Alma Mater Studiorum - Università di Bologna

DOTTORATO DI RICERCA IN

AUTOMOTIVE PER UNA MOBILITÀ INTELLIGENTE

Ciclo 34

Settore Concorsuale: 09/C1 - MACCHINE E SISTEMI PER L'ENERGIA E L'AMBIENTE

Settore Scientifico Disciplinare: ING-IND/08 - MACCHINE A FLUIDO

DEVELOPMENT OF ADVANCED COMBUSTIONS USING CYLINDER PRESSURE SIGNAL

Presentata da: Giacomo Silvagni

Coordinatore Dottorato

Nicolò Cavina

Supervisore

Vittorio Ravaglioli

Co-supervisore

Nicolò Cavina

Esame finale anno 2022

PhD Course: 573 - Automotive for Intelligent Mobility (AIM)
Curriculum: Energy Systems, Powertrains, Vehicle Performance

Cycle: XXXIV
SSD: ING-IND/08 - MACCHINE A FLUIDO
SC: 09/C1 - MACCHINE E SISTEMI PER L'ENERGIA E L'AMBIENTE

Development of Advanced Combustions using Cylinder Pressure Signal

Author: Eng. Giacomo Silvagni

PhD Coordinator: Prof. Nicolò Cavina

Advisor: Eng. Vittorio Ravaglioli
Co-advisor: Prof. Nicolò Cavina

Final Exam Year 2021

Niente nella vita va temuto,

dev'essere solamente compreso.

Ora è tempo di comprendere di più,

così potremo temere di meno.

(Marie Curie)

RINGRAZIAMENTI

Durante la stesura di questo elaborato, spesso mi sono soffermato a ripensare alle emozioni e alle sensazioni che mi hanno accompagnato nello svolgimento di queste attività. Emozioni forti, contrastanti e intense ma, del resto, la natura del mio essere non poteva che generare quel tipo di sensazioni. E ugualmente intensi sono stati i momenti condivisi con le persone che mi hanno accompagnato, taluni loro malgrado, in questo percorso di formazione. Tante sono state le sfide che mi sono state proposte e che ho accettato, sposato, odiato e amato allo stesso tempo. Per questa esperienza, un ringraziamento doveroso va al Professor Fabrizio Ponti che, diversi anni fa, ha messo a disposizione questo tema di ricerca e ha scommesso su di me, quando probabilmente in pochi l'avrebbero fatto. In secondo luogo, mi preme ringraziare i Proff. Corti e Moro, ed i tecnici presenti in laboratorio per gli spunti di riflessione e i suggerimenti forniti durante questo percorso. Indubbiamente, senza il vostro supporto, questa strada sarebbe stata molto più difficile.

Questo dottorato è stato per me un percorso di forte crescita, in cui ho consolidato conoscenze tecniche pregresse e appreso da zero altri concetti che, inevitabilmente, mi erano ignoti. Tuttavia, è a livello personale che ad oggi, ad anni di distanza, ho riscontrato l'arricchimento maggiore e che, a mio modesto parere, è quello che realmente conferisce valore. Un forte ringraziamento va, pertanto, all'Ing. Vittorio Ravaglioli che è stato per me un Virgilio moderno, guida instancabile e di eccezionale pazienza, senza il cui costante supporto e quotidiano esempio questo percorso non sarebbe stato altrettanto formativo.

In questo intenso viaggio, formato da un'altalena di alti e bassi, si sono creati legami forti, indissolubili, veri. Per questo motivo, un grazie va a tutti i miei colleghi passati e presenti che hanno condiviso con me momenti di estrema leggerezza e di inevitabile amarezza e scoramento. Ma, fra i molti, uno in particolare è essenziale per me elevare sopra gli altri. Un ringraziamento speciale va all'Ing. Lorenzo Raggini, amico sincero prima che collega stimato. Grazie, inoltre, alla mia famiglia e, in egual misura, ai miei formidabili amici che hanno reso ogni momento più leggero, consentendomi di affrontare con il sorriso tutte le insidie in cui mi sono imbattuto.

In conclusione, valutando nel complesso questo percorso segnato in modo indelebile dagli avvenimenti della vita quotidiana, posso tranquillamente affermare, in tutta umiltà, una profonda personale soddisfazione, generata dall'insieme di ogni singolo elemento sopra menzionato. Questa mia sensazione è stata riassunta in modo più che efficace da un gigante della scienza:

"Non so come il mondo potrà giudicarmi ma a me sembra soltanto di essere un bambino che gioca sulla spiaggia, e di essermi divertito a trovare ogni tanto un sasso o una conchiglia più bella del solito, mentre l'oceano della verità giaceva inesplorato davanti a me."

--- Sir Isaac Newton

Table of Contents

Abstract

Zero-carbon powertrains development has become one of the main challenges for automotive industries around the world. Following this guideline, several approaches such as powertrain electrification, advanced combustions, and hydrogen internal combustion engines (Hy-ICE) have been aimed to achieve the goal. Among these, the so-called Low Temperature Combustions (LTC), characterized by a simultaneous reduction of fuel consumption and engine-out emissions, represent one of the most studied solutions moving towards a sustainable mobility.

Previous research demonstrates that Gasoline partially premixed Compression Ignition combustion (GCI) is one of the most promising LTC techniques. Mainly characterized by the high-pressure direct-injection of gasoline and the spontaneous ignition of the premixed air-fuel mixture through compression, GCI combustion has shown a good potential to achieve the high thermal efficiency and low pollutants in compression ignited (CI) engines required by future emission regulations. Despite its potential, GCI combustion might suffer from low combustion controllability and stability, because gasoline spontaneous ignition is significantly affected by slight variations of the local in-cylinder thermal conditions. Therefore, to properly control gasoline PPC assuring the maximum performance, a deep knowledge of the combustion process, i.e., gasoline auto-ignition mechanism and the effect of the engine control parameters on the combustion and pollutants, is mandatory.

This PhD dissertation focuses on the study of GCI combustion in a light-duty compression ignited engine. Starting from a standard 1.3L diesel engine, this work describes all the activities made moving toward the full conversion of the engine. A preliminary study of the GCI combustion was conducted in a “Single-Cylinder” engine configuration highlighting the combustion characteristics and the dependencies on the control parameters. Then, the full engine conversion was performed, and a wide experimental campaign allowed to confirm the benefits of this advanced combustion methodologies in terms of pollutants and thermal efficiency. The analysis of the in-cylinder pressure signal allowed to study in depth the GCI combustion and develop control-oriented model aimed to improve the combustion stability.

0. Introduction and Aim

0.1 Future Trends for Sustainable Mobility

Nowadays, the increase in global temperature together with the rise of transported people and goods has forced governments and institutions around the world to establish strict regulation on pollutants and CO2 emissions. On December 12, 2015, in Paris, 195 governments agreed to the text of the most significant global climate agreement in history. Known as the Paris Agreement, the international deal commits nearly every country in the world to lowering greenhouse gas emissions to curb the dangerous effects of climate change. The Paris Agreement strives to limit global temperature increases to 1.5˚C (and 2.0 ˚C as upper limit) [1], as scientists caution that the effects of temperatures rising any higher would be catastrophic and potentially irreversible, while ensuring sustainable food production and economic development, Figure 1.

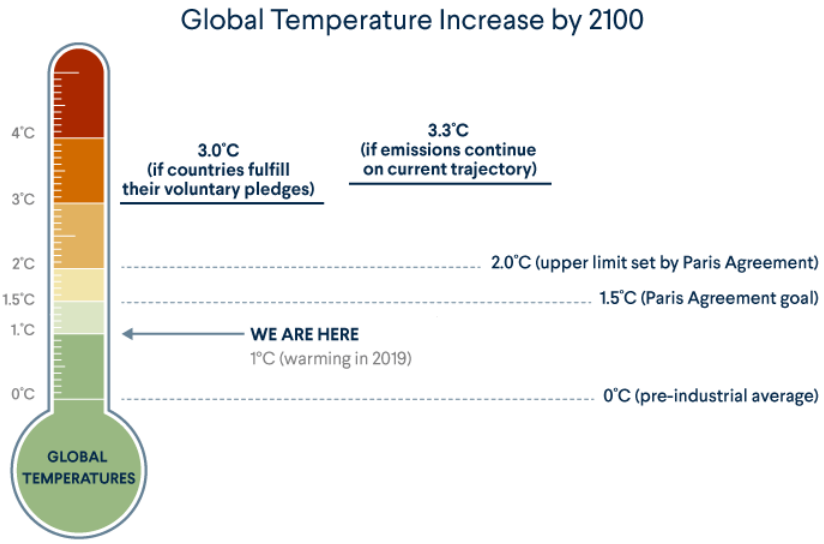

Figure 1. Paris Agreement Targets in temperature increase [1]

While previous climate agreements, most famous before Paris Agreement is the Kyoto Protocol, mandated that countries to reduce their emissions by fixed standards, with Paris Agreement all countries set their goals based on their economic abilities. This radical change of perspective has inducted responsibility of each country following a common goal: to preserve our Earth.

To effectively reduce Greenhouse gases (GHG) emissions it is crucial to know where they are coming from, and which sectors contribute the most. Figure 2 shows the breakdown of emissions by sector. The overall picture that can be seen from the reported diagram is that almost three-quarters of emissions come from energy use, while the remaining 25% come from agriculture, industry, and waste. This means there is no single or simple solution to tackle climate change. Focusing on electricity, or transport, or food, or deforestation alone is insufficient reaching net-zero emissions [2].

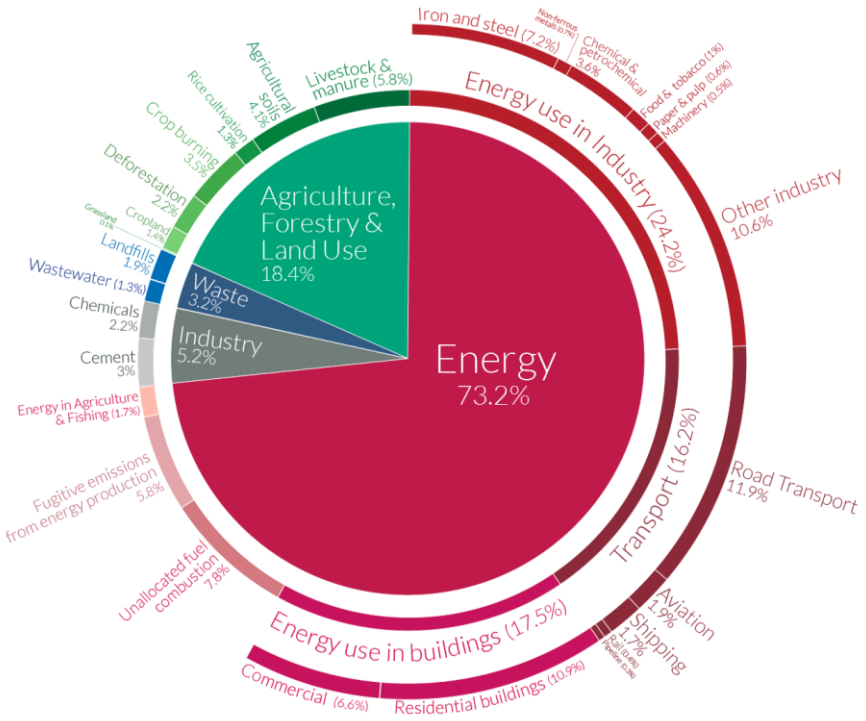

Figure 2. Global GHG sources [2]

In 2017, the top ten emitters of greenhouse gases accounted for more than two-thirds of global emissions, Figure 3. Among the world's largest economies, the India's case is very singular from the GHG emissions point of view [3]. According to Climate Action Tracker, which monitors the Paris Agreement, India is the only top ten emitter whose current policies are on track to help keep global temperature increases below 2˚C. Despite India is considered one of the newly emerging economies (with high request of energy), the attention in climate change stands it as an example of sustainable and rational economy. India's actions are totally focused on overcoming fossil fuel for power generation, transport, and industrial productions. The use of renewable energy sources, such as solar, and the creation of additional forests, which generates a reduction in total greenhouse gas emissions, represent the key points of the Indian green deal.

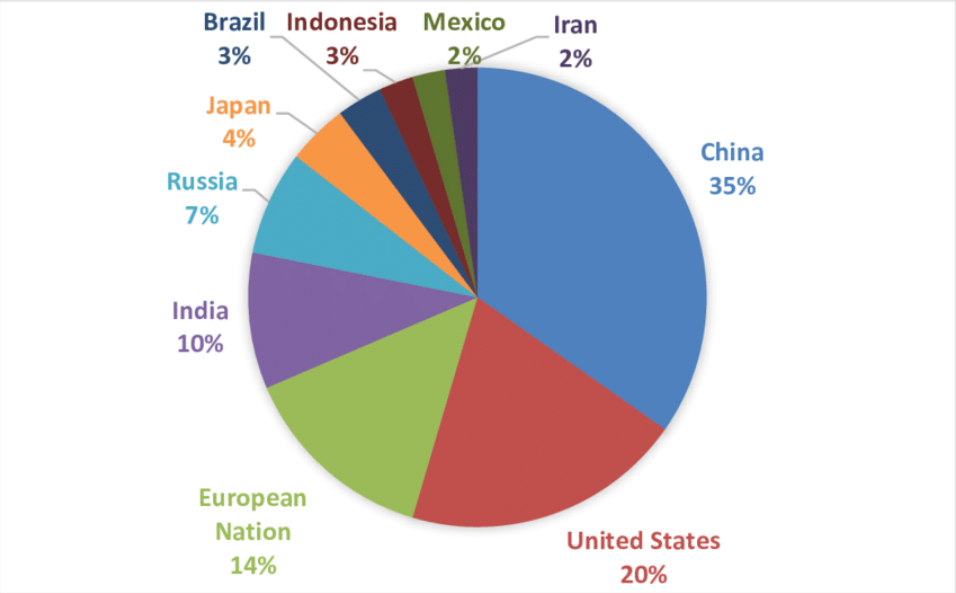

Figure 3. Top ten GHG emitters [3]

Unfortunately, the bigger part of the countries does not comply with the minimum requirements to achieve the Paris Agreement goals. As reported in Figure 4, in 2018 the planned measures of nine of the top ten GHG emitters are highly or critically insufficient to reach the target of maximum global temperature rise of 2˚C. However, the COVID-19 pandemic period strongly highlighted the need of cleaner and more sustainable economy able to avoid future global health and economics shocks. In this scenario, all the governments around the world are developing new green deals with huge investment aimed to improve and develop energy saving, renewable energies and new energy technologies.

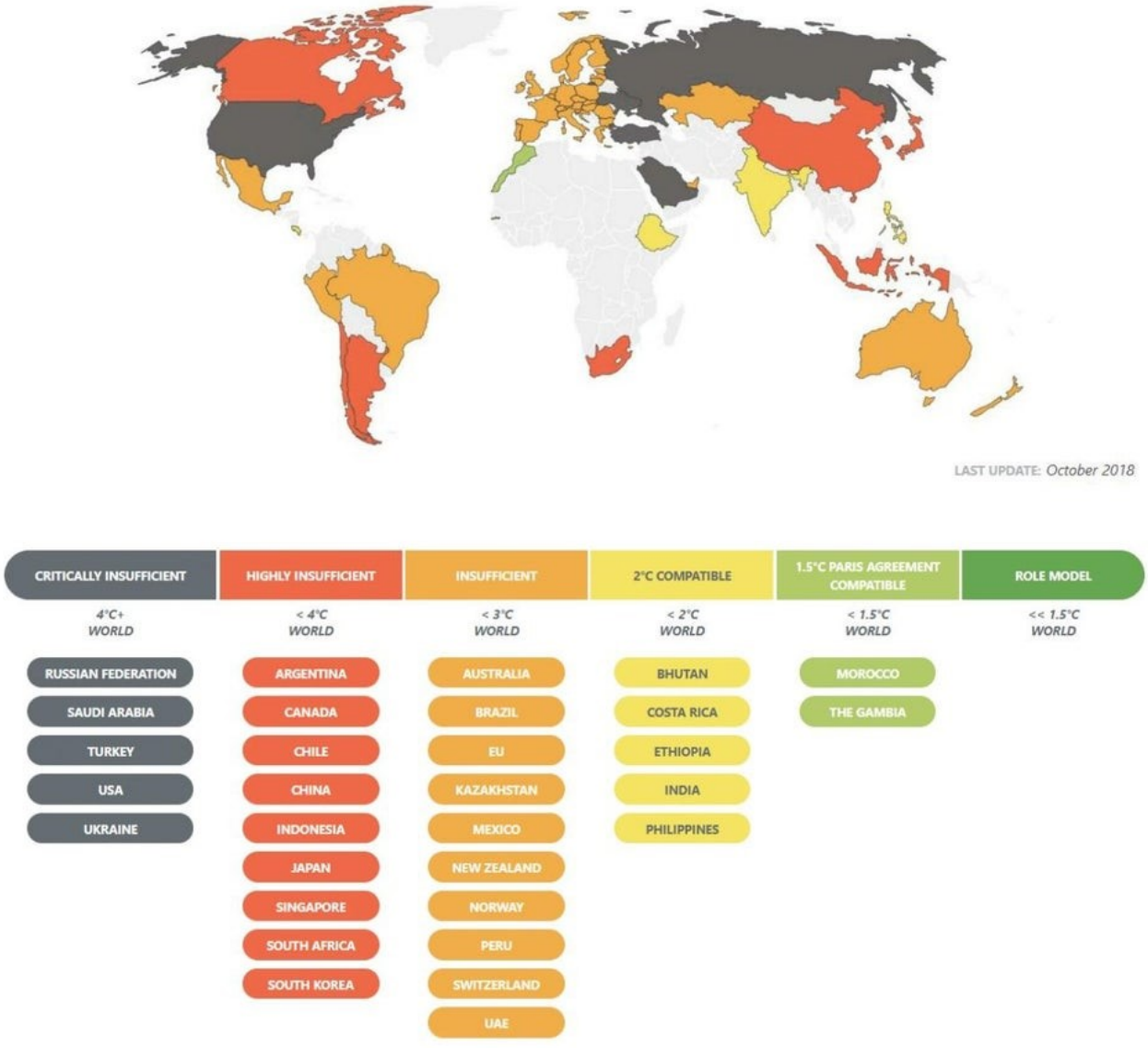

Figure 4. Projections on Paris Agreement goals achievement until 2018 around the world [4]

Since the global economies are still based on fossil fuels, such as carbon, petrol, or natural gas, the bigger part of the GHG production comes from the energy use in buildings and industries, as shown in Figure 2. With the aim of complying the Paris Agreement target, the fossil fuels replacement with renewables sources of energy (solar, geothermal, wind power) or cleaner energy production technologies such as nuclear fusion is strictly mandatory. Unfortunately, this change of perspective cannot be considered shortly drivable mainly because it will require huge investments, big technological empowerments, and relevant infrastructural modifications. However, in the meantime, the actual available technologies give a short-term solution to reduce the impact of transport in terms of global GHG.

As mentioned before, transports account a remarkable contribution in GHG emissions thus, this sector will be strongly modified realizing cleaner and more sustainable vehicles. It is crucial to point out that to adequately consider the impact of the vehicle in GHG production, it is mandatory to consider the carbon dioxide produced among its life cycle. Vehicle life-cycle GHG emissions refers to those emissions produced in the manufacture, maintenance, and disposal of a vehicle, and in the production and combustion on the fuel that powers it. It is obvious that this approach, called *cradle-to-grave*, strongly modifies the consideration regarding the total amount of pollutants generated by a vehicle fleet and, therefore, it requires a disruptive change of policies, both in terms of industrial processes and technical solutions on engine development. Following this guideline, several technologies and solutions have been studied and others are under development aimed to decarbonize road transport by 2050 (Paris Agreement's challenge), and they can be summarized as follow:

1. **Battery Electric Vehicles (BEVs)**
2. **Fuel-Cell Electric Vehicles (FCEVs)**
3. **Hybrid Electric Vehicles (HEVs - ICE based)**
4. **Hydrogen ICE (Hy-ICE)**
5. **Advanced Combustions (LTC)**
6. **Biofuels**

Battery Electric Vehicles (BEVs)

Battery Electric Vehicles (BEVs) are fully electric vehicles with rechargeable batteries and no internal combustion engine. As shown in Figure 5, all energy to run the vehicle comes from the battery pack which is recharged from the grid. BEVs are zero emissions vehicles, as they do not generate any harmful tailpipe emissions or air pollution hazards caused by traditional petrol-powered vehicles.

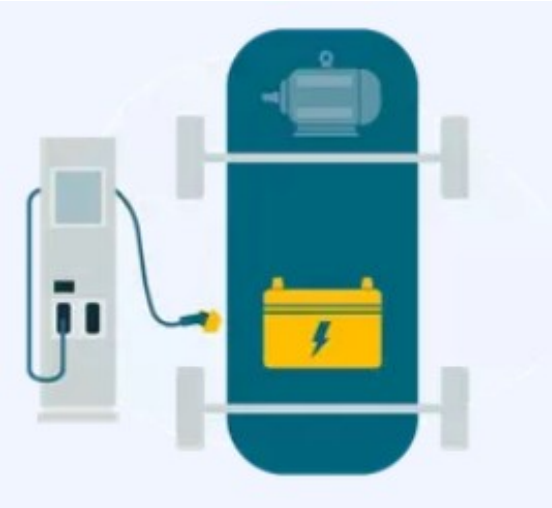

Figure 5. Battery Electric Vehicles (BEVs) power generation layout [5]

Fuel-Cell Electric Vehicles (FCEVs)

Fuel cell electric vehicles (FCEVs) are powered by hydrogen. They are more efficient than conventional internal combustion engine vehicles and produce no tailpipe emissions and they only emit water vapor and warm air. As reported in Figure 6, FCEVs use a propulsion system like that of electric vehicles, where energy stored as pure hydrogen in a tank on the vehicle is converted to electricity by the fuel cell. Furthermore, they are equipped with other advanced technologies to increase efficiency, such as regenerative braking systems that capture the energy lost during braking and store it in a battery.

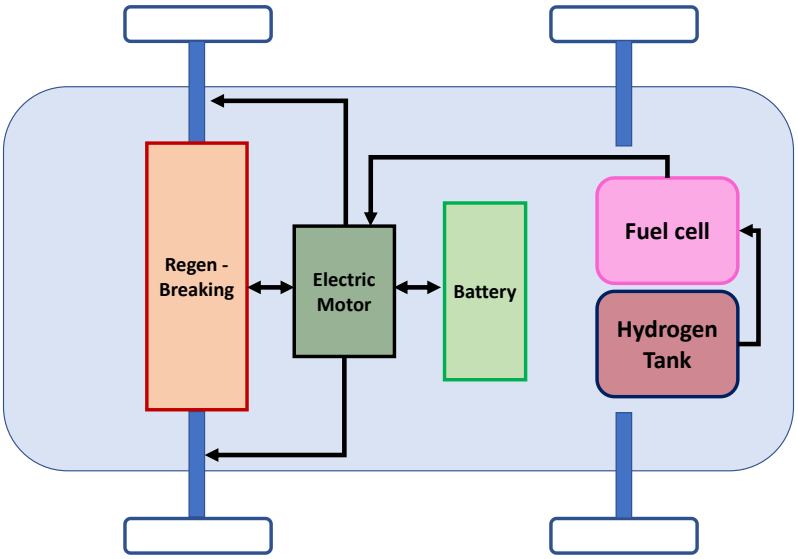

Figure 6. Fuel-Cell Electric Vehicles (FCEVs) power generation layout [6]

Hybrid Electric Vehicles (HEVs - ICE based)

Hybrid Electric Vehicles (HEVs), have both ICE engine and an electric motor to drive the car. All energy for the battery is gained through regenerative braking, which recoups otherwise lost energy in braking to assist the engine, typically a gasoline engine, during acceleration. In a traditional ICE based vehicle, this braking energy is normally lost as heat in the brake pads and rotors. Since regular hybrids cannot plug into the grid to recharge, alternative approaches, such as Plug-in Hybrid Electric Vehicles (PHEVs), have been developed to increase the efficiency of HEVs.

As clearly visible in Figure 7, PHEVs have both an engine and electric motor to drive the car. Like regular hybrids, they can recharge their battery through regenerative braking. They differ from standard HEVs by having a much larger battery and being able to plug into the grid to recharge. While typical HEVs can (at low speed) travel 1-2 kilometers before the gasoline engine turns on, PHEVs can go anywhere from 10-40 kilometers before their ICE provide assistance. Once the all-electric range is depleted, PHEVs act as regular hybrids, and can travel several hundred kilometers on a tank of gasoline. As a result, despite a weight increment generated by bigger battery pack, the extended range run in full-electric mode increase the overall efficiency of PHEVs in urban cycles (extremely critical for emissions).

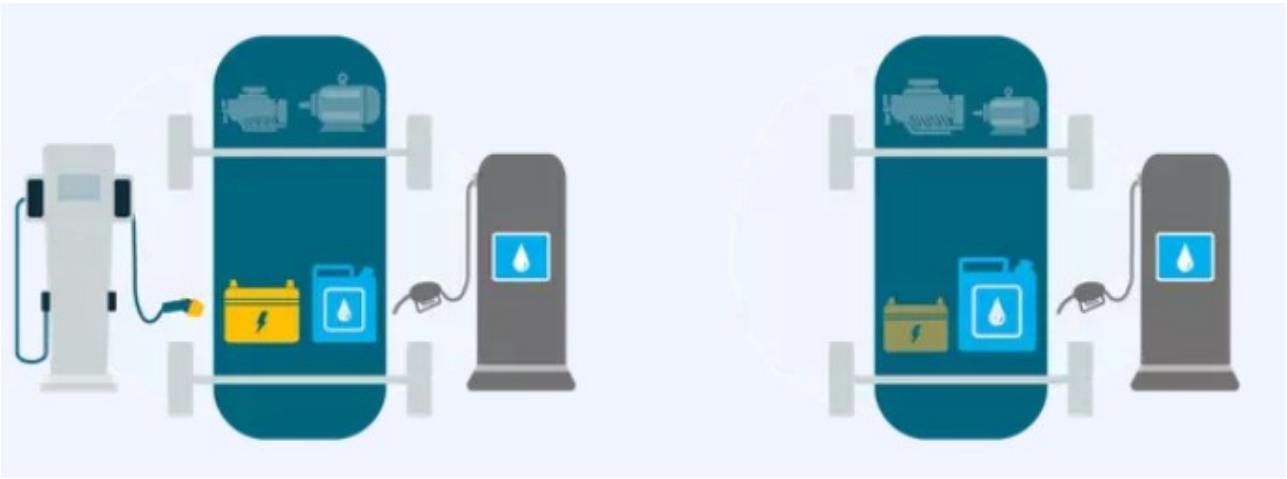

Figure 7. Plug-in Hybrid Electric Vehicle (PHEVs) (left) and Hybrid Electric Vehicles (HEVs) (right) power generation layouts [5]

Hydrogen ICE (Hy-ICE)

Because hydrogen is one of the numerous elements found in the atmosphere, it is readily available and one of the most useful alternatives to fossil fuels today. As a result, most of research have been focused on fuel standard ICE with hydrogen (Hy-ICE) replacing standard fuels, Figure 8, and they proved to be a very promising technology with high efficiency and low pollutants for both for light and heavy-duty engine and off-road applications (even coupled with electric powertrain). Despite the hydrogen production needs huge amount of energy which comes from fossil fuels (called *grey hydrogen*), the Hy-ICE are still not competitive from the cradle-to-grave standpoint with respect to HEVs or PHEVs. However, since the future trends on energy production are oriented to increase hydrogen production using renewable energy sources (called *green hydrogen*), Hy-ICE might represent a concrete solution moving toward a sustainable mobility.

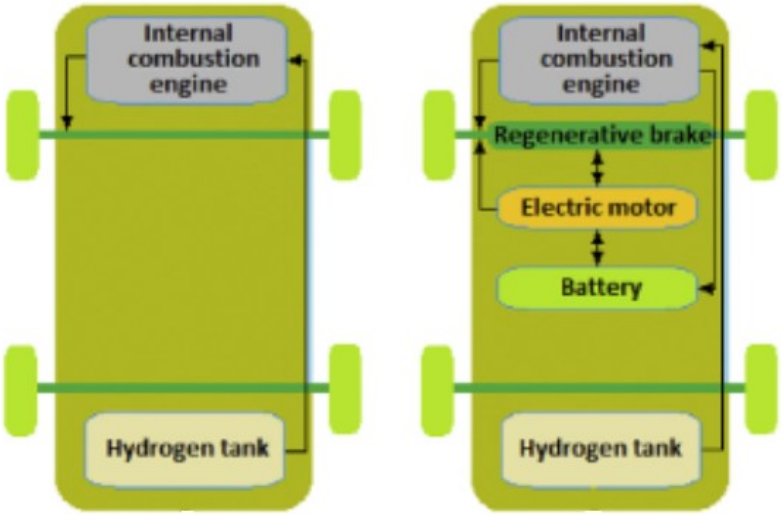

Figure 8. Hy-ICE typical power generation layouts: standard Hy-ICE (right) and Hybrid Hy-ICE (left) [7]

Advanced Combustions (LTC)

Over the past years, the more and more stringent emissions regulations, especially for nitrogen oxides (NOx), soot production and GHG emission, promoted a great amount of research in the field of advanced combustion approaches. Such solutions, called Low Temperature Combustions (LTC), have shown a good potential to replace conventional combustions mainly because of their high efficiency and low emissions with respect to conventional combustions, Figure 9.

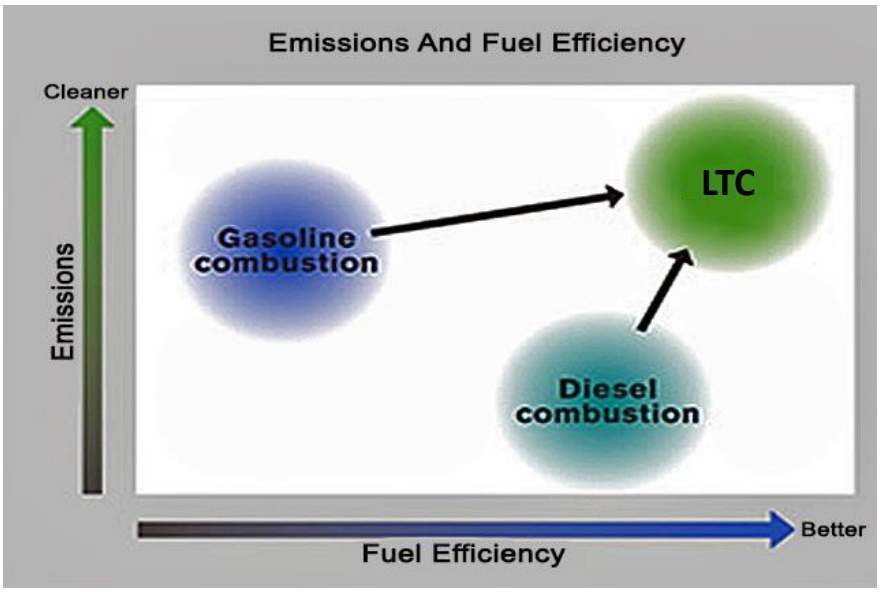

Figure 9. Better than efficiency and emission of LTC combustion [8]

LTC identifies not just one but a group of combustion technologies which differ mainly in charge preparation procedure and ignition strategy. Several methods have been developed to obtain proper level of charge homogenization such as, variable compression ratio, multiple injection strategies, in-cylinder charge motion systems (tumble flaps, ducts, and piston shape optimization). Typically characterized by the very lean combustion of an air-fuel mixture, LTC have been studied to explore their potential in the field of developing cleaner and more efficient internal combustion engines.

Since LTC proved to be an effective solution to limit emission and pollutants in IC engines, the main challenge which limited their diffusion is the controllability of the combustion process and, therefore, they are continuously under development (especially their integration in hybrid powertrains).

Biofuels

Biofuels are any kind of fuel made from plant or animal material, such as corn ethanol and palm biodiesel. Biofuels can reduce life cycle GHG emissions compared to petroleum because the carbon emitted from their combustion was previously sequestered from the atmosphere in the plants from which the biofuel was made. There are, however, other sources of GHG emissions along the life cycle of biofuels and typically come from cultivating, harvesting, and transporting the feedstock and producing and transporting the biofuel. As a result, since biofuels are typically blended into gasoline and diesel (at a rate of 10% or less) and manly due to regional differences in crop and biofuel production, that could strongly modify their GHG emissions, it is not clear that food-based biofuels are any better for the climate than petroleum.

Figure 10 reports an overview of the life cycle GHG emission for the actual solutions and technologies in transport industry and it can be notice that today, also BEVs and FCEVs have too high GHG emissions mainly related to the energy production process (that involves fossil fuels) to fuel these vehicles. Furthermore, despite only BEVs and FCEVs have the potential to achieve the magnitude of life cycle greenhouse gases (GHG) emissions reductions needed to meet Paris Agreement goals, the battery-pack related challenges (energy storage, aging and weight), the lack of charging/filling infrastructure and the cost have hindered a wide diffusion of these technologies.

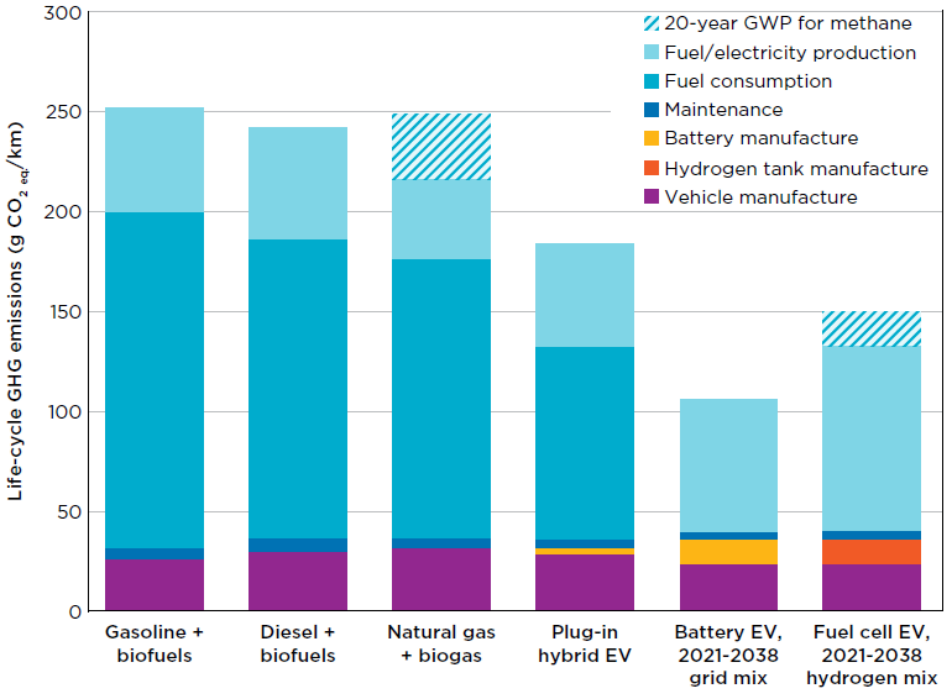

Figure 10. Life-cycle GHG emissions for global typical medium-size passenger cars registered in 2021 [9]

However, considering the evolution of the materials and industrial processes (especially in the energy production from renewable sources) it is expected that these solutions will replace in the long-term the internal combustion engines (ICE) both in high and light-duty vehicles. Figure 11 shows the life cycle GHG emission projections until 2050 for the above-mentioned solutions with the renewable energy. By looking at Figure 11, it clearly arises that to fully decarbonize transports is mandatory the integration of zero-carbon solutions, such as HEVs and FCEVs, with renewable energy sources.

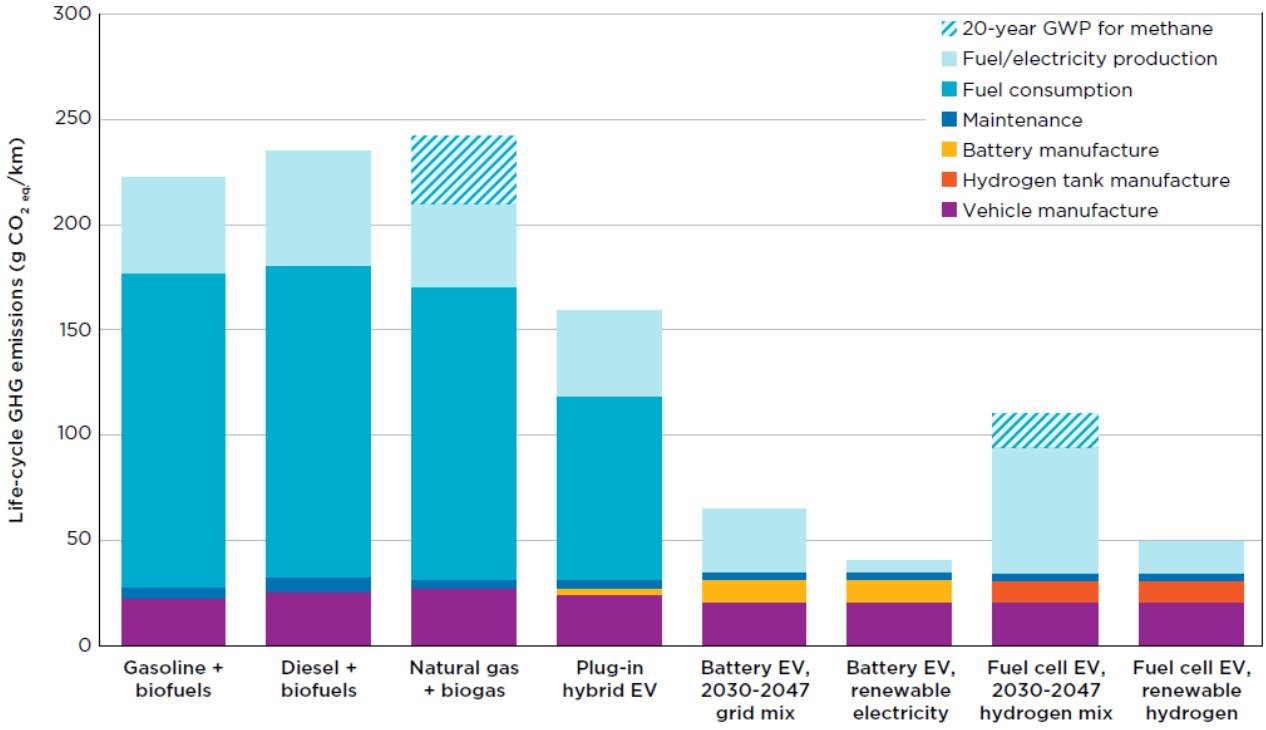

Figure 11. Life-cycle GHG emissions for global typical medium-size passenger cars registered in 2030 [9]

0.2 PhD dissertation structure

Among the solution under studied to decarbonize transport, the PhD research activity described in this dissertation is focused on the development of advanced combustion methodologies (LTC).

After an introduction on LTC, facilities and instruments used during the whole activity, the PhD research tried to give its contribution to the improvement on the knowledge about one of the most studied LTC called Gasoline partially premixed Compression Ignition combustion (GCI) by observing the combustion process using the in-cylinder pressure sensor.

The first part of the activity has been focused on the experimental investigation of GCI combustion in one of the four cylinders of an extremely diffused light-duty diesel engine, while the other three cylinders kept the engine in a stable operating condition, called "*Cylinder Laboratory mode*". By the analysis of the collected data, it has been possible to study the impact of the main control parameters on combustion stability and controllability. A huge part of activity has also been conducted to improve the knowledge regarding gasoline autoignition and to define its dependencies on the control parameters.

Once defined a set of control parameter which guarantee GCI combustion stability in "*Cylinder Laboratory mode*", the second part of the activity has been focused on the full engine conversion from diesel to GCI engine. In this way, all the additional systems needed to stabilize GCI combustion from the cranking stage has been developed and mounted in the test cell. Furthermore, to overcome the limitations given by the standard engine electronic control unit (ECU) performing tests very far from the manufacturer calibration conditions, a fully programable engine ECU has been used to control the engine. By using a custom ECU and its integration with the test bench control system it has been possible to explore this advanced combustion in very different operating conditions. The experimental campaign conducted in the fully converted GCI engine confirmed the potential of this combustion both in terms of pollutants reduction and increase in efficiency.

The third part of the PhD activity concerned the development of model-based control-oriented strategies aimed to improve GCI combustion stability and controllability. For this purpose, since the gasoline autoignition plays a crucial role assuring the combustion stability, a dedicated experimental activity has been carried out to develop a thermodynamic ignition delay model able to predict the start of ignition position as a function of the boost temperature and pressure.

Moreover, since GCI uses multiple injections to improve the combustion stability, a proper control of the injected mass, especially with very small injection pulses with small relative distance, is mandatory. For this reason, the last part of this dissertation shows the experimental activity and modeling carried out to compensate the pressure waves propagation effects in a standard common-rail high-pressure injection system fueled with gasoline.

1. Advanced Combustion Methodologies

Nowadays, road transportation is still mainly based on the use of internal combustion engines (ICE), therefore the increase of engine efficiency and the reduction of pollutant and greenhouse emissions are of fundamental importance to minimize its environmental and health impact. High levels of efficiency can be achieved through compression-ignited (CI) engines, which are currently the most efficient and reliable engine technology used in automotive applications. However, CI engines are usually powered by the high-pressure direct injection of Diesel, which leads to a combustion process that is heterogeneous by nature. Such combustion process is characterized by the simultaneous production of a significant amount of particulate matter and NOx, both severely limited by current emission regulations, Figure 12. To overcome the mentioned problems, over the past years a large amount of research has been carried out to investigate innovative combustion techniques, called Low Temperature Combustions, characterized by high efficiency and low emissions.

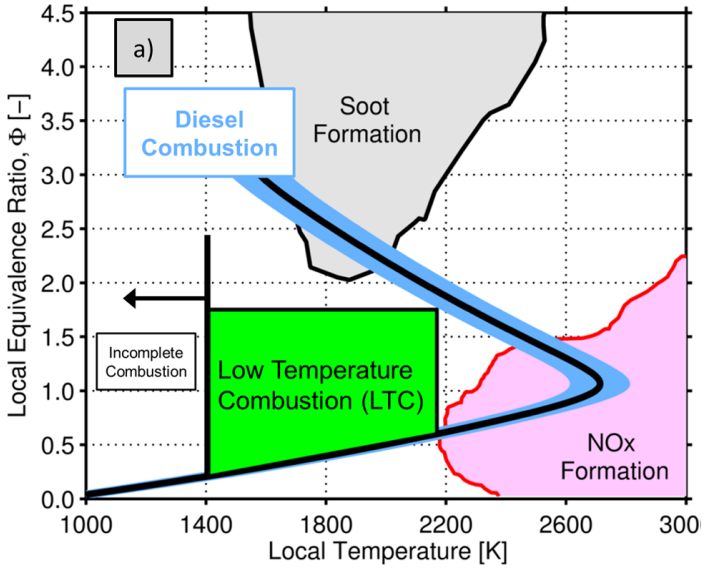

Figure 12. Different kinds of combustion concept in term of flame temperature referred to its chemistry (equivalence ratio) [10]

1.1 Low Temperature Combustions

Low Temperature Combustions (LTC) is a general term used to refer to all the advanced combustion concepts where the overall goal is to achieve lower peak combustion temperature which advantageously alter the chemistry of NOx and soot formation.

Basically, both NOx and soot emissions are derived from the mixing characteristics of air -fuel and combustion temperature. As well reported in literature, NOx generally forms when peak combustion temperatures are above 2000 K and soot in fuel rich conditions and temperatures above 1700 K. Hence, by limiting the peak combustion temperatures with certain level of premixing of fuel with in-cylinder charge prior to ignition we can achieve reduction in both NOx and soot emissions, and it is possible either by extensive premixing to lean equivalence ratio (~0.5) or by use of EGR.

The main LTC concept is to make a very lean mixture, as homogeneous as possible, potentially able to self-ignite almost instantaneously and volumetrically (generating very short combustion). However, to maximize benefits of such combustion methodologies, it is crucial to overcome limitations related to these self-ignited processes. Several works in literature reported main challenges performing LTC, such as high combustion noise, high cyclic and cylinder-to-cylinder variation, limited power density (related to guarantee the engine

reliability). Furthermore, since these advanced combustions are typically chemically driven, mixture preparation (assuring a proper level of stratification) represent the critical aspect which could compromise the combustion stability. Thus, very complex combustion model coupled with engine control strategies, using closed loop contribution based on combustion feedbacks by in-cylinder pressure sensors, are needed to stabilize the combustion over the whole engine operating range. As a result, despite such methodologies are considered a very promising solutions able to limit GHG emission until total dropout of petrol-based ICE, the above-described challenges have hindered their wide diffusion for commercial uses.

Generally, for LTC, it is important to highlight that leaner and more homogeneous mixture led to lower NOx and PM emissions, but also reduce ignition controllability. To achieve these goals, several techniques moving toward the LTC concept and trying at the same time to solve LTC challenges have been proposed. Such solutions mainly differ in charge preparation procedure and ignition strategy. The most relevant LTC technologies are:

- **Homogeneous Charge Compression Ignition (HCCI)**
- **Premixed Charge Compression Ignition (PCCI)**
- **Stratified Charge Compression Ignition (SCCI)**
- **Reactivity Controlled Compression Ignition (RCCI)**
- **Spark Assisted Compression Ignition (SACI)**
- **Turbulent Jet Ignition (TJI) and Torch Ignition (TI)**

Homogeneous Charge Compression Ignition (HCCI)

The HCCI mode consists in the compression ignition (auto-ignition) of homogeneous (premixed) air-fuel mixture in the engine cylinder coupling the benefits from both conventional combustions (CI and SI) methodologies, Figure 13. In HCCI combustion, a nearly homogeneous charge (fuel–air mixture) enters in the engine cylinder during intake stroke and, due to the rise of pressure and temperature during compression stroke, the whole charge releases energy simultaneously. Hence, combustion duration is very short and occurs close to top dead center (TDC) mainly because whole charge releases energy at the same time in the combustion chamber. These combustion characteristics represent the main limitation for HCCI especially at high loads.

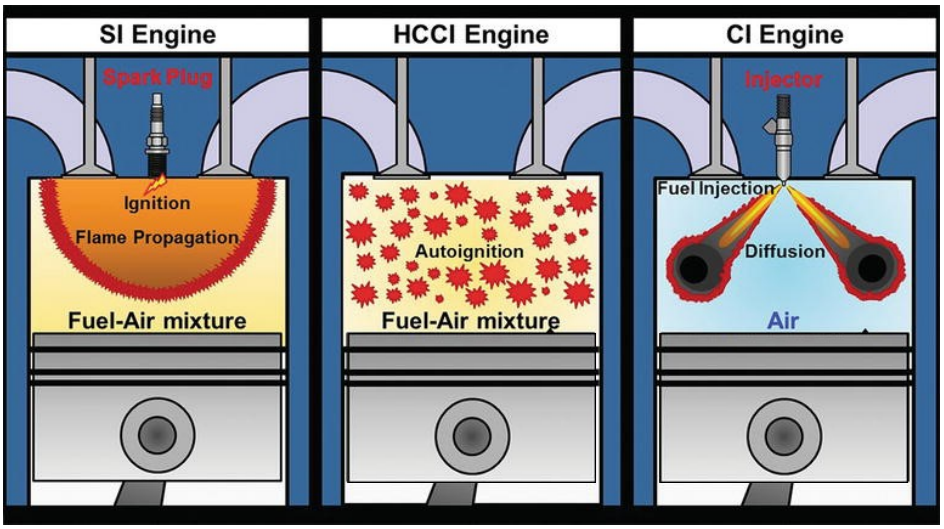

Figure 13. HCCI characteristics compared to conventional combustions (SI - CI) [11]

Since HCCI is governed by chemical kinetics (charge preparation, type of fuel, charge pressure and temperature), the main challenges are related to the control of the combustion phase and rate assuring combustion stability and engine reliability [11].

In this operation mode, power output is controlled by varying the fuel flow rate, and engine is operated unthrottled like CI engines with high compression ratio. The HCCI engine is operated on globally leaner mixture to control the combustion rate, which leads to lower combustion temperature. Premixed charge and lower combustion temperature in HCCI combustion process leads to ultralow NOx and soot emissions. However, since the air-fuel mixture is typically realized using port fuel injection (PFI) systems which does not guarantee a total charge homogenization, also HCCI engines might be characterized by fuel concentration inhomogeneities generating high values of HC and CO.

Premixed Charge Compression Ignition (PCCI)

Conventional diesel engine combustion has a soot–NOx trade-off, and generally, methods of reducing soot lead to increases in NOx emissions and vice-versa. Using diesel, to obtain simultaneous reduction in soot and NOx emissions, charge must be well mixed (premixed charge) to avoid regions with unfavorable carbon–oxygen ratios, charge must also be rich enough to prevent misfire, and combustion results into lower combustion temperatures, Figure 14.
To achieve PCCI combustion, which is typically realized with diesel mainly because its high reactivity reduces the ignition delay, proper manage of injection strategies (injection timing and position) is mandatory to generate a high degree of air-fuel mixing before ignition. Since diesel is a non-volatile fuel, to create a premixed mixture, PCCI engines are equipped with high-pressure direct injection systems which perform early injections (during compression stroke, far from TDC) improving air-fuel mixing. Fuel rich pockets, which form due to imperfect homogenization, are useful for triggering auto-ignition and controlling the combustion phasing. As a result, due to good air-fuel mixing realized with early injections, low NOx and soot emission is achieved with PCCI combustion.

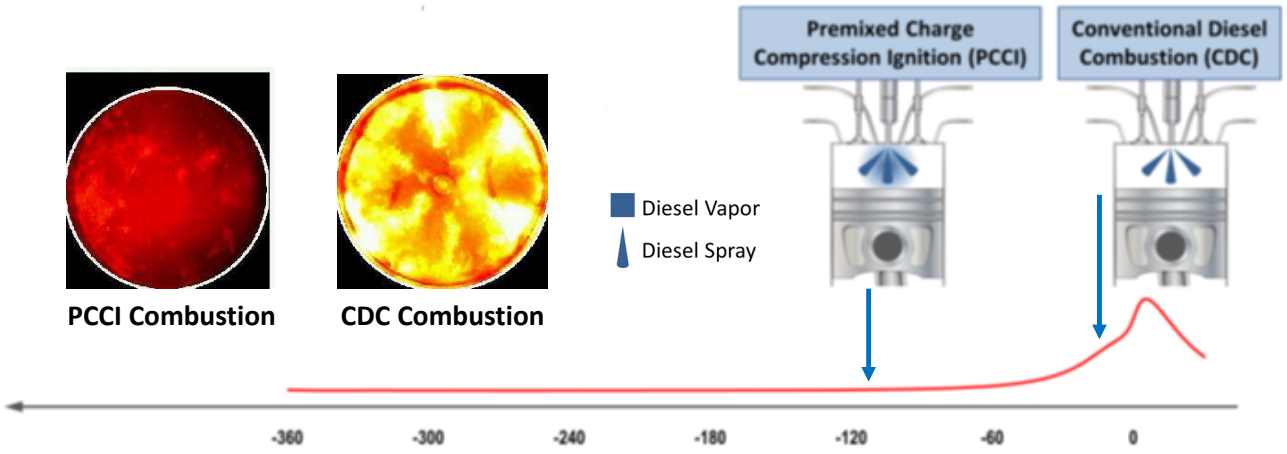

Figure 14. PCCI concept with respect to CDC combustion [10]

On the other hand, as described for HCCI combustion, high level of homogenization leads fast and dangerous combustion at high loads. Hence, to limit the combustion knocking at high loads, PCCI combustion is performed using high dilution typically with external EGR. However, the use of high charge dilution, wrong injection strategy and not optimized geometrical arrangement of engine components (i.e., combustion chamber shape, injector geometry, ducts shape) may affect combustion stability and increase pollutants, especially at low loads. For these reasons, proper control of the combustion process (phase and intensity) represents the main challenges for PCCI combustion without decreasing the thermal efficiency.

Stratified Charge Compression Ignition (SCCI)

As explained before, inhomogeneities (thermal and fuel stratifications) play a key role controlling premixed combustion in compression ignited engines. Since it is very difficult to create or control thermal stratification (typically created by heat transfer and convection in the combustion chamber), to increase PCCI controllability, combustions with different levels of fuel stratification have been studied demonstrating their potential in pollutant reduction without penalizing the thermal efficiency. Fuel stratification is typically achieved by varying the fuel injection timings or by using multiple injection strategies. This strategy creates zones of different fuel concentrations in the combustion chamber, which leads to sequential auto-ignition. The zones with higher fuel concentration auto-ignite first and comparatively lower concentration zone next. Sequential auto-ignition leads to reduce the combustion knocking and increases the combustion duration.

The advantage of fuel stratification mainly depends on the autoignition reactivity of fuel (which typically increases using supercharging, i.e., high boost pressure): the more autoignition reactivity the more fuel has potential to start burning with proper fuel stratification. As widely reported in literature, the high volatility of gasoline and its high autoignition reactivity at high boost pressure allow to overcome the knocking limitation of diesel PCCI combustion at high loads. These strategies generally called Stratified Charge Compression Ignition combustion (SCCI), which has various names by different group of researchers such as Gasoline Compression Ignition (GCI), gasoline Partially Premixed Combustion (gasoline PPC) or Low Temperature Gasoline Combustion (LTGC), always uses gasoline-like fuel directly injected in the combustion chamber with high-pressure injection systems. The gasoline SCCI strategies can be divided into three main categories: partial fuel stratification (PFS), moderate fuel stratification (MFS) and heavy fuel stratification (HFS) based on degree of fuel stratification in the combustion chamber, Figure 15.

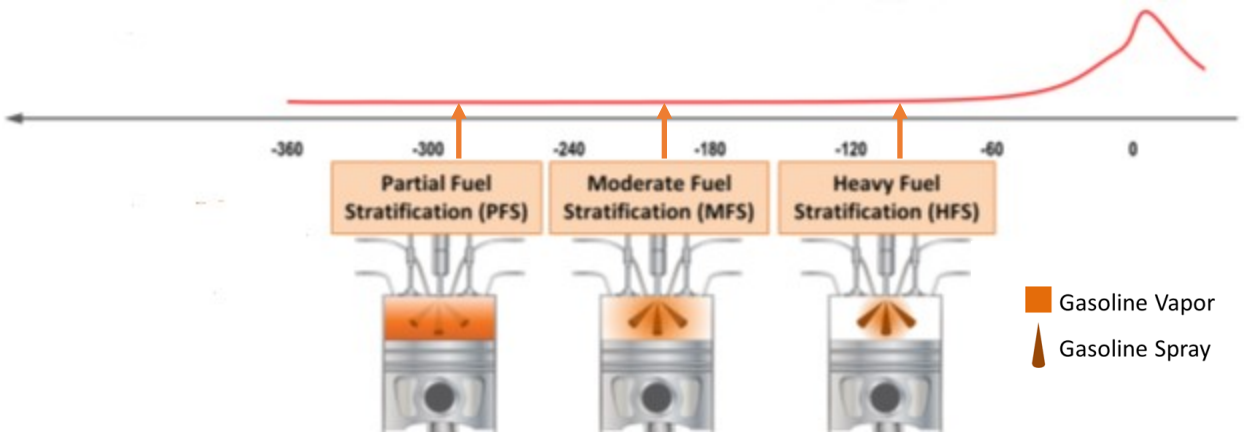

Figure 15. SCCI main concepts at different level of fuel stratification [10]

In PFS strategy, homogeneous part of charge is prepared by either PFI or very early DI fuel injection, and stratification is created using subsequent direct injection of fuel (small quantity). The ratio between the PFI (or very early DI injection) and DI injection defines the charge stratification. In the MFS strategy, stratification level is higher in comparison to PFS, and it is increased by reducing the amount of premixed fuel. Generally, in MFS strategy, all the fuels are injected directly in the cylinder during compression stroke and a fuel injection event near TDC is used to start the combustion. The HFS strategy has highest level of fuel stratification, and it typically has very less premixed fuel. Multiple high-pressure (higher in comparison to PFS and MFS) direct injection events relatively close to TDC is used for charge preparation in HFS strategy. It is important to underline that in SCCI combustion, to promote charge stratification, internal charge motions (typically generated by piston bowl shape, injection spray and ducts shape) are minimized.

As explained before, in gasoline SCCI mode, fuel injection strategy is crucial to manage gasoline compression ignition. The fuel injection strategy can have one, two or three injections per cycle in cylinder during compression stroke which rapidly vaporizes (thanks to high injection pressure) and mixes with air creating the desired level of charge stratification to obtain controlled heat release and stable ignition. Figure 16 reports different injection strategies for PFS, MFS and HFS respectively.

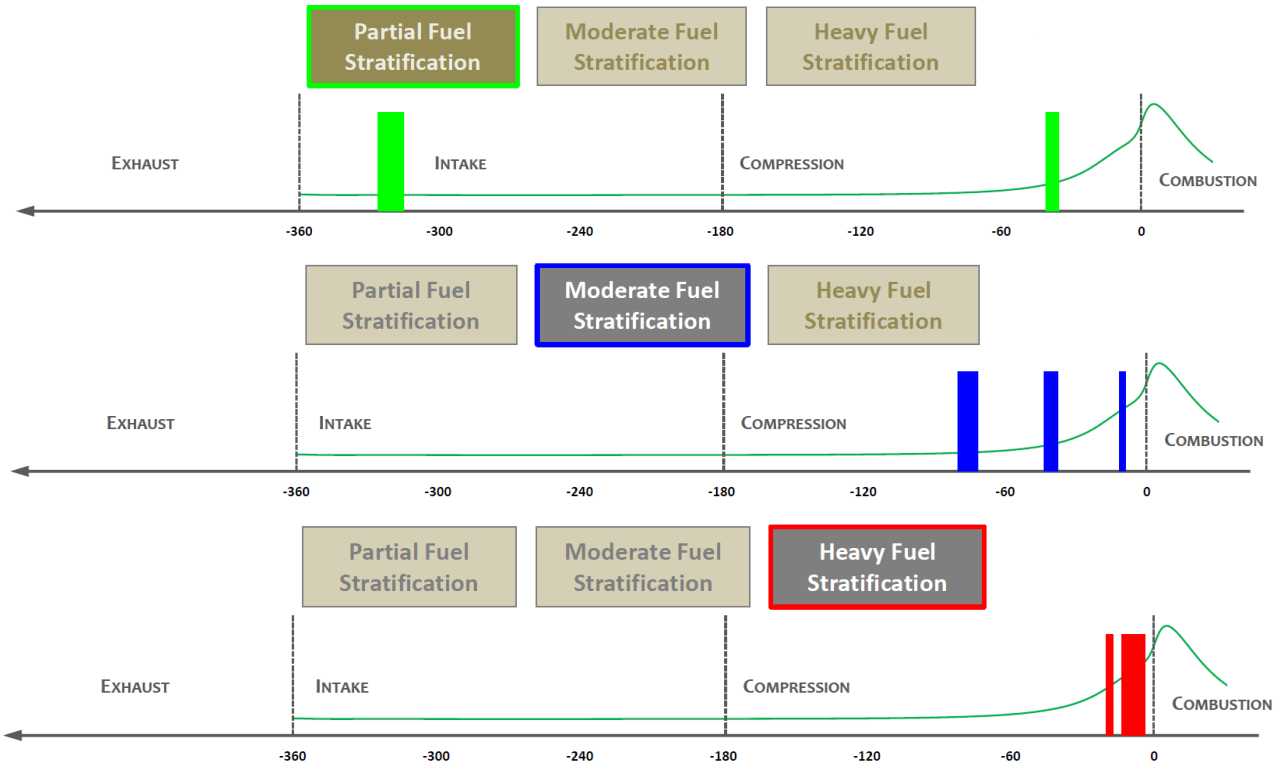

Figure 16. PFS, MFS and HFS injection strategies [10, 11]

As it occurs in CDC, the ignition phase for HFS strategy is governed by injection timings. As a result, combustion phasing can be easily controlled on a cycle-to-cycle basis through injection management. Since the lower stratification of MFS and PFS, the ignition phase management (which defines the combustion controllability) becomes harder mainly because the higher ignition delay of the mixture. Furthermore, moving toward PFS the air-fuel chemistry becomes predominant and therefore, slight variations of charge pressure and temperature may affect the combustion stability, generating knocking or misfiring even at mid loads.

As explained in literature [10, 11], the pollutant emissions (NOx and soot) of SCCI are strongly related with the level of fuel stratification and decrease as mixture becomes more homogeneous. Therefore, high dilution with EGR is required in HFS strategy for LTC operation and decrease NOx emissions (EGR level is still below than the quantity involved in PCCI). As a result, despite high stratification generates benefits both in terms of pollutants production and thermal efficiency, the combustion management problems (i.e., ignition and combustion phase management), related to an even more chemically driven combustion process, represent the main obstacles on the SCCI diffusion in production engines. As mentioned in the introduction paragraph, this PhD dissertation is focused on the study of the GCI combustion, one of the above-described SCCI combustions, in a standard light-duty compression ignited engine.

Reactivity Controlled Compression Ignition (RCCI)

Reactivity-controlled compression ignition (RCCI) strategy is also in the category of partially premixed compression ignition, and it uses two fuels of different reactivities. In this strategy, two fuels with different auto-ignition reactivities (high and low reactivity) are used for charge preparation by in-cylinder fuel blending. By using multiple injections strategy coupled with appropriate external EGR level, RCCI combustion duration and phase can be controlled assuring high thermal efficiency along with simultaneous reduction of NOx and soot emissions to ultralow level. Figure 17 schematically illustrates RCCI combustion concept.

The low reactivity fuels (gasoline-like fuels) are injected in intake manifold using port fuel injection (PFI) system, which premixes with air during intake stroke, due to their volatile nature. The high reactivity fuel (diesel-like fuels) is directly injected in the cylinder using direct injection (DI) system with a single, or multiple injections strategy during compression stroke. Once the high reactivity fuel is injected near TDC and releases its energy (with very low ignition delay), the "near homogeneous" air-fuel mixture starts burning. As a result, the ratio of low and high reactivity fuel (typically represented by diesel fraction, DF) and injection timings of high reactivity fuel can be used to control the RCCI combustion process.

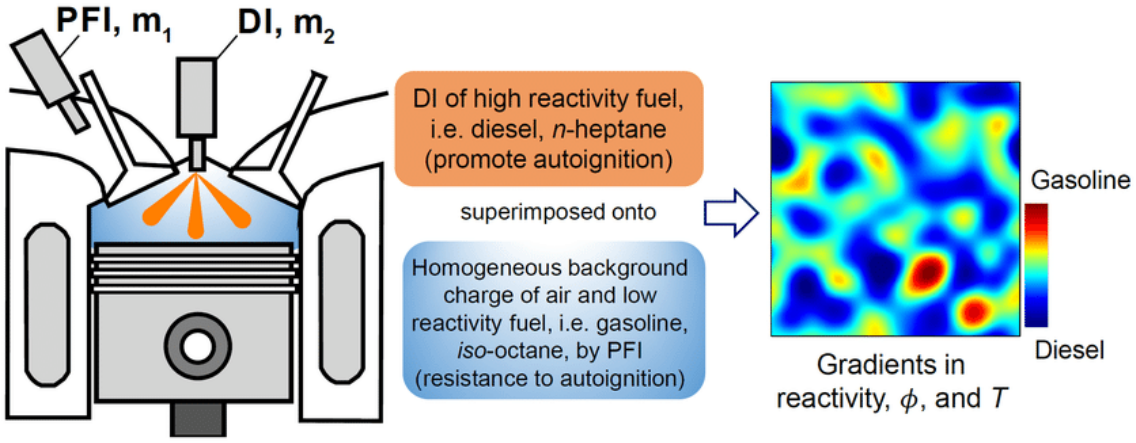

Figure 17. RCCI main characteristics [12]

It is important to underline that using high DF, the combustion controllability improves but the stratification increases producing high NOx and soot. To maximize benefits of RCCI combustion, it is preferable to run the engine with low DF. The combustion process will be even more chemically driven with a very small operating range: low loads are unstable due to high cycle-to-cycle variability, and high loads are dangerous due knocking.

Spark Assisted Compression Ignition (SACI)

Spark-assisted compression ignition (SACI) is a technique to trigger the HCCI combustion improving the controllability of the whole combustion process [13, 14]. By using an external ignition source, SACI combustion can switch from conventional SI combustion to "externally triggered HCCI" over the whole engine operating range overcoming the well-known HCCI limitations both at high (knocking) and low (misfires) loads. During the "externally triggered HCCI" it is possible to obtain the benefit of a standard HCCI both in terms of pollutants and efficiency.

As made for HCCI, a dilute (by using external EGR) homogeneous mixture is prepared in the manifold or very early in the intake stroke. However, a small amount of fuel is injected late in compression stroke to achieve a fuel-rich mixture near the spark plug for promoting SI. The propagating flame, called first combustion phase, near spark plug (small kernel is created) increases pressure and temperature in the cylinder, leading to auto-ignition in the surrounding homogeneous diluted charge which releases energy simultaneously (second combustion phase) in a short time, Figure 18.

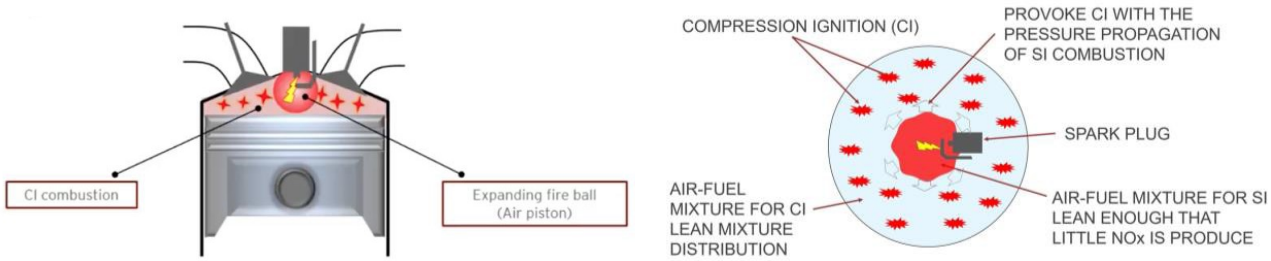

Figure 18. SACI main characteristics [9]

It is important to underline that to correctly perform SACI combustion there are two main requirements on the charge preparation: the relative air-fuel ratio and temperature must be adequately high to sustain flame propagation (first combustion phase), which is fast enough to consume fraction of charge, and the compressed gas pressure and temperature must be sufficiently low such that the charge does not auto-ignite until the end of the first combustion phase.

Typically, SACI engine is started in SI mode to tackle the cold start problem of HCCI and then shift to "externally triggered HCCI" mode for lower engine load operations. At higher engine loads, engine can be shifted back to SI operation mode avoiding knock. As a result, the use of spark plugs to trigger the combustion is considered a key enabler on the development of high efficiency SI–HCCI hybrid systems. Despite frequent SI–HCCI transition is required due to load variations during real engine operation (to avoid combustion instability and to guarantee engine reliability), the SACI management represent one of the main challenges for SACI combustion. Furthermore, many works are focused on increasing the HCCI operating range in SACI engine, to maximize benefits of the homogeneous charge combustion.

Turbulent Jet Ignition (TJI) and Torch Ignition (TI)

As widely explained in the previous sections, the leaner is the mixture the more efficient is the combustion providing the same torque. However, despite spark ignited engines are characterized by high controllability too high value of relative air-fuel ratio generates flame quenching and, consequently, generating misfire. As a result, several technologies, called pre-chamber combustion systems have been proposed able to perform ultra-lean combustion overcoming the ignitability limitation of the mixture.

Turbulent Jet Injection (TJI) and Torch Ignition (TI) systems are both based on the use of a prechamber, located on the top of the cylinder head, in which overlooks the spark plug. The spark plug ignites an almost stoichiometric mixture inside the prechamber. Then, when the flame front reaches prechamber orifices it accelerates itself with or without quenching. If the flame front quenches passing through orifices, ignition process is called TJI, otherwise if the flame front survives passing through orifices, ignition process is called TI. Both systems reduce the ignition delay and highly accelerate the combustion process making possible the ignition of an ultra-lean premixed in cylinder mixture. Ultra-lean operation (with relative air-fuel ratio greater than 2), performed with pre-chamber technologies in spark ignited engines, has demonstrated the ability to increase thermal efficiency and significantly reduce emissions of nitrogen oxides (NOx) due primarily to lower mean gas temperatures.

As mentioned before, the key point of pre-chamber technologies is to create an almost stoichiometric mixture inside the prechamber. Two different technical solutions have been proposed depending on the prechamber fueling system, Figure 19. Active prechamber generates the stoichiometric mixture inside the prechamber by using a supplementary injector, typically integrated in the prechamber housing, which creates proper relative air-fuel ratio with high level of stratification for each operating conditions. Passive prechamber is simply composed by an additional housing covering the top of the spark plug. It is obvious that since passive prechamber is cheaper with respect to active prechamber (only the spark plug replacement is needed compared

to additional injector and redesign of the cylinder head), reaching stoichiometric conditions inside the prechamber at each load and speed is a very hard task. As a result, proper management of prechamber over the whole engine operating range represent the main challenge of this advanced combustion.

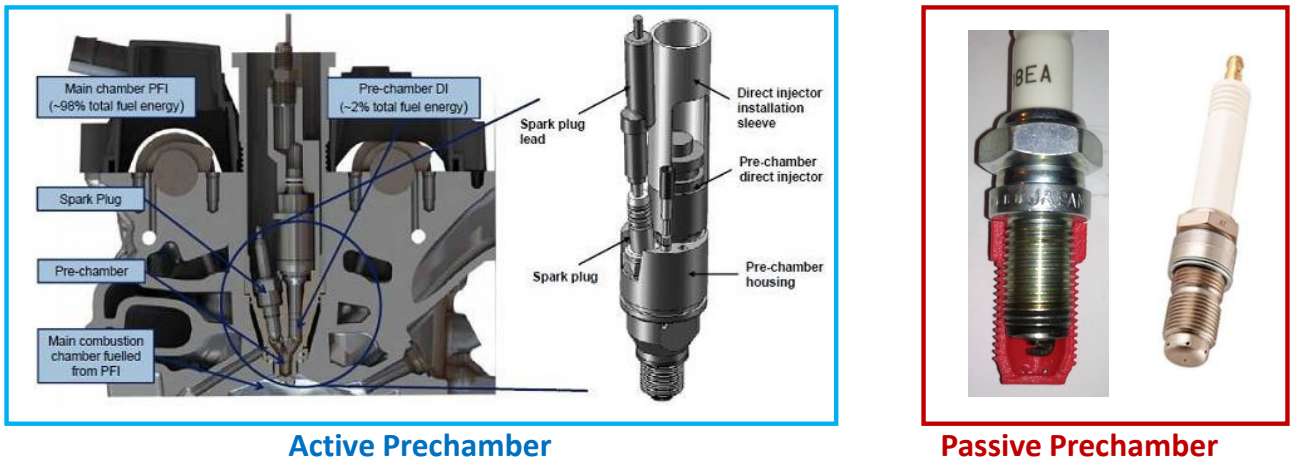

Figure 19. TJI main components architectures [13, 14]

1.2 Combustion Analysis

Combustion analysis is performed through the so-called *indicating analysis* that involve determination of indexes relative to the combustion process [15]. Starting from the knowledge of the geometrical data of the engine under study, to perform the combustion indexes calculation two main sensors are strictly required: the in-cylinder pressure sensor, which provides the pressure trace during the engine cycle through a specific hole in the cylinder head, and the speed sensor, which allows to calculate the instantaneous position of the crankshaft, Figure 20. By coupling these two signals, all the information about the combustion process can be easily derived by specifically developed acquisition systems, called *indicating systems* (mainly because it refers to the *indicated diagram,* p-V diagram during engine cycle).

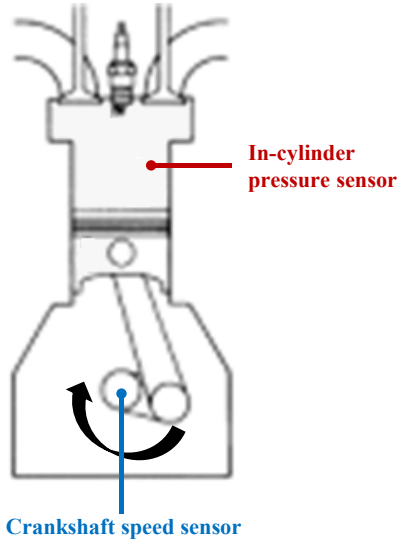

Figure 20. In-cylinder pressure and Crankshaft speed sensors positioning

Modern indicating systems can calculate in real-time, i.e., by the end of the current engine cycle, synthetic indexes of the last combustion and can send them to the ECU as synthetic information. Such solutions are called *in-cylinder sensing technologies*, Figure 21, and they are typically used as feedback for control strategies aimed to improve the engine efficiency and the reliability. Mainly because of cost and durability of the in-cylinder pressure sensors, these systems are used in the test bench, when the engine is under development or for racing applications but their use in common automotive applications is still limited.

Figure 21. In-cylinder Sensing Technology [16]

As mentioned before, to obtain the *indicator diagram*, the link between the volume swept during the engine cycle and the crankshaft position can be derived by geometrical consideration based on the crank mechanism reported in Figure 22. Variation of volume $\frac{dV}{d\theta}$ for different crankshaft angles θ can be calculated using Equation 1:

$$\frac{dV}{d\theta} = A_p \frac{ds}{d\theta} = A_p r f(\theta) \tag{1}$$

with $f(\theta)$, called crank funcion is:

$$f(\theta) \approx sin(\theta) + \frac{\lambda}{2} sin(2\theta) \tag{2}$$

and the geometrical parameter of the engine are:

- A_p, piston bore
- r, radius of crank
- s, piston stroke
- l_{rod}, rod lenght
- $\lambda = \frac{r}{l_{rod}}$

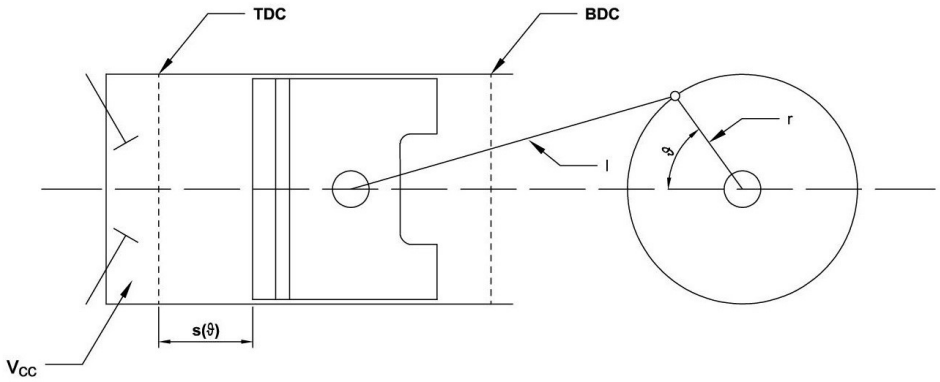

Figure 22. Schematic of Crank mechanism [15]

Based on the *indicator diagram* reported in Figure 23 (right), which are directly derived from the in-cylinder pressure signal showed in Figure 23(left) and the volume swept by piston during the engine cycle, the main combustion indexes related to combustion characteristics and performances which are immediately obtainable are:

- **Indicated Work (L_i),** which represents area in indicator p-V diagram such on in Figure 23 on the right. Indicated work takes in account work done by operating fluid on piston in a complete engine cycle.

$$L_i = \int_0^{720} p\frac{dV}{d\theta}d\theta = A_{pist}r\int_0^{720} pf(\theta)d\theta \tag{3}$$

- **Indicated Mean Effective Pressure (IMEP),** which refers, by definition, to indicated work per cycle per engine capacity unity. IMEP is a very important index used to compare different type of engines. Indicated work is strictly related to IMEP through engine displacement, that is volume swept by piston between bottom dead center BDC and top dead center TDC.

$$IMEP = \frac{\int_0^{720} p(\theta)dV}{Vc} \tag{4}$$

- **Indicated Torque (T_i),** which is strictly related to indicated work and represent the torque only provided by the combustion without mechanical losses.

$$T_i = \int_0^{720} \frac{dL_i}{d\theta} = A_{pist}rf(\theta)p(\theta) \tag{5}$$

- **Indicated Power (P_i)**, where n is the engine speed in cycle per second and express the power generated by the combustion. Indicated power does not consider power losses for friction and losses during engine cycle and due to auxiliary devices driven by crankshaft.

$$P_i = V_c \, IMEP \, n \tag{6}$$

- **Indicated Specific Fuel Consumption (ISFC),** where m_f is the fuel mass flow rate and it is used to quantity the raw effiency of the combustion process without consider any kind of auxiliary or mechanical frictions and losses

$$ISFC = \frac{m_f}{P_i} \tag{7}$$

- **Peak Pressure Rise Rate (PPRR** or $\boldsymbol{R_{max}}$**),** which represents the roughness of the combustion.

$$PPRR = max\,(\frac{dp}{d\theta}) \tag{8}$$

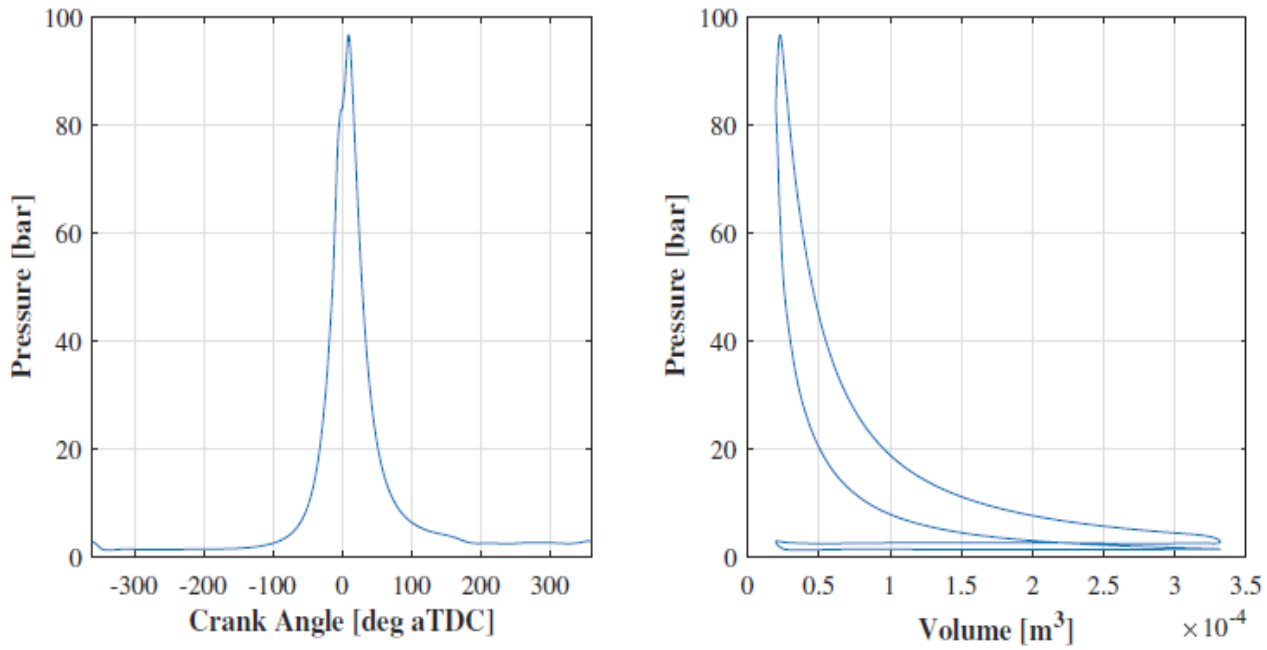

Figure 23. In-cylinder pressure Trace (left) and its respective Indicator Diagram (right)

In addition, detailed information about combustion process can be derived looking at the way the heat is released during combustion. The energy balance during combustion is showed in Figure 24 and expressed by Equation 9, where:

$$\delta Q_{ch} = dU_s + \delta Q_{ht} + dL - hdm \tag{9}$$

- δQ_{ch}, is heat released during combustion
- δQ_{ht}, is heat exchanged through walls
- dU_s, is internal energy variation of open system considered
- dL, is work done by gases on piston
- hdm, is enthalpy lost due to gas leak through elastic tights

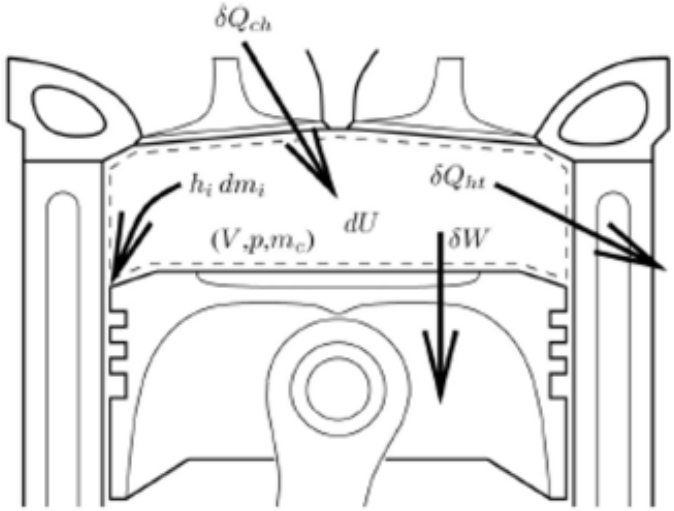

Figure 24. Energy Balance during combustion [15]

By considering the internal energy variation definition as reported in Equation 10:

$$dU_s = d\big(mu(T)\big) = mc_v dT + u(T)dm \tag{10}$$

and the work done on the piston, Equation 11:

$$dL = pdV \tag{11}$$

the energy balance can be rewritten as:

$$dQ_n = dQ_{ch} - dQ_{ht} - (u - h)dm = mc_v dT + pdV \tag{12}$$

Remembering the gas equation and deriving with respect to the temperature as showed in Equation 13:

$$dT = \frac{1}{mR}(Vdp + pdV) \tag{13}$$

Where, $R = c_p - c_v$ is the universal gas constant and c_p and c_v represent the constant pressure specific heat and constant volume specific heat respectively.

The **Rate of Heat Release** (***ROHR***) during the combustion process can be easily obtained substituting Eq. 13 into Equation 12 and defining the specific heat ratio as $\gamma = \frac{c_p}{c_v}$:

$$RoHR = \frac{\gamma}{\gamma - 1} pdV + \frac{1}{\gamma - 1} Vdp \tag{14}$$

Furthermore, the **Cumulated Heat Release** (***CHR***) can be directly calculated by the integration of *RoHR* over an engine cycle

$$CHR = \int_0^{720} \frac{\gamma}{\gamma - 1} pdV + \frac{1}{\gamma - 1} Vdp \tag{15}$$

ROHR is an index of combustion velocity: its peak value refers to maximum combustion velocity with its relative angular position. Moreover, useful parameters related to combustion phase and propagation can be derived directly from ***ROHR*** and ***CHR*** curves, such as:

- ***SOC***, angular position representing the start of combustion. It can be defined in different ways both considering *RoHR*, such as crank angle at which a specific combustion velocity is overcame, and *CHR* crank angle where 5% of the injected fuel released its energy

- ***CA50***, represents the centre of combustion and indicates the crank angle where 50% of injected fuel have burnt, named also ***MFB50***. It contains information about ignition and the flame propagation velocity

- ***CA90***, crank angle where 90% of the injected fuel have burnt, named also ***MFB90,*** meaning the end of the combustion process

- ***Combustion duration***, is the angular distance between end and start of combustion (***CA90-SOC***) and gives information about the overall combustion process velocity

During the PhD activity, the previously defined combustion parameters allowed to deeply analyze the LTC methodology subject of this dissertation obtaining crucial information regarding the combustion stability and controllability. Moreover, by comparing the combustion indexes calculated in different engine conditions, it has been possible to define the limits and the possibilities in terms of efficiency and performance of the GCI combustion in the light-duty compression ignited engine used during the activity.

1.3 Cylinder Pressure Sensor

In-cylinder pressure signal is the most important sensor to quantify and analyze the performance of internal combustion engines. Such signal is strongly correlated to the way combustion takes place in the cylinder and it is typically obtained through piezoelectric transducers, Figure 25.

Figure 25. Different kinds of In-cylinder pressure sensors [17]

Piezoelectricity is the property of a crystalline material to polarize and generate a difference of potential after a deformation. These kinds of transducers are made up by an elastic membrane with one side in touch with the fluid whose pressure must be calculated, and the other one with a piezoelectric material, as *quartz*, to which membrane transmits a force given by the product of unknown pressure and effective area. Piezoelectric plate changes its shape according to pressure variation and free at surfaces electric charges in quantity directly proportional to deformation and so to unknown pressure. When piezoelectric plate is deformed, it hands out electrical charges on its surfaces, directly proportional to the pressure which caused the deformation; this electrical charge cumulation causes a difference of potential between surfaces of the plate, called *piezoelectric effect*, Figure 26.

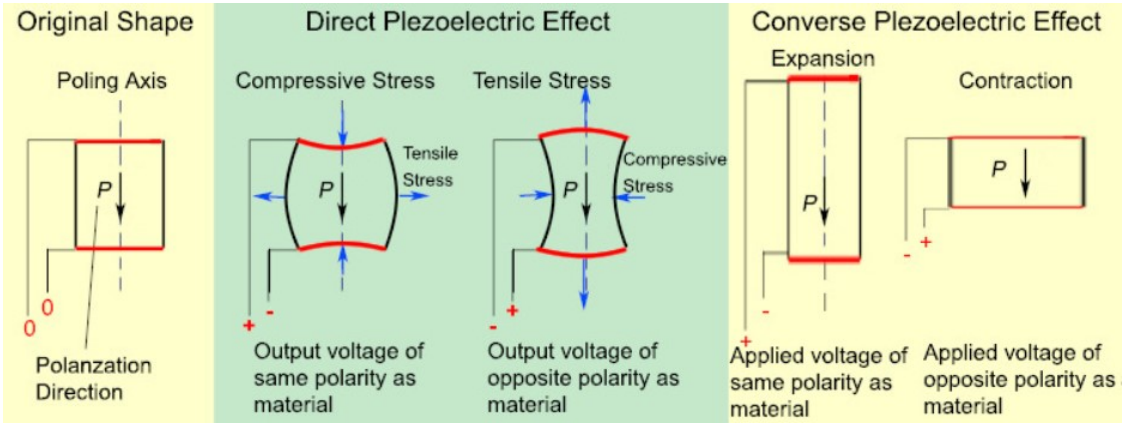

Figure 26. Piezoelectric effect in quartz [18]

Charge cumulation is in the order of *pC/bar*, and the relative voltage signal is consequently small; therefore, to be commuted into a readable pressure signal, voltage signal must be amplified with a charge amplifier: transducers plus charge amplifier system electrical scheme are shown in Figure 27.

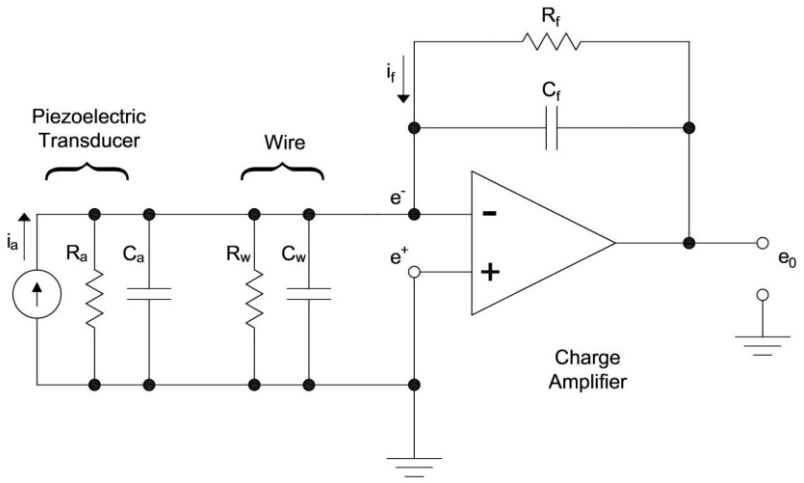

Figure 27. Electric representation of a pressure transducer and charge amplifier [19]

As mentioned before, the amount of charge accumulated (Q) on the surface of the plates is proportional to deformation (x) with k_q, and therefore to pressure (p) with k_p, following Equation 16:

$$Q = k_q x = k_p p \tag{16}$$

As a result, the difference of potential e_0 in accordance with the capacitor scheme can be evaluated as:

$$\mathrm{e}_0 = \frac{Q}{C_a} = \frac{k_q x}{C_a} \tag{17}$$

As reported in literature, piezoelectric transducers can be designed as a current generator, in which a current i_a is generated following a pressure variation, Equation 18:

$$i_a = \frac{dQ(t)}{dt} = k_p \frac{dp(t)}{dt} \tag{18}$$

By the analysis of the electrical scheme reported in Figure 27, in which i_a, $R_a$and $C_a$are respectively current, resistance and capacity of the pressure transducer, $R_w$and $C_w$represent resistance and capacity of the wire which links piezoelectric sensor to charge amplifier, R_f and C_f are the resistance and capacity of the operational amplifier feedback it is possible to calculate the charge amplifier transfer function which shows the conversion from electrical unit (voltage) to physical unit (pressure).

Based on Figure 27, feedback generates a "*virtual short-circuit*" such that it is possible to consider $e^- = e^+ = 0$. "*Virtual short-circuit*" is a condition that allow to solve high gain operational amplifiers problem with negative feedback, and it consist in set equal to zero difference of potential between inputs (*short-circuit*) and set equal to zero current entering the operational amplifier itself (*virtual*). This condition allows to suppose that current through R_a, C_a, $R_w$and C_w is zero and, therefore, the circuit can be simplified as schematized in Figure 28.

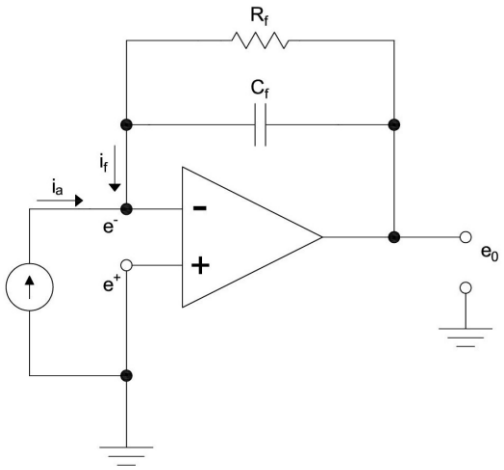

Figure 28. Pressure transducer and charge amplified simplified scheme [19]

Under such hypothesis, it is possible to apply the first Kirchhoff law to the node at the top of the charge amplifier (minus symbol), considering i_C and i_R the current through capacitor and resistor respectively:

$$i_a = k_p \frac{dp(t)}{dt} = i_C + i_R = \frac{dQ_C}{dt} + \frac{e_0}{R} \tag{19}$$

Expanding the Eq. 19 and integrating it can be obtained the ***charge amplifier electric function,*** Equation 20:

$$P(t) = \frac{C}{k_p} e_0(t) + \frac{1}{Rk_p} \int_0^t e_0(\tau) d\tau + P(0) \tag{20}$$

It is important to point out that $P(t)$ is a periodic signal and, hence, it could be expressed as sum of simple periodic sine/cosine function with Fourier series and, obviously $P(0)$ represents the null frequency, i.e., the mean of pressure signal. By applying the Fourier expansion, Eq.20 can be rewritten as:

$$P(j\omega) = \frac{C}{k_p} E_0(j\omega) + \frac{1}{Rk_p j\omega} E_0(j\omega) = \frac{C}{k_p} \left(\frac{RCj\omega + 1}{RCj\omega}\right) E_0(j\omega) \tag{21}$$

Finally, starting from Eq.21 it can be obtain the ***charge amplifier transfer function,*** related to a high pass filter with *time constant,* $\tau = RC$, and *cut-off frequency,* $f_c = \frac{1}{2\pi RC}$, Equation 22:

$$\frac{E_0(j\omega)}{P(j\omega)} = G(j\omega) = \frac{k_p}{C} \frac{RCj\omega}{RCj\omega + 1} \tag{22}$$

By observing Eq. 22, it can be noticed that due to saturation phenomena, the *cut-off frequency* can not be too small. Since the integral contribution of the charge amplifier and de-amplification of low frequency components can not be neglected, the mean component of the pressure signal will be lost and a distortion of the pressure signal occurs, called *drift*.

The above-described problems related to the pressure acquisition toolchain can affect the calculation of the combustion indexes. As a result, solutions have been developed to overcome the signal distortion and to compensate the mean value of the pressure signal. In modern charge amplifier, the drift compensation is already implemented by the amplifier manufacturers with hardware solutions, typically adding an additional resistor in the middle between the charge amplifier and the sensor, fixing the problem.

Regarding the pressure signal mean value recovering, the compensation is typically performed in two ways:

a) ***Pressure referencing with external sensor***
b) ***Pressure referencing with polytropic reconstruction.***

Considering the first method, by using an external absolute pressure sensor, typically mounted on the intake manifold (MAP sensor), the indicating system, which perform signal processing, allows to estimate the mean value of the in-cylinder pressure signal from the simultaneous acquisition of the MAP sensor when the intake valves are open. In this way, the signal coming from the piezoelectric sensor will be correctly referred to the actual intake conditions, cylinder-by-cylinder. However, not always the MAP sensor is available in the indicating system, hence the pressure referencing can be obtained by the reconstruction of the pressure trace following a polytropic thermodynamic transformation, Equation 23.

$$pV^{\gamma} = costant \tag{23}$$

Considering two measured pressure values during compression stroke, (when the intake valves are closed), the polytropic transformation shown in Eq. 23 can be written as follow:

$$p_{1\_true}{V_1}^{\gamma} = p_{2\_true}{V_2}^{\gamma} \tag{24}$$

As explained before, pressure needs a reference value, therefore:

$$p_{1\_true} = p_{1\_raw} + offset \tag{25}$$

Placing Eq. 25 into Eq. 24 the offset can be calculated as function of considered raw pressure and volume in conditions 1 and 2 and the heat specific ratio, Equation 26. It is important to highlight that the polytropic pressure referencing method might be affected by a wrong γ selection, which depends on the kind of fluids that are involved during compression stroke, i.e., only air or air-fuel mixture. For this reason, if possible, it would be preferable to use MAP pressure referencing method to avoid errors and uncertainties when combustion indexes are calculated.

$$offset = \frac{p_{2\_raw}{V_2}^{\gamma} - p_{1\_raw}{V_1}^{\gamma}}{{V_1}^{\gamma} - {V_2}^{\gamma}} \tag{26}$$

2. Gasoline Compression Ignition Combustion Development

In this chapter, GCI combustion investigation in a standard light-duty compression ignited engine is described. First, the engine characteristics and the test bed layout adopted for the whole experimental activity are discussed out. Since the aim of the PhD course was the study of the GCI combustion in a conventional engine, layout modifications, which have been one of the main tasks of the PhD course, are described reporting the obtained experimental results. By the analysis of the collected data during each step, it has been possible to plan and realize the following one moving toward a fully converted GCI engine.

2.1 Engine and Test Bed Control Systems

The whole PhD activity was based on a common light-duty 1.3-liter compression-ignited turbocharged engine installed in a test cell. In its standard configuration, the engine under investigation is a Common-Rail Multi-Jet Diesel engine, Figure 29, equipped with an injection system designed to operate at a maximum pressure approximately equal to 1600 bar. The technical characteristics of this engine are summarized in Table 1.

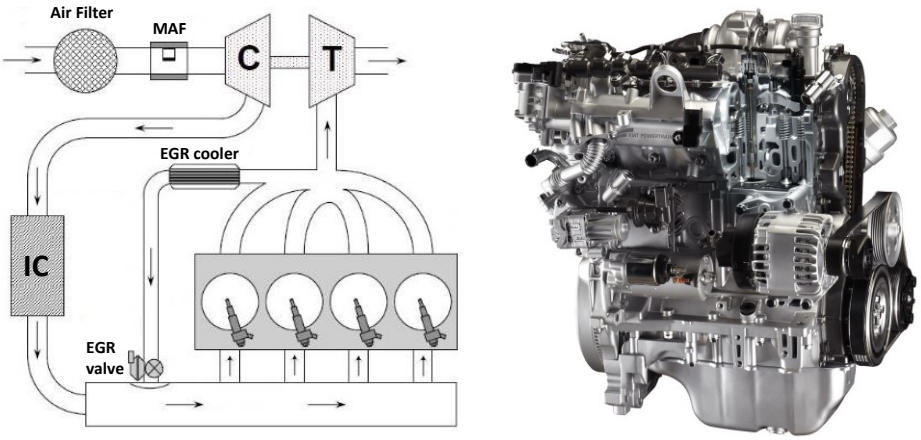

Figure 29. Engine Layout [20]

Since one of the aims of the activity is the pollutants evaluation running the engine in GCI mode, the exhaust line was modified removing catalyst and Diesel Particulate Filter (DPF). Furthermore, to improve air cooling during the experimental activity, the standard intercooler (air-air heat exchanger, which decreases the air temperature after the centrifugal compressor) was replaced with a more efficient water intercooler (externally managed). The technical characteristics of this engine are summarized in Table 1. Despite its small dimension, the air path of this engine is equipped with a variable geometry turbine (VGT) and a high-pressure water cooled EGR system. These systems allow to improve engine efficiency, performance, and reduce pollutants: VGT improves the turbocharger response both at low and high loads, and the EGR system significantly reduces the nitrogen oxides production (the thermal inertia of the recirculated gases limits the flame temperature during combustion). Despite its high efficiency and reliability fueled with diesel, such engines will be strongly penalized by the future emission regulations mainly because the more and more complex pollutant reduction systems and their management (required to respect new limitations) will dramatically impact on costs and fuel consumption. As a result, thanks to their technical characteristics such kind of engines are good candidates to evaluate the potential of GCI combustion in terms of pollutant reduction and thermal efficiency using a close-to-production engine.

Displaced volume	1248 cc
Maximum Torque	200 Nm @ 1500 rpm
Maximum Power	70 kW @ 3800 rpm
Injection System	Common Rail, Multi-Jet
Bore	69.6 mm
Stroke	82 mm
Compression ratio	16.8:1
Number of Valves	4 per cylinder
Architecture	L4
Intake System	Turbocharged with variable geometry turbine, HP-liquid cooled EGR
Firing Order	1-3-4-2

Table 1. Engine technical characteristics

The global management of an engine test cell is typically demanded to a single or multiple process units which perform a real-time acquisition and control of each element of the test bench. Figure 30 shows the test bench systems layout in our application.

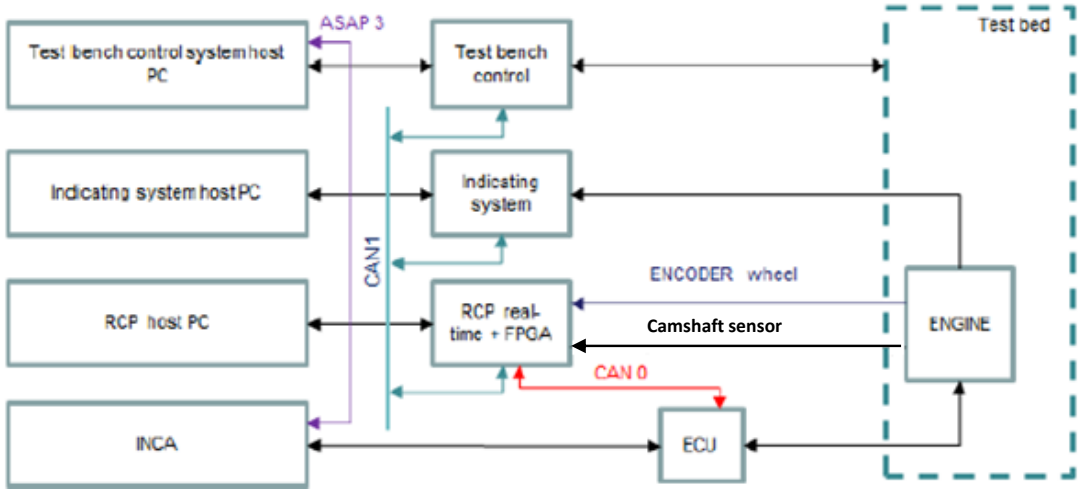

Figure 30. Test bench systems layout [21]

As can it be noted, since the PhD activity was focused on studying an advanced combustion methodology, the layout was a bit unusual with respect to a standard test cell for engine calibration. Several additional hardware and respective host interfaces each other were integrated in the reported layout. The test bench layout is composed by four main systems:

1) **Test bench controller:** this system, typically made by a real-time PC, performs external sensors acquisitions, external driver management, manages alarms and recovery procedures
2) **Indicating system:** this system acquires the in-cylinder pressure sensors and calculates combustion indexes in real-time
3) **RCP system:** this system allows to manage external hardware or to implement custom engine control strategies interfacing with the engine ECU
4) **ECU:** standard hardware for the engine control using INCA software, provided by ETAS

In our application, the main tasks of the test bench system are listed below:

a) Test cell environmental conditions acquisition: pressure, temperature, and humidity

b) Pollutants-emission systems management

c) Fuel consumption measurement systems management

d) Engine ECU management assuring proper engine operating conditions

e) Intake air temperature and engine water temperature management using heat exchangers

f) Remote control of eddy-current brake to guarantee a stable engine operating point

g) Dyno signals acquisition such as torque, speed, and engine power output calculation

h) Additional engine-mounted sensors acquisition (pressure, temperature, air-flow rate, turbo speed, …) for monitoring purpose

i) External systems management through analog/digital signals generation

j) Recovery strategy management improving the safety of the test activities when anomalies are detected

k) Test automation and logging utilities integration

All listed functionalities were developed by using NI-VERISTAND, a reliable software platform provided by National Instruments specifically designed for testing application. Through VERISTAND and its basic functionalities it was possible to integrate and manage external instrumentations improving the whole testing facility. Furthermore, VERISTAND allowed to easily communicate with external systems by using the most diffuse communication protocol, such as CAN interface, RS-232 interface and ASAM/ASAP communication protocol. In this way, it was possible to connect the above-described systems each other aimed at having an exhaustive and immediate understanding of the acquired data.

By using the above-described layout, to perform combustion analysis and real-time monitoring all the quantities which could affect the combustion stability, in addition to the standard sensors, the engine was also equipped with:

- Four piezoelectric AVL GH14P pressure sensors, one for each cylinder
- Additional pressure sensors to monitor engine oil, fresh air, and exhaust path
- K-type thermocouples to measure temperature of each fluid on the engine such as, fresh air, engine oil, water and exhaust gases
- Optical encoder for accurate crankshaft angular measurement
- Accelerometers for non-intrusive combustion indexes estimation
- Linear lambda sensor (UEGO) for oxygen estimation in exhaust gases
- NOx sensor for nitrogen oxides measurement
- AVL Balance 733s for fuel consumption measurement
- AVL Smoke Meter 415s for soot measurement

Technical specifications about most important sensors and measurement systems are available in Appendix A.

During whole PhD, starting from the discussed test bed system layout, modifications both on hardware and software were made to correctly test GCI combustion without the limitations of the standard testing layout. By the analysis of the signals coming from each sensor, during the whole activity it was possible to highlight the effect of the engine control parameters on GCI combustion both in terms of combustion stability and performance (pollutants/emission and efficiency) and to develop control strategies improving the management of GCI in a compression ignited engine.

2.2 Experimental investigation of GCI Combustion with "Cylinder Laboratory" mode

As reported in literature [22, 23], since GCI combustion is a kind of SCCI, to obtain the compression ignition of a low reactivity fuel (RON 95 gasoline in our case) the mixture preparation plays a crucial role. Therefore, to generate a stable GCI combustion there are some crucial aspects to consider. Mixture preparation process, air thermodynamics conditions which promote the charge autoignition and combustion management (load, phase, and knock) represent the main challenges regarding GCI combustion. As a result, the full engine conversion from standard CDC to GCI engine was carried out step by step, each one focused on the empowerment of the knowledge of the gasoline autoignition and how can it be managed with the hardware mounted on the engine (in a near production configuration).

The first activity of the PhD was focused on a preliminary experimental GCI combustion investigation, named "*Cylinder Laboratory*" mode, fueling only one of the four cylinders with gasoline while the others three cylinders keep the engine in stable operating conditions. The experimental results highlighted that to perform stable and controllable GCI combustion, respecting reliability limits in the considered engine, multiple injections (typical pilot-pre-main injection pattern) and proper boost pressure and temperature are required.

As reported in literature [24-26] and confirmed by experimental results [27-30], performing GCI combustion with multiple injections, wrong positioning of pre-injections might compromise the combustion stability, generating misfire or knock. With poor combustion of pre-injections, pressure and temperature in the combustion chamber does not increase sufficiently to reduce the ignition delay of the following main injection, responsible to manage combustion phase and torque. As a result, assuring a complete and efficient combustion of the pre-injections plays a crucial role in the GCI combustion management. Once defined the number of injections needed to correctly manage GCI combustion, to increase the engine operating range without compromise the combustion stability, an experimental activity on the gasoline autoignition was carried out defining proper pre-injections timing which maximize their efficiency.

The last step of the activity carried out using the "*Cylinder Laboratory*" mode was to test the advanced combustion methodologies covering its typical operating loads (mid-high load) collecting information about its fuel consumption reduction potential with respect to CDC. Furthermore, it was possible to obtain a raw calibration able to stabilize the GCI combustion in the engine under study. The obtained calibration set was used in the following part of the study, where the engine was fully converted in GCI engine.

2.2.1 "*Cylinder Laboratory*" mode Experimental Layout

As explained before, the first part of the activity was focused on the experimental investigation of gasoline spontaneous ignition in a compression ignited engine to evaluate how injection pattern design, injection pressure variation and intake conditions (air temperature and boost pressure) affect efficiency, stability, and impulsiveness of the combustion process. To do so, engine was modified to perform the "*Cylinder Laboratory*" mode [29, 30], in which one cylinder (fueled with gasoline) tested the LTC while the 3 cylinders fueled with diesel provided the load needed to keep the engine in stable conditions (mainly rpm and boost pressure).

An additional common-rail fuel system (high pressure pump, rail, and ducts) was added fueling one of the 4 solenoid injectors with commercial 95 RON gasoline, while the others were kept in a standard configuration (diesel-fueled), Figure 31.

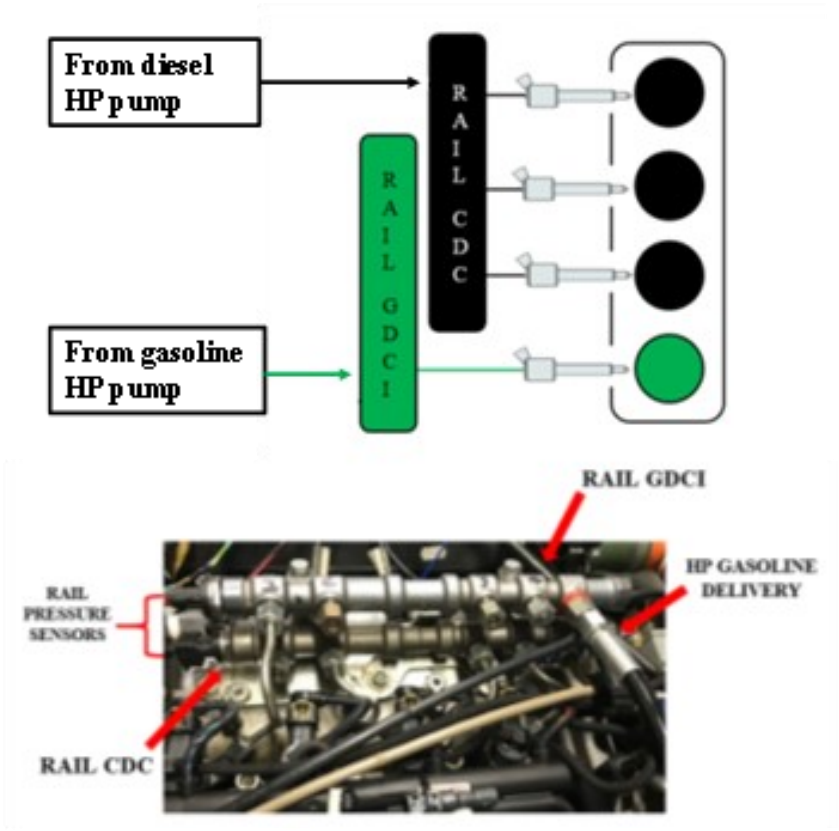

Figure 31. High pressure fuel systems in "Cylinder Laboratory" mode

To control the additional fuel system, a specifically designed control strategy was implemented in a Rapid Control Prototyping (RCP) system based on a National Instrument hardware (cRio 9082). Gasoline pressure management was simply performed changing the duty cycle of the flow control solenoid valve, which manages the gasoline flow upstream the high-pressure pump. Through a PID controller, the RCP system acquired the gasoline pressure signal (coming from the rail-mounted pressure sensor) and changed the PWM command according to the difference between target and feedback gasoline pressure. Furthermore, the RCP system also managed the gasoline injector both in terms of number of injection pulses per cycle, injections positioning and durations (injected mass in each injection). To do so, the RCP system acquired the signal coming from the encoder installed in the flywheel and calculated in real-time the angular position of the crankshaft. Once the injection strategy was chosen (for each injection: Start of Injection angle, SOI, and duration, Energizing Time, ET) the RCP communicated with the standard ECU via CAN bus the calculated values overwriting the default ones (thus the electrical command for the gasoline injector has been generated by the ECU).

In the "*Cylinder Laboratory*" mode, no intake/exhaust systems modifications were made. Therefore, the management of the intake conditions (boost pressure and temperature) was obtained using the standard engine-mounted devices (air cooler and turbocharger with VGT actuator). Through the test bench layout described in the previous section and reported in Figure 32, with the modifications needed to perform the "*Cylinder Laboratory*" mode, was possible to study GCI combustion in several engine conditions. By the study of the collected data, it was possible to define a preliminary engine calibration (assuring stable and safe combustion process in the laboratory cylinder), to highlight the main dependencies of the engine control parameters and to clarify the limits of the GCI combustion in the engine under study.

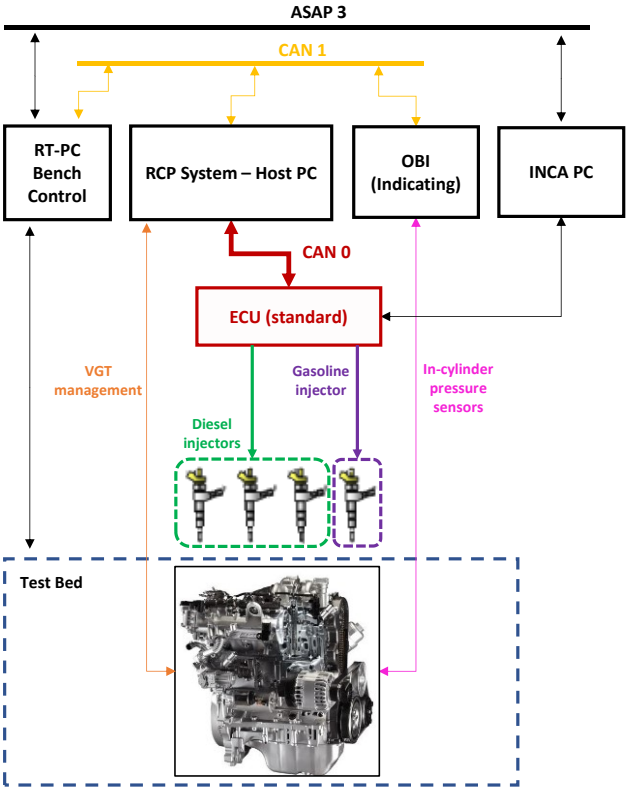

Figure 32. Scheme of the experimental layout used in the "Cylinder Laboratory" mode

2.2.2 Preliminary experimental investigation of GCI combustion

As reported in literature, GCI combustion stability mainly depends on injection strategy, mixture preparation and thermodynamic conditions of the charge. As a result, to preliminary investigate the GCI combustion, the experimental activity was focused on highlighting these aspects. The test was divided into 3 main parts:

- ***a) GCI with single injection strategy***
- ***b) GCI with double injection strategy***
- ***c) GCI stability evaluation***

The results of the activity allowed to define the characteristics and the critical issues of the combustion process in the engine under study.

GCI with single injection strategy

The first experience was focused on finding the ignition point of the air-fuel mixture. To do that, a fixed amount of gasoline, equal to 10 mg/stroke, was injected at different start of injection (SOI) angles. The SOI sweep was performed retarding the SOI of 2 degrees every 10 seconds at constant gasoline rail pressure.

The use of the "*Cylinder Laboratory*" mode allowed to keep the engine in stable operating points (by the torque delivered by the others three cylinders fueled with diesel), assuring proper intake pressure and temperature and constant engine speed, even when the gasoline cylinder did not generate torque. Since many works in literature tested GCI combustion, engine parameters such as boost pressure, engine speed and fuel pressure were selected in accordance with the values reported in literature. The engine conditions during the SOI sweep performing GCI combustion with single injection are summarized in Table 2.

Engine Speed [rpm]	Injected Mass [mg/str]	Gasoline Pressure [bar]	Boost Pressure [mbarA]	Air quantity [mg/str]
2000	10	500	1500	500

Table 2.Engine operating point during GCI single injection strategy test

The most critical aspect to be managed was the injection of gasoline, performed using the same solenoid injectors used in the standard operating mode for diesel injection. Consequently, the standard injector map (stored in the ECU) could not be used to accurately control the injected mass (the ET stored in the standard map is not correct when gasoline is injected). Therefore, fuel consumption was checked (and corrected, if necessary, by managing the ET) comparing its volume with the one provided by the AVL Balance during each test, therefore ensuring the proper injected mass.

Test results in terms of IMEP, MFB50 and R_{max} during the SOI sweep are reported in Figure 33. By looking at Figure 33it is possible to see that misfires occurred from SOI = 40° bTDC till approximately SOI = 34° bTDC, where maximum pressure peak rise rate R_{max} starts to rapidly increase. After that value of SOI, the IMEP keeps almost constant at 5.8 bar and MFB50 at 2 deg aTDC with very low cycle-to-cycle variation.
Since the R_{max} reached during the SOI sweep overcame the reliability limit of the engine (fixed by the manufacturer at 10 bar/deg), the test was interrupted approximately at 50 sec to avoid mechanical damage. This behavior can be easily explained through the combustion analysis based on the in-cylinder pressure signal.

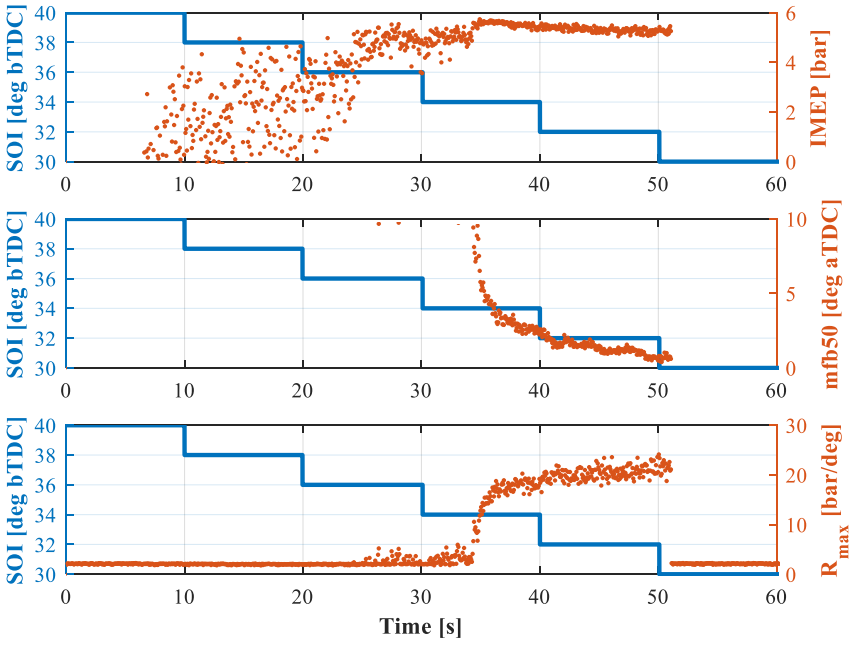

Figure 33. Combustion indexes during GCI single injection strategy SOI sweep

In-cylinder pressure acquired at the most critical point (SOI 30 deg bTDC) compared to a misfire (SOI 40 deg bTDC) is reported in Figure 34 (left). By the comparison of these two engine-cycles clearly arises that the bigger amount of energy introduced by the fuel is released in a very short timing generating very high maximum cylinder pressure, close to the reliability limit (140 bar). At right of Figure 34, ROHR and CHR confirms the very small combustion duration leading an almost-constant volume combustion.

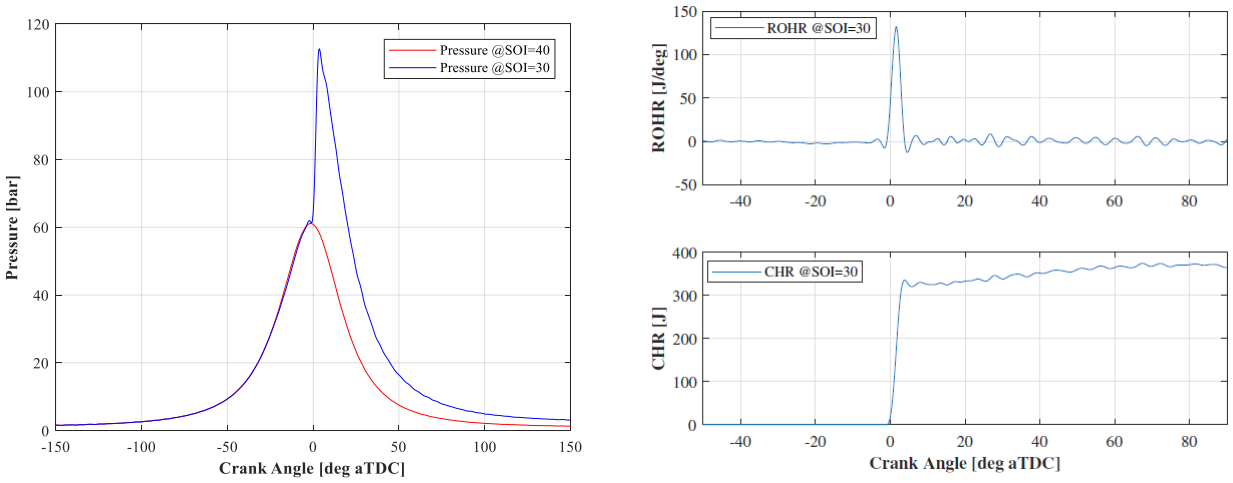

Figure 34. In-cylinder pressure (left) and RoHR-CHR (right) at SOI 30 deg bTDC performing GCI with single injection strategy

Explanation behind this behavior, taken from the literature and confirmed by the reported data, is a distinctive feature of the premixed combustions. Since GCI combustion is chemically driven, the ignition delay of the created air-fuel mixture depends on thermodynamic (pressure and temperature) condition of the charge. As a result, with early SOI, air pressure and temperature inside the cylinder (which will be mixed with fuel) are low and this leads to high ignition delay (ID) and consequently misfires. At the opposite, when the fuel is injected in proper thermodynamic condition, the ignition delay decreases, and the mixture can release its energy near the TDC and producing torque. However, since with the GCI single injection strategy the amount of injected fuel is introduced through a single pulse injection, the mixture is almost homogeneous and, therefore all the charge releases energy simultaneously. To confirm this, it is interesting to observe Figure 33 in which retarding SOI, the IMEP rises while MFB50 gets closer to TDC with very high values of R_{max}.

Despite the reported results showed very dangerous conditions in terms of engine reliability, it was proved that is possible to perform GCI combustion in the engine under study without internal hardware modification (combustion chamber, ducts shape and injection systems). For this reason, the following step was focused on knock limitation by using a different injection management aimed at increasing the GCI operating range.

GCI with double injection strategy

Due to the unpredictability and the excessive mechanical stresses following a single injection, literature suggests splitting injection pattern into two or more single injections going through a "multi-jet" pattern. At first, a double injection strategy was tested splitting the injected mass in two injection pulses: the earlier called Pre, and the last called Main. By using a standard "multi-jet" injection system, each injection can be managed in duration (Energizing Time, ET) and position (Start of Injection, SOI). Therefore, the distance between two injections, called Dwell Time (DT), will be a consequence of the other parameters.

However, how well documented by the literature, due to the hydraulic dynamic effects on the injection system, the use of very close multiple injections might modify the total injected mass (this aspect will be widely discussed further in the PhD dissertation). Thus, to correctly perform GCI combustion with two injection pulses, the injection controller changes the SOI pre to keep DT constant. In this way, the effect of DT during tests can be neglected. Figure 35 reports the scheme of the injection pattern used testing GCI with double injection strategy. Thanks to the RCP system, by changing the injection parameters and overwriting these values on standard ECU, the percentage of split can be imposed, allowing to test different repartitions on each injection and check the effect on GCI combustion.

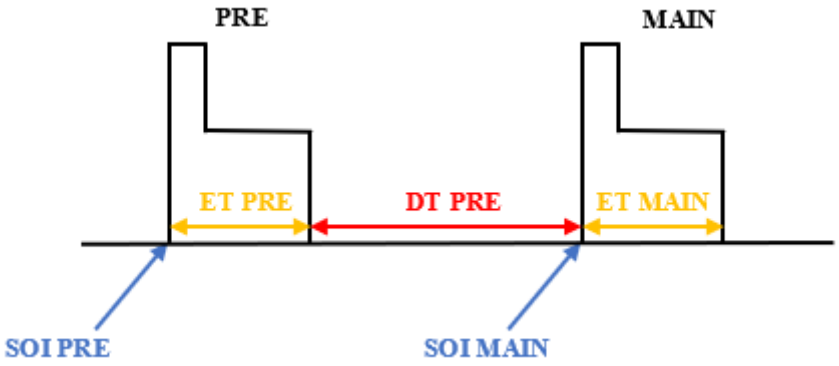

Figure 35. Double injection strategy management

To verify the effect of fuel splitting on GCI combustion, 10 mg/cycle of fuel were divided in two consecutive injections in the same engine operating point, reported in Table 2, tested with single injection. Different values of fuel percentage split were tested, starting from 80% up to 20% of fuel injected in the first injection. Regarding the injections positioning, by looking at the obtained results testing GCI with single injection strategy, it arises that, in this engine, gasoline autoignition can be obtained placing the fuel injection near 32 deg bTDC. Hence, the first injection was placed near 32 deg bTDC while the last injection was placed close to TDC based on similar works found in literature about GCI combustion with double injection (in which the main injection is placed very close to TDC). Furthermore, to avoid interaction between injections DT was kept constant, therefore during the split percentage sweep small differences of SOI pre occurred. Finally, SOI of main injection was set at 7 deg to verify the impact of the percentage split on combustion phase. Table 3 summarized the injection parameters used testing the effect of fuel percentage split on GCI combustion.

Test ID [#]	% Pre INJ [%]	% Main INJ [%]	SOI Pre [deg bTDC]	SOI Main [deg bTDC]
1	80	20	32.4	7
2	70	30	32	7
3	60	40	31.7	7
4	50	50	31.3	7
5	40	60	30.9	7
6	30	70	30.6	7

Table 3.GCI with double injection strategy: injection split

Figure 36 shows the in-cylinder pressures while running GCI combustion with double injection strategy varying the fuel split between injections. By looking at Figure 36 it can be noticed that decreasing the fuel injected in the first injection, the combustion process will become longer and smoother also limiting the maximum in-cylinder pressure. As occurred testing GCI with single injection strategy, the presence of the bigger amount of fuel in the first injection (with injection timing that guarantee the gasoline autoignition), generates a near homogeneous air-fuel mixture which, once ended the ignition delay, burns simultaneously. Since the first combustion increases temperature and pressure in the combustion chamber, the remaining injected fuel release energy instantaneously because the ignition delay of the newer air-fuel mixture is near zero. Confirmation about this can be found in Figure 37 which shows RoHR and CHR. As it can be seen, moving from 80% to 60% of fuel quantity in the Pre, the combustion will be a bit slower (RoHR maximum lower) but the shape of the RoHR remain the same. This could be explained by the amount of energy released by the first injection that still produces a very small ignition delay for the following injection. Moving to even lower injected quantity, the combustion shape changes, which means that two different combustion dynamics occur: one (slower) referred to the combustion of the first injection and the following faster.

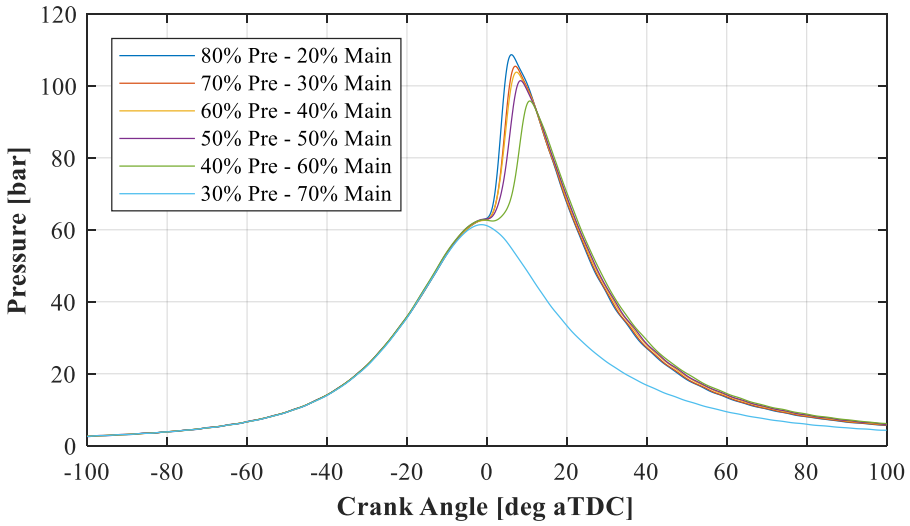

Figure 36. Effect of different fuel percentage split on GCI combustion

The air-fuel mixture created with even smaller Pre injection will be more and more lean and, consequently, its combustion less efficient generating lower temperature and pressure in the combustion chamber. As a result, the ignition delay of the mixture generated with the second injection will be longer and, hence it will burn slower at bigger volume. Decreasing more that 40% the fuel injected in the first injection, the air-fuel mixture will be too lean exceeding the ignitability range and, therefore, misfire will occur.

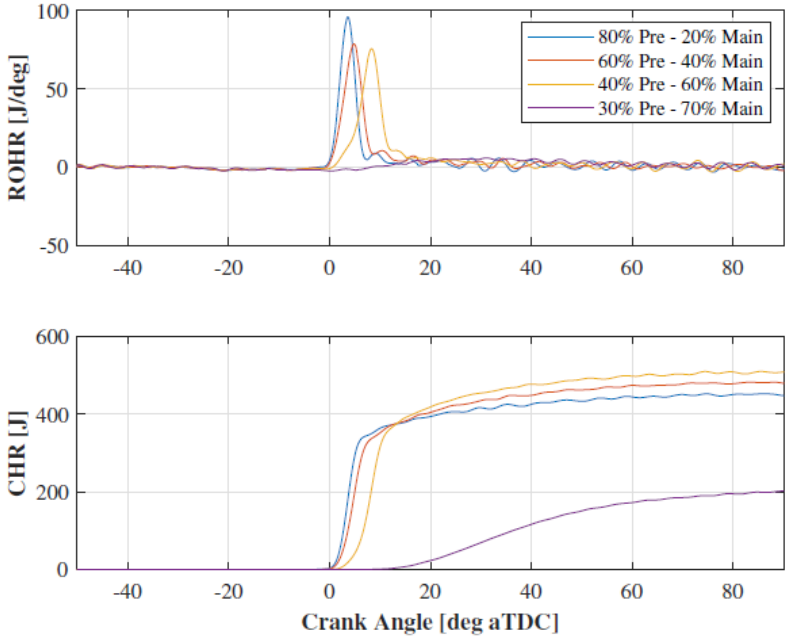

Figure 37. Effect of different fuel injection split on ROHR and CHR with double injection strategy

All the above-mentioned considerations can be obtained also by the analysis of the combustion indexes reported in Figure 38: IMEP and MFB50. The values of PPRR are reported below each point as a number. As it can be noticed in Figure 37, 40% Pre is the most convenient fuel split strategy running GCI with double injection in the analysed engine condition both in terms of torque (IMEP) and reliability (PPRR below than the manufacture reliability limit). Moreover, by looking at the coefficient of variation of IMEP, calculated for each condition and reported in Figure 37, it clearly arises that the cycle-to-cycle variability is very low even dividing the injection, which underlines the robustness of the combustion process.

It is important to highlight that even in the most unreliable and inefficient tested conditions (80% Pre), the injection split improves IMEP and decreases PPRR with respect to single injection strategy: the combustion knocking moves from 23 to 13.4 bar/deg and the IMEP increases from 5.8 to 6.8 bar.

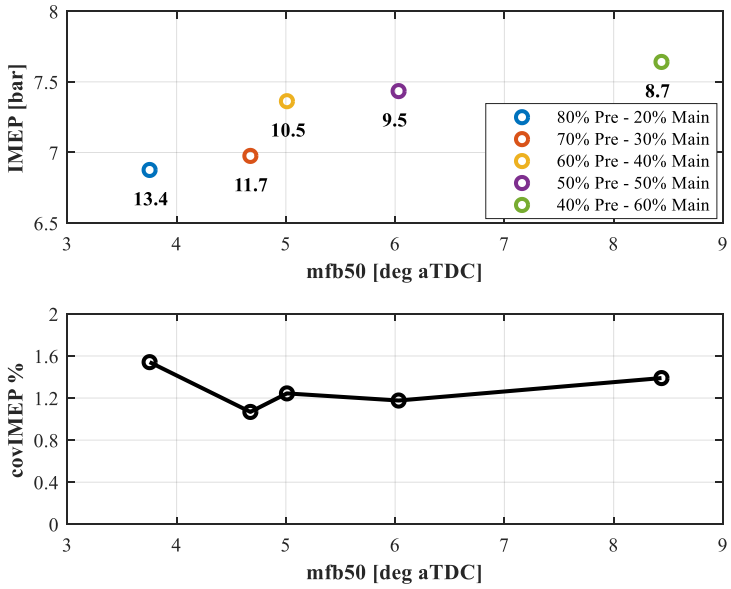

Figure 38. Effect of different fuel injection split on IMEP, MFB50 and PPRR and combustion stability (covIMEP) with double injection strategy

Despite splitting the injection improved GCI combustion controllability assuring stable and reliable operating point, the obtained combustion shape does not allow to increase the engine load without generating reliability problems. By looking at Figure 39 where GCI with single (called "*Unijet*") and double injection (called "*Bijet*") are compared, it clearly arises that with the injection split the in-cylinder pressure trace becomes smoother and the maximum value significantly decrease. However, the shape remains very close to the ones generated with a single injection. As a result, it is impossible to further increase the engine load performing single or double injections.

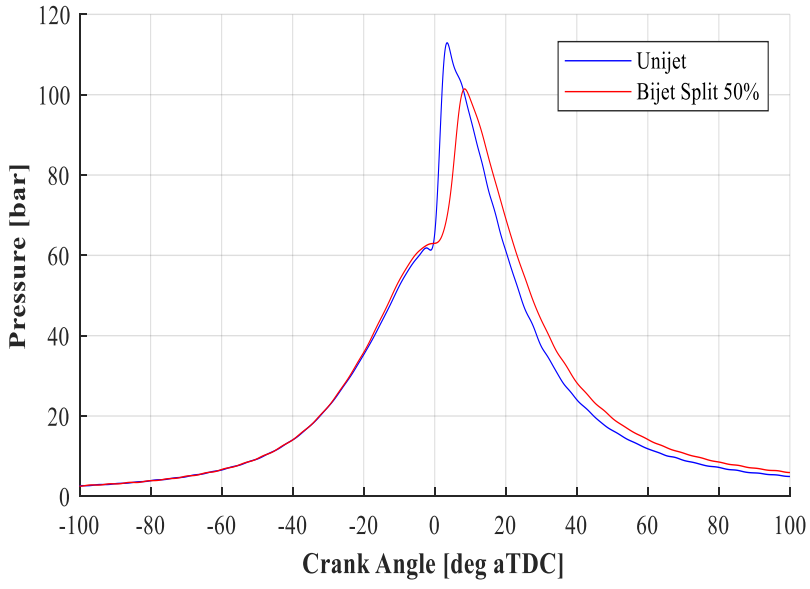

Figure 39. Comparison between in-cylinder pressure trace performing GCI combustion with single and double (50% Pre - 50% Main) injection strategy

Once verified the benefit on combustion controllability splitting the injection, the second activity carried out running the GCI cylinder with double injection strategy was to study how could be managed the combustion phase through the injection. To do this, dedicated tests were carried out performing a rigid movement of the injection pattern. Figure 40 reports the normalized electrical signals of each injection during sweeps.

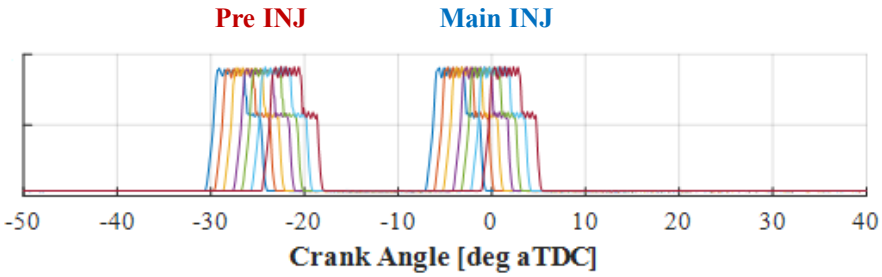

Figure 40. Injection pattern management strategy testing combustion phase controllability in GCI with double injection

To maximize combustions stability during the tests, by looking at the results obtained by the experimental activity on injection split, two different percentage of fuel split were selected, 50% Pre and 60% Pre. The test consisted in a rigid movement of the injection pattern, DT were kept constant for each percentage of split tested, starting from a knocking condition (R_{max} over than 10 bar/deg) until combustion instability occurs. During each test, the engine load was set at IMEP = 8 bar and manually adjusted compensating the efficiency loss due to retarded combustion. Additional information about the engine operating conditions during the injection movement tests are summarized in Table 4. Figure 41 reports the experimental results obtained moving the injection pattern both with gasoline pressure of 500 bar.

RPM	IMEP [bar]	Boost Pressure [mbarA]	Injected Fuel [mg/cycle]	Intake Temperature [°C]	% Pre INJ [%]	% Main INJ [%]	SOI Pre [deg bTDC]	SOI Main [deg bTDC]
2000	8	1500	10	75	50	50	**31 to 25**	**7 to 1**
2000	8	1500	10	75	60	40	**31 to 24**	**7 to 0**

Table 4. Engine operating condition during injection pattern movement tests in GCI with double injection strategy

By looking at the combustion indexes reported in Figure 41, it clearly arises that changing the position of the injections in the engine cycle, the combustion phase moves following the same direction. Moreover, by retarding the combustion phase, knocking decreases producing smoother and more reliable combustion. As a result, if a robust combustion of the first fuel jet is guaranteed, GCI combustion can be effectively managed by changing the injection position.

It is important to underline that increasing the fuel quantity in the first injection, due to higher temperature and pressure generated by the combustion of the first air-fuel mixture, the ignition delay of the second injection decreases anticipating the center of combustion with higher R_{max}. Moreover, since the energy released by first combustion with 60% Pre rises, it was possible to slightly increase (with respect to 50% Pre) the operating range (bigger MFB50) avoiding misfires. Despite smaller MFB50 and higher R_{max}, the injections management proved to be effective to control the combustion phase even changing the injection split.

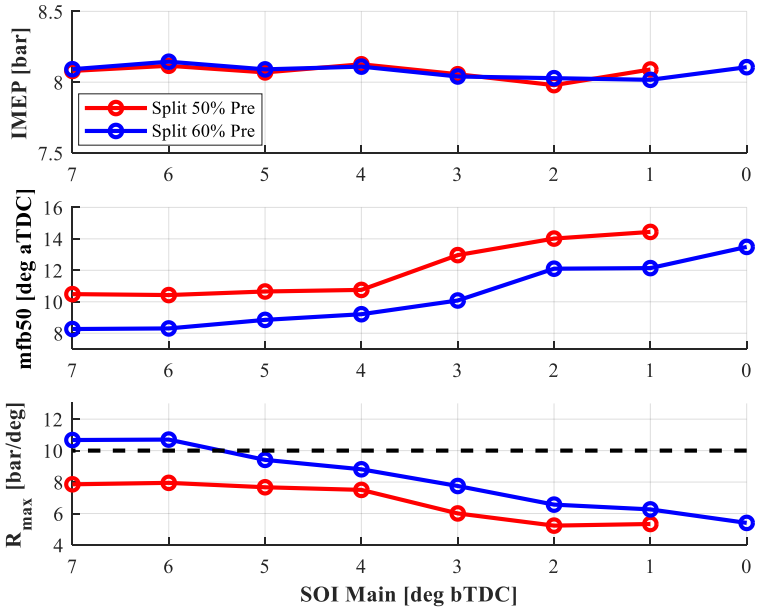

Figure 41. Effects of injection rigid movement on combustion indexes in GCI with double injection strategy

However, the benefit on R_{max} reduction of combustion phase is insufficient to test higher loads (because is always close to the reliability limit of the engine) performing the double injection strategy. By splitting the injection in two different fuel jets with a percentage of the total injected fuel, the more load is increased bigger become the amount of fuel in the first injection. As demonstrated, increasing the fuel injected in the Pre injection the combustion will become more impulsive producing knock. As a result, to properly manage GCI combustion at high load more complex injection strategy is needed.

Since the double injection strategy proved to be effective running stable and controllable GCI combustion, further activities were carried out to highlight the effect of the main control parameters on combustion stability such as, intake temperature and boost pressure. The following section describes the obtained results aimed at improving the knowledge of GCI combustion.

GCI combustion stability evaluation

As reported in literature, to obtain consistent and reliable gasoline autoignition, thermodynamics conditions of the charge play a crucial role. Therefore, wrong boost pressure and air temperature selection could compromise the combustion stability and generate misfire.

To verify how the thermodynamic conditions of the charge impact on the GCI combustion in our engine, two different kinds of test were carried out: boost pressure scan and air temperature scan. Each test was conducted starting from a stable and safe (in term of mechanical stress) GCI operating conditions up to the occurrence of misfires. Table 5 summarizes the GCI operating conditions of each test both with gasoline pressure of 500 bar.

RPM	IMEP [bar]	Boost Pressure [mbarA]	Injected Fuel [mg/cycle]	Intake Temperature [°C]	% Pre INJ	% Main INJ	SOI Pre [deg bTDC]	SOI Main [deg bTDC]
2000	8	**Sweep from 1500**	10	75	50	50	31	5
2000	5	1550	10	**Sweep from 75**	50	50	28	14

Table 5. Engine operating conditions during GCI stability evaluation changing boost pressure and intake temperature

Figure 42 shows the effect of boost pressure variation (real-time controlled adjusting the position of the VGT actuator) on GCI combustion. As it can be seen during the sweep, as long as boost pressure is high enough to assure favorable thermodynamic conditions for the gasoline autoignition (with the selected SOI Pre), the combustion generate torque with low cycle-to-cycle variability, from 0 sec to 17 sec. Due to further decrement of the boost pressure, from 17 sec to 20 sec, the center of combustion starts retarding mainly because the ignition delay of the mixture increases. In this zone, since the autoignition of the mixture is always guaranteed, no significant modification on IMEP production is recorded. Starting from that point, further reduction in boost pressure generates unstable combustions and misfires. In this condition, the thermodynamics of the mixture are far from the condition which guarantee a stable gasoline autoignition with the selected position of the Pre injection.

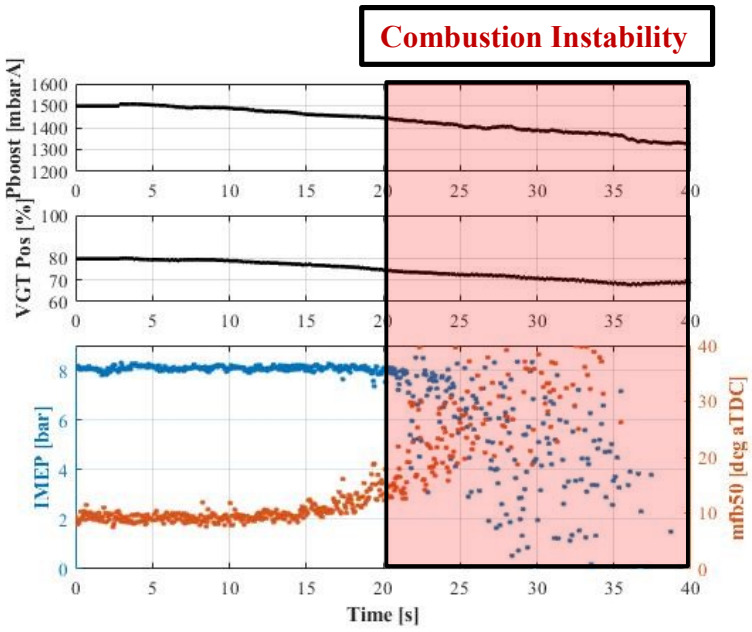

Figure 42. Effect of boost pressure on GCI combustion stability

Almost the same effect on combustion process is generated by the reduction of the intake temperature. Figure 43 reports an intake temperature transient from 75 °C to 45 °C (controlled using the air cooler installed in the middle between the compressor and the intake manifold). By looking at Figure 43, once the air temperature starts decreasing (at 8.5 sec), combustion retards and then becomes unstable (after 1.5 seconds). Since it is known that both pressure and temperature affect the ignition delay of the mixture, this behavior can be explained in the same way as done for the boost pressure effects [29, 30]. By the comparison of the above-described transient tests, it seems that the gasoline ignition delay (and consequently the whole GCI combustion) is affected more by the temperature than pressure because the instability occurs faster than in pressure sweep. However, since the position of the first injection contributes to define the gasoline autoignition, these tests can not clarify the contribution of pressure and temperature to the ignition delay and, then more investigation aimed at clarifying this aspect is needed.

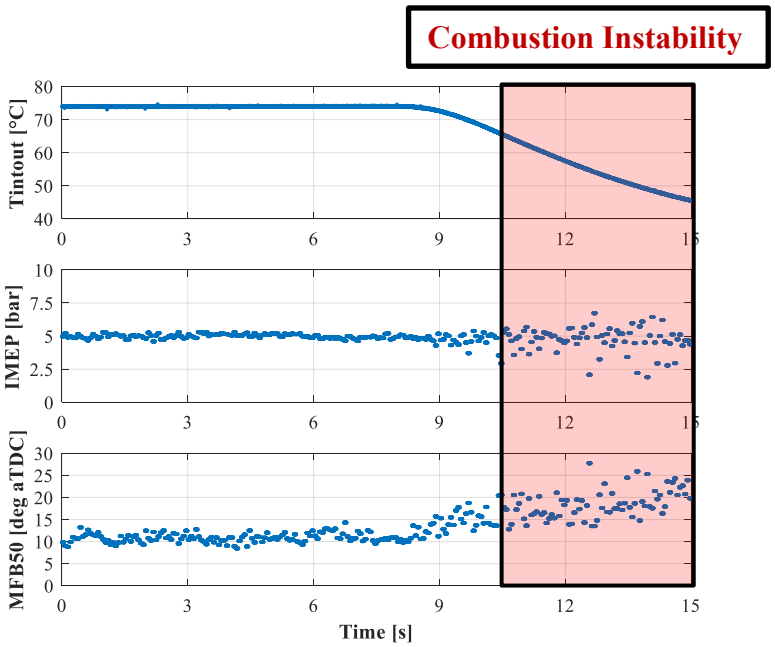

Figure 43. Effect of intake temperature on GCI combustion stability

2.2.3 Experimental Investigation on gasoline auto-ignition

The above-described experimental findings showed that to control GCI combustion [30], it is crucial to guarantee a robust combustion of the fuel injected in the first injection. By the analysis of the reported results, it was demonstrated that both boost pressure and intake temperature strongly affect GCI combustion stability and, therefore the calibration of these parameters represent one of the key points managing GCI. Furthermore, once boost pressure and air temperature were correctly selected, by using a proper timing of the first injection running GCI with double injection strategy, it was possible to control the position of the center of combustion reducing PPRR without compromising combustion stability.

The experience made testing GCI with double injection strategy suggests that to properly manage this advanced combustion methodology, a more complex injection strategy is needed. As a result, to develop effective and reliable complex injection strategy, a deeper knowledge of the ignition mechanism of the first injection is mandatory. For this reason, this part of the PhD dissertation describes the experimental activity carried out to investigate the gasoline auto-ignition process through the analysis of combustion of with small quantity of fuel and how the main control parameters modify the gasoline auto-ignition.

During this activity, two different amounts of gasoline (used in previous activities) were investigated: 2 and 4 mg/stroke. For each fuel mass, three different fuel pressures were selected, i.e., 300, 500 and 700 bar. Each combination of gasoline mass and injection pressure was tested with different combinations of intake pressure and temperature: two levels of intake pressure (1450 and 1550 mbar) and two levels of intake temperature (20 and 75 °C), were investigated. During all the mentioned tests, several steady-state tests were run changing the SOI from 50 to 10 deg BTDC. The whole set of experimental tests was analyzed, the goal being to highlight the effect of each control parameter on heat release and ignition delay. Table 6 reports the engine conditions used during the experimental activity.

RPM	Boost Pressure [mbarA]	Gasoline Pressure [bar]	Injected Fuel [mg/cycle]	Intake Temperature [°C]	SOI [deg bTDC]
2000	1450	300	2	75	**Sweep 50 to 10**
2000	1450	500	2	75	**Sweep 50 to 10**
2000	1450	700	2	75	**Sweep 50 to 10**
2000	1450	300	2	20	**Sweep 50 to 10**
2000	1450	500	2	20	**Sweep 50 to 10**
2000	1450	700	2	20	**Sweep 50 to 10**
2000	1550	300	2	75	**Sweep 50 to 10**
2000	1550	500	2	75	**Sweep 50 to 10**
2000	1550	700	2	75	**Sweep 50 to 10**
2000	1550	300	2	20	**Sweep 50 to 10**
2000	1550	500	2	20	**Sweep 50 to 10**
2000	1550	700	2	20	**Sweep 50 to 10**
2000	1450	300	4	75	**Sweep 50 to 10**
2000	1450	500	4	75	**Sweep 50 to 10**
2000	1450	700	4	75	**Sweep 50 to 10**
2000	1450	300	4	20	**Sweep 50 to 10**
2000	1450	500	4	20	**Sweep 50 to 10**
2000	1450	700	4	20	**Sweep 50 to 10**
2000	1550	300	4	75	**Sweep 50 to 10**
2000	1550	500	4	75	**Sweep 50 to 10**
2000	1550	700	4	75	**Sweep 50 to 10**
2000	1550	300	4	20	**Sweep 50 to 10**
2000	1550	500	4	20	**Sweep 50 to 10**
2000	1550	700	4	20	**Sweep 50 to 10**

Table 6. Engine operating conditions during the experimental investigation on gasoline autoignition with small amount of fuel

Since the standard fuel consumption measurement system (AVL Balance 733s) was not enough accurate to precisely measure the gasoline mass flow during autoignition investigation, a high accuracy flow meter (FlowSonic LF), characterized by a measurement range compatible with the small mass flow rates introduced inside GCI cylinder, was installed in the gasoline line before the high-pressure pump.

As made for the previous analyzed GCI operating conditions, the combustion analysis was performed through the calculation of the RoHR and CHR during the combustion process. However, RoHR calculation performed through Eq.15 does not consider the losses due to heat transfers through the walls and blow-by. This aspect was not negligible in this study, because when small amounts of fuel are injected, the heat exchanged through the crevices or the cylinder walls can be comparable to the one which produces a pressure increase captured by the in-cylinder pressure sensor. If the amount of (positive) energy released during the combustion process is comparable with the negative contribution (blow-by and heat transfer through the walls), it might be difficult to perform detailed studies of the ignition process, because some of the phenomena of interest might be hidden by the losses.

To automatically compensate the mentioned negative contributions, each RoHR trace, calculated from the pressure measurements, was corrected removing the heat release trace calculated during a motored test (no fuel injected) run in the same condition of engine speed, intake pressure and temperature.

This procedure was applicable because it was possible to keep the boost pressure at its target value also when the injection was deactivated in GCI cylinder (this is done using the three cylinders fueled with diesel, main features of "*Cylinder Laboratory*" mode). Figure 44 demonstrates that the discussed procedure is suitable to compensate the effects of the losses, returning the gross RoHR released during the combustion process. In addition, it is interesting to notice that the gross RoHR in Figure 44 shows a negative and a positive region. The negative part corresponds to the vaporization stage (negative because the fuel receives heat), while the positive part is the combustion stage (positive because the fuel releases heat).

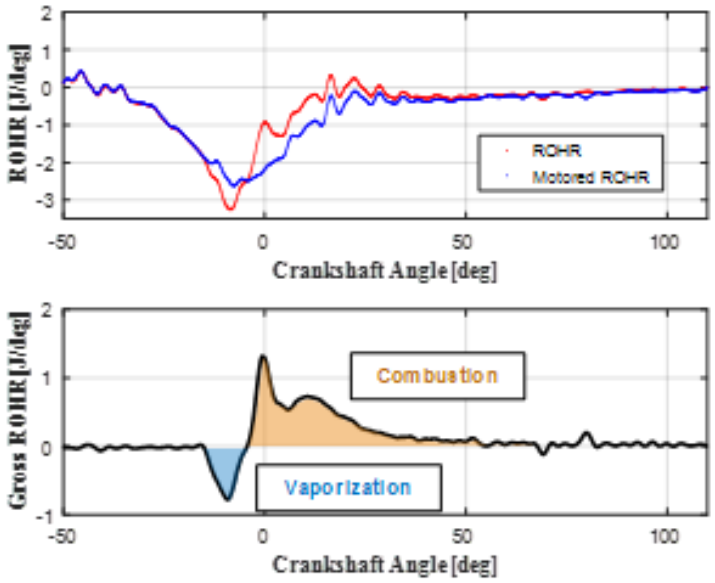

Figure 44. Gross RoHR calculation for a test run at 2000 rpm, boost pressure 1550 mbar, intake temperature 75°C and gasoline pressure 300 bar (4 mg/stroke)

The use of the calculated gross RoHR was fundamental to properly analyze the effects of intake conditions, injection pressure and SOI variation on the vaporization and combustion stage in the tested operating conditions. Given an investigated steady-state condition, the first aspect to be noticed is that SOI variation has a remarkable impact on both vaporization and combustion phase. To clarify this consideration, Figure 45 reports the result of the SOI sweep performed injecting 4 mg/stroke, keeping boost pressure at 1550 mbar, intake temperature at 75°C and gasoline pressure at 300 bar. As it can be observed, to obtain a good efficiency of the combustion stage, i.e., a high CHR, it is necessary to select the optimal SOI (approximately 26 deg BTDC in this case). It is easy to notice that SOI also influenced the vaporization phase, since the vaporization speed (represented by the minimum values of the negative ROHR portion) is slow for very advanced injections (high SOI), reaches its maximum at intermediate SOI values and decreases again when a retarded SOI (near the TDC) is applied. This result is obviously due to the different average temperatures experienced by the fuel mass during its vaporization (given the injected mass, faster vaporizations correspond to higher temperatures).

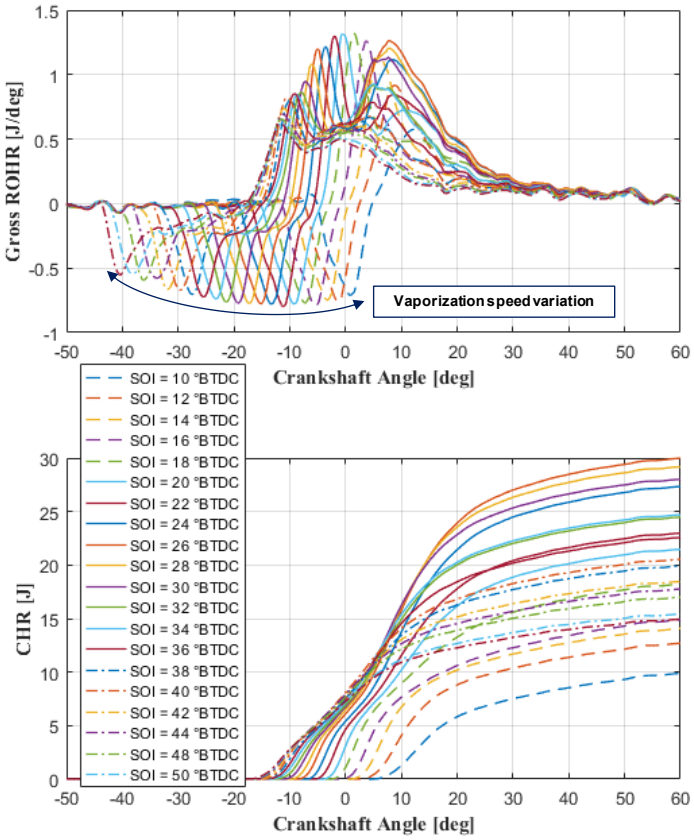

Figure 45. Gross RoHR and CHR variations during a SOI sweep (2000 rpm, 4 mg/stroke, boost pressure 1550 mbar, intake temperature 75°C and gasoline pressure 300 bar)

The results reported in Figure 45 clarify the importance of the optimal SOI selection to guarantee a reasonable combustion efficiency for the small amounts of gasoline injected (with the prospect of using it as first injection of a multi-injection pattern), but the effect of this quantity has to be combined with the effects due to the variation of the other control parameters.

As an example, Figure 46 at left shows that even if SOI was kept at a constant value (26 deg BTDC) the measured gross ROHR varied with the variation of the intake conditions. When high boost pressure and intake temperature is used, the combustion process is characterized by 2 steps: a premixed combustion portion followed by a diffusive combustion. This means that the combustion process started with gasoline auto-ignition further propagates and generates the second ROHR peak. When pressure or temperature are reduced, the second ROHR peak disappears, probably because of the slower propagation of the combustion process, which stops when it reaches too lean regions of the combustion chamber (the injected fuel has more time to propagate inside the combustion chamber and therefore to reduce the local relative air-fuel ratio before being reached by the flame). This result suggests that, with the perspective of a multiple injection pattern, the first injection should be performed in operating conditions that guarantee good combustion stability and efficiency, i.e., the ones in which the first pre-mixed combustion is able to further propagate within the combustion chamber. To do so, a minimum level of intake pressure and temperature needs to be guaranteed, together with the proper choice of the injection phase.

To clarify this aspect, Figure 46 at right summarizes the effect of different intake condition on the combustion efficiency (calculated as maximum of CHR) in terms of ignition delay of the mixture (ID, crucial when chemically driven combustions are considered), calculated using Equation 27.

The very low energy released could affect all standard definitions of the start of combustion such as, CA05 or CA10. As a result, since for the investigation of the combustion of small fuel quantity injected the gross RoHR was calculated, an unconventional definition of start of combustion, SOC defined as angular position where was reached 0.2 J/deg of combustion speed ($\theta_{RoRH\_0.15}$), was used.

$$ID = SOC - SOI = \theta_{RoRH\_0.15} - SOI \qquad (27)$$

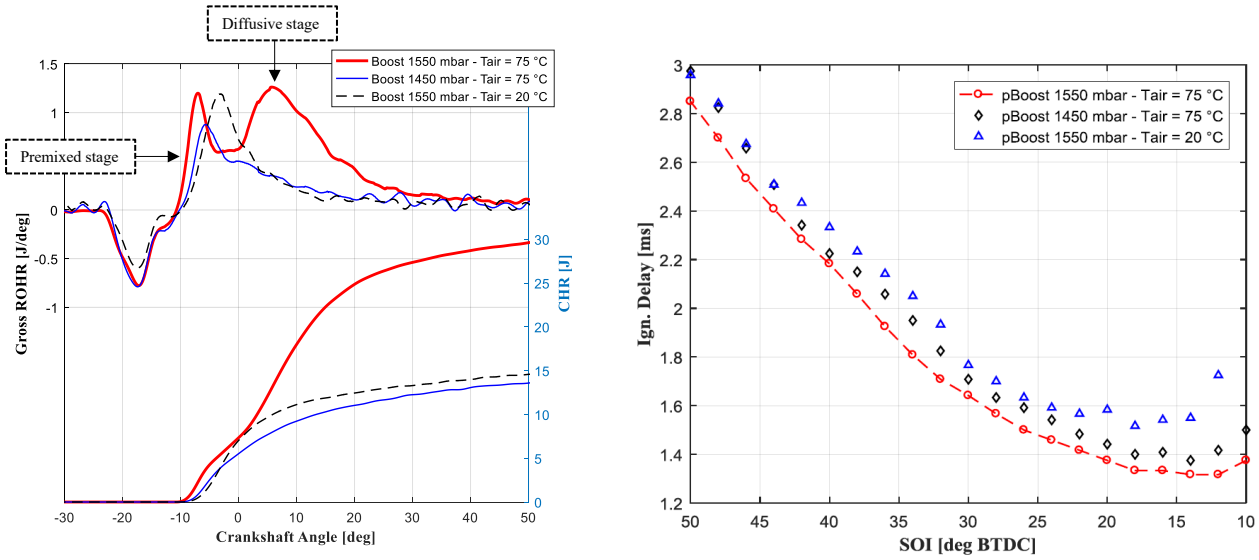

Figure 46. At left RoHR and CHR for 3 tests run at 2000 rpm, SOI 26 deg BTDC injecting 4 mg/stroke at 300 bar and changing the intake conditions: at right comparison between ignition delay during SOI sweep at different intake conditions

As expected, the minimum ignition delay is obtained in the "hottest" condition, i.e., the one in which both intake pressure and temperature are kept at the maximum value. It is interesting to notice that the measured ignition delay usually decreases when SOI is retarded (moving to TDC), except for very retarded injections (SOI lower than 15 deg BTDC), where the ignition delay tends to increase again. As a matter of fact, the ignition delay is not only influenced by the charge temperature in correspondence of the SOI, but by the average charge temperature in the time interval between SOI and SOC. For very retarded values of SOI, the ignition delay increases because the combustion process starts in the expansion stroke, where motored cylinder pressure and temperature are already decreasing. The above-described effect of ignition delay on combustion efficiency changing intake conditions with gasoline pressure of 300 bar are summarized in in Figure 47.

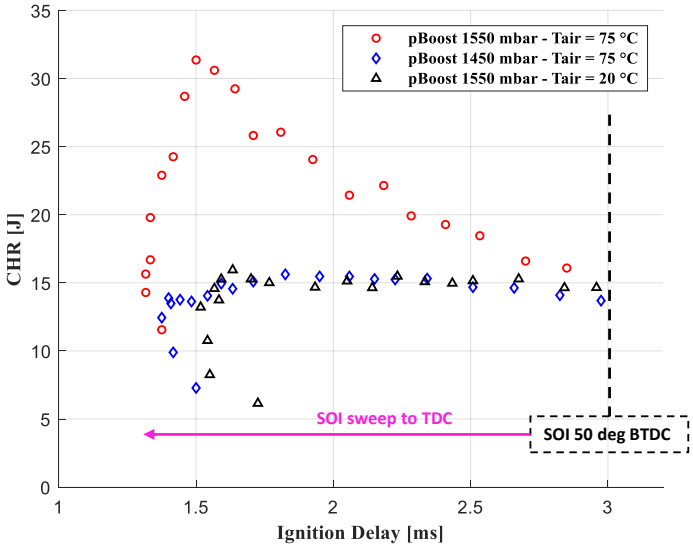

Figure 47. Effect of ignition delay on combustion efficiency at different intake conditions

The comparison of similar tests performed at different injection pressures also highlights the effect of this parameter on the combustion process. Figure 48 reports a comparison between three tests in which SOI (26 deg bTDC) and intake conditions were kept approximately constant (boost pressure 1550 mbar and intake temperature 75 °C) while varying only the injection pressure. As it can be observed, the pressure increases significantly accelerated the vaporization process, which resulted in more negative peaks of the calculated gross RoHR (higher fuel pressures guarantee a better air-fuel mixing and smaller fuel drops).

Another aspect to be noticed is that faster vaporization and better jet penetration also affected combustion efficiency (by varying the quality of the local air-fuel mixture). In this case, when the fuel pressure was increased, the diffusive combustion portion disappeared because the better air-fuel mixing accelerated the formation of ultra-lean regions in which the combustion process did not propagate. On the contrary, all the gross RoHR traces showed similar premixed portions, located in different angular position according to injection pressure.

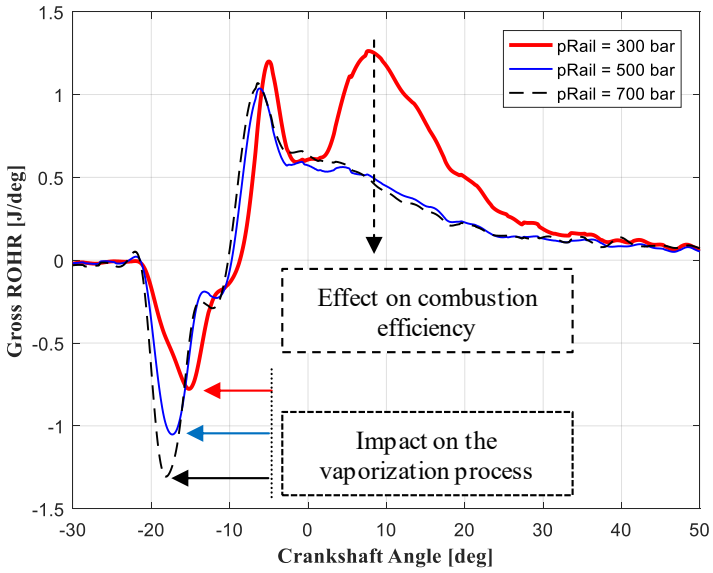

Figure 48. Gross RoHR for 3 tests run at 2000 rpm, SOI 26 deg BTDC injecting 4 mg/stroke at 300 bar and changing the gasoline pressure

The effects of different fuel pressure on combustion process during the whole SOI sweep are reported in Figure 49. For each injection pressure tested, the ignition delay variation (Figure 49 left) follows the same trend meaning that the impact of SOI on combustion phasing can be considered constant by varying gasoline pressure. Since higher fuel pressure improves the vaporization and the mixing of the mixture, given a fixed SOI, the ignition delay decreases by rising the injection pressure.

Moreover, despite improved mixing, with high fuel pressure the presence of ultra-lean zones avoids the flame propagation in the combustion chamber and, therefore the combustion efficiency will be lower. Figure 49 at right reports a comparison between combustion efficiencies during SOI sweep at different gasoline pressure. By looking at Figure 49, it clearly arises that the efficiency of the combustion (with approximately constant intake conditions and fuel quantity) decreases by increasing fuel pressure.

As shown in Figure 48 and Figure 49, the ignition delay deviations measured when the injection pressure is varied seems to be correlated with the variations of the vaporization process, i.e., to the different duration of this stage and the different air-fuel mixing obtained. As a matter of fact, a strong correlation between ignition delay and the minimum value of gross RoHR can be observed in Figure 50.

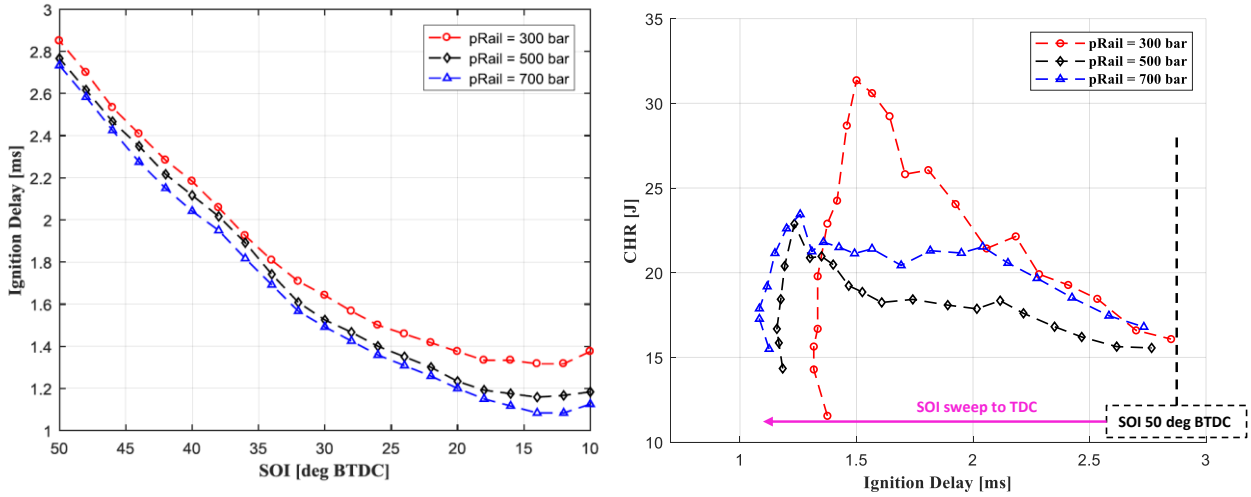

Figure 49.At left comparison between ignition delay during SOI sweep at different gasoline pressure; at right, effect of ignition delay on combustion efficiency at gasoline pressure

As expected, the above-described results confirm the existence of a strong correlations between the ignition delay of the combustion and fuel pressure and charge thermodynamic conditions (boost pressure and intake temperature). With the aim of developing complex injection strategy (which guarantee combustion stability and controllability over whole GCI operating range) based on pre-injections, all the collected data was crucial to improve the knowledge of the ignition mechanisms of small amounts of gasoline in our engine.

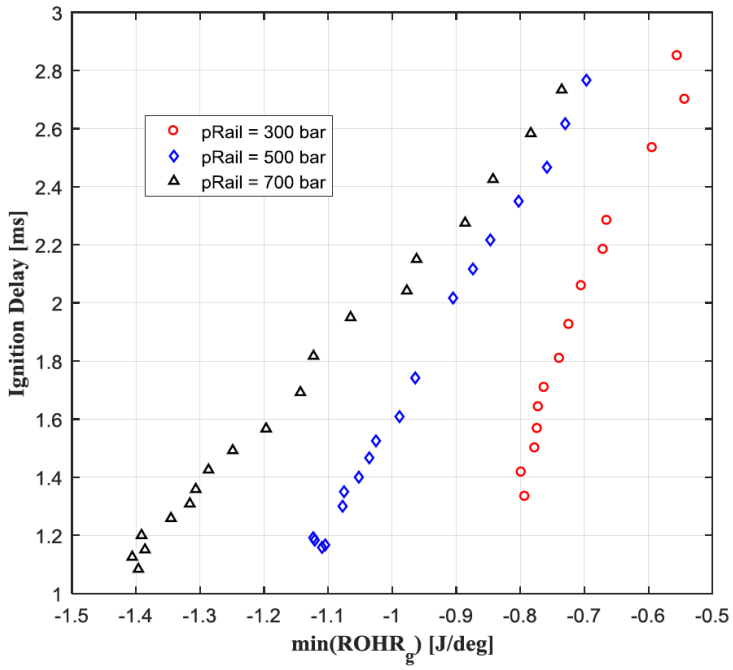

Figure 50.Ignition delay vs minimum value of gross RoHR for 3 SOI sweeps run injection 4mg/stroke and changing the fuel pressure with boost pressure 1550 mbar and intake temperature 75 °C

2.2.4 Experimental Investigation of the main engine control parameters on GCI combustion stability and efficiency

The experimental results obtained testing GCI combustion with double injection strategy proved that to guarantee stable and reliable combustion process over its typical operating range (higher than IMEP = 8 bar), more complex injection strategy (multi-jet) is needed.

With the perspective of designing a multi-jet process, it was demonstrated that the first crucial aspect to be guaranteed is the robust ignition of the first injection (Pilot injection). As widely described before, even though this injection usually introduces small amounts of fuel (1-2 mm3/stroke), its combustion is fundamental to increase pressure and temperature inside the cylinder and reduce the ignition delay of the following injections and properly design the heat release trace. However, this injection behaves nearly as an HCCI combustion (chemically driven process), therefore it is very sensitive to slight variations of the cylinder thermal conditions. Because of relevance of the combustion of Pilot injection, to study in deep gasoline auto-ignition mechanisms in our engine, a wide experimental activity was performed and described in the previous section of the PhD dissertation.

Once the stability of the ignition process was guaranteed, the injection pattern can be designed using many degrees of freedom. According to literature and experience (confirmed by the experimental tests) a reasonable way to limit the degrees of freedom is the choice of a multi-injection pattern (Pilot, Pre, and Main injection), where the amount of fuel injected in Pilot and Pre is equal to 1 mm3/stroke. Schematic of the multi-injection pattern used, and its parameters are reported in Figure 51.

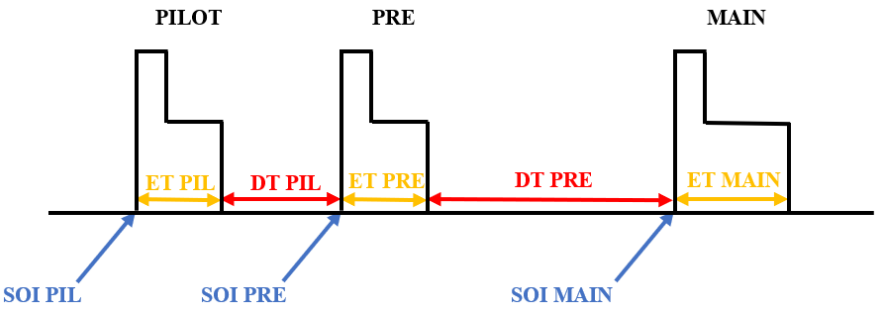

Figure 51. Multi-injection strategy management

With regard to the Dwell Time between Pilot and Pre injections (DTPil), it was kept nearly equal to the one used in the standard diesel calibration (compatible with the dynamic of the injector's needle and pressure waves in the fuel system). Since for each analyzed operating point the injection parameters of Pilot (SOIPil and ETPil) and Pre (SOIPre and ETPre) were fixed, the control of the center of combustion was performed varying the start of the Main injection (SOImain) through RCP system. The load of GCI cylinder was managed by changing ETmain to guarantee selected IMEP.

First, by using the above-described "*Cylinder Laboratory*" mode performing GCI combustion, the attention was initially focused on the effect of rail pressure variation on the combustion process. In the previous section of this dissertation, the effect of gasoline pressure on the auto-ignition process was highlighted. As a matter of fact, higher pressures increase jet penetration and reduce the size of the injected fuel drops, consequently accelerating fuel vaporization and therefore reducing the ignition delay, improving combustion stability. Bearing in mind the above consideration, to guarantee combustion stability it is crucial to design the proper injection pattern in different load conditions (more fuel might modify the local air-fuel mixing). To perform a robust GCI combustion and design a progressive heat release, a proper stratification must be guaranteed. When the combustion is run at low load (long ignition delay), excessive rail pressures increase the homogeneity of the charge (the fuel has time to propagate throughout the combustion chamber), which results in unacceptable combustion impulsiveness (high PPRR). On the contrary, when the load is increased (reduction of the ignition delay) the injection pressure must be increased to guarantee the desired stratification in a shorter time. Table 7 summarizes the operating points characteristic and the injection pattern parameters used during these tests. The above consideration is confirmed by experimental observations (Figure 52) obtained performing GCI combustion with multi-injection pattern at low load (IMEP = 8 bar).

RPM	IMEP [bar]	MFB50 [deg bTDC]	Boost Pressure [mbarA]	Gasoline Pressure [bar]	SOI Pil [deg bTDC]	QPil [mg/stroke]	SOI Pre [deg bTDC]	QPre [mg/stroke]	SOI Main [deg bTDC]
2000	8	12	1900	500	40	1	22	1	4
2000	8	12	1900	700	33	1	23	1	0

Table 7. Engine operating condition running GCI combustion at low load with multi-injection pattern at different gasoline pressure

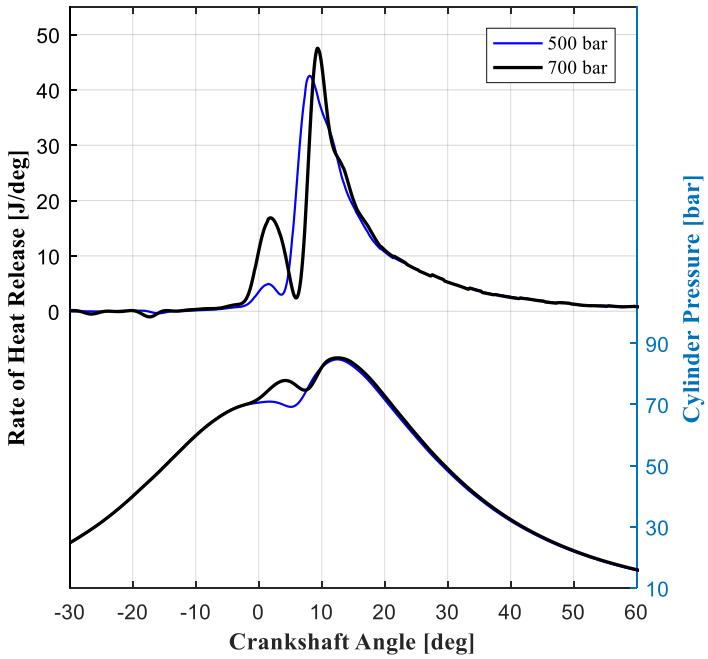

Figure 52. RoHR and in-cylinder pressure measured testing GCI combustion at 2000 rpm, IMEP=8 bar (multi-injection pattern) and varying the rail pressure (500/700 bar)

As it can be observed in Figure 52, the combustion process can be easily designed using an injection pressure equal to 500 bar and choosing a proper set of injection parameters for the 3-injection pattern. If the injection pressure is increased at 700 bar, the impulsiveness of the combustion process increases. This results in higher pressure derivatives (high PPRR) and lower controllability, because the combustion process is acceptable only over a limited range of MFB50 and it is easy to reach knocking or misfiring conditions [28].

The opposite occurs when the engine is run at higher loads. To test this operating condition, the cylinder fueled with gasoline was run at 2750 rpm and IMEP = 14 bar. The injection patterns used during the test reported at higher engine speed are summarized in Table 8. From the observation of Figure 53 clearly arises the potential related to the use of higher injection pressures. As a matter of fact, at high loads, increasing the rail pressure seems to be an effective way to reduce combustion impulsiveness and keep the maximum PPRR below the reliability limit.

RPM	IMEP [bar]	MFB50 [deg bTDC]	Boost Pressure [mbarA]	Gasoline Pressure [bar]	SOI Pil [deg bTDC]	QPil [mg/stroke]	SOI Pre [deg bTDC]	QPre [mg/stroke]	SOI Main [deg bTDC]
2750	14	12	2000	500	40	1	22	1	12
2750	14	12	2000	700	33	1	23	1	6

Table 8.Engine operating condition running GCI combustion at high load with multi-injection pattern at different gasoline pressure

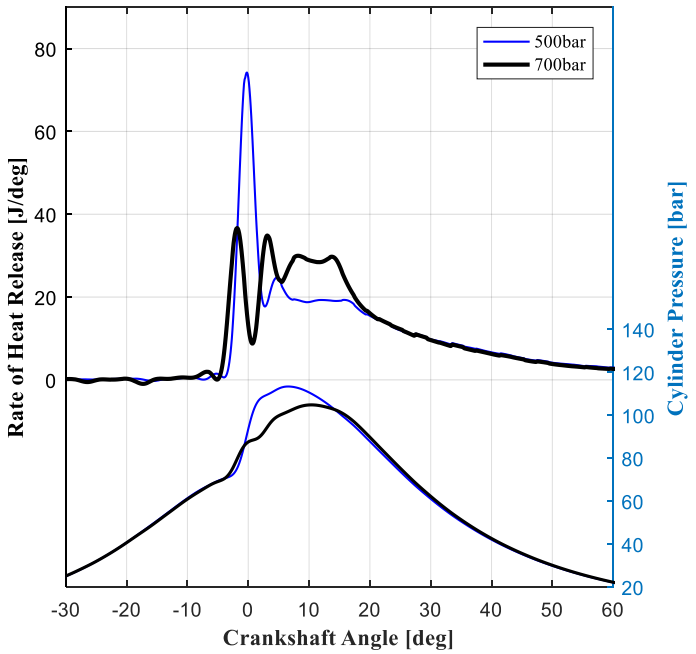

Figure 53. ROHR and in-cylinder pressure measured during tests run in PPC mode at 2750 rpm, IMEP=14 bar (3-injection pattern) and varying the rail pressure (500/700 bar)

Based on the above-discussed experimental observations, the effect of rail pressure variation was further investigated to quantify the impact of rail pressure variation on PPRR reduction, Indicated Specific Fuel Consumption (ISFC) and combustion stability. To highlight the impact of rail pressure variation on efficiency and stability, the center of combustion was varied performing CA50 sweeps ranging from the misfire limit (retarded combustion) to advanced combustion phasing, mainly limited by the maximum PPRR achieved. To run the sweeps, the same approach shown in Figure 54 has been used: the start of Pilot and Pre was kept constant (for each pressure, the SOI that optimizes the combustion efficiency of the 2 pre-injections was selected) while the center of combustion was changed varying the applied SOImain.

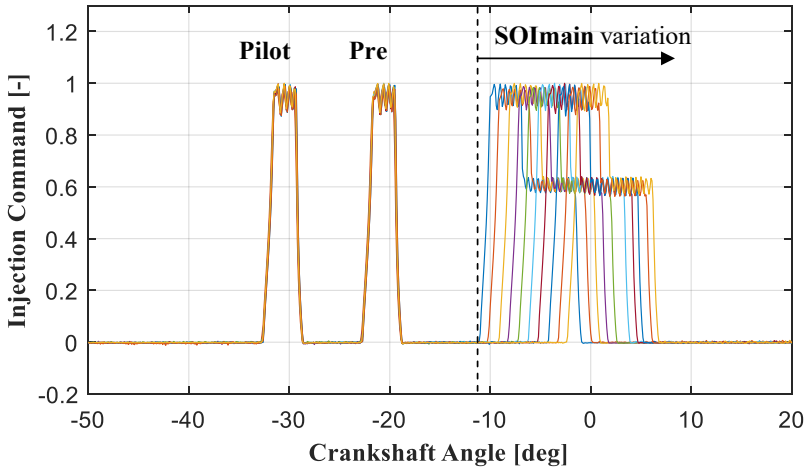

Figure 54. Multi-injection strategy management during CA50 sweep

The tests were performed activating a closed loop controller, implemented in the RCP system, that automatically varied SOImain and ETmain to keep CA50 and IMEP at a constant target value. The structure of this controller, which uses as inputs the combustion indexes calculated by the indicating system, is shown in Figure 55. As it can be observed in Figure 55, the center of combustions was kept at a proper target value changing the Start of Main Injection, while load (IMEP) was kept constant varying the Main Energizing Time, i.e. (at constant rail pressure) the amount of fuel injected. During the CA50 sweep, the variation of ETmain is obviously necessary to compensate the variation of the torque efficiency, which is maximum in correspondence of an optimal CA50 value. The variation of the amount of fuel injected compensates the torque efficiency variation and guarantees a constant indicated torque delivery during the whole CA50 sweep. As made for the previous experimental activity (testing GCI combustion with small quantity of gasoline), fuel consumption was accurately measured through the Flowsonic flow meter.

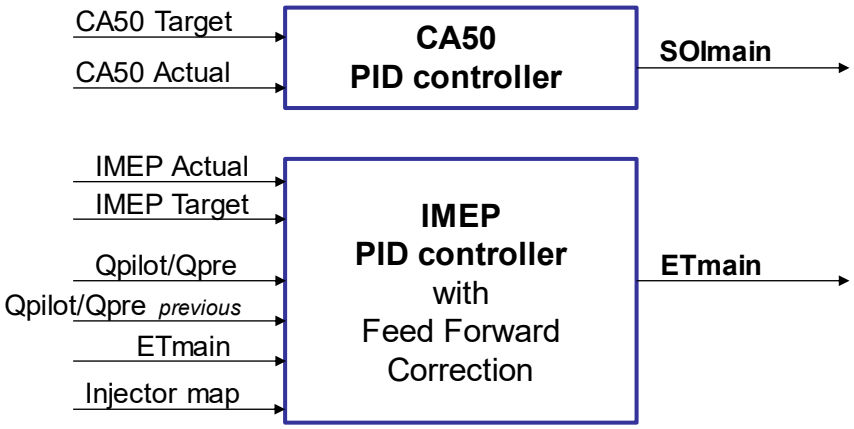

Figure 55. Scheme of the IMEP and CA50 closed-loop controller implemented in the RCP system.

Figure 56 reports a comparison between 3 CA50 sweeps performed at 2750 rpm, IMEP = 14 bar and setting the rail pressure equal to 500, 700 and 900 bar. From the observation of Figure 56 arises that increasing the rail pressure has a slight impact on the ISFC, which shows its minimum in correspondence of a CA50 nearly equal to 8 deg. In this case (relatively high load), the rail pressure increase seems to have a beneficial impact on combustion efficiency, since the minimum ISFC reported in Figure 56 is achieved during the sweep at 900 bar. It is also interesting to notice that the optimal ISFC, measured at this load in GCI mode, is low also compared to the corresponding fuel consumption measured in standard CDC operation, which is nearly equal to 198 g/kWh.

Since increasing injection pressure up to 900 bar seems to be slightly beneficial (at least in terms of ISFC), it is interesting to focus the attention on 3 tests run nearly with the same center of combustion. To do so, Figure 57 shows a comparison between the average pressure and heat release traces measured during 3 tests run with CA50 nearly equal to 12 deg. Although the increase of rail pressure seems to be beneficial to improve the ISFC, Figure 57 shows that there is another crucial aspect to be considered, i.e., the impulsiveness of the combustion process. In the discussed operating point, the test run at 500 bar results in unacceptable values of PPRR.

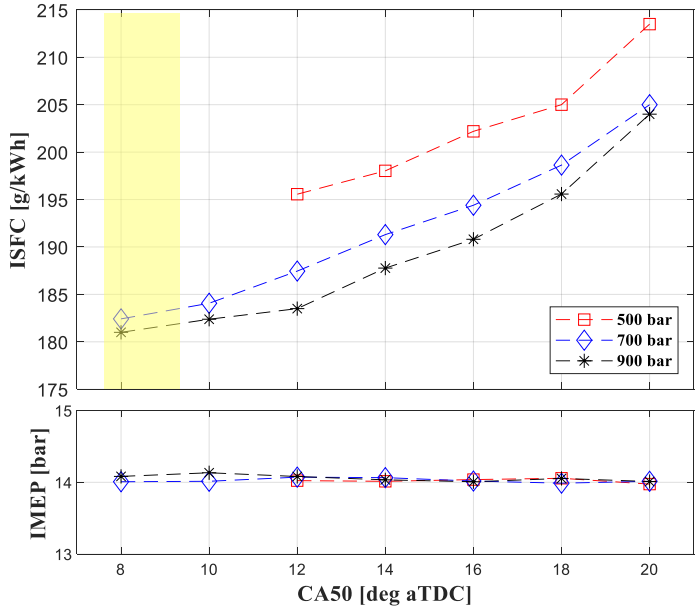

Figure 56. ISFC (top plot), IMEP and CoV (bottom) measured during the CA50 sweeps run GCI combustion (multi-injection pattern) at 2750 rpm, IMEP=14 bar, gasoline pressure of 500, 700 and 900 bar

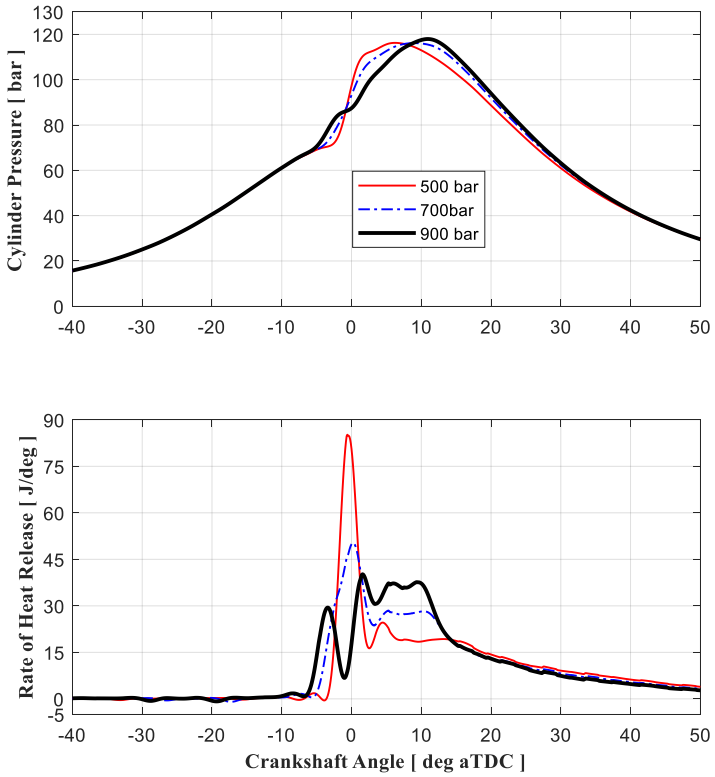

Figure 57. In-cylinder pressure and RoHR for tests run at 2750 rpm and IMEP=14 bar, varying gasoline pressure from 500 to 700 and 900 bar (injection pattern optimized for each rail pressure). Tests with CA50 nearly equal to 12 deg

While anticipating the combustion process (i.e., moving the CA50 to the Top Dead Center), the measured PPRR tends to increase at all the investigated rail pressures. However, the use of high rail pressures provides a significant PPRR reduction potential. As clearly visible in Figure 58, in the investigated operating point (2750 rpm, IMEP = 14 bar), the PPRR measured during the sweep carried out at 500 bar exceeds the maximum acceptable PPRR (10 bar/deg) when the CA50 is nearly 12 deg, which is significantly less efficient than the optimal operating condition. The sweep run at 700 bar is also critical in terms of PPRR, because the optimal efficiency CA50 is hardly reachable (its PPRR is nearly equal to the maximum acceptable PPRR, therefore a slightly advanced CA50 would immediately lead to unacceptable PPRR values).

On the contrary, the entire CA50 sweep run at 900 bar is characterized by an acceptable impulsiveness, since the maximum measured PPRR always remains below the reliability limit. This occurs also when an extremely advanced center of combustion is reached, such as 8 deg aTDC. The results discussed above could be (at least partially) explained by the variation of the combustion duration (defined as CA90-CA05) reported in Figure 58. This quantity clearly shows that increasing the injection pressure fastens the combustion process, probably reducing the losses in cylinder walls and exhaust.

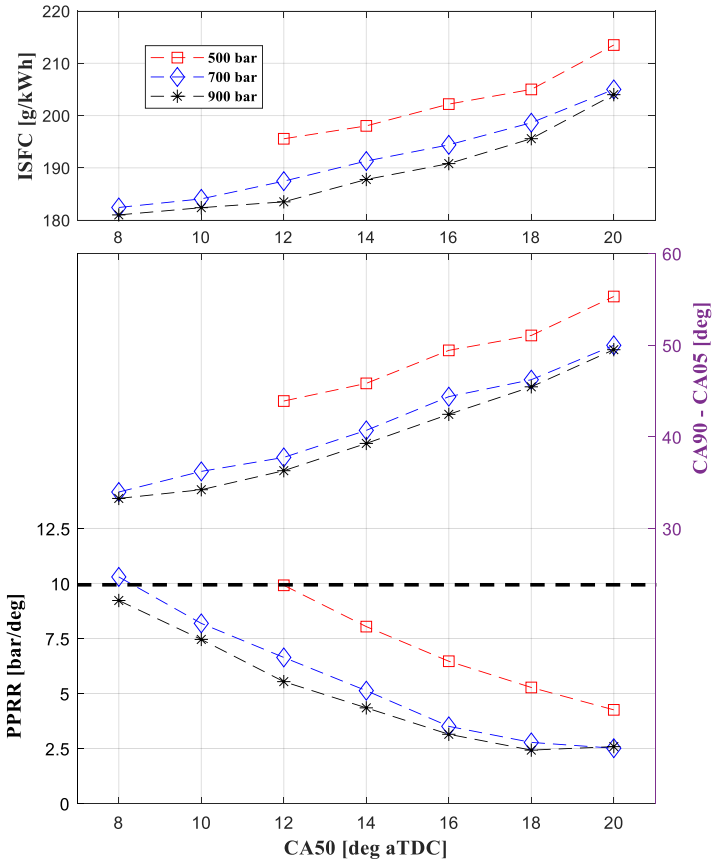

Figure 58. ISFC, combustion duration (CA90-CA05) and PPRR measured during the CA50 sweeps run at 2750 rpm, IMEP=14 bar, gasoline pressure of 500, 700 and 1000 bar. Different CA50 ranges available at each rail pressure level

The above considerations for the test run at IMEP = 14 bar are obviously valid also for operating points run at higher loads. If the load of the GCI process is further increased, the use of an injection pressure nearly equal to 900-1000 bar becomes even more crucial. It is worth mentioning that higher loads of the cylinder run in GCI mode were tested, reaching the maximum of IMEP = 18 bar. In all the tested conditions, the use of a rail pressure up to 1000 bar allowed achieving the maximum efficiency CA50 without exceeding the established reliability limitations (maximum acceptable PPRR).

The obtained results proved the importance of injection pressure as an effective lever to properly design the combustion process of an engine operated with GCI combustion. The tests also quantified the maximum range of injection pressure necessary to operate in GCI mode over its whole operating load range.

Even though the obtained combustion process (using multi-injection strategy) is stable and reliable in all the tested load conditions, it is worth bearing in mind that gasoline compression ignition is extremely sensitive to the intake thermal conditions. As already mentioned, all the investigated CA50 sweeps were performed modifying intake temperature boost pressure to guarantee a stable and efficient combustion of the gasoline masses injected in Pilot and Pre.

Since in real driving applications the intake conditions are not always under control, some of the sweeps run in reference conditions were also tested reducing the intake temperature (kept nearly equal to 26 °C). To quantify the impact of cold intake conditions on the combustion process, some reference injection patterns were tested keeping constant the optimal injection pattern identified in hot conditions (only ETmain has been varied by the closed-loop controller to maintain the IMEP constant during the 2 tests). As it can be observed in Figure 59, which reports 2 engine cycles performed using the same injection pattern (identified as optimal during the sweep at fuel pressure = 500 bar), the intake temperature reduction completely modifies the combustion process also using multiple injections.

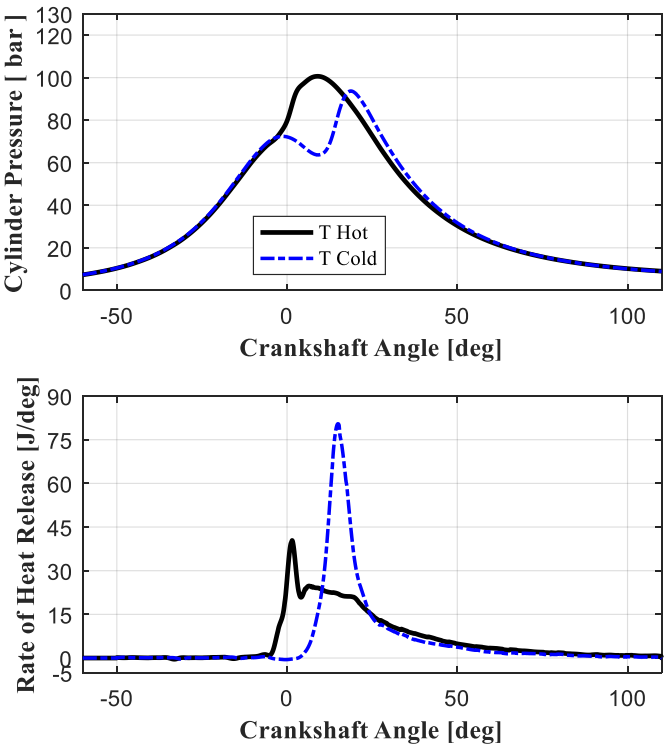

Figure 59. In-cylinder pressure and RoHR for tests run at gasoline pressure = 500 bar, 2000 rpm and IMEP=14 bar (same injection pattern). Comparison between hot and cold conditions

As noticed testing GCI with double injection strategy, the intake temperature reduction significantly increases the ignition delay of the pre-injections (Pilot and Pre). As a result, the fuel injected in Pilot and Pre ignites later and auto-ignites together with the fuel introduced during the Main injection. This is clearly visible from the observation of the heat release trace reported in Figure 59, which shows an impulsive premixed combustion (with high PPRR) for the test run in cold intake conditions (blue trace). On the contrary, the heat release identified as optimal in reference conditions (black trace) shows a premixed combustion followed by a diffusive combustion portion.

Similar considerations apply to the tests run using higher injection pressures, as visible in the comparison reported in Figure 60 (optimal calibration identified in reference conditions at 1000 bar). In this case, the cold test still shows a low premixed peak (in which part of the fuel injected during pre-injections auto-ignites), however this peak is much lower and significantly retarded with respect to the corresponding peak in the test run in reference intake conditions (hotter air temperature). Also in this case, during the cold test the impulsiveness of the combustion process is significantly higher, although the higher injection pressure mitigates the differences with respect to the ones identified in the comparison at 500 bar.

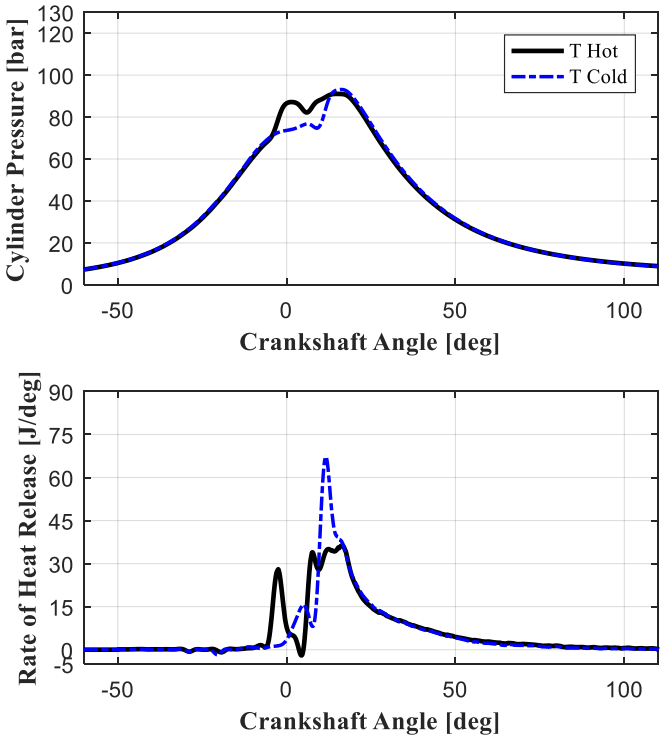

Figure 60. In-cylinder pressure and RoHR for tests run at gasoline pressure = 1000 bar, 2000 rpm and IMEP=14 bar (same injection pattern). Comparison between hot and cold conditions

The results reported in Figures 59 and 60 demonstrate that the intake temperature variation has a remarkable impact on the effectiveness of the combustion process also using multiple injection pattern. This result is mainly motivated by the increase of the ignition delay of the air-fuel mixture, already analyzed in literature and confirmed by the results reported in previous sections of the PhD dissertation.

Despite multiple injection strategy proved to be effective controlling GCI combustion over its typical operating range (mid-high loads), the effectiveness of the combustion process (assured by a robust autoignition of the first fuel jets) will be influenced by other load-dependent parameters, such as local air-to-fuel ratio, charge temperature and amount of residuals. As a results, to improve the stability of the GCI operation (running far from the calibration conditions) an ignition delay model become necessary.

Unfortunately, measuring the mentioned quantities, with the discussed experimental layout, is critical. As a matter of fact, due to the geometry of the standard exhaust line, it is very difficult to obtain a reliable measurement for the relative air-fuel ratio for the single cylinder run with gasoline. In addition, gasoline auto-ignition mechanisms are significantly affected by the hot residuals trapped in the cylinder, here determined (in terms of amount and composition) also by the operating conditions of the three cylinders fueled with diesel. Finally, this experimental layout is critical in terms of measurement of the pollutants produced by the engine, mainly because the exhaust manifold collects the exhaust gases coming from all the 4 cylinders, which are mixed upstream the turbine (configuration necessary to control boost and backpressure via VGT, but critical to measure the emissions). Due to the above discussed limitations, a large amount of work was performed to improve both hardware and control software, the goal being to develop a 4-cylinder compression-ignited engine operated with gasoline over its whole load range.

2.3 Experimental Investigation of GCI Combustion in a fully converted 4-cylinder light-duty compression ignited engine

The first stage of this work, performed running only one cylinder with GCI combustion, allowed investigating the combustion of gasoline in the compression-ignited engine under study and determining a baseline calibration (injection pattern and air system) suitable to achieve combustion stability over the whole engine load range. The second part of the experimental activity was focused on verifying the benefits of this LTC methodology both in terms of pollutants and efficiency. To do so, hardware and software were improved to obtain a 4-cylinder compression-ignited engine fully converted to run GCI combustion. Figure 61 shows the test bench layout for 4-cylinder GCI engine testing: both hardware and software improvements will be discussed above in the next section.

Figure 61. Test bench layout for 4-cylinder GCI engine testing

2.3.1 Experimental Layout Improvements

In terms of hardware improvements, the main modification to run the 4-cylinder gasoline engine was the use of a volumetric compressor (before the centrifugal compressor) necessary to provide, from the cranking stage, enough boost pressure to auto-ignite gasoline (and consequently start the engine). To achieve this, the above-described experimental layout was modified adding a roots volumetric compressor (Eaton Compressor M24) upstream the standard dynamic compressor. To keep in motion the volumetric compressor, a mechanical connection through a tooth belt with an electric motor (5.5 kW and maximum rotational speed equal to 3000 rpm) was realized. Then, the external supercharger was controlled (together with the turbocharger) to guarantee a specific target boost pressure from the cranking stage. To correctly integrate the supercharger in the air path of the engine, stand and pipes were designed. Figure 62 reports the 3D representation of the roots stand for placing the external supercharger system and the real component mounted on the test bed.

It is important to underline that the volumetric compressor is used only to start the engine: when a load which allows controlling the boost pressure directly with the VGT actuator is reached, the compressor is switched off and by-passed. All the operating points run with the 4-cylinder PPC configuration were performed with the volumetric compressor switched off and by-passed. Therefore, no negative work (spent on the compressor) needed to be taken into account in the calculation of the engine efficiency.

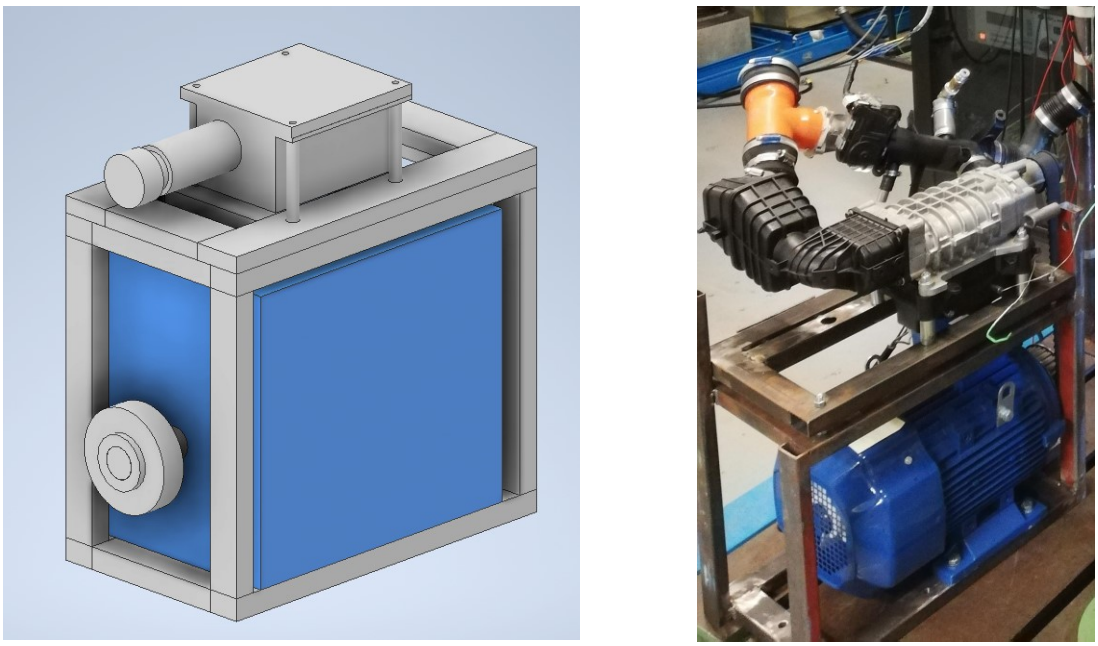

Figure 62. Volumetric compressor

Furthermore, an air heater with diathermic oil (kept at a controllable target temperature using the TEMPCO T-REG HCE 609/15 0 heater) was installed in the middle between the dynamic compressor and the intake manifold. The additional heater enabled the accurate control of the intake temperature in any operating condition, which was also beneficial to stabilize the combustion process in cold-start conditions. It is important to underline that to correctly manage the air temperature using hot diathermic oil flow to fuel the intercooler, the standard plastic water-air heat exchanger was replaced by a more reliable aluminum oil-air heat exchanger. Figure 63 shows the TEMPCO unit, and the custom metallic intercooler used to improve the intake air temperature controllability. As described in the test bench layout section, to quantify the engine-out emissions obtained with the 4-cylinder GCI configuration, a Continental SNS14 NOx probe and an AVL 415S Smoke Meter were installed in the exhaust line.

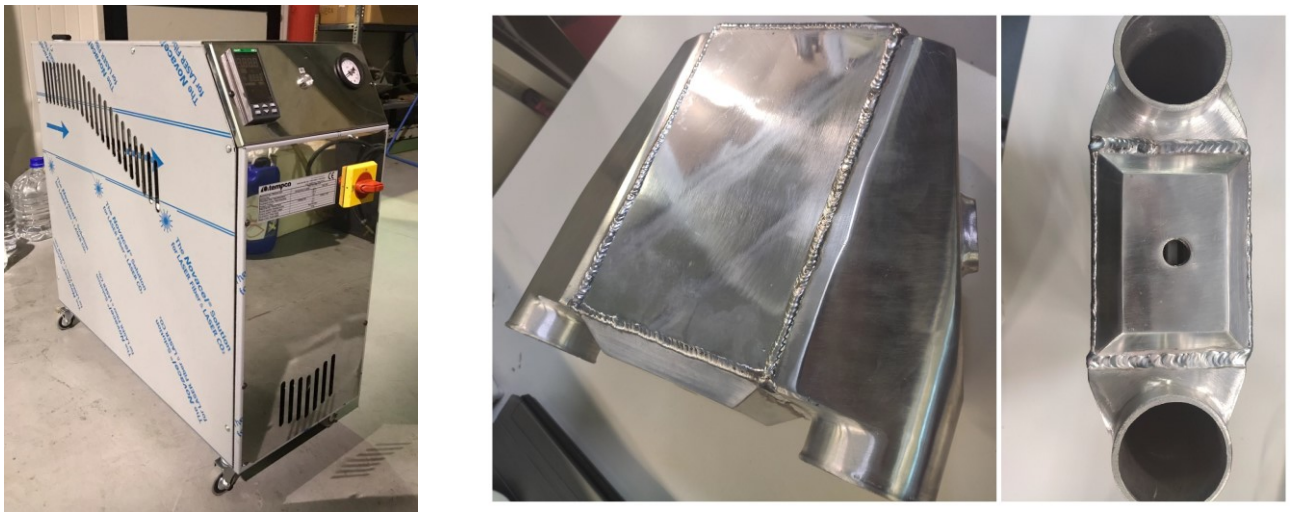

Figure 63. TEMPCO unit (left) and heat-exchanger (right)

Together with the before described hardware improvements, the engine control system was also modified to manage the fully converted 4-cylinder GCI engine. The standard ECU was removed, and the whole control strategy was implemented in an open ECU (Spark by Alma Automotive, programmable using LabView software). The control strategy, implemented in the open ECU, manages the fuel system (only gasoline was used in this second stage of the activity), the actuation of the injection patterns (defined with the activity performed on the single cylinder and further optimized in the 4-cylinder configuration) and the actuators of the air system (standard and additional components).

The programmable ECU (Spark) reported in Figure 64, also implements the closed-loop combustion controller schematized in Figure 55: the ECU receives the combustion indexes calculated by the indicating system via CAN bus and real-time adjusts the injection pattern to maintain indicated torque and center of combustion at a calibrated target value. As a result, the RCP system was only used to communicate with TEMCO system through the already integrated RS485 protocol, without any task controlling the engine. Figure 65 and Figure 66 show the upgraded test bed control systems and their integration with the improved hardware respectively.

Figure 64. Spark ECU (left) and its integration as engine control unit (right)

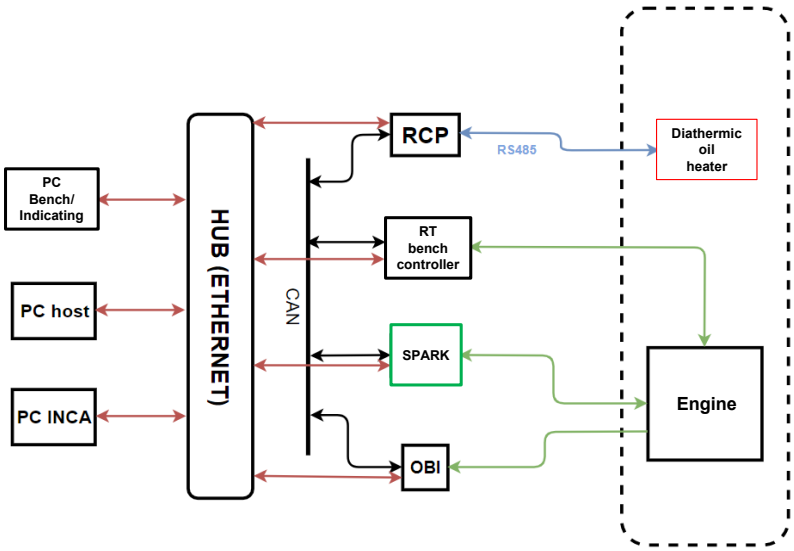

Figure 65. Scheme of the improved test bed control systems

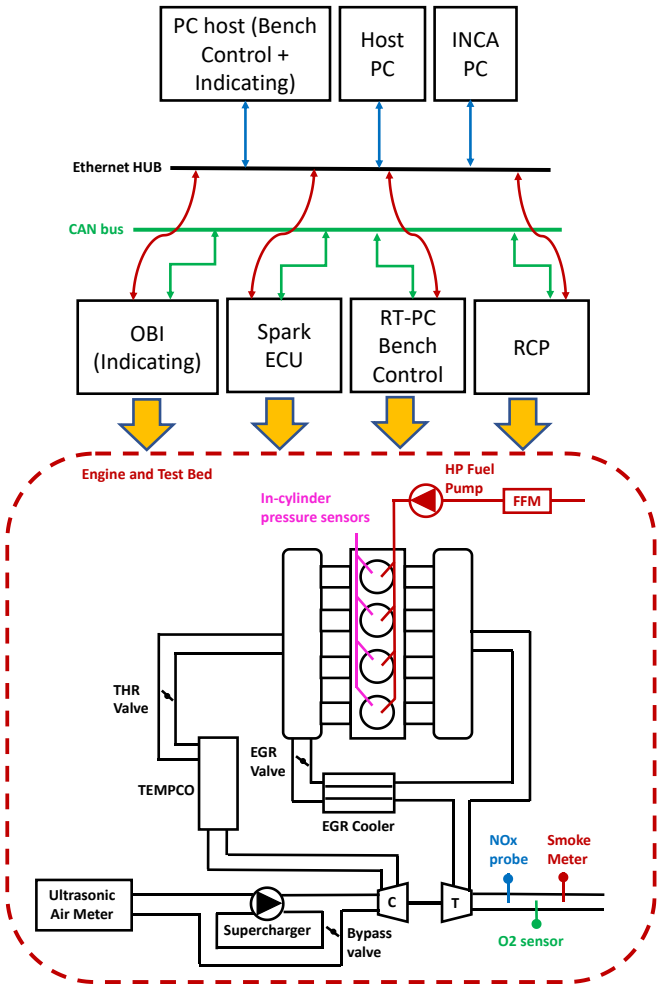

Figure 66. Scheme of the fully converted GCI engine and control system layout

2.3.2 Experimental Investigation of the main control parameters on GCI combustion emissions and efficiency

The 4-cylinder GCI engine was tested and optimized in different speed and load conditions. This stage of the activity started from the base calibration obtained with the "*Cylinder Laboratory*" activity, slightly modified because of the different boost pressure management performed in the fully converted configuration. As a matter of fact, when all the 4 cylinders are operated with GCI combustion (and deliver nearly the same amount of torque), exhaust temperature and pressure can vary significantly with respect to the "*Cylinder Laboratory*" mode (where the values of these quantities are affected by the operating conditions of the 3 cylinders fueled with diesel). Different exhaust conditions vary mass and temperature of the hot residuals which strongly impact gasoline auto-ignition mechanisms. Although the mentioned differences might generate small discrepancies between the absolute performance measured in single-cylinder and 4-cylinder configuration, the same trends highlighted during single-cylinder operation were confirmed. In addition, the experimental tests run in 4-cylinder GCI mode highlight the impact of the injection parameters (especially injection pressure) on the engine-out emissions. It is important to highlight that the engine was kept in its standard configuration (injection systems, piston, turbocharger). The use of a low-lubricating fuel, such as gasoline, affects the reliability of the standard high-pressure diesel pump, also increasing energy losses and brake specific fuel consumption (BSFC). As a results, the thermal efficiency of GCI combustion was evaluated by considering ISFC (instead BSFC).

Since combustion stability was guaranteed by a multiple injection pattern, as already mentioned, the CI engine under study was tested in GCI mode over a wide range of loads and speeds. The main limitation to the use of GCI combustion in the layout under study is that the boost pressure needs to be maintained high enough to guarantee a robust gasoline auto-ignition. For the engine under study, this results in a minimum boost pressure around 1.5-1.6 bar (the lower limitation varies with the intake temperature), which limits the minimum load at which combustion can be operated in stable conditions nearly at IMEP = 5 bar (if the load is further reduced, the relative air-fuel ratio becomes too lean). Due to the above limitation, the engine was tested in the load range between 6 and 18 bar IMEP and in the speed range between 1750 and 3000 rpm. The performance obtained with the 4-cylinder strategy was compared with the performance obtained running the same engine with standard diesel combustion. It is important to underline that, to verify the results obtained with the 4-cylinder configuration with the single cylinder, at first the comparison between GCI and CDC was performed deactivating the EGR system (for both GCI and CDC), which obviously results in relatively high NOx emissions. Then, to define how GCI combustion are far from the engine-out emission of a standard calibrated CI engine, similar tests were carried out highlighting the need of EGR also running the LTC. Finally, the effect of EGR on GCI combustion and pollutants production was tested [30].

GCI combustion vs CDC combustion: comparison without EGR

The analysis of acquired data clarifies the potential of the tested LTC, when performed in the CI engine under study. Figure 67 shows the results obtained operating the engine at 2000 rpm and IMEP = 8 bar. As it can be observed, the variation of the injection pressure has a remarkable impact on all the reported performance indexes and on the measured emissions. In correspondence of the optimal center of combustion (8 degCA), the minimum ISFC reaches nearly 178 g/kWh, significantly lower than the optimal value obtained using Diesel (EGR deactivated in both cases). In terms of pollutant emissions, GCI shows a slight reduction of soot and a remarkable reduction of NOx compared to CDC.

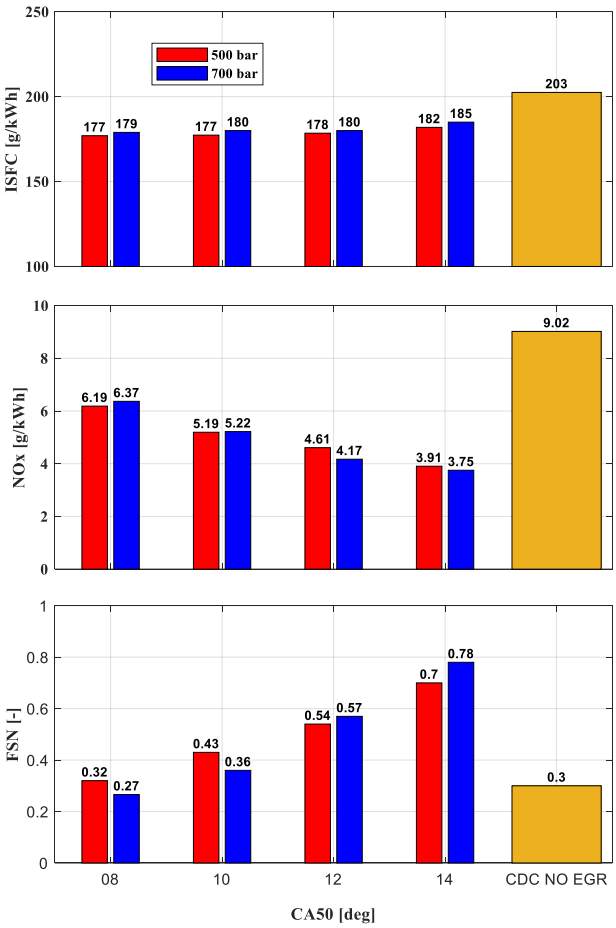

Figure 67. Comparison between ISFC, NOx and soot emissions for tests run, in GCI and CDC mode, at 2000 rpm and IMEP=8 bar (EGR deactivated)

It is interesting to notice that the CDC reference was obtained injecting the fuel at 870 bar, while the optimal test run in GCI mode was operated at a significantly lower pressure (between 500 and 700 bar) [28]. This means that the work spent to increase the fuel pressure, with gasoline, will be lower, therefore an extra benefit in terms of BSFC will be obtained because of the injection pressure reduction. Since, in this work, the experimental activities were performed using the standard common-rail injection system (not optimal to manage gasoline direct injection in terms of efficiency and reliability over time), the measured BSFC is not compared (with CDC).

Similar results can be obtained running the engine at higher engine speed, where the selection of the proper injection pressure is even more crucial to achieve the optimal performance in terms of combustion efficiency and engine-out emissions reduction. As an example, Figure 68 reports the performance of a test run at 2750 rpm and IMEP = 14 bar. From the observation of these results, clearly arises the potential of GCI operation in the compression-ignited engine under study (maximized in correspondence of the optimal MFB50, i.e., 8 deg aTDC).

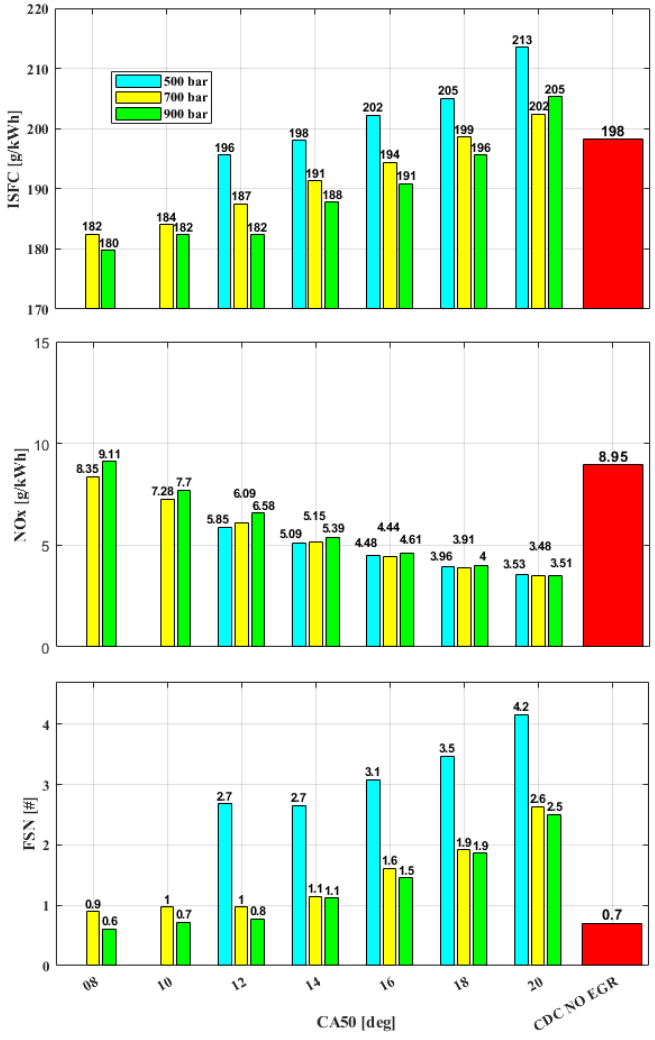

Figure 68.Comparison between ISFC, NOx and soot emissions for tests run, in gasoline PPC and CDC mode, at 2750 rpm and IMEP=14 bar (EGR deactivated)

Moreover, it is important to notice that GCI combustion does not require the use of extremely high injection pressures. ISFC and engine-out emissions running the engine in GCI mode (both at 700 and 900 bar) are lower than the ones of the reference CDC, operated with a rail pressure nearly equal to 1150 bar. Due to the lower injection pressure, it is reasonable to expect that the LTC methodology will lead to a further BSFC gain mainly because the high-pressure fuel system will require less energy (compared to CDC operation) to keep the fuel at the target pressure.

GCI combustion vs CDC combustion: distance from standard CDC engine

As already discussed, this work was carried out keeping the EGR deactivated both in CDC and GCI mode [30]. The comparison between coherent tests performed running the engine in standard CDC, clearly highlights the potential of GCI combustion, i.e., the improvement of combustion efficiency and engine-out emissions. However, as already mentioned, the emission regulations strongly limit the pollutants productions of the internal combustion engines (especially NOx) and, therefore, the use of EGR is mandatory to respect the rules. Since the engine under study was kept in standard layout and calibration, to verify how far GCI combustion without EGR is (in terms of the engine-out emissions) from a calibrated CDC engine three different engine conditions were tested. The experimental investigation was focused on three main operating points, characterized by different loads and speeds: two tests were run at 2000 rpm, one at high load (14 bar IMEP)

and the other at low load (8 bar IMEP); the third operating condition was run at higher rotational speed (3000 rpm) and intermediate load (10 bar IMEP). Table 9 reports the tested engine operating conditions during this activity. The selected engine conditions span a significant portion of the load-speed range of the engine under study and can therefore provide useful information about the potential related to the use of GCI combustion in a modern homologation cycle (with respect to standard CDC). The conclusions drawn analyzing the operating points will be useful to estimate the performance of the engine in the intermediate (in terms of load and speed) operating conditions.

Engine Point name	Engine Speed [rpm]	IMEP [bar]	MFB50 [deg bTDC]	Boost Pressure [mbarA]	Gasoline Pressure [bar]	Intake Temperature upstream manifold [C]
Low-load	2000	8	From 6 to 14	1.5/1.6	500/700/900	50
High-load	2000	14	From 8 to 14	1.9/2.0	500/700	50
High-revs	3000	10	From 8 to 18	1.9	500/700	50

Table 9. Engine operating conditions testing GCI in 4-cylinder mode

Figure 69 reports pollutants and thermal efficiency measured during the CA50 sweep performed at 2000 rpm and 14 bar IMEP (High-load). By looking at Figure 69, the trend of NOx and FSN with respect to CA50 variation clearly emerges. As a matter of fact, for all the tested gasoline injection pressures, retarding the center of combustion results in a NOx reduction and an increase in FSN. Since it is well known that retarded combustions generate lower pressure and temperature peaks during the combustion process, the trends visible on the measured pollutants were expected and can be easily explained. On the other hand, it is interesting to highlight that the ISFC measured in GCI mode is always lower or equal to the one measured with standard CDC. The optimal thermal efficiency is achieved in correspondence of the most advanced values of CA50 (8 and 10 deg) at all the tested injections pressures.

As regards rail gasoline pressure effects, as widely described in the previous sections of this work, due to the impact exerted on the mixing process, specific values of gasoline pressure must be chosen to generate a stable and efficient combustion and avoid high levels of pollutants in each operating condition. Considering the tests reported in Figure 69, the lowest value of gasoline pressure (500 bar) generates high levels of FSN if compared with the higher gasoline pressure values analyzed.

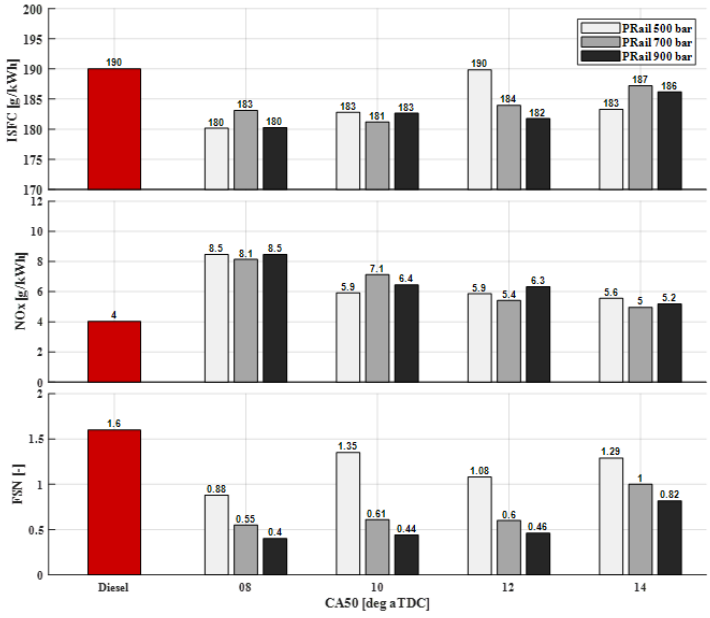

Figure 69. Comparison of ISFC, NOx and soot emissions between Diesel Reference and GCI combustion (without EGR) during CA50 sweep for mid-load operating condition at 2000 rpm, IMEP=14 bar

In Figure 69 are also shown the Diesel reference values set for each parameter (ISFC, NOx and FSN) to provide information about the need to improve PPC management making this combustion methodology convenient both in terms of emissions and efficiency with respect to standard calibrated CDC engine. It is important to underline that the reported CDC conditions (Diesel) were obtained testing the above-described 1.3L engine in standard conditions, both in terms of engine layout and calibration, defined by the engine manufacturer. It is worth mentioning that the base (standard) calibration for CDC operation (rail pressure, CA50, boost pressure, EGR rate) is mainly determined by the need to comply with the pollutant emission regulations (tailpipe emissions), and not necessarily aimed at achieving the maximum possible thermal efficiency. As a result, the refence CDC conditions (Diesel) do not represent the most efficient (minimum ISFC) CDC calibration reachable with this engine but can be considered a reference for GCI mode. To guarantee the coherence between efficiency and emissions measured both in CDC and GCI combustion, all the experimental tests were run using the same engine and test bench layout (in-cylinder pressure sensors, fuel consumption sensor, NOx probe and FSN measurement sensor were not changed).

From such comparison it is possible to observe that, despite efficiency and FSN show a promising potential, gasoline PPC (operated without EGR) always produces higher amounts of NOx with respect to the Diesel combustion. This result suggests that the use of EGR might be crucial, in gasoline PPC, to mitigate NOx emissions. It is interesting to notice that the CDC reference was obtained injecting the fuel at approximately 1150 bar, while the optimal tests run in PPC mode were operated at significantly lower pressures.

Figure 70 shows that similar considerations also apply to the test run at 3000 rpm and IMEP = 10 bar (high revs). In this case, the investigated CA50 range was extended (from 8 to 18 deg aTDC) to better highlight the effect of combustion retard on the efficiency. The observed trend confirms that the optimal ISFC is obtained in correspondence of the most advanced CA50 values. In particular, the ISFC obtained at 8-10 deg is significantly lower that the ISFC for the optimized standard CDC condition. GCI combustion seems to be very promising also to reduce particulate matter, especially using an injection pressure approximately equal to 700 bar. On the contrary, without external EGR, the NOx emissions are always too high, also for retarded combustion phases.

Similar conclusions can be drawn also analyzing the tests carried out at 2000 rpm and IMEP = 8 bar (low-load), but in this case the impact of gasoline pressure on pollutants is less evident, as shown in Figure 71. Low-load conditions are characterized by the combustion of small quantities of fuel in large amounts of air (in this test the relative air-fuel ratio was close to 2.4, mainly due to the need to maintain the boost pressure higher than 1.5 bar to guarantee a robust gasoline auto-ignition). Consequently, increasing the injection pressure at very high levels is less crucial to obtain a good air-fuel mixing.

From the analysis of the 3 investigated points, it appears clear that improving Diesel performance reducing simultaneously ISFC, NOx and FSN, would not be possible running GCI mode without EGR and, as a result, the impact of external recirculated gases on GCI combustion must be investigated. This aspect will be thoroughly discussed in the following section.

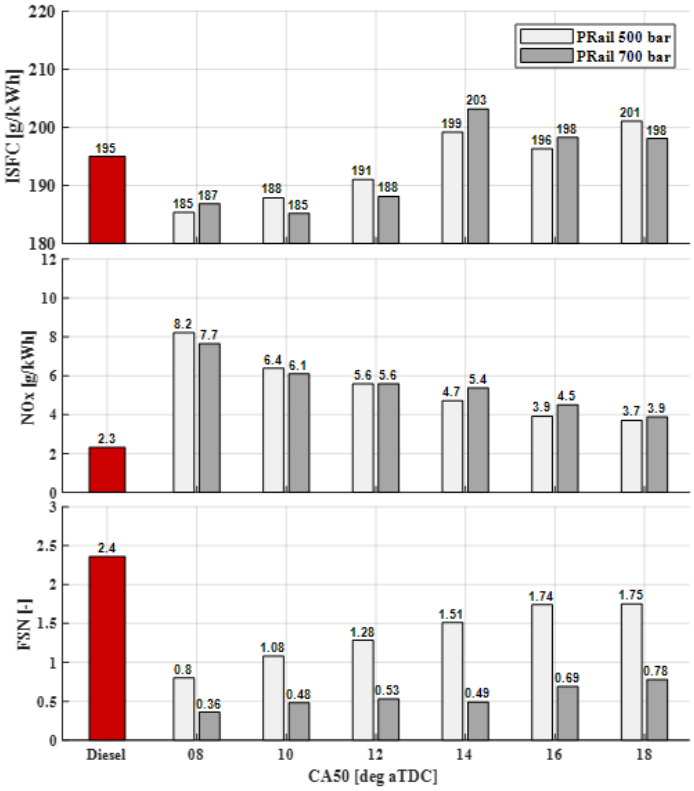

Figure 70. Comparison of ISFC, NOx and soot emissions between Diesel Reference and GCI combustion (without EGR) during CA50 sweep for high-revs operating condition at 3000 rpm, IMEP=10 bar

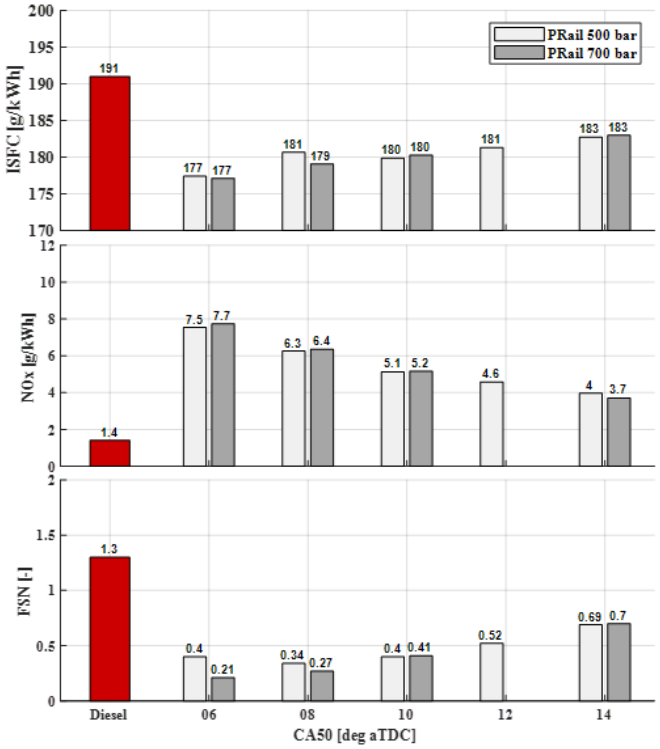

Figure 71. Comparison of ISFC, NOx and soot emissions between Diesel Reference and GCI combustion (without EGR) during CA50 sweep for low-load operating condition at 2000 rpm, IMEP=8 bar

GCI combustion vs CDC combustion: the use of EGR in GCI combustion

As previously explained, EGR investigation is necessary, to improve GCI engine-out emissions (i.e., the trade-off between NOx and particulate matter) trying to increase the performance with respect to standard CDC, used in this work as a reference condition. Starting from the information collected during tests without EGR, for each engine operating condition, an optimal set of injection parameters was selected: optimal injection pattern, gasoline, and boost pressure.

To properly investigate the effect of EGR under different rpm and load conditions, it was necessary to quantify the EGR mass and calculate the so called EGR rate defined in Equation 28, in which m_{Cyl} and m_{EGR} are the total mass trapped inside the cylinder and the mass of recirculated gases, respectively.

$$EGR_{Rate} = \frac{m_{EGR}}{m_{Cyl}} \tag{28}$$

To determine the defined EGR rate, it is first necessary to quantify the total mass trapped in the cylinder (m_{Cyl}). For this purpose, a filling model able to predict the total amount of air and external EGR trapped in the cylinder was developed. The model is based on the measurements of in-cylinder pressure and air flow (from the additional ultrasonic flow meter, reported in Figure 66, at the beginning of the intake line). In general, the in-cylinder trapped mass is composed by the sum of fresh air m_{Air}, internal residual gases m_{RG} and external EGR m_{EGR}, as shown in Equation 29.

$$m_{Cyl} = m_{Air} + m_{RG} + m_{EGR} \tag{29}$$

First, the model was developed keeping the EGR valve closed. Applying the well-known ideal gas equation, the contributions of fresh air and internal residuals were estimated. As shown in Equations 30, these masses can be determined referring to specific pressures and temperatures measured in different stages of the engine cycle. Residual gases were calculated as the mass trapped inside the combustion chamber at the end of the exhaust stroke (V_{CC}) when the piston reaches the top dead center (TDC). In this condition, it is possible to consider in-cylinder pressure and temperature approximately constant and equal to the values acquired by the pressure and temperature sensors mounted on the exhaust line, P_{Exh} and T_{Exh} respectively.

$$m_{RG} = \frac{P_{Exh}V_{CC}}{RT_{Exh}} \tag{30}$$

Once the internal residuals were quantified, the estimation of the total charge can be based on the information provided by the in-cylinder pressure sensors. During the intake stroke there are different contributions which impact the cylinder filling process. Previous research shows that residuals and valve timing have a strong impact on cylinder filling, mainly by reducing the effective volume compared to the geometrical volume (V_{cyl}) [31, 32]. For these reasons, two volume reduction contributions (with respect to V_{cyl}) were introduced, which represent the volume loss because of the expansion of the hot residuals from exhaust to intake pressure (ΔV_1) and the volume loss due to late intake valve closure (ΔV_2, difference between the cylinder volume in correspondence of the bottom dead center and volume in correspondence of the intake valve closure). Equation 31 and Equation 32 define these two volume reductions.

$$\Delta V_1 = V_{CC}\left(\frac{P_{Exh}}{P_{Int}}\right)^{1/\gamma} - V_{CC} \quad (31)$$

$$\Delta V_2 = V_{BDC} - V_{IVC} \quad (32)$$

In the discussed model, P_{Int} was considered constant and equal to the mean value of the measured in-cylinder pressure trace during the intake stroke (intake valve open), while the charge temperature was set equal to the measurement provided by the sensor installed in the intake manifold (T_{Int}). Finally, the gas constant R was set at 287.05 J/(kgK). Equation 33 summarizes the cylinder filling model used to estimate the mass of fluid introduced in the cylinder at IVC (from the intake manifold), i.e., the sum of fresh air and external EGR.

$$m_{Air} + m_{EGR} = \frac{P_{Int}(V_{Cyl} - \Delta V_1 - \Delta V_2 - V_{CC})}{RT_{Int}} \quad (33)$$

Figure 72 shows a comparison between the total mass trapped in the cylinder (m_{Cyl} , estimated using the model reported in Eq. 33) and the measurement performed by the air flow meter as a function of the EGR valve position. It is important to notice that, while performing the EGR valve scan reported in the top subplot of Figure 72, the position of the VGT actuator was continuously adjusted to maintain the boost pressure approximately constant. As it can be observed, when the EGR valve position is lower than 5%, both VGT position and measured amount of fresh air are almost constant. Consequently, the mass of external EGR does not change with respect to the condition at EGR equal to zero.

The discussed cylinder filling model [30] was validated comparing the estimated fresh charge (fresh air only) with the measurement provided by the ultrasonic air flow meter during tests operated without EGR. The analysis of the bottom subplot of Figure 72 shows the different contributions of m_{Cyl} during the EGR valve sweep. By comparing the estimated fresh air (blue bar) and the air flow measurement without external EGR (EGR valve position below than 5%) the model shows an accuracy approximately of 2%. It is important to underline that EGR also changes charge composition and temperature, which vary the gas constant and, consequently, introduce a small error in the in-cylinder mass evaluation. Due to the absence of a gas analyzer, the chemical composition of the charge cannot be evaluated using the discussed experimental layout. Furthermore, another small error in the estimation of the masses is due to the use of a constant specific heat ratio γ (it should be varied with the temperature of the charge). However, it is reasonable to consider the model acceptable during the whole EGR valve sweep, since the mentioned errors are small (compatible with requirements for control-oriented models) and do not affect the relative comparison between operating tests run in different opening positions of the EGR valve.

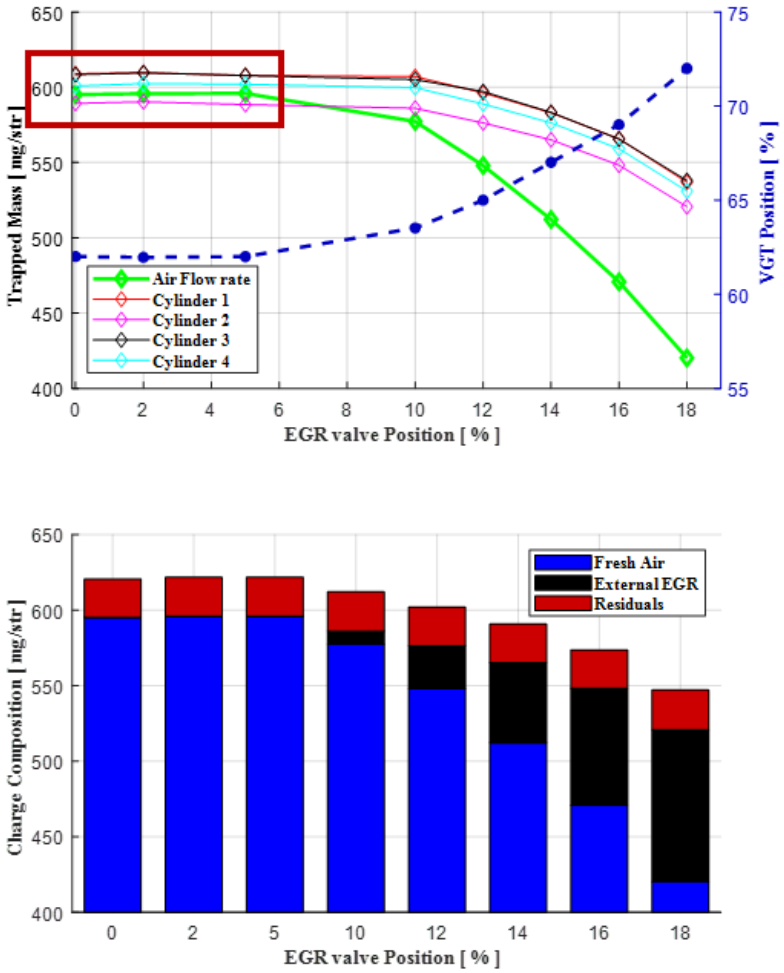

Figure 72. Cylinder Filling model behavior and validation, top subplot, during EGR valve sweeps and charge composition for cylinder 2, bottom subplot (Fresh air, residuals and external EGR). The VGT actuator movement allows to keep boost pressure at its target value.

To highlight the impact of EGR on combustion process and pollutant emissions production, several EGR valve sweeps were carried out for each one of the three engine operating conditions previously described. In addition, to correctly identify the best operating condition in terms of both pollutants and efficiency, GCI combustion was tested considering different CA50 values. As explained above, during these experimental tests, both IMEP and CA50 were kept at their target values activating the combustion controllers schematized in Figure 55, while the boost pressure controller kept intake pressure at a constant value compensating the turbine power reduction generated by the (partial) exhaust flow recirculation. Table 10 summarizes the best operating conditions obtained for each engine operating point analyzed, hereafter referred to as optimal conditions.

Engine Point name	Engine Speed [rpm]	IMEP [bar]	MFB50 sweep [deg bTDC]	Best MFB50 [deg bTDC]	Boost Pressure [mbarA]	Gasoline Pressure [bar]	Intake Temperature upstream manifold [C]
Low-load	2000	8	From 6 to 14	**14**	1.5	500	50
High-load	2000	14	From 8 to 14	**12**	2.0	700	50
High-revs	3000	10	From 8 to 18	**12**	1.9	700	50

Table 10. Optimal engine operating conditions considered for EGR rate sweeps

Figure 73 shows the effect of EGR on ISFC in the tested engine operating points (reported in Table 10). As expected, increasing the CA50 at constant EGR valve position, the IFSC will rise (lower thermal efficiency). As explained before, since the EGR makes the combustion process slower, increasing the EGR valve position at a constant CA50 (keeping constant the intake/exhaust pressures) the combustion process will be characterized by higher fuel consumption. The operating conditions run at low (2000 rpm / IMEP 8 bar) and high (2000 rpm / IMEP 14 bar) load, reported in Figure 73 a) and b) respectively, clearly highlight the impact of the EGR and CA50 on ISFC. Furthermore, since higher engine speeds promote charge mixing, the operating condition reported in Figure 73 c) (3000 rpm / IMEP 10 bar) shows less pronounced dependency on the EGR because better air-fuel mixing is always achieved.

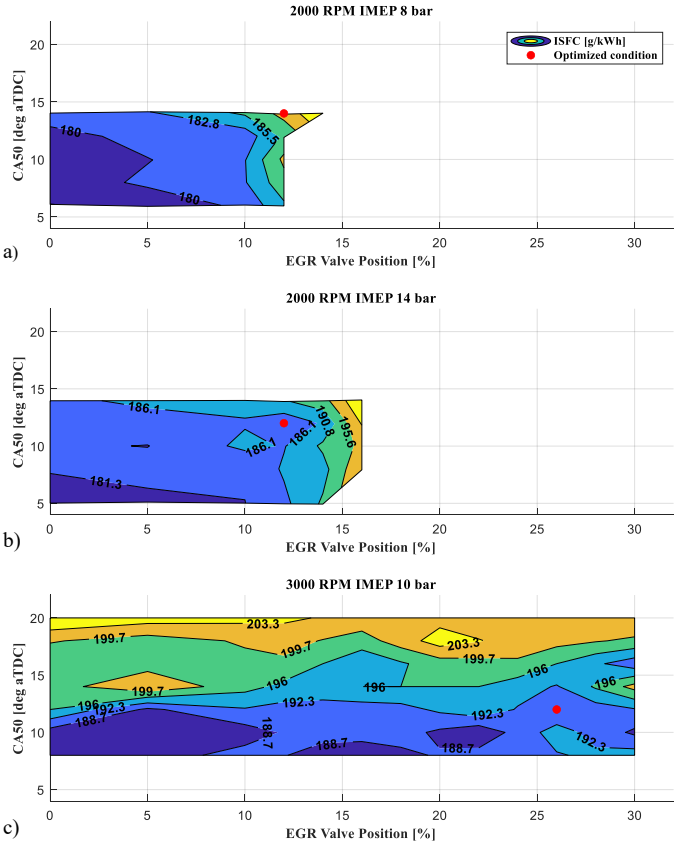

Figure 73. Impact of EGR on ISFC performing a CA50 sweep in different engine operating points: a) 2000 rpm – IMEP 8 bar, b) 2000 rpm – IMEP 14 bar and c) 3000 rpm – IMEP 10 bar.

Figure 74 and Figure 75 show the pollutants (NOx and FSN) measured during the experimental activity. As for the standard CI combustion process, NOx concentration decreases while increasing the EGR rate, mainly because of the lower oxygen content of the mixture, slowing down the combustion process. The main drawback using EGR is the FSN increment. As a matter of fact, due to lower oxygen concentration and poor air-fuel mixing (not enough to fully oxidize the injected fuel until the end of combustion), particulate matter will rise. Those trends can be observed both at high and low load and for different engine speeds. It is important to underline that combustion instability limits the GCI operating range (especially at low load) and therefore reduces the applicability of this combustion approach. The reported maps also show the best pollutants-efficiency trade-off for each analyzed conditions (red dots). Such optimized conditions identified through this experimental activity confirm that, to limit NOx production, GCI combustion needs high values of EGR.

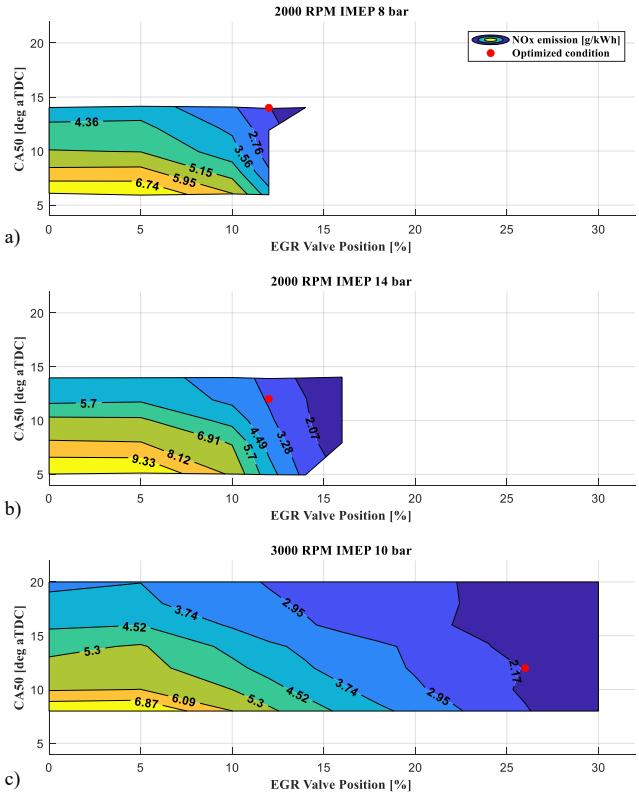

Figure 74. Impact of EGR on NOx production performing a CA50 sweep in different engine operating points: a) 2000 rpm – IMEP 8 bar, b) 2000 rpm – IMEP 14 bar and c) 3000 rpm – IMEP 10 bar.

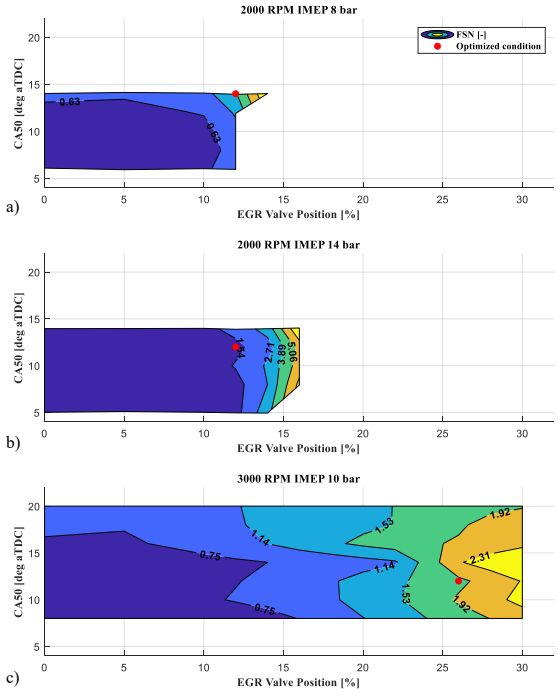

Figure 75. Impact of EGR on FSN production performing a CA50 sweep in different engine operating points: a) 2000 rpm – IMEP 8 bar, b) 2000 rpm – IMEP 14 bar and c) 3000 rpm – IMEP 10 bar.

Since the aim of this activity was to study the effect of EGR on GCI combustion, a deeper analysis of the impact of the exhaust gases on combustion process and performances using the in-cylinder pressure sensors was performed [30]. Focusing the attention of the best MFB50 for each engine operating conditions (identified through the previous activity), further considerations about the effect of EGR on gasoline autoignition and combustion propagation were made. By using the developed cylinder filling model and the measured air flow, it was possible to calculate the EGR rate for each test and, consequentially, to identify the best condition (fresh air-EGR) for minimizing both thermal efficiency and pollutants production.

The effect of EGR on efficiency and pollutants for the high-load operating point run at 2000 rpm – 14 bar IMEP is reported in Figure 76. As a matter of fact, increasing EGR rate until 14%, NOx concentration strongly decreases, while efficiency appears to remain almost constant and FSN slowly increases from 0.6 to 2.13. A comparative analysis of ISFC and pollutants with respect to the Diesel reference condition (Figure 76) clearly shows that 9% might be selected as the EGR rate assuring the efficiency/pollutants trade-off for this condition. In this case, ISFC, NOx and PM are all significantly improved with respect to the calibrated CDC, while higher EGR rates would produce a quick rise in FSN and ISFC, also exceeding the Diesel reference thresholds.

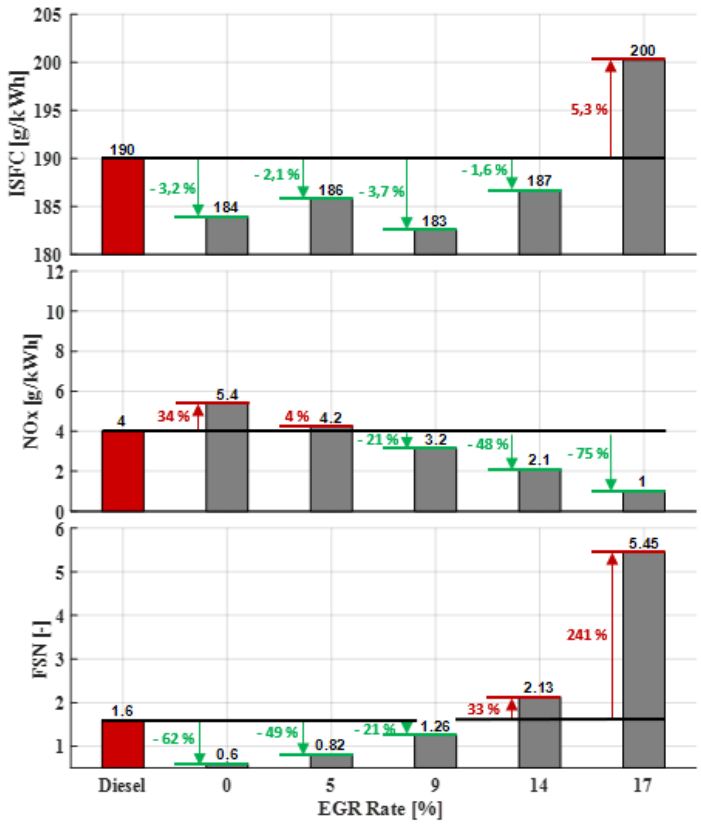

Figure 76. Comparison of ISFC, NOx and soot emissions between GCI combustion with external EGR for the high-load operating condition at 2000 rpm, IMEP=14 bar, CA50 12 deg and Diesel Reference

As for the standard CI combustion process, charge dilution with external EGR decreases the amount of oxygen available for fuel oxidation and the peak combustion temperature, consequently the quantity of NOx produced decreases. Furthermore, particulate matter increases, mainly because oxygen and air-fuel mixing are not enough to fully oxidize the injected fuel until the end of combustion. This is clearly shown in Figure 77, which reports the relative air-fuel ratio measured during the EGR rate sweep.

Furthermore, it is interesting to focus on intake and exhaust temperatures during EGR sweeps. Figure 77 clearly shows the rise in both temperatures as the EGR rate increases. In fact, the temperature of the recirculated gases is usually higher than the temperature of the fresh air, as a result, when EGR is recirculated, the intake manifold temperature increases. Due to the engine layout, the EGR comes from the exhaust to the intake manifold directly through the cylinder head. Therefore, since the air temperature before intake manifold was kept constant thought TEMCO unit, the rise of intake manifold (and then exhaust) temperature showed in Figure 77 during EGR rate sweeps is mainly a consequence of the thermal mixing of fresh air (constant 50°C) and exhaust gases. Thus, if hotter fresh air is used at the end of the combustion process, exhaust gases will become even hotter resulting in an increase in exhaust gas temperature (bottom subplot of Figure 77).

It is important to clarify that also the lambda decrease might explain the rise of the intake temperature. However, by observing the tests with EGR rate below 14% reported in Figure 77, since both engine load and the center of combustion were kept constant during the EGR rate sweeps (fuel consumption and combustion duration can be considered constants), the lambda is decreasing due to the lower oxygen content of the mixture. Therefore, the rise of intake temperature for such conditions is generated only by the presence of hot exhaust gases in the intake manifold. When the EGR rate becomes greater that 14 %, the big amount of exhaust gases recirculated significantly slows down the combustion process decreasing the combustion efficiency (lower lambda values) and generating even higher exhaust temperature, and consequently higher intake temperature.

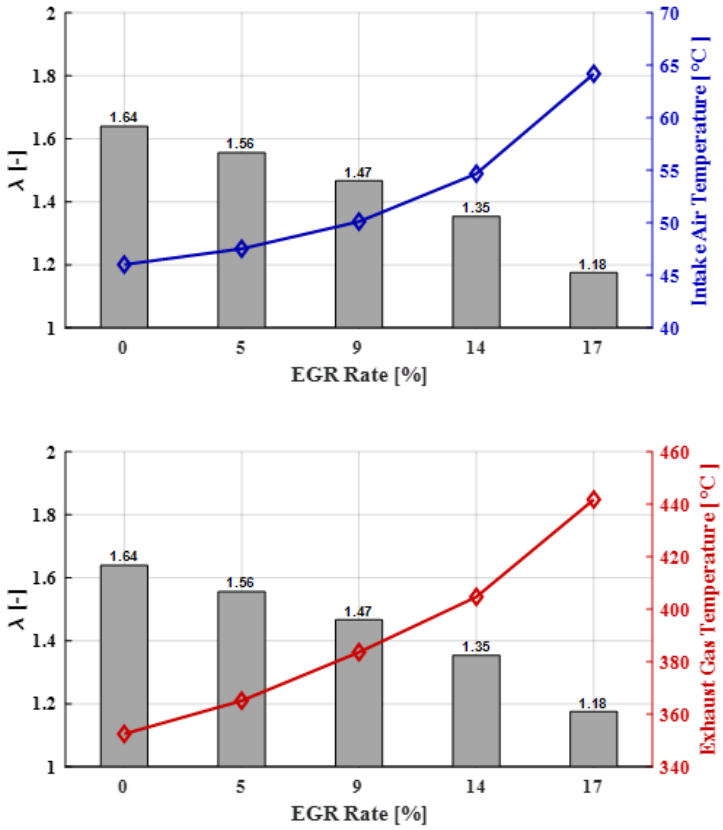

Figure 77. Lambda, Intake Air Temperature and Exhaust Gas Temperature during EGR rate sweep for high-load operating condition at 2000 rpm, IMEP=14 bar, CA50 12 deg

Figure 78 shows the effect of EGR on combustion duration (defined as CA10-90) and PPRR. It is important to notice that an increase in the EGR rate causes longer combustions for the same reasons above explained, however it seems to be ineffective on PPRR. This aspect will be better discussed later, where the impact of EGR on PPRR will be verified, comparing two different CA50 conditions.

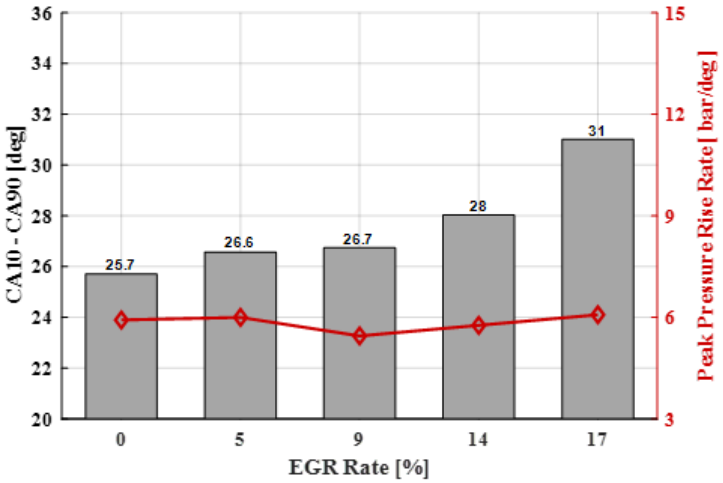

Figure 78. Combustion duration and Peak Pressure Rise Rate (PPRR) during EGR rate sweep for high-load operating condition at 2000 rpm, IMEP=14 bar, CA50 12 deg

To further explain how EGR affects the behavior of gasoline PPC, the acquired cylinder pressure traces were compared. As an example, Figure 79 shows 100 consecutive pressure traces (grey traces) and its average (red trace) for the high-load operating point (2000 rpm – 14 bar IMEP – CA50 12 deg aTDC) operated without (top subplot) and with external EGR (bottom subplot).

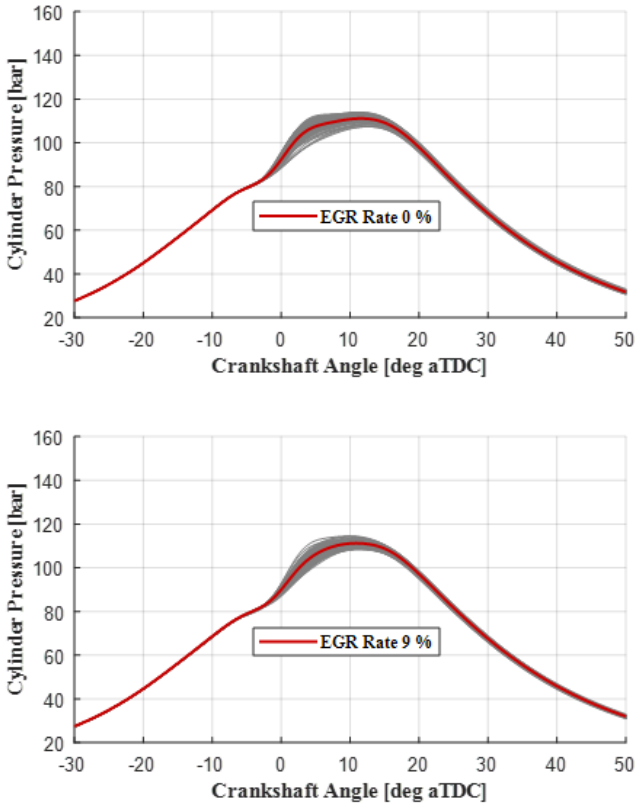

Figure 79. In-cylinder pressure measured for high-load operating condition at 2000 rpm, IMEP=14 bar, CA50 12 deg. EGR rate effect on combustion process. EGR rate 0% (top subplot) and 9% (bottom subplot)

As it can be observed, cycle-to-cycle variability is very low in both cases (with and without EGR). Despite the average pressure traces look reasonably similar, the major impact of external EGR is visible on the start of the combustion process, i.e., on the ignition mechanism of the Pilot injections. Focusing the attention on the pressure traces in Figure 79, especially on the angular region between 0 and 5 deg, it is easy to notice that the first stage of the combustion process is strongly affected by the recirculated gases. In fact, the pressure trace obtained without EGR is characterized by a rapid pressure rise until 5 deg, then the combustion process becomes slower until the maximum pressure peak is reached (approximately at 10 deg). When the external EGR is used (EGR rate approximately 9% in this case), the above-described rapid pressure rise disappears, highlighting that EGR slows down the ignition process of gasoline.

To further highlight the effect of EGR on the start of the combustion process (especially on the ignition of the Pilot injections), the analysis of the RoHR (average value of 100 consecutive cycles) calculated from the in-cylinder pressure traces measured during the EGR sweep reported in Figure 76 was performed. It is interesting to notice that the combustion process clearly shows two main stages: a pre-mixed portion (impulsive, long ignition delay) mainly related to the combustion of the amount of fuel introduced during the Pilot injections, and a diffusive portion mainly related to the combustion of the fuel introduced with the Main injection (ignition delay reduced by the energy released by the combustion of the Pilot injections).

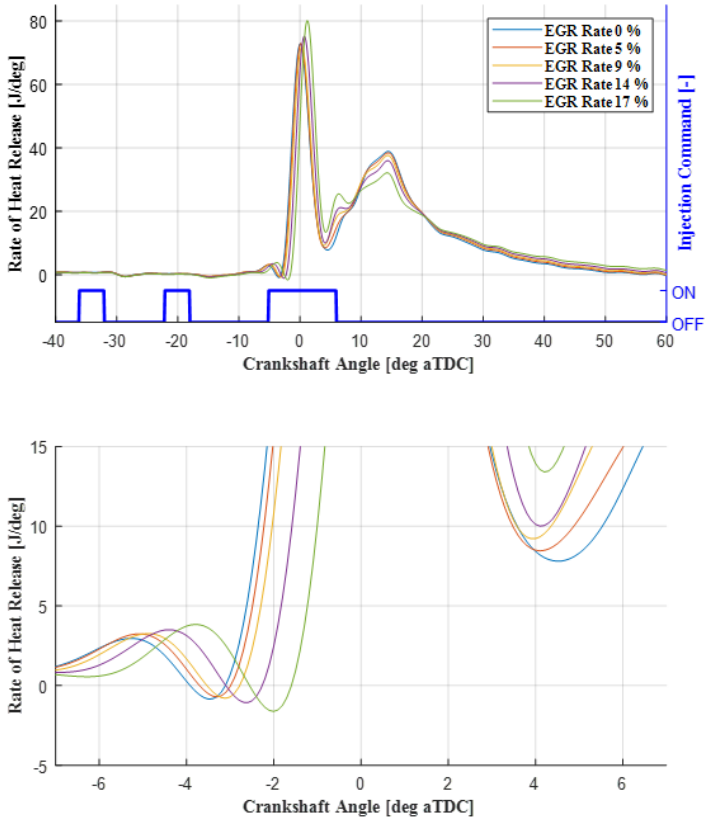

Figure 80. RoHR traces during EGR rate sweep for high-load operating condition at 2000 rpm, IMEP=14 bar, CA50 12 deg [32]

With the aim of highlighting the effects of EGR on GCI combustion, Figure 80 shows the RoHR of the "high-load" operating condition with different EGR rates. From the analysis of Figure 80 clearly arises that the presence of exhaust gases strongly affects the combustion of Pilot injections (and consequently the whole combustion process). Charge composition and stratification strongly impact the ignition mechanisms of pilot injections (chemically driven) in compression-ignited engines [24, 28, 33].

Regarding the ignition phase, the analysis of the heat released confirms that, when charge dilution with the exhaust gases is increased, the first combustion stage becomes more and more impulsive (while all the other control parameters, i.e., injection pattern, rail pressure and boost pressure are kept constant). Despite the intake temperature rise would suggest a decrease of the ignition delay for the pilot injections [35-37], Figure 80 shows that the ignition delay reduction due to the temperature rise is lower than the effects related to the chemical inertia of EGR (which retards the auto-ignition). As a result, the ignition delay of the pre-injections increases with the EGR rate. Furthermore, focusing the attention around the TDC, it is possible to observe that longer ignition delays contribute to the impulsiveness of the pre-mixed (first stage) combustion portion, since the tests run with higher EGR rates show higher RoHR peaks. Longer ignition delays mean that air and fuel have more time to mix, therefore the amount of charge that auto-ignites becomes higher.

The above-described behaviour can be also observed in Figure 81, which reports the PPRR measured with CA50 equal to 5 deg ATDC (same speed and load of the tests shown in Figure 80). In this case, EGR rate equal to 5% slightly fastens the combustion process with respect to the reference test without EGR (the temperature increase due to the hot residuals is dominant and reduces the ignition delay). Then, further EGR rate increases lead to longer ignition delays and more impulsive combustions.

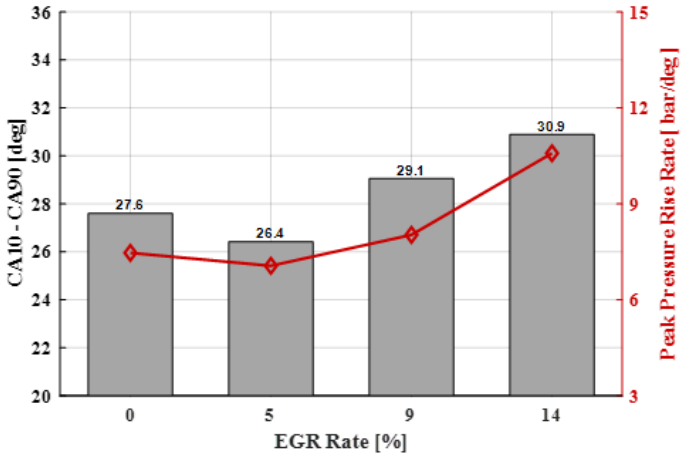

Figure 81. Combustion duration and Peak Pressure Rise Rate (PPRR) during EGR rate sweep for high-load operating condition at 2000 rpm, IMEP=14 bar, CA50 5 deg [32]

In addition, the effect of EGR can be observed also on the diffusive stage of the combustion process, approximately from 10 to 60 deg aTDC in Figure 80. The exhaust gases recirculated in the combustion chamber slow down the mixing process between air and the fuel introduced with the Main injection. As a result, the diffusive combustion portion becomes slower (lower values of RoHR peak) and longer compared to the reference condition without EGR. Figure 78 and Figure 81 summarize the effect of EGR on combustion duration. All the comments about the combustion process confirm the GCI combustion pollutant emissions (NOx and soot) trends reported in Figure 76 for the high-load operating point.

The above considerations, based on the analysed experimental tests, confirm that a proper EGR rate calibration is crucial to operate the engine at the best compromise between efficiency and pollutants (both can be improved with respect to standard CDC) while guaranteeing engine reliability (PPRR lower than 10 bar/deg) [34]. As a matter of fact, the use of recirculated gases affects RoHR shape and combustion location within the cycle, as clearly highlighted by the steady-state tests run varying the EGR rate and keeping constant start and duration of the injections.

All the above-described evidence can be applied also to the “high-revs” operating point (3000 rpm – 10 bar IMEP). Figure 82 shows pollutants and ISFC for the “high-revs” condition. In this operating point, the impact

of EGR (EGR rate from 5 % to 20 %) on combustion efficiency seems to be marginal (ISFC quite constant). A comparative analysis of ISFC and pollutants with respect to the Diesel reference condition (Figure 82) shows that an EGR rate approximately equal to 18% might be selected as the EGR rate reaching the efficiency/pollutants trade-off for this condition (both fuel consumption and emissions are improved with respect to the calibrated CDC). Regarding the emissions of NOx and FSN (Figure 82), the "high-revs" engine condition shows trends similar to the ones already discussed for the for the "high-load" operating point.

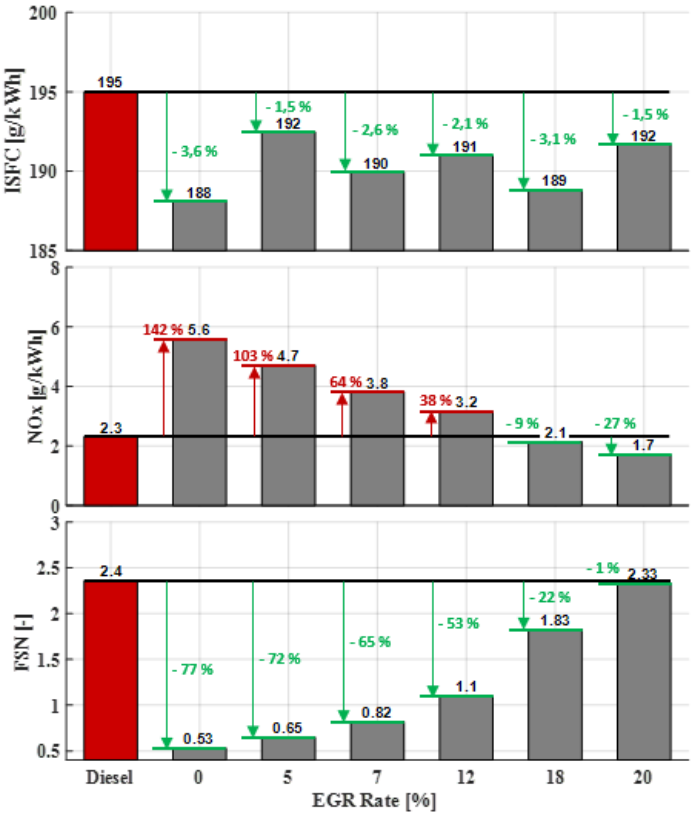

Figure 82. Comparison of ISFC, NOx and soot emissions between GCI combustion with external EGR for high-revs operating condition at 3000 rpm, IMEP=10 bar, CA50 12 deg and Diesel Reference

The comparison between the average pressure traces with and without EGR (Figure 83) still highlights the impact of EGR on the ignition delay. By the analysis of the pressure traces between 0 and 10 deg aTDC, it arises that the first stage of the combustion process is slightly retarded when an EGR rate equal to 18% is used (selected as optimal compromise between pollutants and efficiency).

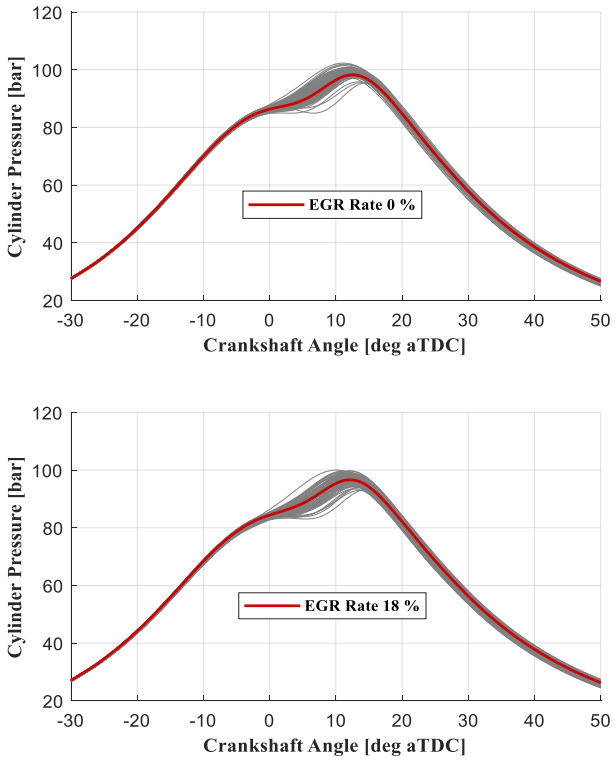

Figure 83. In-cylinder pressure measured for high-revs operating condition at 3000 rpm, IMEP=10 bar, CA50 12 deg. EGR rate effect on combustion process

To analyze more in depth the effect of EGR in the "high-revs" condition, the average RoHR traces, measured during the EGR sweep, were reported in Figure 84. As discussed for the "high-load" condition, exhaust gas recirculation affects both gasoline PPC combustion stages (premixed and diffusive). From the observation of Figure 84, it is possible to notice that, at higher engine speed (3000 rpm), the impact of EGR on the ignition delay varies with the amount of EGR rate. In particular, the charge temperature increase due to the hot recirculated gases fastens the spontaneous ignition of the air-fuel mixture when the EGR rate is lower than 12%, which means that (when the mass of recirculated gases is low) the temperature increase is dominant with respect to the higher chemical inertia due to the exhaust gases. This effect, not clearly visible in the tests operated at 2000 rpm and IMEP = 14 bar, might be (at least partially) explained by the higher turbulence in the cylinder at higher engine speed. When the EGR rate overcomes 12%, the effect of the recirculated gases becomes similar to the one discussed for the "high-load" condition, i.e., the ignition delay soars together with the impulsiveness of the first pre-mixed combustion stage (visible observing the maximum RoHR peak).

As highlighted in the analysis of the "high-load" tests, the presence of the recirculated gases in the combustion chamber also affects the diffusive stage of the combustion. As clearly visible in Figure 84, approximately in the angular range between 15 and 20 deg aTDC, increasing the EGR rate makes the diffusive portion (of the heat release) slower and longer (the presence of exhaust gases slows down the mixing process between air and fuel).

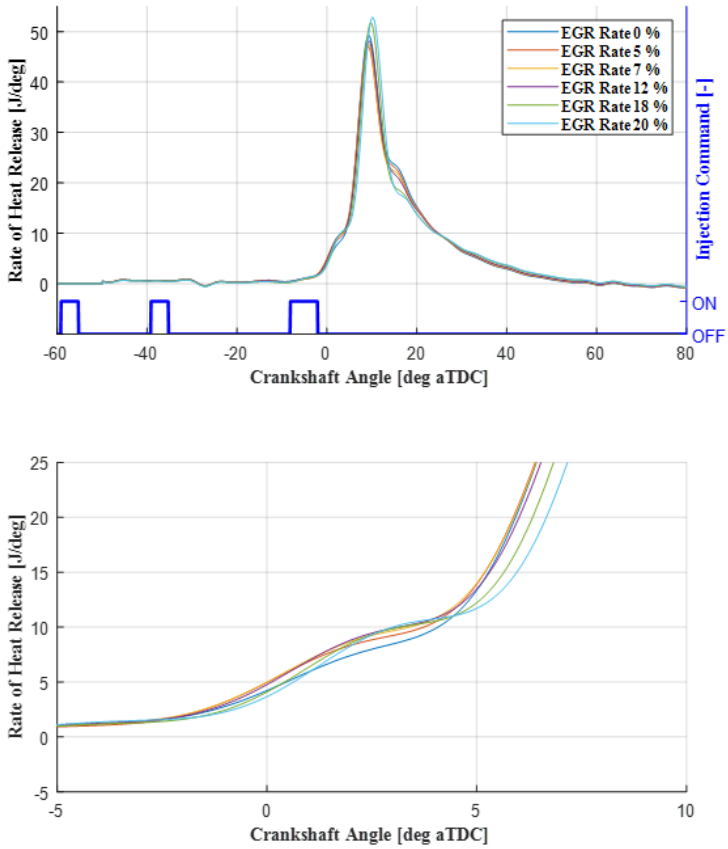

Figure 84. RoHR races for high-revs operating condition at 3000 rpm, IMEP=10 bar, CA50 12 deg. EGR rate effect on combustion process

The last engine operating point analyzed in this part is the "low-load" condition (2000 rpm – 8 bar IMEP), where the engine is operated at the same rotational speed of the high-load point, but with less injected fuel. As already discussed, these sweeps were operated at a leaner relative air-fuel ratio (approximately 2.4) compared to the "high-load" condition (approximately 1.5). When the engine is operated in GCI mode, the relative air-fuel ratio needs to be increased to maintain the boost pressure high enough to guarantee a robust gasoline auto-ignition. For the engine under study, this results in a minimum boost pressure around 1.5-1.6 bar (the lower limitation varies with the intake temperature [35, 36]), which limits the minimum load at which combustion can be operated in stable conditions nearly at IMEP = 5 bar (if the load is further reduced, the relative air-fuel ratio becomes too lean to guarantee a stable combustion process).

As for the previously analyzed operating conditions, Figure 85 shows ISFC and pollutants for the "low-load" engine operating point. In this case, the use of recirculated gases has a remarkable impact also on the measured fuel consumption, probably because adding EGR to a barely stable auto-ignition (operated at very lean relative air-fuel ratio) immediately reduces combustion effectiveness. Regarding the pollutant emissions, trends similar to the ones discussed for the previous operating conditions can be observed: particulate matter increases with the EGR rate, while NOx emissions are reduced. Unfortunately, in this operating point, it is no longer possible to identify an EGR rate clearly beneficial both in terms of combustion efficiency and emissions. As a matter of fact, the use of an EGR rate approximately equal to 14% returns a slight improvement in ISFC and particulate matter but measured NOx emissions exceed the level of the calibrated CDC.

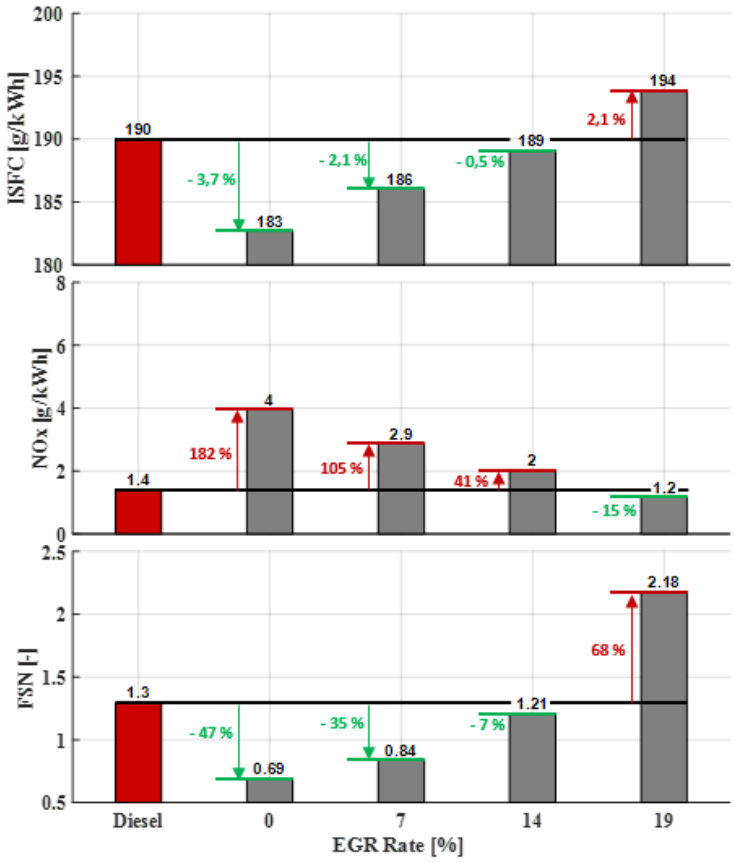

Figure 85. Comparison of ISFC, NOx and soot emissions between GCI combustion with external EGR for low-load operating condition at 2000 rpm, IMEP=8 bar, CA50 14 deg and Diesel Reference

The observation of the pressure traces obtained without and with EGR (Figure 86) confirms that EGR increases the ignition delay of the Pilot injections. Focusing the attention on the angular interval between 0 and 10 deg, it is easy to notice that the first stage of the combustion process is retarded when the EGR rate is equal to 14% (compared to EGR rate = 0%). This is even more visible in Figure 87, where the RoHR calculated from the average pressure traces of the whole EGR rate sweep are compared.

All the previously described effects of the EGR on the GCI combustion are visible also in the average RoHR traces of the "low-load" tests. As it can be observed in Figure 87, moving toward higher EGR rates, the ignition delay of the first premixed stage increases (chemical inertia effect due to the additional exhaust gases). Furthermore, increasing the EGR rate, the diffusive combustion, reported in Figure 87 approximately in the range between 10 and 20 deg aTDC, becomes slower and longer compared to the reference condition without EGR.

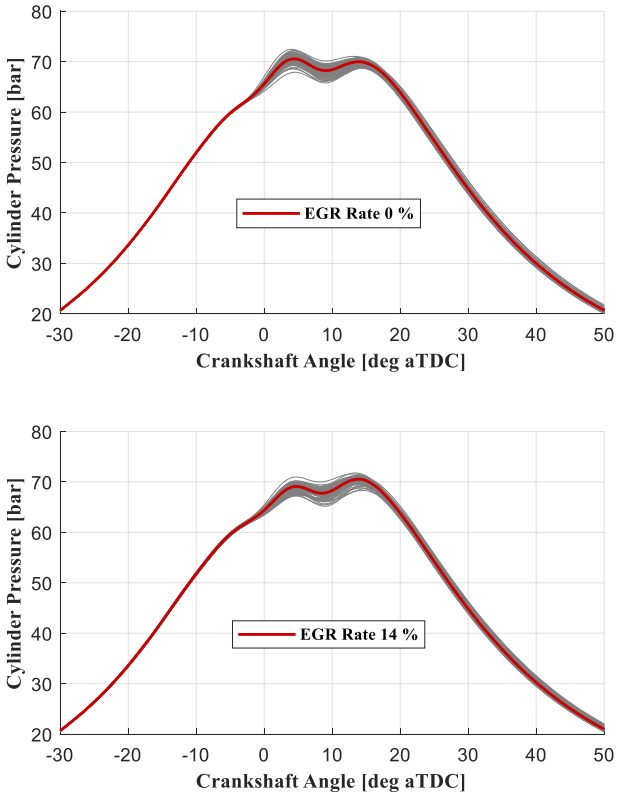

Figure 86. In-cylinder pressure measured for low-load operating condition at 2000 rpm, IMEP=8 bar, CA50 14 deg. EGR rate effect on combustion process

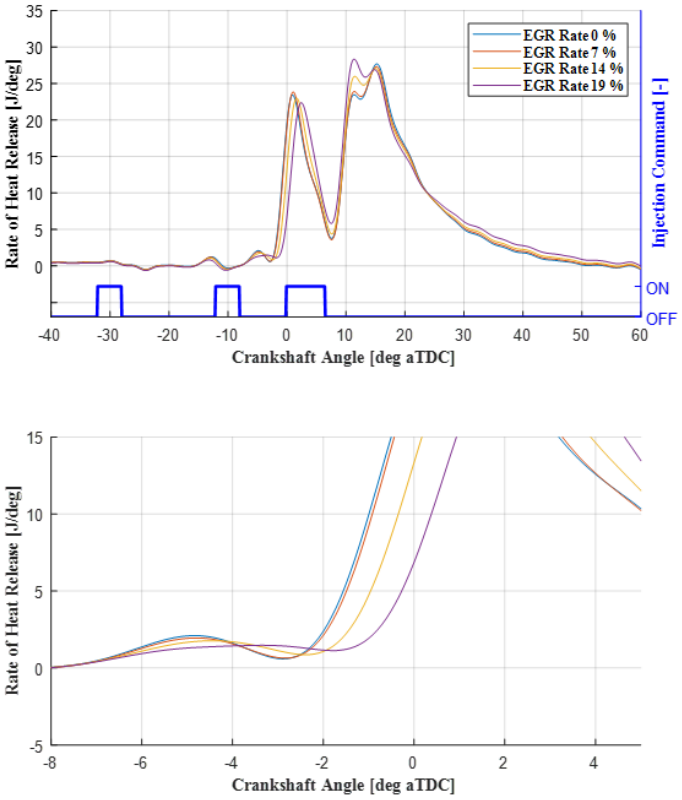

Figure 87. RoHR traces during EGR rate sweep for low-load operating condition at 2000 rpm, IMEP=8 bar, CA50 14 deg

The above-described experimental results proved that it is possible to perform stable and reliable GCI combustion in a very common light-duty compression ignited engine without any hardware modification (external supercharger was used only during cranking) using multiple injections strategy [30]. Several tests were carried out to quantify engine-out emissions and efficiency of the LTC under study. By the analysis of the obtained results, it was possible to verify benefits both in terms of pollutants and efficiency of GCI combustion with respect to CDC in the same engine. It is important to mention that to improve GCI performances (and give benefit compared to CDC), the use of high percentage of EGR rate was needed.

Even though GCI combustion proved to be effective reducing pollutants and efficiency, the management of the combustion process (especially the ignition phase, chemically driven) represents the main challenge on GCI development. Based on the experimental evidence collected during the previous activity, the following sections of the PhD dissertations focuses on control-oriented modelling development aimed at improving combustion controllability and to extend the GCI operating range.

2.4 Model-based Fuel Quantity Correction Strategy for Common-Rail High-Pressure Injection Systems

In the previous sections of this works it was demonstrated the benefit in terms of engine-out emissions and efficiency running GCI combustion in a standard light-duty compression ignited engine. Despite the potential of the considered LTC was proved by the activities described above, to properly control GCI combustion, a high-pressure multiple direct injection strategy is needed. As a matter of fact, previous works clearly show the enormous benefit given by pilot injections both in terms of pollutants reduction, such as NOx, and combustion stability improvements. As for Conventional Diesel Combustion (CDC), the rise of in-cylinder pressure and temperature generated by pilot injections combustion allows minimizing the ignition delay of the following injections, making the whole combustion process more stable and smoother. As a result, a proper management of pilot injections in terms of injected fuel quantity, number of injections and angular positions plays a key role to ensure GCI combustion controllability, especially center of combustion and delivered torque.

To meet such requirements, the high-pressure Common Rail system (CR) represents the most common injection system testing GCI combustion. Thanks to the use of solenoid hydraulic assisted injectors, modern Common Rail systems guarantee fast and accurate injection management also with the high pressures required by gasoline PPC (up to 1000 bar). Despite the high flexibility performing multiple injections with CR systems, hydrodynamic effects, which are generated by the water hammer consequent to the injector nozzle closing after each injection, affect the actual quantity of fuel injected during the following injections, especially when the amount of fuel injected is very low (in the range of 1 mg/stroke) and the relative distance between injections is small (lower than 2000 μsec). As widely discussed in literature, due to the propagation of pressure waves, the mass of fuel injected during the second of two consecutive injection pulses may vary significantly (up to 50%) around the nominal value, producing negative effects on the GCI stability. Thus, a fuel quantity correction strategy is required to achieve accurate fuel injection management.

With the aim of investigating pressure waves and their effects on the injection quantity, several approaches were used. Coppo et al. [37] presented a numerical model for a CR system finding that the hydraulic layout (feed duct length and diameter) and injector nozzle had a relevant impact on pressure wave propagation. Boudy et al. [38] investigated the influence of fuel properties on the pressure wave in the injector feed duct. They found that fuel density is the main property that influences the amount of mass injected, because it changes fuel viscosity and bulk modulus. Based on the above-mentioned findings, many works were focused on clearing pressure waves effects. Su et al. [39] experimentally obtained an ideal filter for the elimination of the water hammer. Gupta et al. [40], Bianchi et al [41, 42] and Ferrari et al. [43-45] showed that water hammer effects can be reduced changing the system layout but increasing the cost of designing and manufacturing of

the whole injection system. Bai et al. [46] presented a correction strategy based on the reconstruction of injected quantity oscillations, for a typical pilot-main injection strategy, without considering the source of this phenomenon, i.e., pressure waves.

In this section of the PhD dissertation, a physical model of pressure waves propagating in a standard high-pressure CR system fueled with gasoline based on the equivalent mass-spring-damper system is presented [47]. Through a specifically designed flushing bench equipped with a high-frequency acquisition system, a wide experimental activity was conducted highlighting pressure waves behavior on the feed duct using different injection strategies. To properly reconstruct pressure waves propagation on the feed duct, a frequency analysis, aimed at finding the main carriers of the pressure waves (both with single and multiple injections) was carried out varying fuel injection pressure and dwell time (DT) between injections. To verify the model applicability and robustness, different fuel, injectors, and placement on the rail were tested. Finally, the obtained results were used to develop a fuel quantity fluctuation correction strategy based on the pressure wave reconstruction during multiple injections of gasoline, which could be directly implemented in the custom ECU improving the GCI combustion management.

2.4.1 Experimental Layout

The experimental activity was carried out on a specifically designed high-pressure CR test bench, based on a light-duty 1.3L diesel engine injection system with 4 solenoid injectors fueled with RON 95 commercial gasoline (same injection system and fuel used during GCI combustion investigation). To study pressure waves under actual operating conditions, the high-pressure line was not changed with respect to the engine-mounted configuration, i.e., pipeline diameter and length were maintained as in the original layout. The main technical characteristics of the CR system under study are summarized in Table 11.

Number of Injectors	4
CR pump	Bosch CP1
Injector type	CRI2-16 M2
Feed duct length	93 mm
Feed duct diameter	20 mm
External Rail length	250 mm
External Rail diameter	200 mm

Table 11. High-pressure Common Rail system technical characteristics.

To simulate the fuel thermal inertia on CR low-pressure side (which is typically composed by long pipes connecting the tank with the high-pressure pump) a diathermic oil thermoregulation unit (TEMPCO T-REG HCE 609/15-O) was installed between the low-pressure pump and the high-pressure pump. The thermoregulation unit allowed to accurately manage the fuel temperature during all tested conditions excluding external thermal effects on the pressure wave propagation, such as frequency or amplitude modifications [26, 48]. Furthermore, to consider the fuel tank thermal inertia, a water-fuel heat exchanger was placed before the low-pressure pump. Finally, the low-pressure line was kept at constant pressure of 4.5 barA (standard condition for the CR system under study) using a mechanical pressure regulator.

To accurately investigate pressure waves and their consequences on the effectively injected fuel, several sensors were mounted on the test bench. In addition to standard CR system sensors, i.e., rail-mounted high-pressure fuel sensor (PRail), low-pressure and temperature fuel sensors, to highlight pressure wave behavior during the injection process, the high-pressure pipe between the rail and the injector was equipped with two piezoresistive pressure sensors Kistler 4067A, one close to the injector (PKist Inj Side) and the other close to the rail (PKist Rail Side). Furthermore, to monitor the oscillations in injected fuel generated by water hammer propagation, two different gasoline consumption measurement systems (AVL BALANCE 733S and high-precision ultrasonic flowmeter FlowSonic FFM LF DP-010-02) were installed on the test bench low-pressure

line. Both measurement systems are fully closed (AVL Balance closed vessel and FFM closed pipe) to avoid fuel evaporation and, consequentially, excluding measurement errors when high volatile fuels are used. Fuel consumption measurement redundancy allowed the definition of proper acquisition strategies for each tested injection pattern, obtaining consistent consumption measurements also with different instruments and small injected quantities. These strategies provided a reliable fuel consumption measurement also when a different fuel was used (the high-precision ultrasonic fuel consumption measurement was not available for both tested fuels). Finally, with the purpose of monitoring the heat exchange between fuel and diathermic oil (on the fuel side), two K-type thermocouples between inlet and outlet of the TEMPCO heat exchanger were mounted. Figure 88 shows the hydraulic layout of the high-pressure test bench.

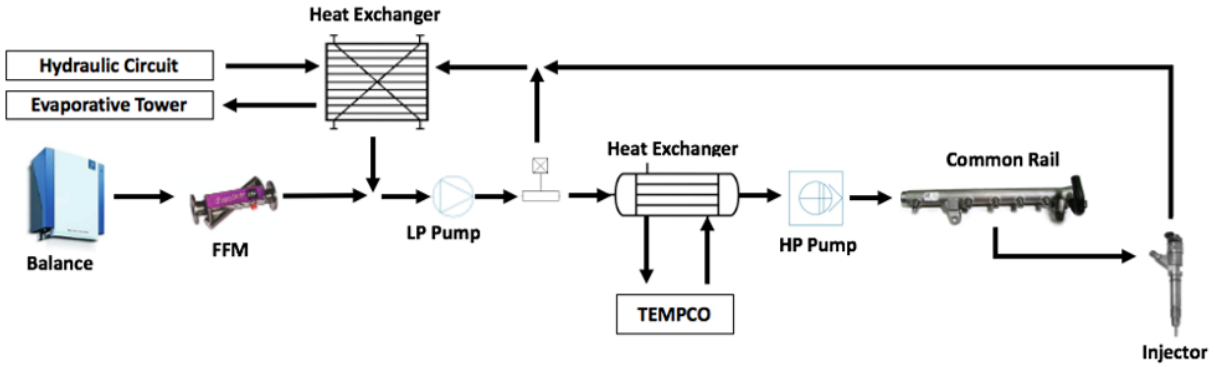

Figure 88. Flushing bench hydraulic layout.

Test bench control and data acquisition were managed by a specifically developed Rapid Control Prototyping (RCP) system based on National Instrument cRIO 9082 using LabView. Selecting proper acquisition frequencies for each signal (100 kHz for high-pressure sensors, to keep all the main carriers of the injection system significantly lower than the Nyquist frequency), the RCP system allowed to collect all the data needed for pressure waves analysis and modeling.

Regarding the fuel pressure management, it was performed keeping in motion the volumetric high-pressure pump with an electric motor (5.5 kW and maximum rotational speed of 3000 rpm) at constant rpm. The mechanical connection between the high-pressure pump and the electric motor, obtained with a toothed belt, was designed with the same gear ratio, used in the on-board application, for the connection between crankshaft and pump (the electric motor rotates twice as fast as the pump). Using the information coming from the encoder mounted on the pump shaft, the RCP system evaluated the pump speed, sending an analog command to a dedicated inverter managing the electric motor. Furthermore, acquiring the rail-mounted pressure sensor, the RCP system was able to manage the PWM command of the pump-mounted solenoid metering valve (MPROP) to keep the fuel pressure at the target value during each test. A picture of the high-pressure CR test bench is shown in Figure 89.

The injection strategy was managed using a fully programmable ECU (SPARK ECU, the same used to manage the fully converted GCI engine), based on National Instruments hardware and LabView software, overcoming the limitations that usually occur when a production ECU with standard control software is used with custom injection patterns. Despite the MPROP valve can be easily managed by SPARK ECU, with the aim of improving the test bench safety during the experimental activity, both MPROP duty and pump speed were managed by the RCP system. Furthermore, to improve testing operations, the injection parameters were controlled and logged using INCA software, provided by ETAS. Figure 90 reports the test bench control layout and the integration between the RCP system and SPARK ECU.

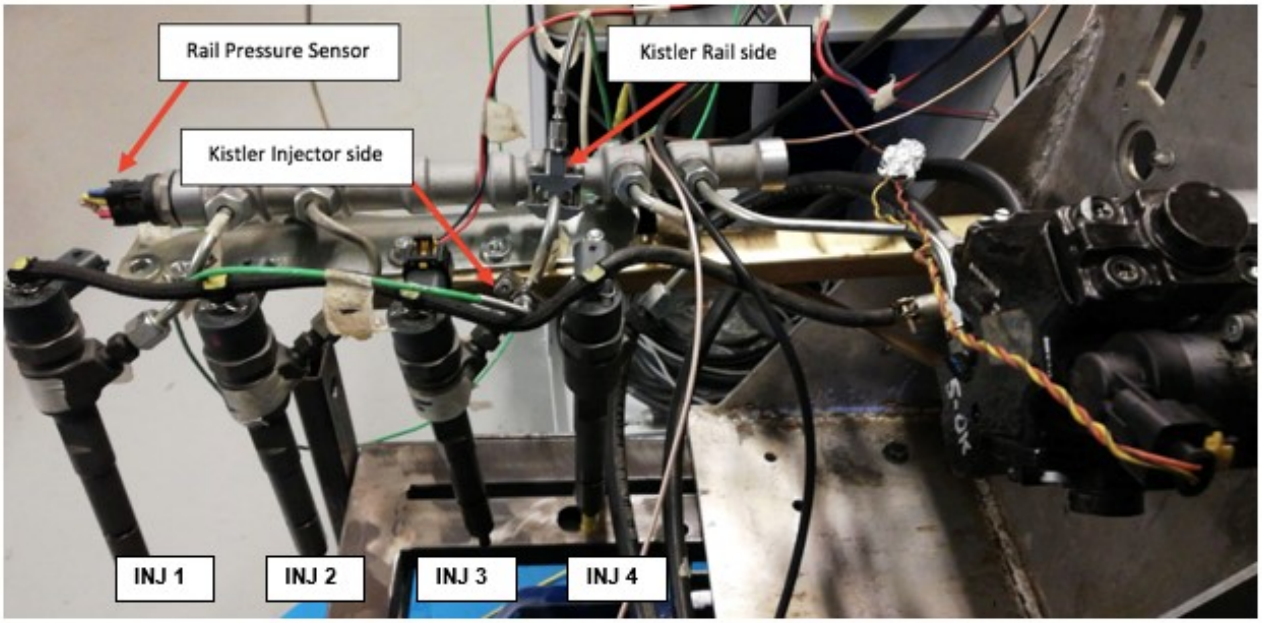

Figure 89. Flushing bench pressure sensors placement.

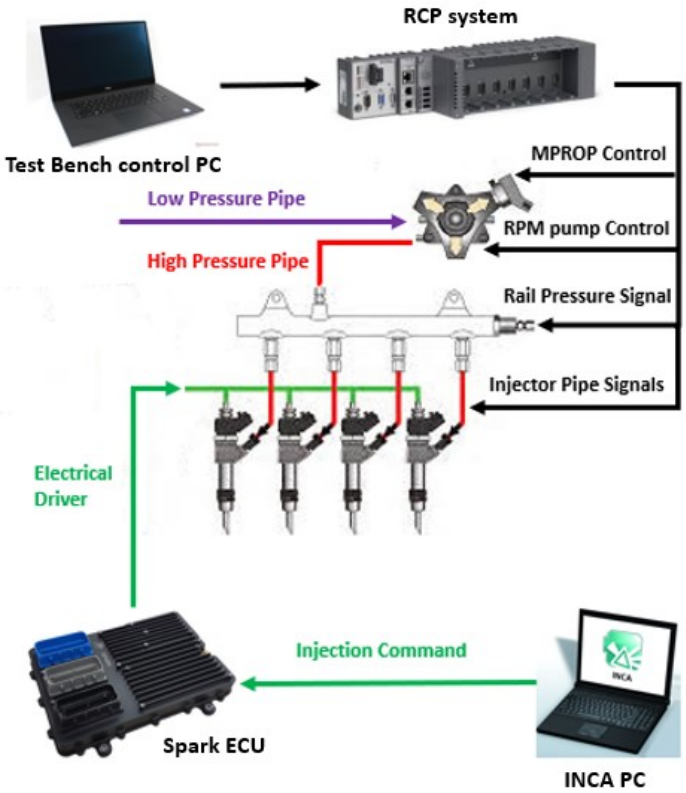

Figure 90. Scheme of flushing bench control and acquisition systems.

2.4.2 Pressure Waves Physical Model

The above-described testing layout, specifically realized for this work, was used to investigate pressure waves under different injection strategies, the goal being to develop a model-based pressure waves reconstruction (and compensation) strategy.

Hydraulic System Behavior Analysis

In literature, several works can be found [45, 48-51] describing the CR system behavior from different points of view: equivalent electrical, rotational, thermal, chemical, and mechanical systems were proposed. Furthermore, they also report that it is possible to obtain transfer functions linking the physical CR system properties with the equivalent system characteristics parameters [40-42, 52-53]. Therefore, with the aim of identifying the best approach to model pressure waves in the CR system, the authors focused the first part of the experimental activity on the study of the system behavior performing gasoline single injections. To do so, the whole experimental activity was carried out keeping 3 injectors closed (but connected to the rail) and activating only one injector.

Figure 91 shows the pressure signals coming from rail-mounted and high-pressure tubing-mounted sensors for a single injection pulse test and injection pressure of 700 bar. By the analysis of the piezoresistive pressure sensors signals, it is possible to notice that, when the injection occurs, a high frequency pressure wave is generated. This wave, produced by the mass discharged from the injector, propagates inside the feed duct from the injection event up to 20 ms after, when its energy is totally dissipated [52-53]. Because of the larger amount of fuel contained in the rail compared to that in the feed duct, and due the pressure drop generated by the duct-to-rail connection, the rail capacity can be considered as infinite, and therefore the rail-mounted pressure signal (PRail) does not contain the information of pressure oscillations. This evidence, confirmed by the literature, suggests that the pressure wave, triggered by the injection, propagates only inside each feed duct without generating cumulative effects in the near ducts.

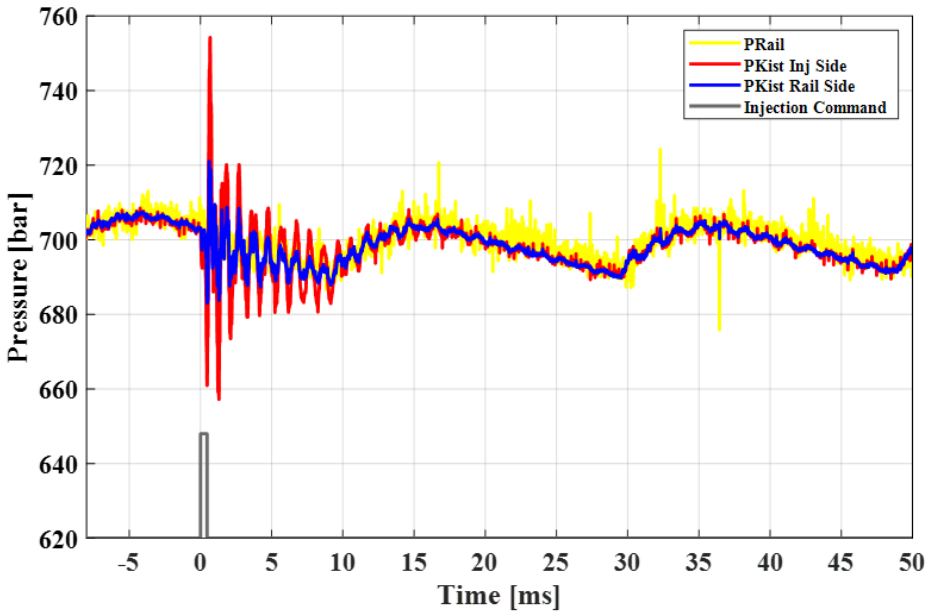

Figure 91. Experimental fuel pressure signals (acquired ad 100 kHz) generated by a single injection (per cycle, only one injector active) pulse strategy at gasoline pressure 700 bar, 1000 pump rpm and ET of 310 µs.

In addition, it is clear from the comparison of the piezoresistive sensors pressure traces that the effects of pressure waves are more visible, in terms of oscillations amplitude, closer to the injector. For this reason, to model the pressure oscillations generated by single and multiple injections, it has been considered the pressure traces coming from the piezoresistive pressure sensor closer to the injector because they represent the instantaneous fuel pressure, which directly determines the injected mass.

Furthermore, it is important to notice that both duct and rail mounted sensors show a low frequency oscillation representing the leakage flow rate compensation due to the closed-loop rail pressure controller behavior. As clearly highlighted by Figure 92 (top subplot), the instantaneous pressure traces acquired by the sensor closer to the injector during different injection cycles show the same high frequency oscillations generated by the injection, but different low frequency oscillations. The position of the leakage flow rate contribution moves on the injection cycle because the pressure controller actuation, which manages the MPROP valve duty cycle keeping constant rail pressure, is not phased with the injection event shifting the leakage compensation with respect to injection pulse.

To highlight the portion of the pressure oscillations related to the injection process, the average of 500 consecutive injection cycles has been considered. As Figure 92 (bottom subplot) clearly shows, averaging the pressure traces mitigated the acquisition noise and the leakage flow rate, highlighting only the pressure wave on interest (which occurs cycle-by-cycle) and its propagation time (from the injection event to 20 ms). Moreover, it is possible to see that the leakage contribution does not affect the bulk of the pressure oscillation (from 0 to 10 ms), but it becomes predominant when the oscillation amplitude decreases (10 ms after the injection event). For these reasons, the hydraulic system modeling was based on the average pressure trace reconstruction. As a result, the fuel system external conditions such as pump speed (even during transient) or the MPROP duty cycle which change only the leakage contribution, do not affect the modeling.

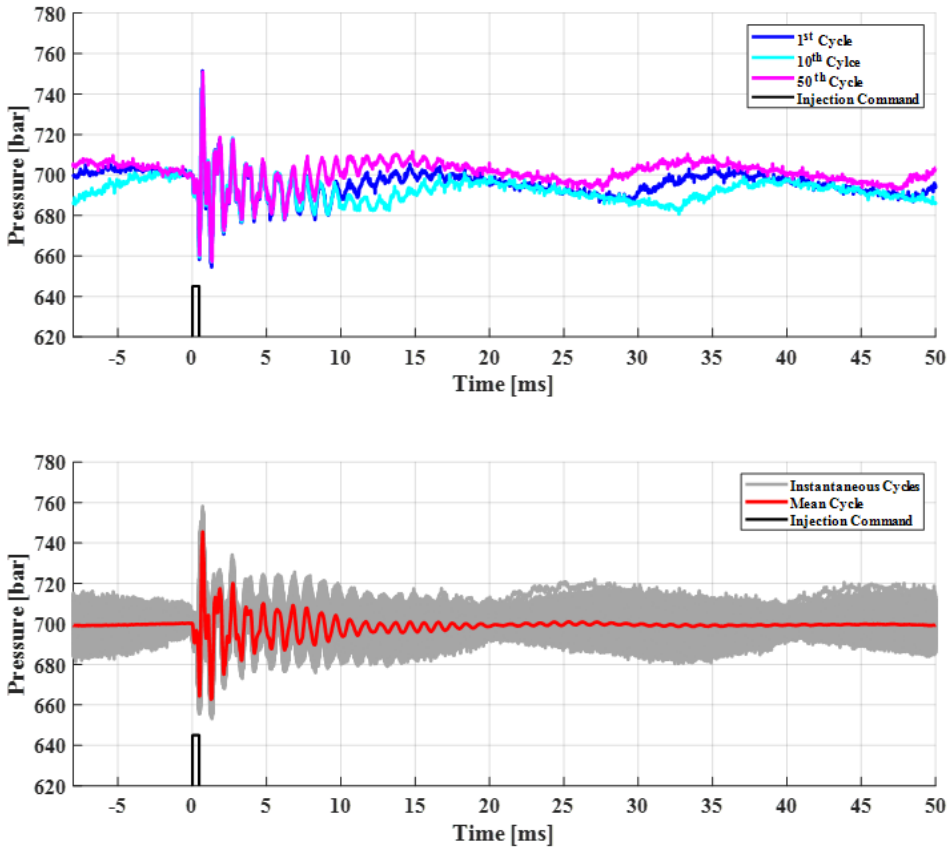

Figure 92. Piezoresistive injector-side pressure signals for (a) different injection cycles (acquired ad 100 kHz) and (b) average of 500 consecutive injection cycles at gasoline pressure 700 bar, 1000 pump rpm and ET of 310 µs.

From the observation of Figure 92 (bottom subplot) clearly arises that the average pressure trace during the injection cycle follows the typical behavior of an underdamped mass-spring-damper (MSD) vibration system. For this reason, to accurately predict the pressure wave in the feed duct triggered by the injection, a mechanical approach was followed. Finally, it is important to underline before the prominent pressure oscillations, the effect of the injector opening dynamics in terms of pressure drop. The upcoming section describes the pressure wave modeling approach based on MSD system.

Hydraulic System Modeling

In agreement with the similarity principle between mechanical and hydraulic system [45, 53], a sum of free responses of one-degree of freedom MSD systems, one for each main carrier contained in the experimental signal, was assumed to model the pressure wave during the injection process.

The free-response calculation for the well-known one-degree of freedom MSD system can be based on the analysis of the system reported in Figure 93 [54].

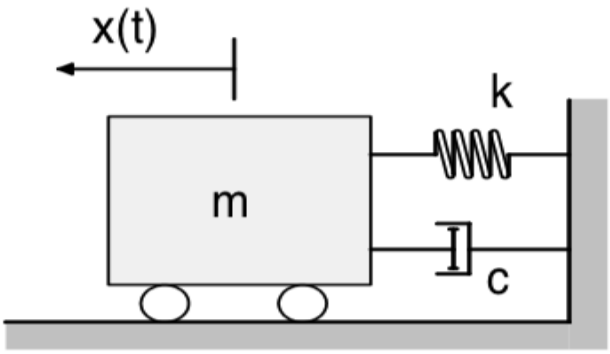

Figure 93. Schematic of Mass-Spring-Damper (MSD) one-degree of freedom system [54].

Equation 34 describes the motion of the system, in which x is pressure on the feed duct. The system parameters *m, k* and *c* represent the fuel inertia of the feed duct and injector, the fuel stiffness, and the damping, respectively.

$$m\ddot{x} + c\dot{x} + kx = 0 \qquad (34)$$

Considering as solution of Equation 34 the typical exponential form shown in Equation 35 [54], the characteristic equation of the vibration system can be obtained. As reported in Equation 36, it is a linear, ordinary homogeneous differential equation with constant coefficients.

$$x(t) = Ce^{zt} \qquad (35)$$

$$mz^2 + cz + k = 0 \qquad (36)$$

Thus, the natural frequency of the vibrational system ω_n, and the damping ratio ξ can be defined as reported in Equation 37 and 38, respectively.

$$\omega_n = \sqrt{\frac{k}{m}} \tag{37}$$

$$\xi = \frac{c}{2\sqrt{km}} \tag{38}$$

For the analysis of the damped system, it is useful to define the damped frequency of the vibrational system ω_d as a function of ω_n and ξ (Equation 39) which represents the actual frequency of the oscillation.

$$\omega_d = \omega_n \sqrt{1 - \xi^2} \tag{39}$$

Solving the differential equation showed in Equation 35 and applying the well-known Euler's formula, the free response of the MSD system can be written as reported in Equation 40, where in addition to the above-mentioned parameters x_0 and v_0 were considered as initial conditions (time equal to zero) of the system.

$$x(t) = e^{-\xi\omega_n t}(x_0\, cos(\omega_d t) + \frac{v_0 + \xi\omega_n x_0}{\omega_d}\sin(\omega_d t) \tag{40}$$

The following section describes the methodology developed by the authors to reconstruct the pressure oscillations during the injection cycle, based on a sum of one-degree of freedom MSD systems free responses, described by Equation 40.

Hydraulic System Characterization

To identify the number of free responses needed to reconstruct the pressure oscillations and highlight the main injection parameters effects on the hydraulic system behavior, such as injection duration (ET) and injection pressure, a frequency analysis for a single pulse injection strategy was performed.

The frequency content of the pressure oscillations can be summarized in Figure 94, which reports the pressure signal power spectrum from 0 to 4 kHz (higher frequencies do not have relevant energy content) for a single pulse injection strategy with gasoline pressure of 500 bar using different ET. It is important to notice that changing the injection duration, i.e., increasing ET, the power spectrum changes in amplitude but not in frequency. It means that the injection duration affects only the amplitude of the response without any modification in terms of frequency content.

The power spectrum, Figure 94, also shows 5 main carriers: the 1st around 16.6 Hz related to the injection frequency, the 2nd at 600 Hz, the 3rd at 830 Hz, the 4th at 1.05 kHz and the 5th at 2.2 kHz related to the system behavior (rail, duct and injector). Considering the identified main carriers, it is possible to notice that the 1st frequency can be neglected because it is not related to the pressure oscillation but only to the injection cycle (the frequency of 16.6 Hz corresponds to 1000 pump rpm, or 2000 engine rpm). The 3rd frequency can be considered the fundamental frequency of the hydraulic system because it shows the biggest amplitude for all the tested conditions. Due to the small distance in frequency and the huge difference in amplitude of the 2nd and the 4th main carriers with respect to the fundamental frequency, their contributions to the pressure fluctuation are not clearly visible in the instantaneous pressure trace. This observation suggests that the 2nd and the 4th frequencies could be neglected while modeling the pressure wave. On the contrary, despite the

smaller amplitude of the 5th frequency (compared to the fundamental frequency), the higher frequency makes it clearly visible in the pressure oscillation.

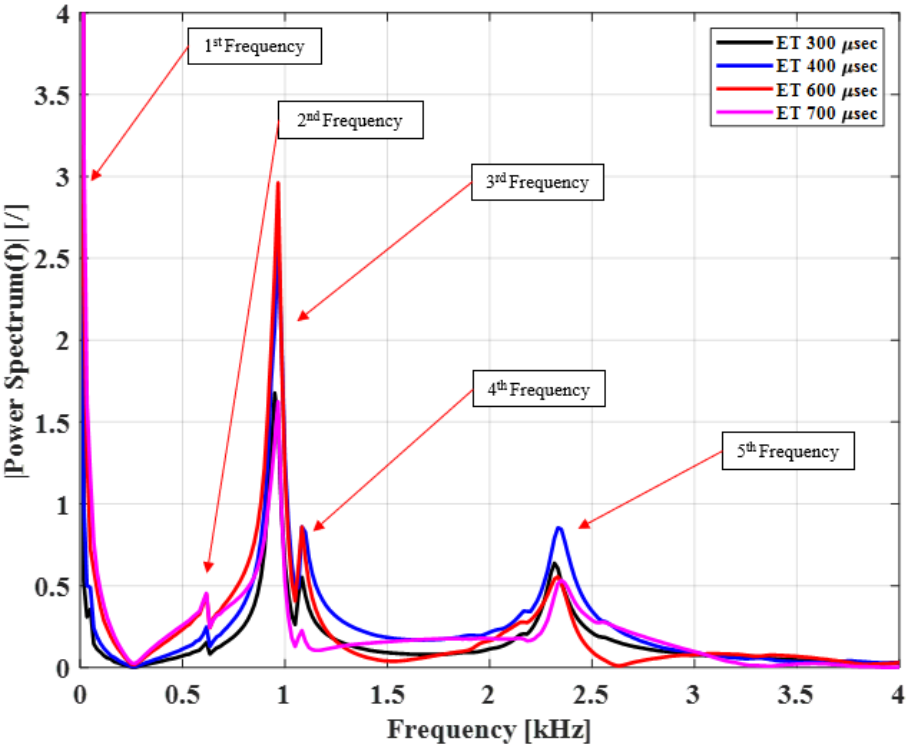

Figure 94. Frequency analysis (power spectrum) of the injector-side pressure signal generated by single injection pulse strategy at different ET with gasoline pressure 700 bar and 1000 pump rpm.

Based on the above-described considerations, to quantify the relevance of each main carrier with respect to the fundamental frequency on the pressure oscillation, the Relevance Carrier Index (RCI) was defined as reported in Equation 41. This index is composed by the product between the relative power ratio (P_{r_x}), which represent the energy contribution of the specific x-th carrier compared to the total energy of the identified main carriers, and the relative frequency distance (ΔF_x) from the 3rd frequency. Equation 42 and Equation 43 define the relative power ratio and the frequency distance, respectively.

$$RCI = P_{r\_x}\Delta F_x \tag{41}$$

$$P_{r\_x} = \frac{P_x}{\sum P_x} \tag{42}$$

$$\Delta F_x = \frac{F_x - F_3}{F_3} \tag{43}$$

Table 12 reports the RCI calculation for the power spectrum showed in Figure 94 at ET = 400 µsec. As it can be seen, despite the amplitude of the 4th and the 5th carriers is similar, the huge differences in the calculated RCI suggests that the 5th frequency cannot be neglected to properly reconstruct the pressure oscillation. On the contrary, it is reasonable to expect that the 2nd and the 4th frequency might be neglected without losses of information in the reconstruction of the pressure fluctuation. This assumption will be further discussed and confirmed, through the analysis of the experimental acquisitions, in the following section.

Carrier Number	Frequency [Hz]	Amplitude [-]	Relative Frequency [%]	RCI [-]
2nd	616	0.247	35.8	1.94
3rd	960	2.596	-	-
4th	1083	0.858	12.8	2.41
5th	2330	0.853	142.7	26.73

Table 12. Table 2. RCI estimation at ET=400 µsec with gasoline pressure 700 bar and 1000 pump rpm.

According to the considerations based on the power spectrum, the pressure wave during the injection process can be modeled as a sum of 2 one-degree of freedom MSD systems free responses, representing the 3rd and the 5th main carriers (which are the larger part of raw signal energy content).

As widely reported in the literature [37, 49, 55], the injection pressure does not modify the hydraulic system characteristics but only the fuel stiffness. Figure 95 clearly shows that changing the fuel pressure (keeping the injected mass constant at 1 mg/str) the power spectrum will maintain its typical shape, but with different frequencies. Increasing the fuel pressure indeed, all carriers move to higher frequencies keeping constant their relative position. Furthermore, it can also be seen that for all the tested injection pressures, the larger part of the energy content of the signal is represented by the 3rd and the 5th main carriers. Once again, the considerations based on the power spectrum confirm that the pressure wave during a single pulse injection strategy can be modeled as sum of the responses of 2 one-degree of freedom MSD vibration systems.

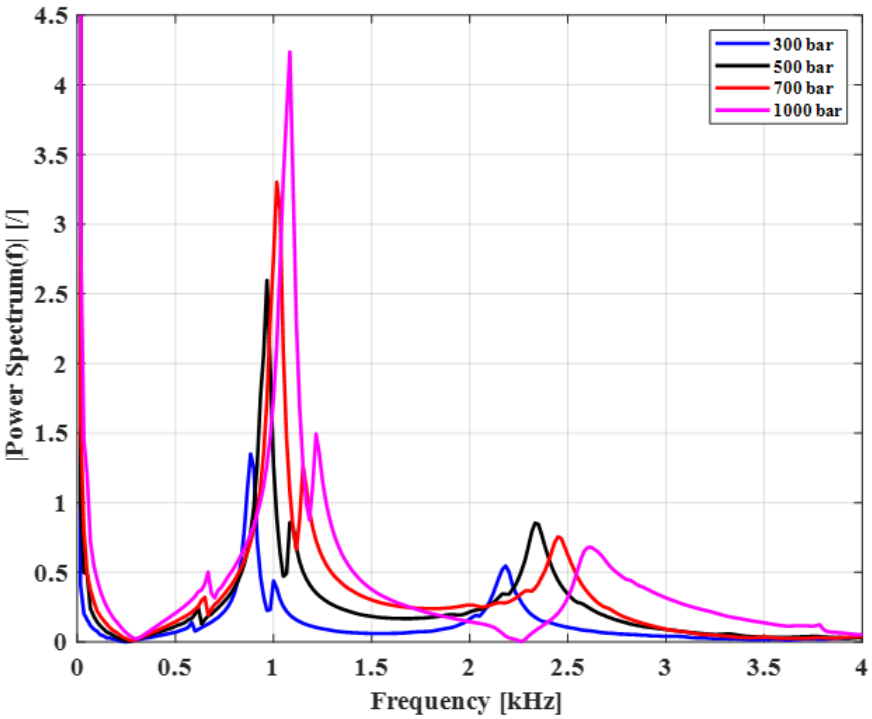

Figure 95. Frequency analysis (power spectrum) of the injector-side pressure signal generated by single injection pulse strategy at different gasoline pressure with same injected mass (1 mg/str) and 1000 pump rpm.

As shown in Equation 40, the one-degree of freedom MSD vibration system free response is a function of the system parameters, i.e., ω_d, ξ, x_0 and v_0. With the aim of obtaining the above-mentioned parameters for both the main carriers (the 3rd and the 5th) a numerical optimization for the single pulse injection strategy was performed. Starting from the general formulation of the free response showed in Equation 40, the optimization process, based on MATLAB *fminsearch* function, calculates the four fundamental parameters (ω_d, ξ, x_0 and v_0) minimizing the distance between the mathematical model and a bandpass filtered pressure signal centered on the analyzed frequency. The optimization process was applied for both the main carriers at all tested conditions in terms of ET and gasoline pressure. Figure 96 and Figure 97 summarize the output of the optimization process (8 fundamental parameters) as a function of ET and gasoline pressure.

Analyzing the obtained maps, Figure 96 and Figure 97, it is important to highlight that all the parameters show clear dependencies with respect to gasoline pressure and ET except ξ_1, ω_{n1} and ω_{n2}. As mentioned previously, the injection duration does not modify the hydraulic system behavior, hence the frequencies (ω_{n1} and ω_{n2}) can be considered constant for different ET and linearly variable with respect to the injection pressure (increasing the rail pressure both frequencies will rise).

Regarding ξ_1, the optimization provides as output very close values for each tested condition and a defined trend cannot be determined. This means that ξ_1 is unsensitive with respect to the injection parameters Consequently, an average (constant) value of ξ_1 can be reasonably chosen replacing the reported map. As clearly visible in Figure 97(b), the situation is slightly different for the 5th main carrier because the damping ratio ξ_2 tends to increase with the rail pressure (for a fixed ET) and decrease for higher values of ET (for a given rail pressure).

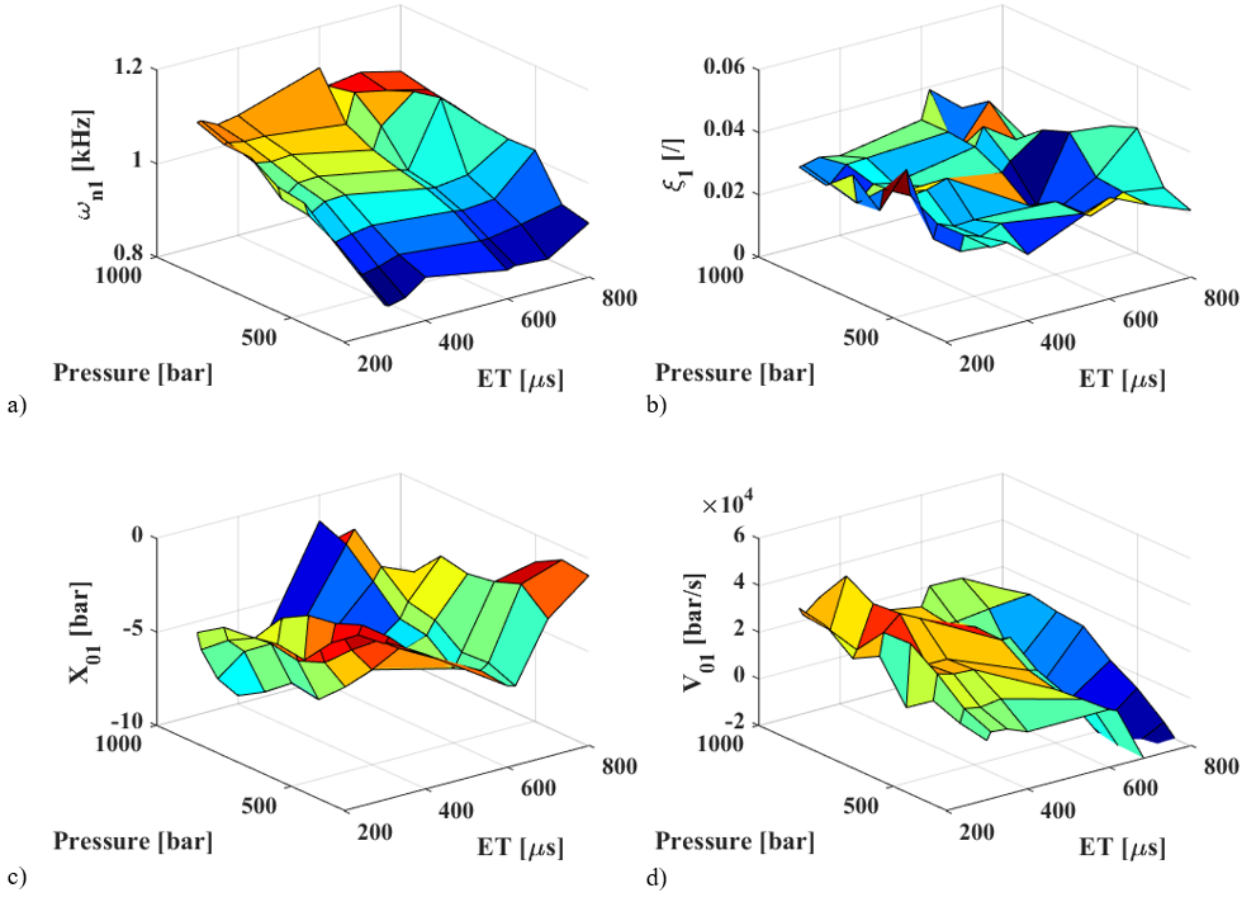

Figure 96. MSD system parameters after the optimization process for the first main carrier as function of injection parameters (injection pressure and ET): (a) frequency ω_d, (b) damping ξ and initial conditions (c) and (d) for x_0 and v_0 respectively.

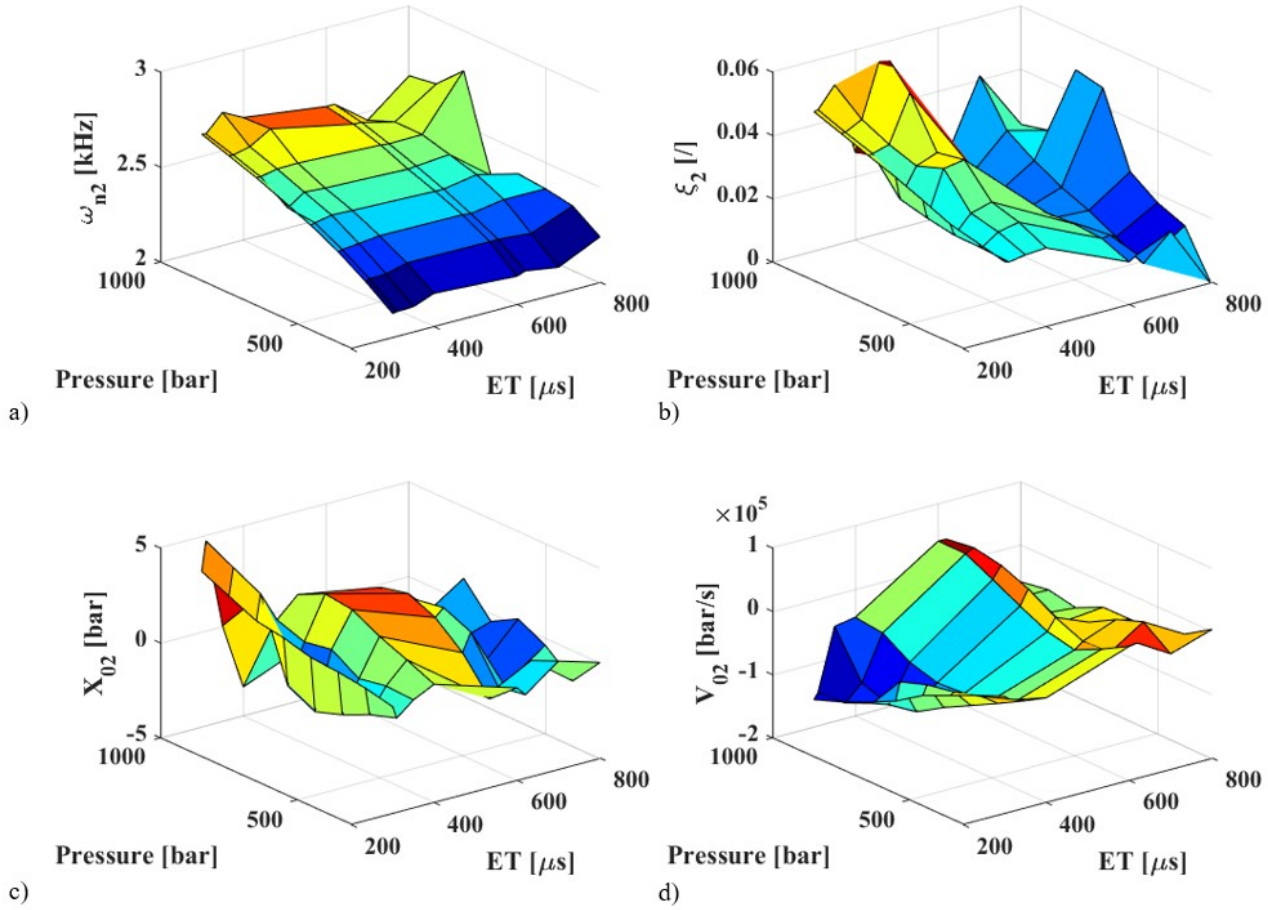

Figure 97.MSD system parameters after the optimization process for the second main carrier as function of injection parameters (injection pressure and ET): (a) frequency ω_d, (b) damping ξ and initial conditions (c) and (d) for x_0 and v_0 respectively.

Figure 94 shows that the complete power spectrum contains many frequencies with lower energy content with respect to the identified main carriers. Since the total energy content of the other frequency is not negligible, considering only the sum of the modelled main carriers would lead to an inaccurate reconstruction of the instantaneous pressure trace. To take into consideration the total energy contribution from frequencies different from the 2 main carriers, the estimated pressure fluctuation was corrected using a set of specifically identified offsets and gains, mapped as functions of rail pressure and energizing time. The last step of the system characterization was to obtain the maps of gain and offset applied to the reconstructed pressure oscillation, which allow compensating the energy content lost by considering a simplified power spectrum (with only two main carriers). The offsets have been determined as the difference between the mean values of the modeled and experimental pressure oscillation, while the gains were calculated as the ratio between the first absolute peaks of the modeled and experimental pressure oscillation. Figure 98 reports the obtained maps. It is interesting to notice that the offset map shows a clear dependence on both ET and rail pressure, while the gain map shows a slight correlation with respect to ET and no evident dependence on the rail pressure.

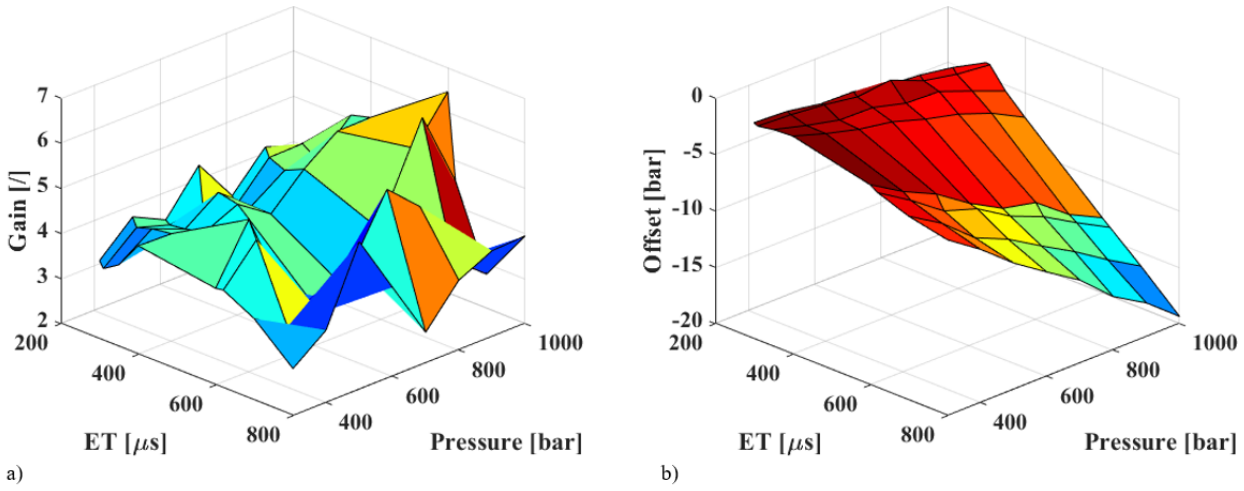

Figure 98. Gain (a) and offset (b) maps for the reconstructed pressure trace.

2.4.3 Pressure Waves Reconstruction Strategies for Single and Multiple injections

After obtaining the hydraulic system characteristics as described in the previous section, the pressure waves reconstructions were derived applying the model-based approach under different injection strategies (single and multiple injections) and conditions, such as injection pressure, ET and relative position between consecutive injections. Since the aim of the modeling approach is to develop a control strategy suitable to mitigate the fuel quantity oscillation during multiple injections of gasoline, typical values of the injection parameters used for the management of GCI combustion were selected. As a result, the single injection strategy was tested varying the rail pressure from 300 to 1000 bar and the injected mass from 1 to 45 mg/stroke (for the highest pressure). Once the pressure waves reconstruction was validated for the single injection strategy, with the aim of verifying the model-based approach applicability also with multiple injections, an experimental activity was carried out performing two consecutive injections with same ET and different DT (defined in Equation 44).

$$DT = \frac{(EOI_1 - SOI_2) * RPM}{10^6} \qquad (44)$$

Table 13 summarizes all tested conditions using gasoline, the goal being to validate the pressure wave reconstruction by comparing them with the experimental pressure trace. It is important to underline that the whole experimental activity was carried out keeping the injector nozzle at the atmospheric pressure (without back pressure). As well known, the back pressure on the nozzle changes the total injected mass (i.e., the injector map which is calibrated with the typical in-cylinder pressure on the nozzle) but does not affect the hydraulic system behavior (especially its characteristic frequencies). As a result, the pressure waves estimation methodology can be considered valid also when the back pressure is varied.

Injection Strategy	Prail [bar]	ET 1 [μs]	ET 2 [μs]	DT [μs]
Single	300 to 1000	300 to 800	-	-
Double	300	400	400	20 to 3800
Double	500	350	350	20 to 3800
Double	700	310	310	20 to 3800
Double	1000	300	300	20 to 3800

Table 13. Test plan of the experimental activity.

Pressure Waves Reconstruction for Single Injection Strategy

First, the goal was to verify the model-based approach robustness reproducing the pressure wave generated by single injection pulse (SI-PWR) using the hydraulic system parameters obtained by the optimization process. Following the control scheme reported in Figure 99, the pressure waves were simulated as the sum of two MSD free responses, one for each identified main carrier (3rd and 5th frequencies). The MSD system parameters were obtained using the above-described maps considering the ET and injection pressure (PRail) as input variables. Finally, by using the offset and gain maps (ET and PRail as inputs) the SI-PWR retrieves the energy content of the neglected frequencies (mainly the 2nd and 4th frequencies).

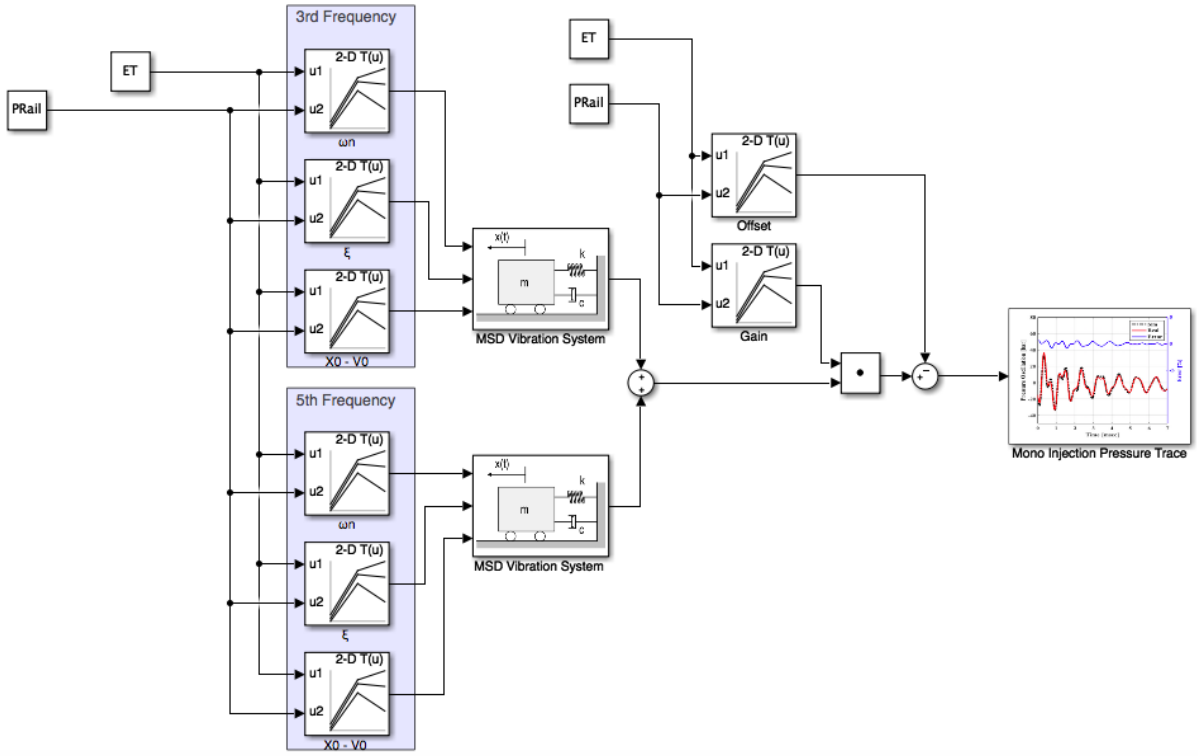

Figure 99. SI-PWR strategy using the MSD model-based approach.

Figure 100 shows the comparison between simulated and experimental pressure wave considering only the oscillation contribution for different ET at gasoline pressure of 700 bar. It is important to underline that the developed model-based approach does not consider the injector dynamics [42], therefore the pressure drop generated by the injector opening was neglected. The pressure waves simulations start from the first pressure drop generated by the mass discharged from the injector. To estimate the simulations accuracy during the propagation phase of the waves, the percentage error was defined as reported in Equation 45. The percentage error definition allows comparing the pressure wave reconstruction accuracy for different injection pressure settings.

$$Error\ \% = \frac{P_{simulation} - P_{acquired}}{P_{Rail}} * 100 \qquad (45)$$

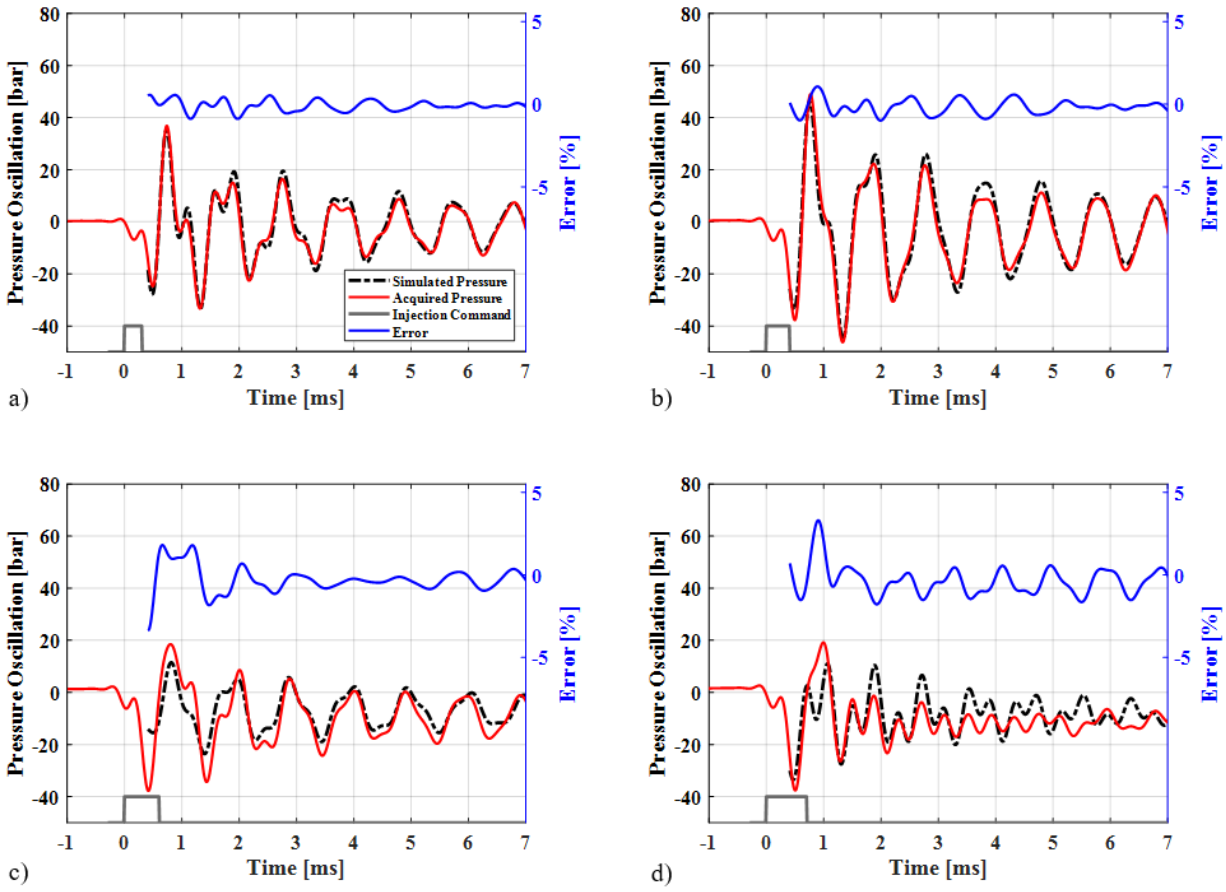

Figure 100. Comparison of experimental and reconstructed pressure waves and instantaneous error evaluation using the SI-PWR strategy with gasoline pressure of 700 bar, 1000 pump rpm and ET of (a) 300 µs, (b) 400 µs, (c) 600 µs and (d) 700 µs.

It is clear by looking at Figure 100, that the model-based approach can predict pressure waves with high accuracy (error +/- 3%), also when the pressure oscillation varies significantly (ET 700 µs) from its typical behavior (ET 300/400/600 µs). Starting from the error definition (Equation 45) during the pressure wave propagation phase, to evaluate the pressure waves reconstruction accuracy for all tested conditions the Root Mean Squared Errors (RMSE) were calculated. Figure 101 summarizes the pressure wave reconstruction in terms of RMSE as respect to ET and injection pressure. The maximum RMSE of 1 % reported in Figure 101 allows considering the model-based approach as valid for the SI-PWR.

To verify the information provided by the RCI index in terms of relevance of each carrier for pressure wave reconstruction, the SI-PWR was tested in two different ways: only considering the fundamental frequency (simplified SI-PWR, with only the 3rd main carrier) and adding the 5th carrier (SI-PWR). The results provided by the simplified SI-PWR were not sufficiently accurate (RMSE higher than 4%) especially for the tests operated at high ET (Fig. 100(d)), where the contribution of the 5th frequency is clearly visible. As a result, the RMS error between the measured and the estimated instantaneous pressure drops to 1% considering, in the SI-PWR, also the 5th carrier. To further validate the information provided by the RCI index, the model was tested also adding the 2nd, the 4th and both carriers, but this resulted in negligible improvements in the instantaneous pressure estimation. For this reason, the final SI-PWR approach was designed considering only the 3rd and the 5th main carriers, as previously suggested by the RCI index.

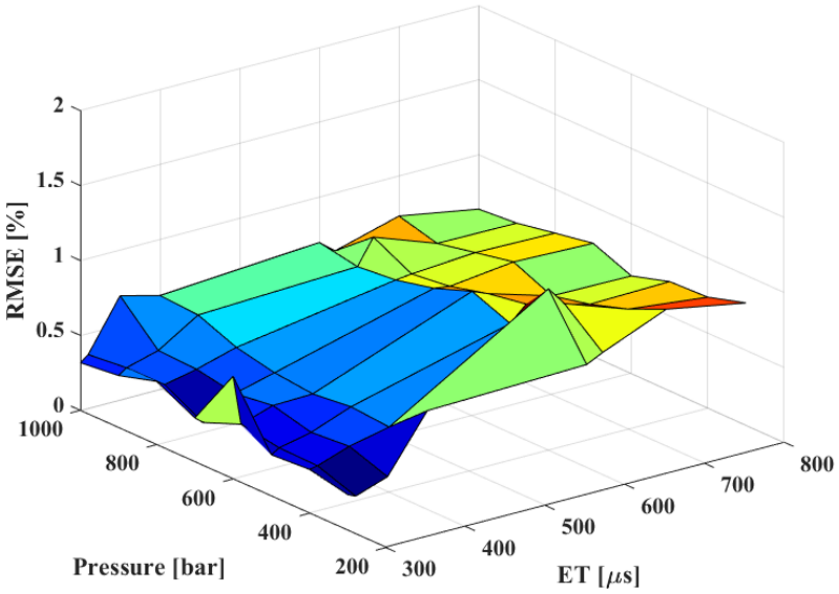

Figure 101. Accuracy evaluation of the SI-PWR strategy (RMSE) using gasoline for all tested condition of injection pressures and ET.

To check the model-based strategy robustness, the SI-PWR was tested by changing fuel type and injectors. As widely reported in literature [48, 56], the Bulk modulus, defined in Equation 46, determines the hydraulic system natural frequencies. Hence, changing fuel from gasoline to diesel, thicker than gasoline, at same injection pressure and temperature the hydraulic system natural frequencies will increase. Keeping constant the hydraulic system layout, the fuel density variation effects on the system behavior was considered as an offset, proportional to the square of the fuels density ratio [48], on the main frequencies values maps (ω_{n1} and ω_{n2}), as stated in Equation 47. Moreover, all the previously obtained hydraulic system parameters (ξ, x_0 and v_0) were kept constant. Figure 102 shows the accuracy of the pressure waves reconstructions in terms of RMSE considering diesel fuel and placing the controlled injector in a different rail position, from position 3 to 1 in Figure 89 (Figure 102(a)) or changing the activated injector (different hardware component but same injector type) with gasoline (Figure 102(b)). Also, for these tested conditions, the low RMSE values underlines the approach validity and robustness in case of single injection strategy.

$$K = \rho \frac{dP}{d\rho} \tag{46}$$

$$\Delta_\omega = 1 - \sqrt{\frac{\rho_g}{\rho_d}} \cong 7\ \% \tag{47}$$

It is important to notice that the model-based approach only considers the injection pressure effect on the hydraulic system parameters. By the Bulk modulus (K) definition (Eq. 46) results that also the fuel temperature can modify the system behavior (because it changes the fuel density). Despite the impact of the fuel temperature on density and Bulk modulus cannot be neglected [56], the model-based strategy implicitly considers this effect thanks to the hydraulic system parameters (ω_n, ξ, x_0 and v_0) optimization for each injection pressure. With the purpose of characterizing the fuel temperature effect on density and Bulk modulus, a hydraulic layout modification is needed adding rail temperature sensors to those already installed before the HP pump. As mentioned before, the presented model was characterized keeping constant the geometry of the injection system i.e., rail (diameter and length) and feed ducts (diameter and length). The variation of such

parameters modifies the hydraulic system characteristics and, consequently, the response of the system, whose information are summarized in the power spectrum, might change considerably. Therefore, to apply the presented model with different hydraulic system geometry, it is mandatory to perform a preliminary frequency analysis defining the minimum number of carriers needed to properly reconstruct the pressure wave. Once established the main carriers, the model parameters can be characterized following the same steps reported in this work and the pressure wave reconstruction can be performed by using the obtained parameters.

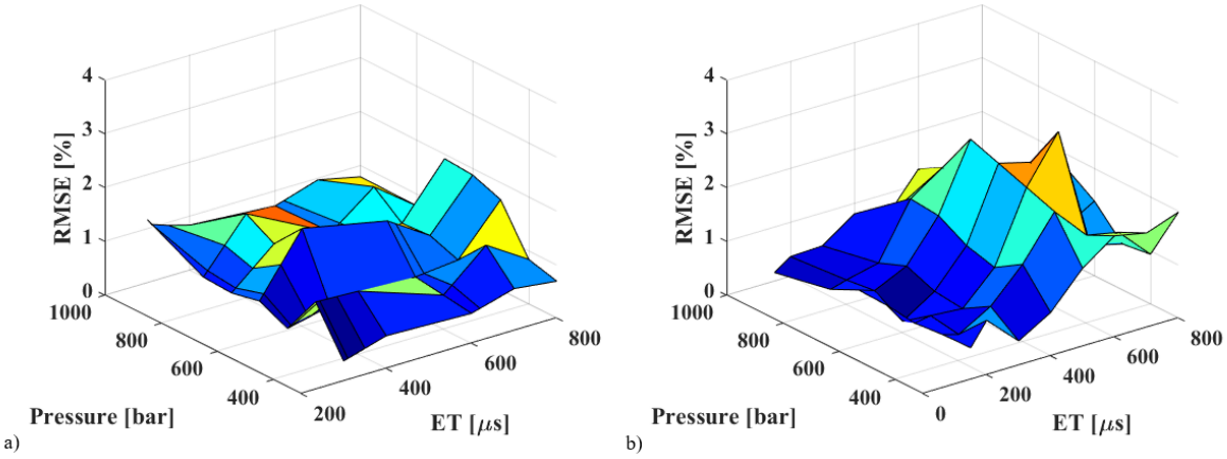

Figure 102. Accuracy evaluation of the SI-PWR strategy (RMSE) using the same injector fueled with diesel and different injector position (a), and different injector (injector placement used for hydraulic system parameters calibration) fueled gasoline (b) for all tested condition of injection pressures and ET.

Pressure Waves Reconstruction for Multiple Injection Strategy

As mentioned before, to properly manage GCI combustion a multiple injections pattern, typically composed by several pilot injections followed by main injection, is needed [57-60]. The pressure oscillation triggered by the first injection pulse strongly modifies the injected quantity of the following injections [42, 51, 55, 61], mainly because the second injection pulse occurs when the pressure wave cannot be neglected yet.

To define the impact of the pressure wave on the total amount of fuel injected with multiple injections, a wide experimental activity testing double injections strategy, summarized in Table 13, was carried out. Figure 103 shows the injected mass (measured), normalized with respect to the theorical total injected mass (calculated using the injector map), at different injection pressures changing the dwell time (DT), from 0 to 3500 μs, between two consecutive injection pulses (ET1=ET2 for each injection pressure) using gasoline. As previously described, the higher the injection pressure, the higher the pressure wave frequency, thus the injected fuel mass oscillation will occur at smaller DT. Figure 103 also reports the hydraulic fusion region (DT < 600 μs): due to the slow injector dynamics, when the injected mass gets high, consecutive injections get very close [40, 52]. Considering the key role of the pilot injections on GCI management, the need of a compensation strategy for the injected fuel is mandatory to ensure the requested fuel mass on pilot injections (typical DT values for multiple injection pattern are from 800 to 2500 μs).

To understand the behavior of the hydraulic system with a multiple injections strategy, the analysis of the pressure waves coming from the piezoresistive pressure sensors near the injector was performed. Figure 104 shows the comparison of experimental pressure wave, triggered by single injection strategy, and the wave triggered by double injection strategy with same ET. The reported pressure traces clearly highlight how the pressure wave generated by two consecutive injections can be considered as sum of two single injection triggered pressure waves, shifted by DT. As a matter of fact, considering two consecutive injections with same ET, the pressure wave generated by the first injection pulse does not modify either the amplitude or the

frequency of the wave triggered by the following injection but only the fuel instantaneous pressure during the active phase of the injector (when the injector nozzle is open).

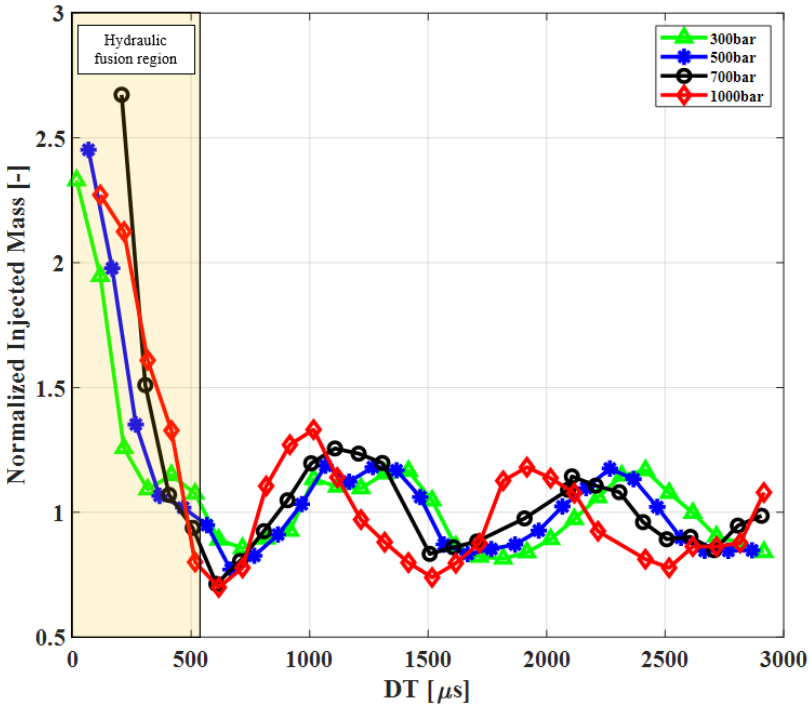

Figure 103. Effects of injection pressure and DT on the effective injected fuel, normalized with respect to the total injected mass, generated by a double injection strategy (ET1=ET2 ~ 1mg/str) using gasoline.

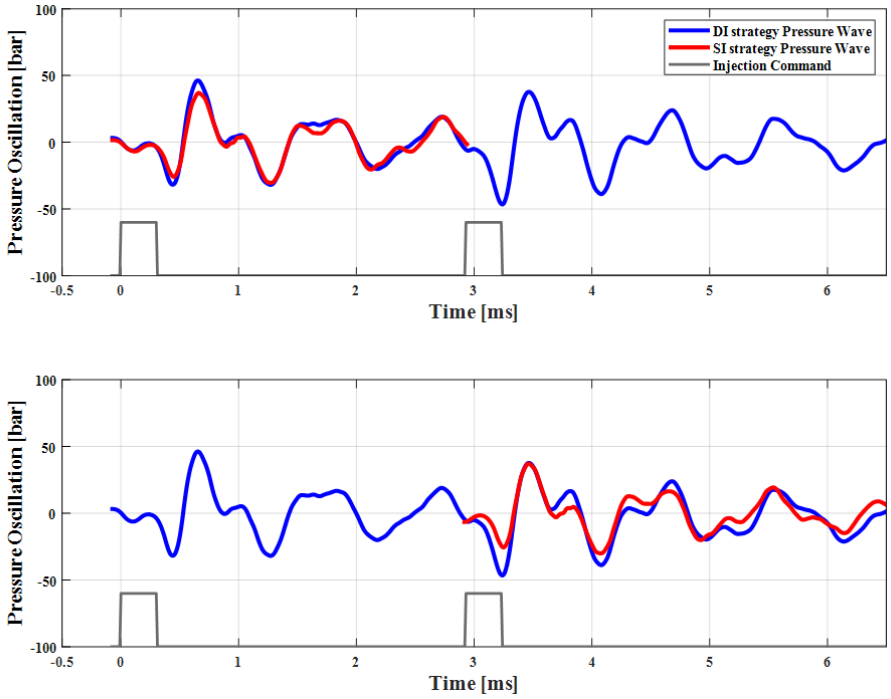

Figure 104. Comparison of experimental pressure wave triggered by double and single injection strategies at gasoline pressure of 700 bar with same ET=310 µs, aligned with (a) first injection pulse and (b) second injection pulse.

Based on the high accuracy on the SI-PWR applying the model-based approach, a pressure wave reconstruction for double injection strategy (DI-PWR) was developed. Bearing in mind the previous considerations, the DI-PWR was built as the sum of two SI-PWR. To simulate the pressure wave triggered by a double injection strategy, the scheme shown in Figure 105 was used, in which the ET for both injections (ET1 and ET2), PRail and DT were chosen as input variables. As it can be seen, the calculation structure replies twice (using the same hydraulic system parameters) the reconstruction strategy described in Figure 99.

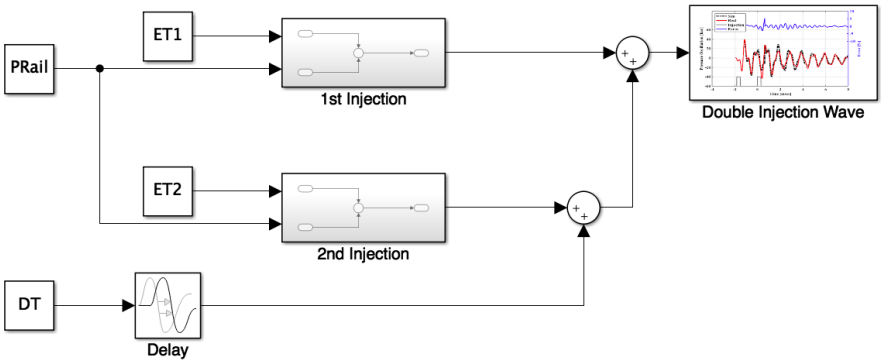

Figure 105. DI-PWR strategy based on the sum of 2 SI-PWR, using the MSD model-based approach.

Figure 106 shows the comparison of simulated and experimental double injection strategy pressure waves (considering only the oscillation contribution) for different DT at gasoline pressure of 700 bar and ET = 310 µs. It can be inferred from Figure 106 that both before and after the second injection pulse, the pressure wave was simulated correctly. Moreover, it is possible to see that the reconstructions are consistent also during the active phase of the injector, providing reliable instantaneous pressure traces also with multiple injections strategies.

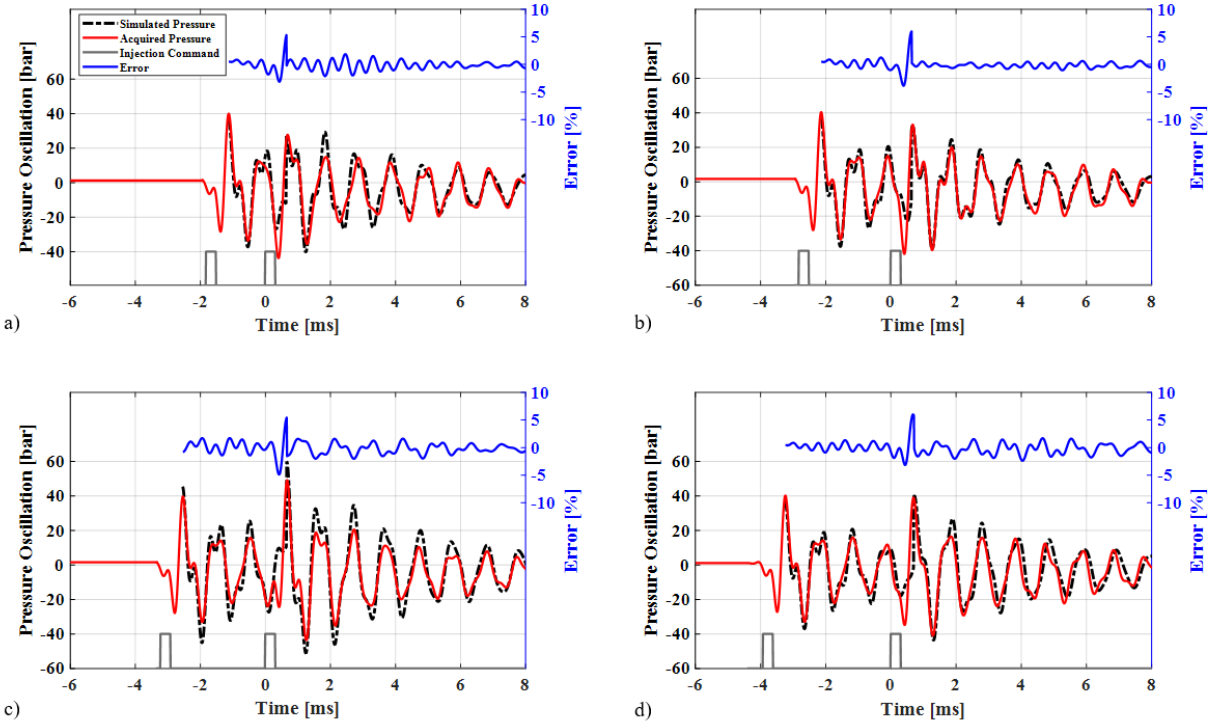

Figure 106. Comparison of experimental and reconstructed pressure wave and instantaneous error evaluation using the DI-PWR strategy with gasoline pressure of 700 bar, 1000 pump rpm, ET of 310 µsec and DT of (a) 1800 µs, (b) 2800 µs, (c) 3200 µs and (d) 3900 µs.

It is worth pointing out that as for the SI-PWR the injector dynamics are neglected (especially during the injector closing), thus the reconstruction accuracy decreases in proximity of the injector closing. As mentioned before, this region (DT from 0 to 600 µs) should be avoided due to the hydraulic fusion, hence this inaccuracy can be neglected. As made for SI-PWR, to summarize the simulations accuracy, RMSE for all tested DT and injection pressures were calculated: results are reported in Figure 107. The maximum RMSE of 2 % allows to consider the model-based approach as valid also for the DI-PWR. Based on the above-described results referring to the modeling phase, the following section describes the developed fuel quantity fluctuation correction strategy (FQC).

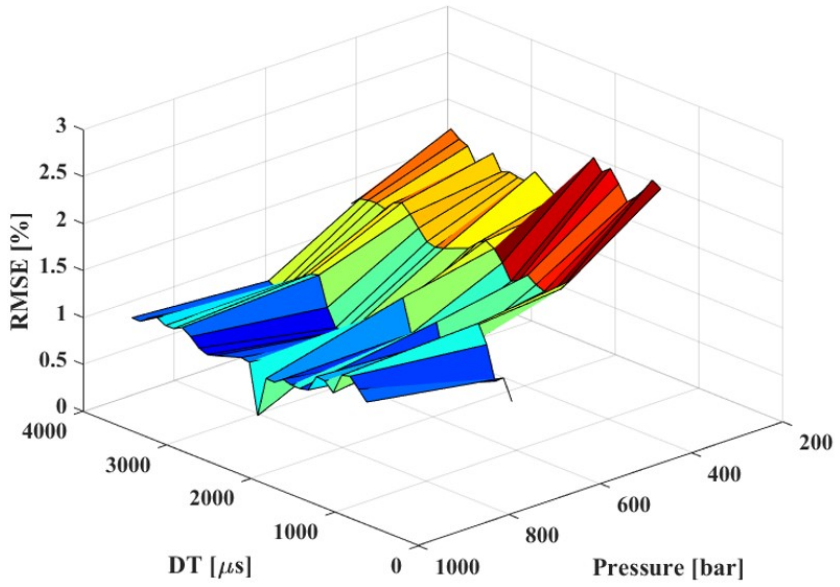

Figure 107. Accuracy evaluation of the DI-PWR strategy (RMSE) using gasoline (ET1=ET2) for all tested condition of injection pressures and DT.

2.4.4 Fuel Quantity Fluctuation Correction Strategy

As explained in the previous section, the occurrence of pressure waves represents one of the most critical issues in CR systems for a proper fuel injection management. The standard fuel dosing control strategies, both for single and multiple injections, are based on the rail-mounted pressure sensor, which does not contain the information of pressure oscillations. Especially for pilot injections, when the requested fuel mass is very low (m_{inj} ~1 mg/str) and DT < 2500 µs, the presence of the pressure oscillations modifies the second pulse injected mass, generating remarkable differences between requested and effective total injected fuel [15, 43, 44]. Thus, a fuel quantity fluctuation correction strategy (FQC) becomes crucial to manage GCI combustion using CR system, whereby the energy released by pilot injections play a key role ensuring the whole combustion process stability [27, 57-60, 62-63].

As a result of the high accuracy given by the DI-PWR, considering the effective pressure coming from the DI-PWR, a fuel injected estimation was performed as the sum of the two injected mass (with ET1=ET2) based on the injector map (without back pressure on the nozzle). Since the pressure wave does not affect the first injection, the injector map provides an accurate estimation of the amount of fuel introduced with the first injection using PRail (coming from the rail mounted pressure sensor) and ET as inputs. With regard to the second injection, to compensate the effects due to the pressure wave propagation triggered by the first injection (injector closure), the estimation of the mass was carried replacing PRail with the average instantaneous pressure trace coming from the DI-PWR in the time interval corresponding to the activation of the second injection.

Figure 108 shows the comparison of measured and estimated (based on the DI-PWR) fuel consumption, normalized with respect to the total injected mass, for different DT at gasoline pressure of 1000 bar using gasoline. Despite the hydraulic fusion phase cannot be replied by the DI-PWR, the estimated fuel consumption oscillations show a good accordance with respect to the experimental both in terms of frequency and amplitude for each DT.

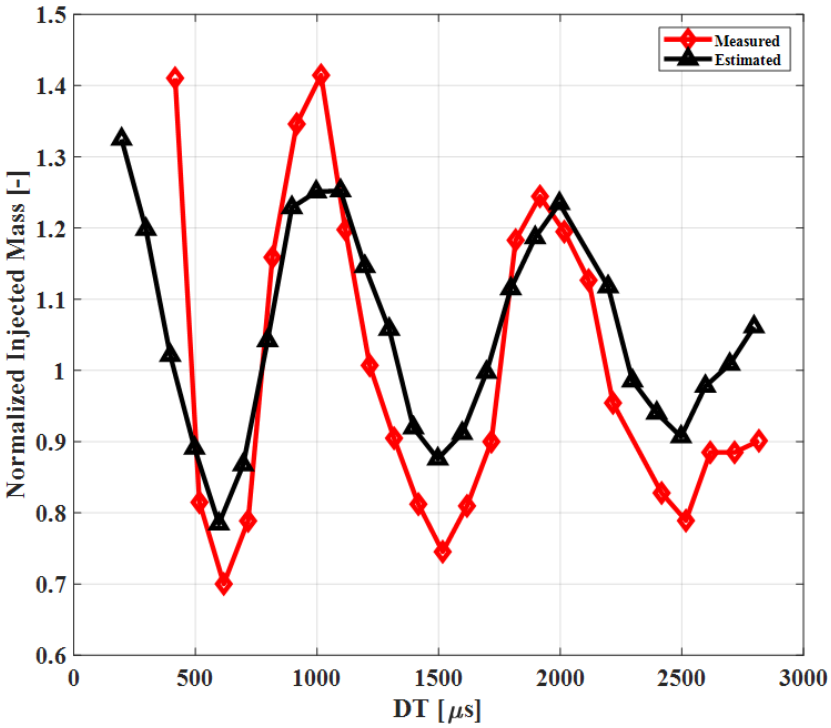

Figure 108. Comparison of fuel quantity injected measured and estimated (with the DI-PWR considering the mean of the instantaneous pressure trace during the second injection active phase) during double injection strategy (ET1=ET2) using gasoline at different DT.

Based on the results obtained comparing the measured and estimated fuel consumption reported in Figure 108, with the aim of reducing the consumption oscillation during multiple injections, an FQC strategy was designed, according to the block diagram reported in Figure 109. Relying on the instantaneous pressure wave reconstruction (applying the DI-PWR) during the second injection active phase, the FQC strategy can reasonably mitigate the fuel injected quantity oscillations due to the effects of the pressure waves. As above described, the standard fuel dosing strategies are based on the rail-mounted pressure sensor which does not contain the pressure oscillations, thus with the aim of considering the pressure oscillations effects on the second injection pulse the rail-mounted pressure signal was replaced by the DI-PWR. Since the pressure wave does not modify the first injected mass, the developed control strategy only modifies ET2, assuring the injected target mass $m_{inj\,2}$. It is important to notice that the FQC strategy is based only on previously defined 3D maps. Hence, after determining the hydraulic system parameter maps using the model-based approach, the FQC strategy can be easily implemented on a standard ECU.

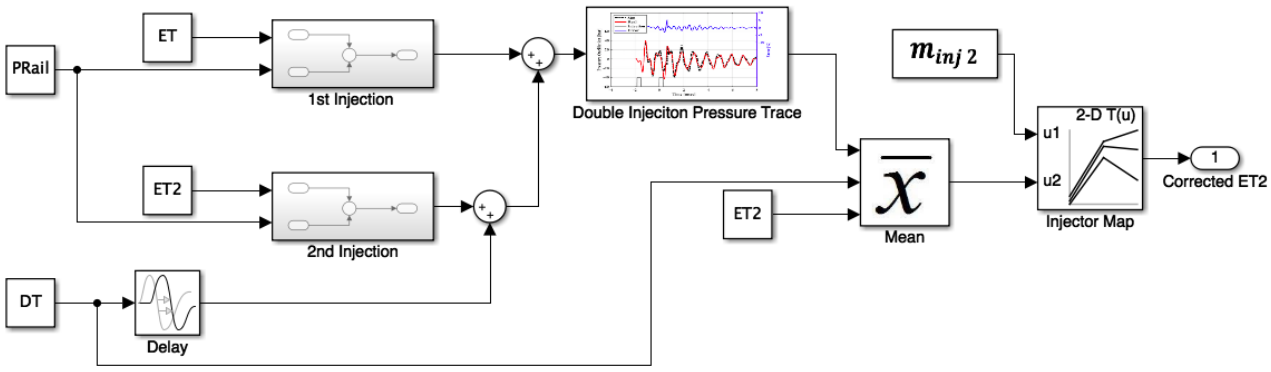

Figure 109. QFC strategy based on DI-PWR strategy using the MSD model-based approach.

2.5 Control oriented Ignition Delay Model for GCI Combustion

The above-described experimental activities carried out running the engine in GCI mode, highlighted the key role of the pilot injections in the combustion management. As widely reported in literature and confirmed by the experimental evidence collected during the PhD activities, to properly manage GCI combustion process, the use of complex injection strategies (composed at least 3 injections: 2 pilot + 1 main) is needed. As explained in the previous sections, the rise of pressure and temperature generated by the combustion of the fuel injected through pilot injections shortens the ignition delay of the following main injection which burns instantaneously when injected. Whereby, the combustion of the pre-injections assumes a key role in the GCI combustion management.

As mentioned before, since the combustion of the first fuel jets in GCI mode is chemically driven (no external source of ignition, such as spark plug, is used) the gasoline ignition mechanisms are significantly affected by chemical kinetics and slight variations of the cylinder thermal conditions. This means that small local variations of air-fuel mixing, and temperature might cause significant variations of the ignition delay, which could compromise the whole combustion stability (consequently generating misfire or knock). Therefore, a detailed knowledge of gasoline auto-ignition mechanisms plays a fundamental role. As a matter of fact, once defined a set of injection parameters, an accurate prediction of the angular position at which the fuel introduced with the first injection starts burning (start of combustion angle, SOC) is necessary to guarantee the combustion of all the following injections and, consequently, assuring a proper GCI combustion management.

This part of the PhD dissertation describes a 0-D control-oriented ignition delay model developed to improve the stability of GCI combustion. To do this, a wide experimental activity was carried out aimed at studying the ignition delay of the first fuel jets running the 1.3L light-duty compression ignited engine fully-converted to perform GCI combustion. By the analysis of the obtained results, a 0-D ignition delay model was developed able to accurately predict the SOC position even changing engine operating conditions. Since the aim of this work was to obtain a control-oriented strategy which improve the GCI combustion controllability, the developed model can be easily implemented in the ECU and used for real-time estimation of the ignition delay (ID). By knowing ID, the ECU might manage the injection pattern parameters to guarantee proper SOC positioning before combustion occurs, avoiding knock or misfire.

2.5.1 Ignition Delay sensitivity analysis

Previous experimental activities on GCI combustion proved that, to manage this kind of SCCI methodology avoiding anomalous phenomena (such as knocking or misfiring), a multiple injection strategy is needed. As widely described, by using multiple injections, the typical shape of the GCI combustion is composed by two typical stages: premixed and diffusive. Figure 110 shows a typical RoHR running GCI combustion.

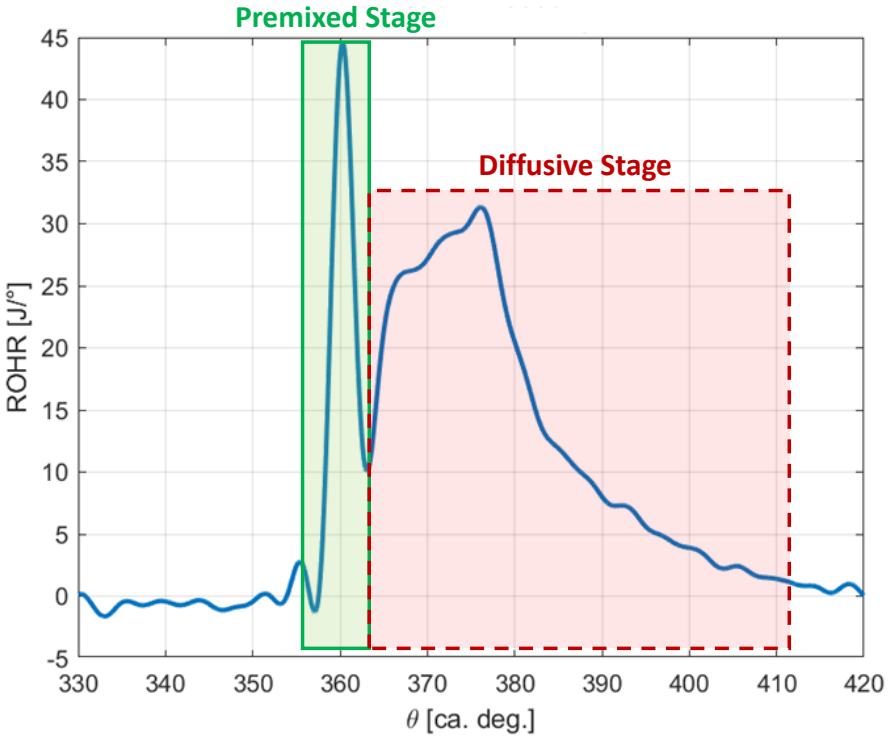

Figure 110. Rate of heat release curve testing GCI combustion at 12 bar of IMEP and 2000 rpm

Due to their high ignition delay, the pilot injections burn together (the unfavorable thermodynamics conditions generate high ID and, therefore, the pilot injections IDs are almost equal), releasing high amount of energy in a short time (premixed stage). After that, the rise of in-cylinder temperature and pressure reduces the ignition delay of the following main injection. Consequently, as shown by Figure 110, the second stage of the GCI combustion is characterized by a smoother energy release (diffusive stage).

Previous results reported in this PhD dissertation proved that GCI combustion can be effectively managed (performing this dual-stage combustion) in different operating conditions without compromising engine reliability. However, to guarantee stable GCI combustion, a robust and efficient premixed stage is needed. Bearing in mind the results coming from the experimental investigation of gasoline auto-ignition with small amount of injected fuel using the "*Cylinder Laboratory*" mode, the main effects of the control parameters on the ignition delay were highlighted. However, due to the presence of the 3 cylinders fueled with diesel, which modify the chemical composition of the residuals and produce different back pressure (assuring proper boost pressure only with 3 cylinder), the results described in the previous section must be further confirmed running the fully converted engine. Since the premixed stage is mainly driven by the chemical composition of the air-fuel mixture and the thermodynamics of the combustion chamber, a sensitivity analysis on the gasoline ignition delay was performed in the fully converted GCI engine.

As defined in Equation 27, ID represents the distance between two angles: the Start of Injection (SOI) and the Start of Combustion (SOC) respectively. Although its simple definition, several approaches were proposed with the aim of calculating ID mainly because of different (and still correct) SOC definition. Despite the SOC detection methodology proposed during the experimental investigation of gasoline auto-ignition using the gross RoHR (because the small amount of energy released was comparable with the energy losses through the cylinder walls) proved to be reliable estimating SOC, the amount of fuel injected with pilot injections (using typical GCI multiple injection patter) was high enough to consider a more common SOC definition. For this reason, Equation 48 defines the ID considering SOC as the crankshaft angle which it is reached 5 J/deg of RoHR. Figure 111 clarifies the SOC positioning for a typical GCI combustion. If the first stage of the combustion reaches (and overcomes) the defined combustion velocity threshold, the rise of pressure and temperature will reduce the ignition delay of the following injection, making GCI stable and controllable.

$$ID = SOC - SOI = \theta_{RoRH\_5} - SOI \tag{48}$$

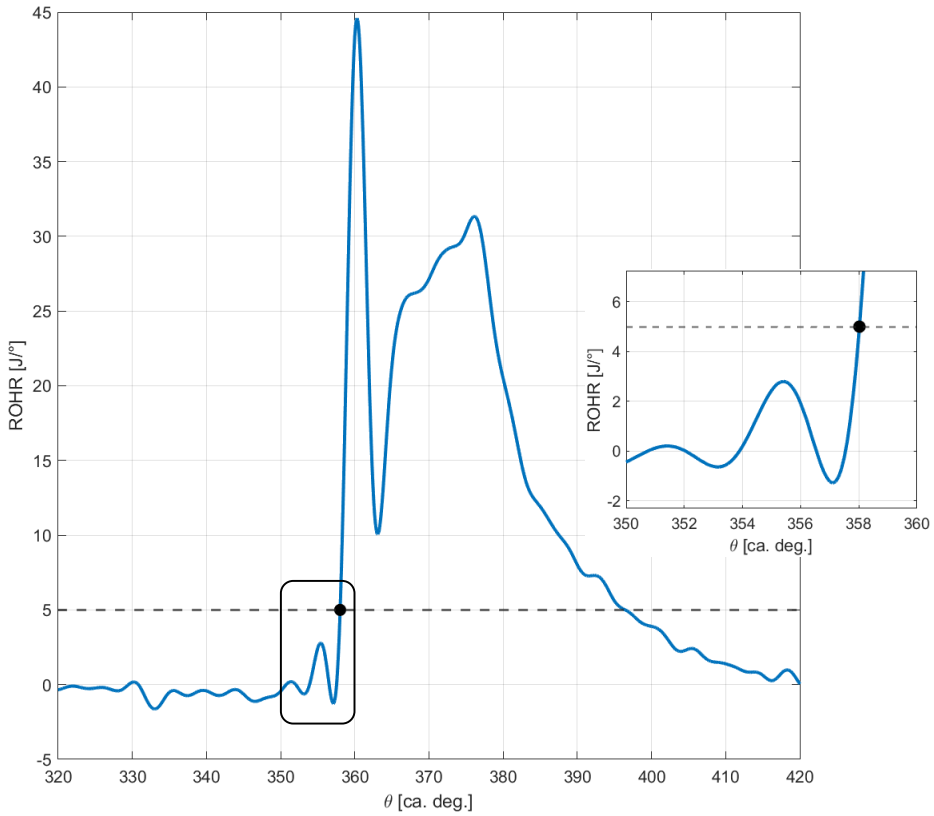

Figure 111. ROHR curve and corresponding ROHR threshold for determining the SOC

Once the ID was identified with good accuracy, with the aim of developing a control-oriented ignition delay, model the activity was focused on verifying the main dependencies of ID on the engine control parameters. To do so, a wide experimental activity was carried out performing a specifically designed testing methodology called *"Switching Pattern"* [64]. During these tests, the GCI engine (4 cylinders fueled with gasoline) was run in a stable operating point, using the calibration obtained by the previous activities, and every 100 engine cycles the main injection was turned off keeping active the previous ones (pilot and pre injections) for only 1 cycle called *"Switched cycle"*. During these tests, other engine control parameters were kept constant at the calibration values. Figure 112 shows an example of switching strategy test in which: cycles n-1 and n+1 represent the complete injection pattern (Pilot+Pre+Main), and cycle n is the switched cycle (Pilot+Pre only).

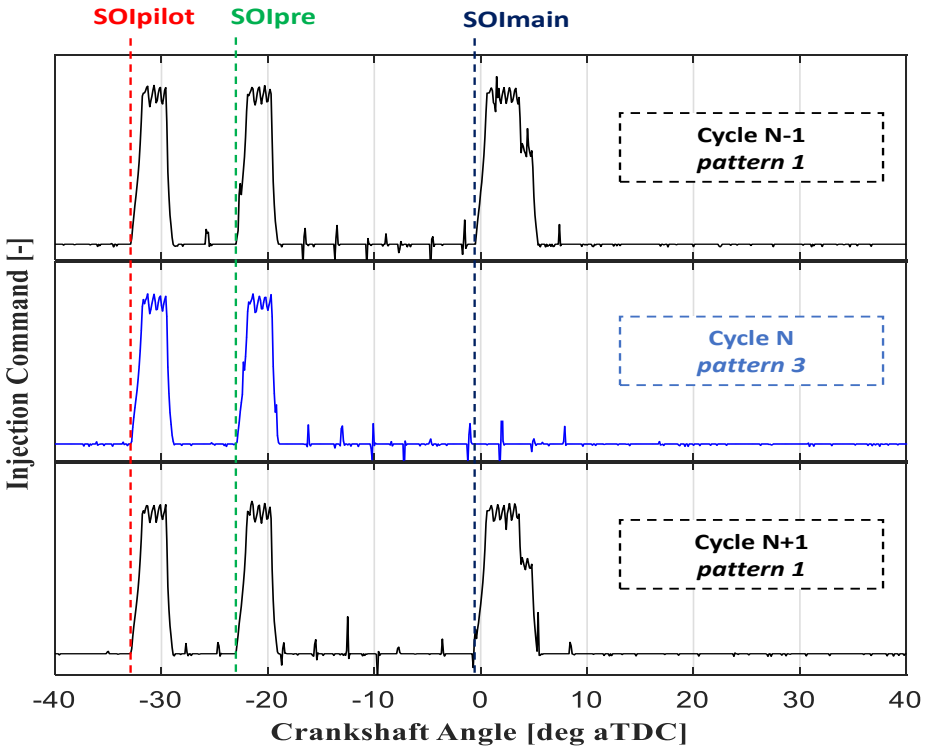

Figure 112. Switching pattern methodology: comparison between the injection commands of both complete (cycle n-1 and n+1) and switched pattern (cycle n)

In this way, the realized combustion occurs with same amount of residual gases and thermodynamic conditions of a GCI running with complete injection pattern (Pilot-Pre-Main) but without chemical-physical interactions generated by the main injection. As a result, the ID of the switched cycle represent the ID of the fuel injected with the pre injections, which combustion is responsible of the whole GCI stability. After performing the switching strategy (only 1 engine cycle was switched), the main injection was turned on again avoiding engine reliability problems (running only 3 cylinders might damage the engine crankshaft). Combustion stability was assured mainly because the dynamic of the combustion controllers (used to keep the engine at a constant IMEP and MFB50) and boost controller were set very slow, and therefore, switching only one cycle, it was possible to neglect the impact of the closed loop controllers on the control parameters. As an example, Figure 113 shows a comparison between RoHR of engine cycles recorded during a switching test. As can it be observed, the red trace represents the RoHR of the switched cycle while the black and grey ones are the instantaneous and averaged RoHR respectively (2000 rpm IMEP 14 bar, MFB50 14 deg bTDC and gasoline pressure 500 bar). By the analysis of this condition, since the chemical-physical interactions produced by the main injection on the first stage of combustion are negligible in a reference GCI combustion (dual stage combustion), SOC can be successfully identified through the analysis of the switched cycle. In that way, it was possible to study in depth the ignition phase of the GCI combustion (mainly determined by the combustion of the pre injections) even changing engine control parameters which could strongly modify the combustion shape (with closer combustion stages the mutual interaction between premixed and diffusive combustions might compromise the SOC detection).

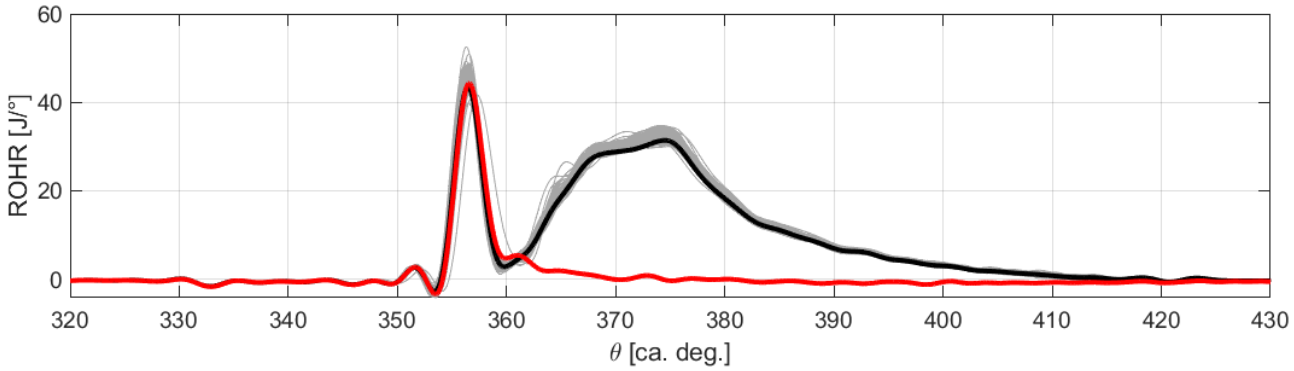

Figure 113. Comparison between average ROHR running the engine with the complete injection pattern (black) and ROHR of the switching cycle (red)

By looking at the literature and by the analysis of the results of previous experimental activities, running GCI combustion with typical engine layout (using high-pressure injection system, multiple injection pattern and EGR) the ID mainly depends on:

a) Gasoline pressure
b) Injection Phasing
c) Intake temperature
d) Intake pressure
e) Mass and temperature of residual gases trapped in the combustion chamber
f) Air humidity
g) EGR rate

Gasoline pressure

As pointed out by the literature [26, 28, 29] and confirmed by the experimental activity carried out in "*Cylinder Laboratory*" mode, the variation of gasoline pressure modifies the fuel vaporization and penetration and therefore, the local relative air-fuel ratio (which determines the ignition points in the combustion chamber) will be different. As a result, the gasoline pressure must be properly chosen to assure favorable local relative air-fuel ratio able to generate pre injections combustion with high efficiency and stability. Since the hardware of the engine was kept constant during whole PhD activities (pistons, fuel system, intake and exhaust manifolds and turbocharger), the effect of gasoline pressure widely discussed running the "*Cylinder Laboratory*" mode, could be reasonably considered valid even testing the fully converted engine.

Injection Phasing

Previous sections of this PhD dissertation highlight that to correctly control GCI combustion, a proper management of the injections is needed. In particular, the stable and reliable GCI combustion was reached using complex injection strategies typically composed by three injections: two anticipated injections with a small fuel jets (Pilot and Pre injections) and one bigger near the TDC (Main injection). By using that injection strategy with proper selection of the pre injections phasing, it was demonstrated that the GCI combustion can be easily and safely managed covering the typical engine operating range of this LTC methodology. A wrong pre-injection positioning might compromise the combustion stability and engine reliability. Since the first injections burns as HCCI combustions, their phasing and quantity play a crucial role in the GCI combustion management mainly because determines the thermodynamic conditions (temperature and pressure) of the charge when the fuel is injected and therefore, the ID. As a result, with the aim of developing an ID model, the pre injections phasing must be considered.

Intake Temperature

As reported by literature [24, 25, 36], performing combustion techniques characterized by spontaneous ignition, the intake temperature (T_{INT}) plays a crucial role on the ignition delay timing because of its contribution in the chemistry of the mixture. Once the air-fuel mixture was created through injection, the thermodynamic conditions affect the autoignition process modifying the required energy to start the combustion. As a result, the higher intake air temperature and pressure the lower ignition delay will be. This phenomenon, well documented by the literature, was highlighted during the experimental activity on the autoignition investigation performed through *"Cylinder Laboratory"* configuration of the engine. Despite the discussed effect could be considered valid also running the fully converted engine, since the air path of the engine was modified introducing the thermoregulation unit (TEMPCO), the dependency of ID on intake temperature was verified though specifically designed tests.

The same engine operating point (IMEP 12 bar at 2000 rpm) was tested at two different intake temperatures: Thigh and Tlow. Table 14 reports the comparison of the control parameters used to evaluate the effect of intake temperature variations on ID. It is possible to note that among the listed variables, the only difference is related to the intake temperature which was increased of roughly 25 °C going from the low temperature test to the high temperature one.

	High Temperature condition	**Low Temperature condition**
Engine speed [rpm]	2000	2000
IMEP [bar]	12	12
Boost pressure [bar]	2.2	2.2
Exhaust pressure [bar]	3	3
Intake temperature [°C]	**77**	**50**
MFB50 [ca. deg aTDC]	12	12
Injection pattern: SOI Pil, SOI Pre, SOI Main [deg bTDC]	[35,21,4]	[35,21,3]
Injection pressure [bar]	500	500
ET_{main} [µs]	686	683

Table 14. Engine operating conditions testing the effect of two different levels of intake temperature on ID

By the analysis of the RoHR reported in Figure 114, it was confirmed the effect of intake temperature on ID. Moreover, by looking at Figure 114, it clearly arises that the intake temperature significantly modifies the way in which heat is released during the combustion process. The rise of intake temperature makes the first combustion stage (chemically driven) faster with shorter ID. Having a higher intake temperature means that the fuel injected during pilot and pre injections will vaporize and mix with the air faster due to the higher charge temperature and therefore it will start burning earlier (low ID) and faster (high RoHR). Furthermore, since the energy released during the first combustion stage is enough to significantly reduce the ID of the main injection, the diffusive stages are similar in both conditions.

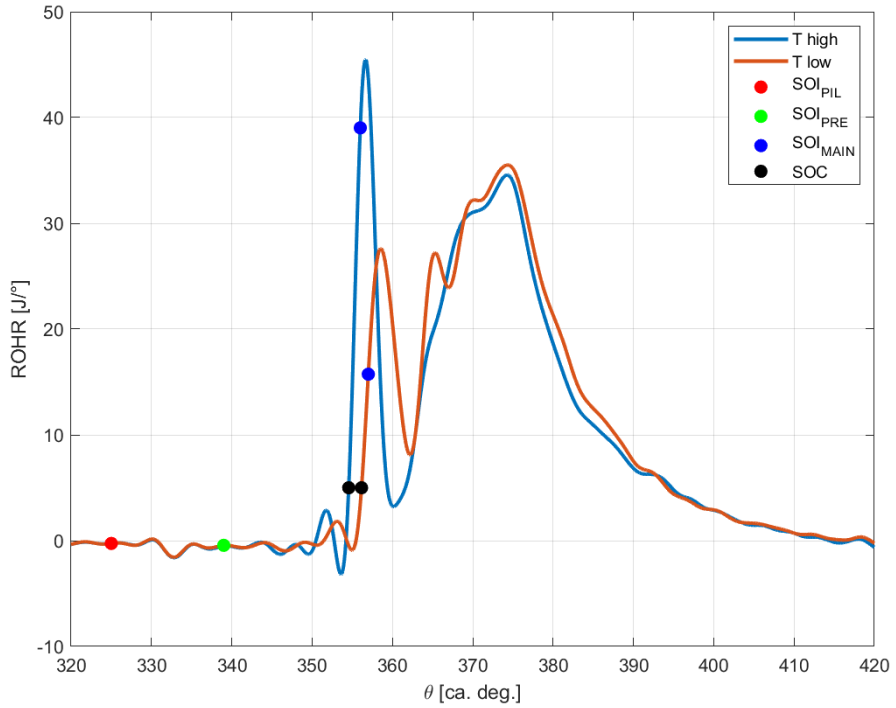

Figure 114. RoHR curves at different intake temperature

Figure 115 shows the cycle-by-cycle evaluation of ID for both analyzed conditions. By looking at Figure 115 it can be noticed that the reduction of the ignition delay when increasing the intake temperature is remarkable. Considering the reported conditions, an increase of intake temperature of 54% (typical variation when the engine is used on the public roads) results into a reduction of ID equal to 7% and, therefore, with the aim of developing a control-oriented ID model the effect of intake temperature variation must not be neglected.

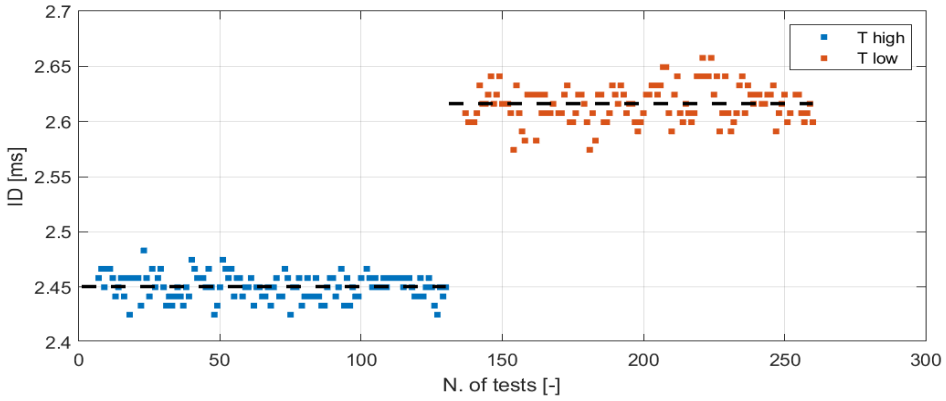

Figure 115. Effect of different intake temperature on ID

Intake Pressure

The other intake variable having a major impact on the ignition delay is the intake pressure. Since the energy required to overcome the autoignition conditions is mainly related to the thermodynamic of the air-fuel mixture, the rise of pressure and temperature will produce the same effect on ID. With the aim of verifying the impact of boost pressure on the ID of the GCI combustion (i.e., the gasoline autoignition dynamic) in the engine under study, specifically designed tests were conducted. Therefore, a boost pressure scan was performed while the others control parameter were kept approximately constant.

Table 15 reports the operating conditions during the boost pressure sweep test. It is important to mention that during the boost pressure sweep, the control parameters of the main injection were changed by the closed loop controllers (CL) to maintain the engine at constant IMEP and MFB50. Reducing the boost pressure, the combustion efficiency will be lower mainly because the lower amount of fresh air (M_{AIR}) hinders the mixing process between air and injected fuel, getting richer mixtures (i.e., low oxygen content) which reduces the thermal efficiency of the combustion.

Engine speed [rpm]	2000
IMEP [bar]	12
Boost pressure [bar]	**Sweep from 2.2 to 1.8**
Exhaust pressure [bar]	3
Intake temperature [°C]	74
MFB50 [ca. deg aTDC]	12
Injection pattern: SOI Pil, SOI Pre, SOI Main [deg bTDC]	[35, 21, CL]
Injection pressure [bar]	500

Table 15. Engine operating conditions during boost pressure sweep

Figure 116 shows RoHR traces running the GCI engine at a different boost pressures. By looking at the first combustion stage, similarly to the intake temperature, an increase of boost pressure results into a reduction of ignition delay. As a result, the first combustion stage will be even more anticipated. It is important to notice that despite the premixed stage of the combustion anticipates progressively, the peak of the first combustion stage of the RoHR reaches approximately the same value during the boost pressure sweep. This aspect could be partially explained through the local air-fuel mixing dynamic.

During the tests, the pilot injections (made by very small fuel quantities) were kept constant. It can be seen from Figure 116 that lowering the boost pressure does not hinder the formation of proper number of local zone in the combustion chamber with proper relative air-fuel ratio able to start burning, but retards only its ignition. As previously observed, the first combustion stage releases enough amount of energy to significantly reduce the ID of the main injection, the diffusive stages take place almost the same angular range during the boost pressure sweep.

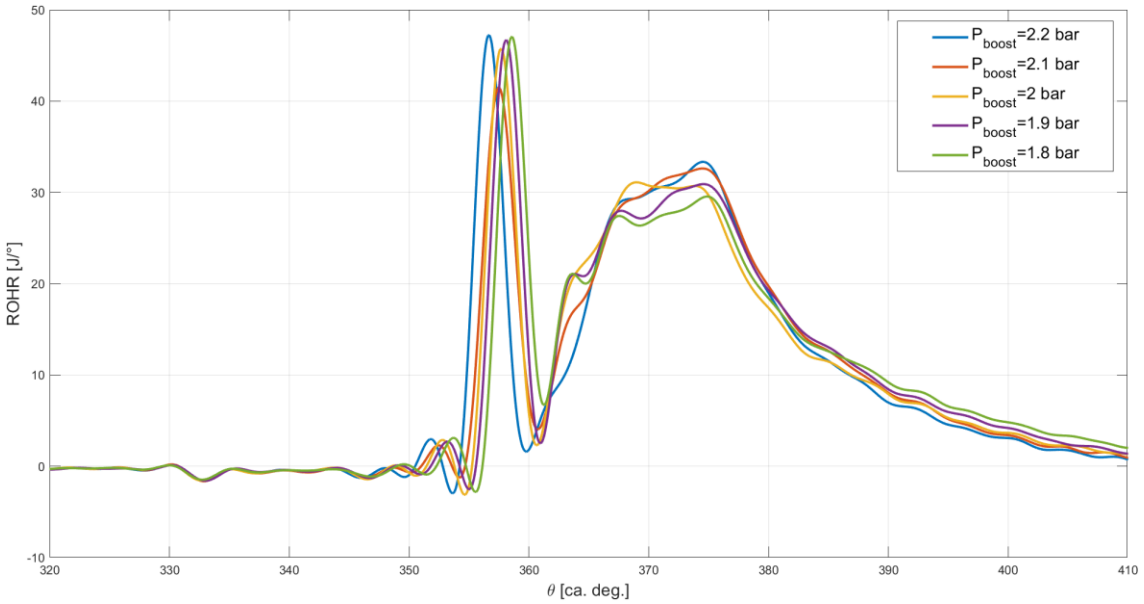

Figure 116. RoHR curves at different intake pressure

To quantify the effect of boost pressure variation on ID, Figure 117 reports the cycle-by-cycle ID evaluation. By observing Figure 117, it clearly arises that for every 0,1 bar of boost pressure increase, the ignition delay is subjected to a reduction of about 0,5 ms. The reported results confirm that also boost pressure have to be considered as fundamental parameter of the control-oriented ID model.

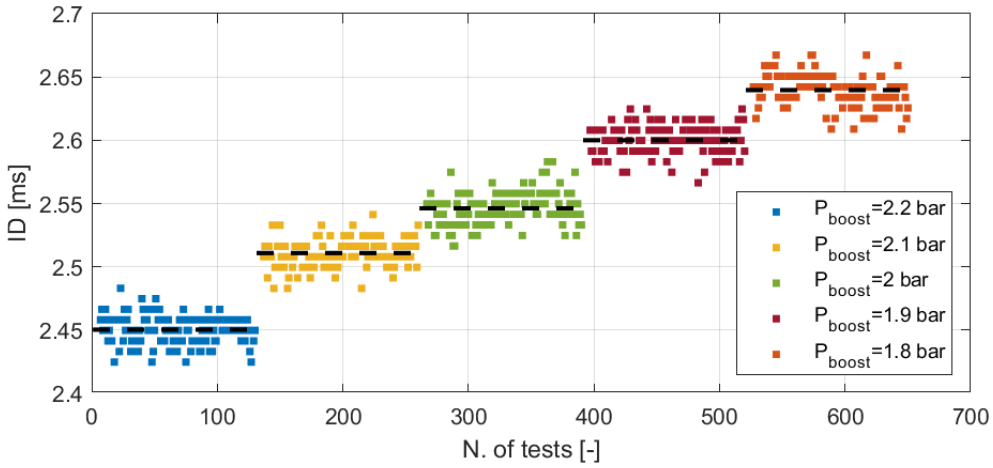

Figure 117. Effect of different intake pressure on ID

Mass and temperature of residual gases trapped in the combustion chamber

Since the premixed stage of the GCI combustion is chemically driven, the charge composition might modify the gasoline autoignition dynamic. In the combustion chamber, fresh air and gasoline are the most present components of the charge. Beyond these, residual gases are always present in the combustion chamber and therefore, their impact on ID must not be neglected. As well known, since residuals are typically composed by carbon dioxide coming from the exhaust stroke of the previous engine cycle, their temperature and quantity (with respect to the fresh air) impact on the autoignition process (of a chemically driven combustion) [31, 32]. As a result, to verify the effects of both temperature and amount of residuals on ID, two different kind of tests running the fully converted GCI engine were carried out.

First, the effect of different residual gases temperature (T_{RG}) was tested. Typically determined by engine load and position of the center of combustion, the temperature of the residuals depends on the temperature reached at the end of the combustion process. As a result, by using the above-described switching strategy, it was possible to highlight the impact of different temperatures of the residuals on ID. Keeping the GCI engine a stable operating point, the switching strategy was enabled in one of the four cylinder while the others engine parameters were kept at a fixed values. Figure 118 shows the RoHR of the recorded engine cycles before and after the switched cycle.

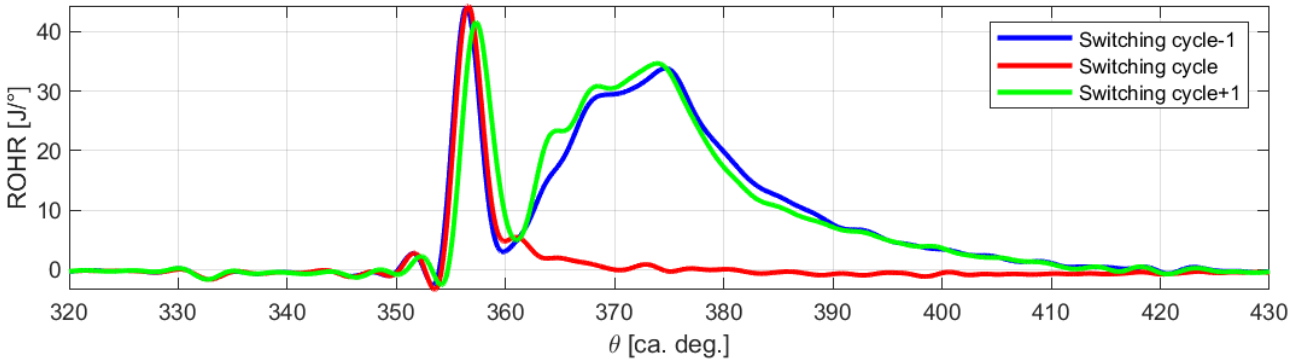

Figure 118. Effect of different residual gases temperature: RoHR for cycles before (blue) and after (green) the switching cycle (red)

As it can be seen, the premixed stage of the engine cycles with hot residuals, made by an efficient combustion process with remarkable engine load, (blue and red traces) are very similar both in terms of ID and magnitude of RoHR. Instead, by looking at the combustion after the switched cycle, the first combustion stage is delayed and slower (lower maximum RoHR is reached) compared to the previous cycles. Despite the switched cycle burns with high efficiency, the exhaust gases temperature will be very low (compared to the previous ones) mainly because of the lack of the main injection, responsible of the engine load production. Once these residuals are mixed with the fresh air (switching cycle+1) a colder charge will be generated charge with consequently longer ID. Moreover, the presence of the lower of temperature due to the colder residuals hinders the formation of proper local air-fuel ratios zones which can release energy (too low local temperature makes it impossible the combustion) and, therefore the maximum RoHR reached in the premixed stage is lower. However, despite the lower and delayed premixed combustion performed with cold residuals, the energy released is high enough to make stable the following diffuse stage (almost equal to blue trace with hot residuals). Very slight differences can be noticed only near 365 c.a. deg where the diffusive stage is a bit faster probably because of the heat released by the premixed stage is not high enough to completely minimize the ignition delay of the fuel injected through the main injection. As a result, the reported results demonstrate the impact of residual gases temperature on ID and therefore, it must be considered on ID modeling.

Previous results demonstrated that the residuals temperature impacts on ID of the first combustion stage because of their mixing with the fresh air. Thus, the higher is the amount of residual gases present in the combustion chamber, the hotter is the charge, with a consequent ID reduction.

As widely described when the cylinder filling model was described, the amount of residuals mainly depends on the cylinder pressure ratio (exhaust and intake pressure, $^{p_{EXH}}/_{p_{ASP}}$). Thus, to verify the dependency of the ID on the mass of residuals, a specifically designed test was carried out changing the exhaust pressure. To do so, the GCI engine was run in stable operating conditions and the amount of residual was varied only changing the exhaust pressure. Table 16 summarizes the operating conditions during the test on investigation of different amount of residuals. It is important to mention that to guarantee the same boost with different exhaust pressure, the boost controller (which manages the VGT actuator) was turned off. Intake and exhaust pressure were manually managed by using VGT coupled with the standard throttle valve (placed before the intake manifold but never used running GCI mode) which reduces the intake pressure at a target value.

	High Exhaust pressure	**Low Exhaust pressure**
Engine speed [rpm]	2000	2000
IMEP [bar]	12	12
Boost pressure [bar]	2	2
Exhaust pressure [bar]	**3**	**2.8**
Intake temperature [°C]	73	73
MFB50 [ca. deg aTDC]	12	12
Injection pattern: SOI Pil, SOI Pre, SOI Main [deg bTDC]	[35,21,4]	[35,21,4]
Injection pressure [bar]	500	500
ET_{main} [µs]	695	699

Table 16. Engine operating conditions testing the effect of two different amount of residuals on ID

Figure 119 clarifies the impact of the amount of residuals on ID for the two different exhaust pressures. The rise of hot residuals quantity increases the charge temperature and, consequently generates a slight reduction of ID. Even if the ratio between residual gases and fresh air is typically around 6% (for the engine under study run in GCI mode), their contributions to the ignition dynamics is not negligible. Hence, with the aim of developing a reliable ID model, both residual gases temperature and mass must be considered.

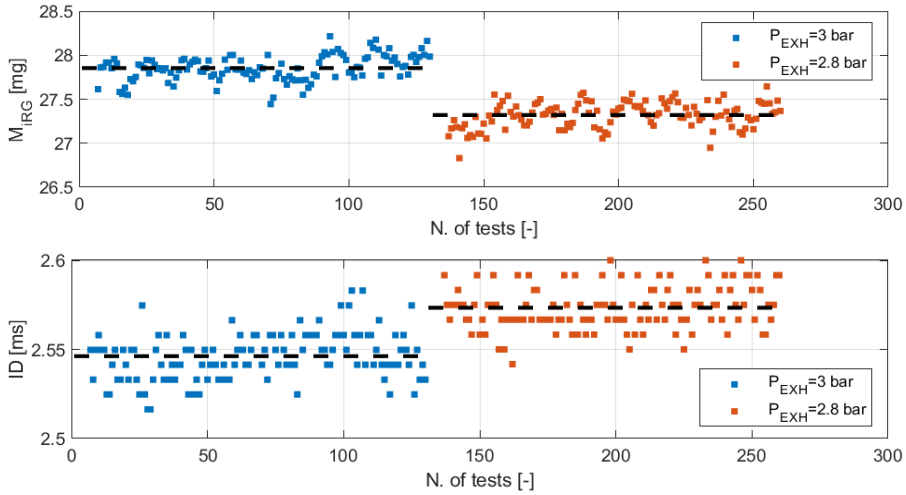

Figure 119. Effect of different residual gases mass on ID

Air humidity

In a spontaneous ignition of a lean air-fuel mixture, the chemical composition of the charge plays a crucial role on auto-ignition process. As above described, the charge of GCI combustion, keeping closed the external EGR, is typically composed by fresh air, fuel, and residual gases. Focusing the attention on the chemically driven stage of the GCI combustion, since the injected fuel (considering pilot injections only) and residuals are the smaller part of the charge, it was demonstrated that the chemical composition of the fresh air impacts ID. In general, the oxygen content of the fresh dry (without water vapor) air defines the (chemical) load of the combustion. However, a certain amount of water vapor is always present in the air, quantified by the relative humidity. As a result, the water vapor reduces the oxygen concentration of the fresh air and obstacles the formation of local zone with favorable air-fuel mixture able to release energy (internal mixing process), decreasing the reactivity of the mixture. Also in this case, the impact of the relative air humidity on the autoignition dynamic of the premixed stage combustion cannot be neglected.

To highlight the effect of the humidity [66] on GCI combustion, the same engine operating point was tested in different days with two relative humidities (Φ) as reported in Table 17.

	Low relative Humidity	**High relative Humidity**
Engine speed [rpm]	2000	2000
IMEP [bar]	12	12
Boost pressure [bar]	2.1	2.1
Exhaust pressure [bar]	3	3
Intake temperature [°C]	73	73
Relative humidity [-]	**25 %**	**40 %**
MFB50 [ca. deg aTDC]	12	12
Injection pattern: SOI Pil, SOI Pre, SOI Main [deg bTDC]	[35,21,4]	[35,21,4]
Injection pressure [bar]	500	500
ET_{main} [µs]	695	699

Table 17. Engine operating conditions testing the effect of two different relative humidity on ID

Figure 120 shows RoHR traces running the GCI engine at a different relative humidity. By looking at the first combustion stage, an increase of relative humidity leads to charge reactivity reduction mainly because of the lower oxygen content in the mixture and therefore, the first combustion stage is delayed. Furthermore, since water obstacles the internal mixing process, the premixed stage of the combustion will be slower (lower maximum values of RoHR curve). It is important to notice that despite the premixed stage of the combustion is delayed, the magnitude of the first combustion stage of the RoHR reaches approximately the same values assuring the reliability of the following diffusive combustion stage. Since the mixing process was delayed due to the presence of a big amount of water, the distance between the two combustion processes (premixed and diffusive) decreases.

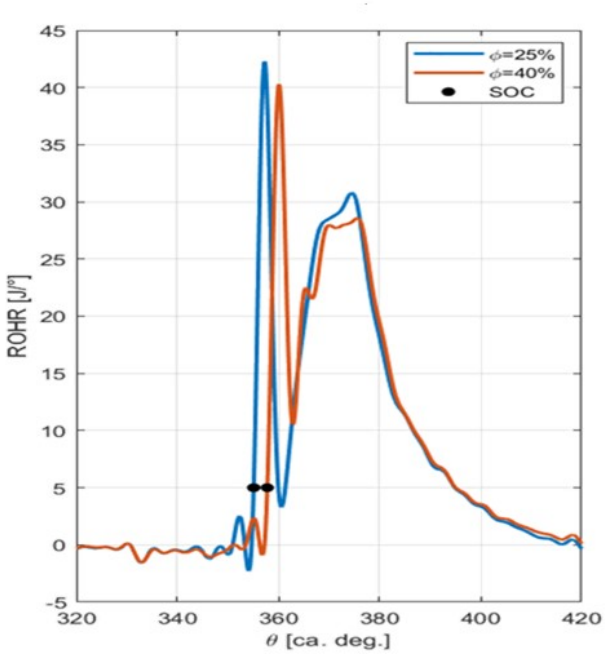

Figure 120. RoHR curves at different relative humidity

To quantify the effect of relative humidity variation on ID, Figure 121 reports the cycle-by-cycle ID evaluation. By looking at Figure 121, it clearly arises that an increase of 60% of the relative humidity (from 25% to 40%) results in a remarkable rise of ignition delay of about 0.25 ms (which is about a 10% increase of ID). The reported results confirm that the effect of air humidity have to be considered in the control-oriented ID model.

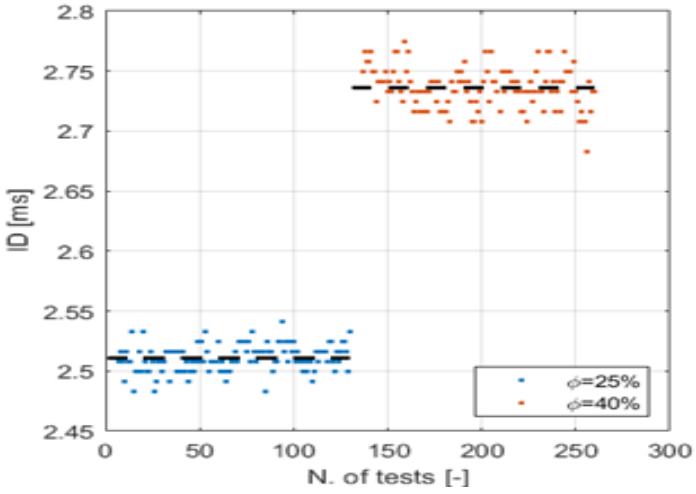

Figure 121. Effect of different relative humidity on ID

EGR rate

As deeply explained in the previous part of the PhD dissertation, GCI combustion needs high rates of exhaust gases recirculation to limit the combustion knocking and reduce NOx emissions [10, 26, 30]. Despite proven benefits using EGR in terms of combustion controllability and engine-out emission, several works demonstrate its impact on the autoignition dynamics in a spontaneous combustion process. Due to the different chemical composition and temperature between fresh air and exhaust gases recirculated in the combustion chamber, the internal mixing process will be modified with a remarkable impact on the whole combustion process, especially on the premixed stage.

To highlight the impact of EGR on the ID of the GCI combustion, an EGR sweep was performed using the fully converted GCI engine in a stable operating point. Table 18 shows the operating running conditions the EGR sweep. It is important to mention that during the EGR sweep the combustion controllers changes the main injection parameters (SOI and ET) to guarantee the targets values of IMEP and MFB50. Due to the EGR valve opening, the turbine is bypassed by a certain amount of exhaust gases and therefore, the intake pressure will be lower. Thus, to keep the boost pressure at a constant value the boost controller changes the VGT position to compensate the amount of exhaust gases flow lost through the EGR valve. Finally, by using the air flow rate measurement provided by the ultrasonic air flow meter, the EGR rate, defined through Equation 28, is calculated for each EGR valve position tested.

Engine speed [rpm]	2000
IMEP [bar]	12
Boost pressure [bar]	1.6
EGR rate [%]	**0-4-7-10-13-17**
Exhaust pressure at 0% of EGR rate [bar]	3
Intake temperature [°C]	45
MFB50 [ca. deg aTDC]	8
Injection pattern: SOI Pil, SOI Pre, SOI Main [deg bTDC]	[34, 20, CL]
Injection pressure [bar]	500

Table 18. Engine operating conditions during EGR rate sweep

As it can be noticed by looking at Figure 122, the use of EGR delays the SOC. As well explained by the literature, despite the increment in intake temperature given by the exhaust gases recirculation should reduce the ID, increasing the EGR rate the combustion will be even more delayed. This phenomenon could be explained through the worsening of the internal mixing process generated by the EGR. Since the presence of EGR reduces the oxygen content of the charge and therefore, increasing the EGR rate the SOC of the premixed stage will be delayed. Moreover, given that the chemical inertia of the EGR slows down the formation of the local zones with favorable relative air-fuel ratio able to release energy, with high percentage of the EGR rate the premixed stage will be even more impulsive mainly because a bigger amount of air-fuel mixture auto-ignites simultaneously.

The presence of the EGR has a remarkable effect also on the diffusive stage of the combustion. As shown by Figure 122, the presence of EGR also slows down the internal mixing process (between air and fuel) of the main injection, which dominates the diffusive stage. As a result, the second part of the combustion will be slower (lower RoHR trace) and longer (the end of combustion, near zero RoHR, is reached with bigger crank angle).

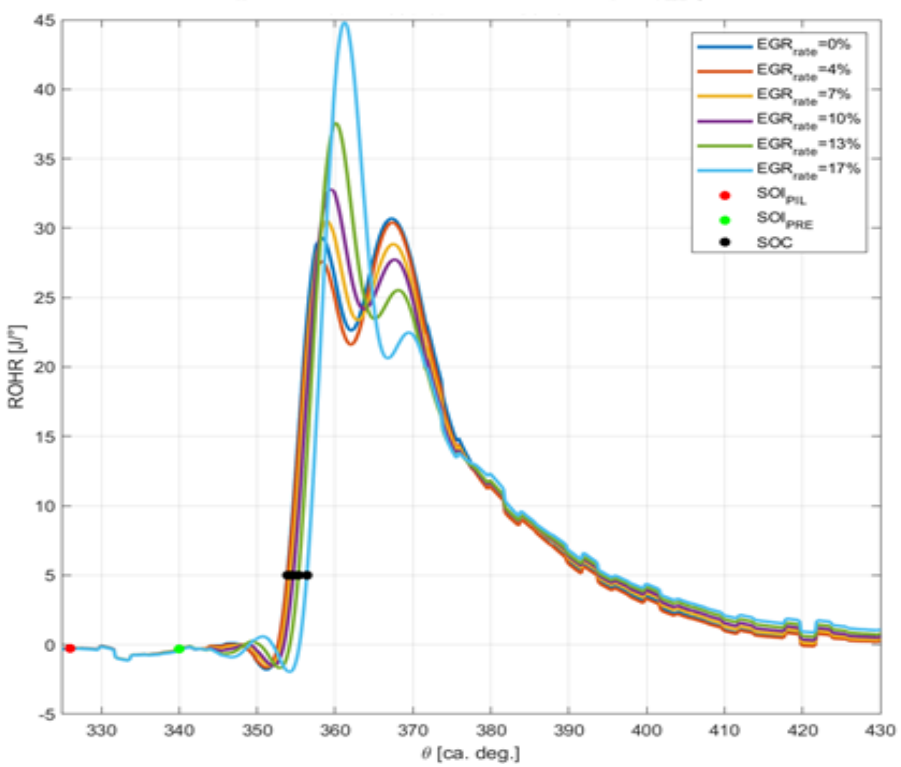

Figure 122. RoHR curves running GCI with different EGR rates

To quantify the effect of EGR rate variation on ID, Figure 123 reports the cycle-by-cycle ID evaluation for different EGR rates. By observing Figure 123, it clearly arises that increasing the EGR rate the ID will be bigger. Since GCI combustion can not be run without high EGR rates, the reported results confirm that also EGR rate have to be considered as fundamental parameter of the control-oriented ID model.

It is important to bear in mind that during the intake stroke, part of the available volume inside the cylinder is occupied by hot (with respect to fresh air and EGR) residual gases which rises increasing the EGR rate (due to the bigger back pressure generated by the VGT to keep boost pressure at a target value). Despite the visible impact on ID reduction of the residuals, when GCI is run with EGR, even increasing the amount of residual gases, their benefit is completely overwhelmed by the reduction of reactivity of the mixture caused by the EGR. This aspect can be notice by the analysis of the Figure 123. Comparing the ID of 0% and 4% of EGR rate condition, it clearly arises the effects of both residual gases and EGR. Despite the presence of EGR, which should increase ID, the bigger amount of hot residuals compared to 0% EGR rate (opening the EGR valve the exhaust pressure rises and consequently residuals increase) compensates the EGR effect keeping the ID at almost constant value, the same recorded without EGR. Once the EGR rate overcomes that condition, the ID will rise following the EGR rate increment.

The goal of this part of the PhD dissertation was to highlight which are the variables that significantly influence the ignition delay of the premixed stage of typical GCI combustion. The following paragraph describes the control-oriented ignition delay model developed to further increase the stability of the GCI combustion in the engine under study.

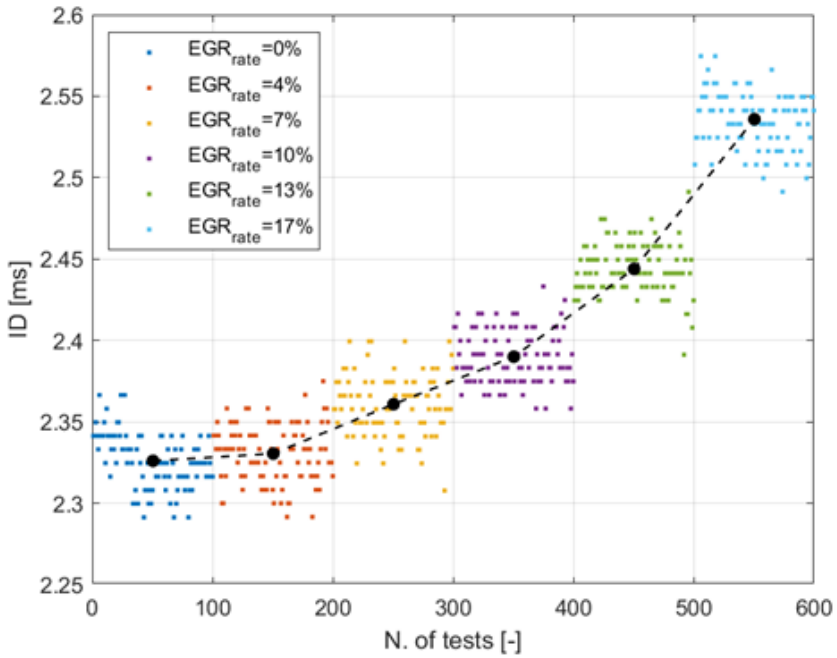

Figure 123. Effect of different EGR rates on ID

2.5.2 Ignition Delay Model development and calibration

As widely documented by the literature [15], the global behavior of a reacting system, such as spontaneous combustion, can be modelled as an Arrhenius-type expression, Equation 49, where k is the kinetic constant, A is the preexponential factor, T is the absolute temperature, E_a is the activation energy, and R_u is the universal gas constant.

$$k = A\, exp\left(-\frac{E_a}{R_u T}\right) \tag{49}$$

The general one-step fuel/air reaction describing the oxidation process of a fuel is given by Equation 50 where a and b are the number of moles of the oxidant and the combustion products, respectively.

$$Fuel + a * Oxidant \rightarrow\ b * Combustion\ Products \tag{50}$$

The global reaction rate q regarding that process can be expressed by Equation 51.

$$q\ \cong A * [\,Fuel] * [Oxidant]^a * exp\left(-\frac{E_a}{R_u T}\right) \tag{51}$$

By using the ideal gas state equation ($pV=mRT$) and the definition of the equivalence fuel/air ratio (φ), the global reaction rate can be assumed to be a function of the pressure, the temperature, and the equivalence ratio [15]. Since the ID is inversely proportional to the rate of the pre-reactions preceding the combustion process, it can be expressed by Equation 52.

$$ID = A * p^{-n} * \varphi^{-m}\ \ exp\left(-\frac{B}{T}\right) \tag{52}$$

However, despite it was proved that this relation could predict ID of a spontaneous ignition process considering fuel with a constant chemical properties (which define E_a), the variability in the fuel chemistry (commercial gasoline may vary by production batch) and the difficulty of correctly estimating (high uncertainties are always present) the model parameters (*A, n, m, and B*) reported in Equation 52 makes the presented approach difficult to use for control purpose. As a result, with the aim of developing a control-oriented model for ID estimation, a simpler approach was followed.

The above-described sensitivity analysis allowed to identify the effects (and their relative dynamics) of the variables which typically affect the ID of GCI combustion. The outcome of that analysis is summarized in Table 19. As mentioned before, the GCI combustion stability can be guaranteed by using a multiple injection strategy with two small pre-injections followed by the main injection. The results showed in the previous section of this work demonstrated that for the engine under study, two small injections around 1 mg/str each are needed to generate stable and reliable GCI combustion. For this reason, to study the ID of the GCI combustion both number of pre-injections and the injected quantity of each were kept approximately constant. By the different nature of the reported quantities, they can be combined in two classes: Thermodynamic and Chemical-Physical variables.

		Relation with the ID
Thermodynamic variables	T_{INT}	$\propto^{-1}$
	T_{RG}	$\propto^{-1}$
	SOI_{PIL} $[ca.deg.BTDC]$	$\propto$
Chemical-Physical variables	M_{AIR}	$\propto^{-1}$
	p_{EXH}/p_{ASP}	$\propto$
	EGR_{rate}	$\propto$
	ϕ	$\propto$

Table 19. Effects of both thermodynamic and chemical-physical variables on the ignition delay

According to the physical approach, the experimental data collected during the ID sensitivity analysis suggest that ID depends on both thermodynamics and chemical-physical properties of the air-fuel mixture. As a result, two parameters called T_{SOI} and M_{eq} which summarize the thermodynamics and chemical-physical properties of the mixture respectively were developed.

The thermodynamic parameter of the model (T_{SOI}), defined by Equation 53, collects the information of the charge temperature in the combustion chamber when the first fuel jet is performed. In Equation 53, the temperature of the mixture when the first fuel jet is introduced in the combustion chamber (SOI Pil) is obtained thought the isentropic compression of the charge starting from the intake closure (IVC).

$$T_{SOI_{PIL}} = T_{IVC}\left(\frac{V_{IVC}}{V_{SOI_{PIL}}}\right)^{\gamma_{comp}-1} \qquad (53)$$

While combustion chamber volumes reported in Equation 53 (V_{IVC} and $V_{SOI_{PIL}}$) can be directly calculated through geometrical consideration on the engine characteristics (IVC) and control parameters (SOI PIL), the charge temperature is obtained as weighted average between the charge components. Equation 54 shows the weighted average between the components of the charge in the combustion chamber at the intake valve closing: fresh air ($M_{CYL_{intake}}$) coming from the intake manifold (T_{man}) and residual gases of the previous combustion (m_{RG} at T_{RG}).

$$T_{IVC} = \frac{M_{CYL_{intake}} * T_{man} + m_{RG} * T_{RG}}{M_{CYL_{intake}} + m_{RG}} \qquad (54)$$

By looking at the parameters reported in Equation 54, $M_{CYL_{intake}}$ and m_{RG} can be easily calculated by using the cylinder filling model described in the previous section of this dissertation. It is important to mention that in case the EGR rate is equal to 0%, $M_{CYL_{intake}}$ measures only the mass of air entering the cylinder; conversely, whenever the EGR rate is different from 0%, $M_{CYL_{intake}}$ is given by the mass of air (by the ultrasonic flow rate measurement) plus the mass of EGR, Equation 55.

$$\begin{cases} M_{CYL_{intake}} = m_{Air} & if\ EGR_{rate} = 0\% \\ M_{CYL_{intake}} = m_{Air_{Flow\ rate}} + m_{EGR} & if\ EGR_{rate} \neq 0\% \end{cases} \quad (55)$$

Considering the temperature reported in Equation 54, T_{man} comes directly from the intake manifold temperature sensor, while T_{RG} is obtained considering the cooling process of residuals until the fresh air is incoming in the combustion chamber. As well known, once the intake valves are already wide open, the fresh air start entering in the combustion chamber when the intake pressure overcomes the in-cylinder pressure, Equation 31. During the intake stroke (intake valve is open and exhaust valve is closed), the in-cylinder pressure progressively decreases due to the volume increment (ΔV_1) at the beginning of the piston movement towards the BDC. As a result, until proper pressure value able to generate the air flow through the intake valve in the combustion chamber is reached, the residuals will progressively get colder following the isentropic expansion reported in Equation 56.

$$T_{RG} = T_{Exh}\left(\frac{V_{cc}}{(\Delta V_1 + V_{cc})}\right)^{\gamma_{Exh}-1} \quad (56)$$

Equation 54 and 56 show two different adiabatic coefficients mainly because different gas (charge or exhaust gases) temperature might vary significantly c_p and, consequently generate different γ values (especially γ_{Comp}). To consider that aspect, since the proved accuracy of the cylinder filling model, the c_p and, consequently γ calculation were performed based on the in-cylinder temperature by using the gas ideal law, reported in Equation 57, from the intake valve closing to the exhaust valve opening (when the system can be considered closed).

$$T_{cyl} = \frac{p_{cyl}(\theta)V(\theta)}{R_{air}(M_{CYL\_intake} + m_{RG})} \quad (57)$$

Once calculated the experimental in-cylinder temperature for every cycle, it is possible to evaluate γ during each cycle by means of the following expression reported in Equation 58, in which $c_P(T_{cyl})$ is modelled by means of the following polynomial expression showed in Equation 59. Once the isentropic coefficient during the whole engine cycle is available, by windowing and averaging the γ curve in the considered zone (form IVC to SOI Pil) it was possible to obtain γ_{Comp} for each analyzed engine condition (γ_{Exh} is obtained by using the exhaust gases temperature sensor and considering standard *R* constant for exhaust gases). Figure 124 shows the in-cylinder temperature and the corresponding isentropic coefficient within the angular interval ranging from IVC to EVO.

$$\gamma_\theta = \frac{c_P(T_{cyl})}{c_V(T_{cyl})} = \frac{c_P(T_{cyl})}{c_P(T_{cyl}) - R_{air}} \quad (58)$$

$$c_P\left(T_{cyl}(\theta)\right) = 1403.06 - 360.72 * \left(\frac{1000}{T_{cyl}(\theta)}\right) + 108.24 * \left(\frac{1000}{T_{cyl}(\theta)}\right)^2 - 10.79 * \left(\frac{1000}{T_{cyl}(\theta)}\right)^3 \quad (59)$$

Thus, as reported above, $T_{SOI_{PIL}}$ not only depends on the start of injection of the first fuel jet (i.e. retarding SOI_{PIL} will result into a higher $T_{SOI_{PIL}}$), but it also determined by the temperature of the mixture at the intake valve closure (i.e., T_{IVC}); which, in its turn, depends on both intake temperature and temperature of residuals as well as the mass entering the cylinder and the mass of residual gases which already were inside the cylinder, even considering the external EGR. It is important to bear in mind that one of the effects of recirculating exhaust gases is an increase of intake manifold temperature (T_{man}). Hence, increasing the EGR rate will consequently result into an increase of $T_{SOI_{PIL}}$.

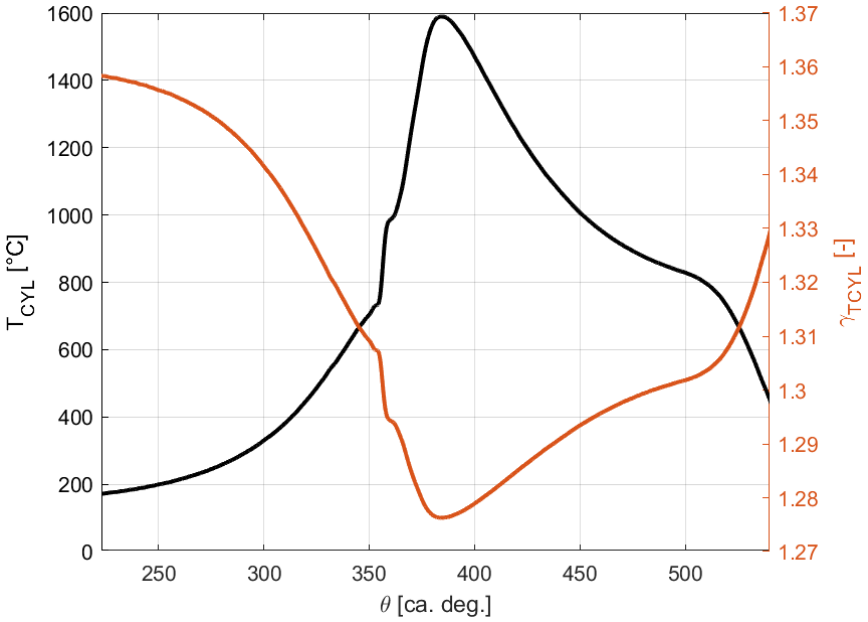

Figure 124. Variation of in-cylinder temperature and γ within the angular interval IVC-EVO

The chemical-physical variable of the ID model (M_{eq}) aims to quantify the chemical potential of the charge prior to the pilot injection. Considering the dependencies on ID highlighted during the sensitivity analysis and summarized in Table 19, the chemical potential of the charge can be expressed by Equation 60, in which M_{O_2} is the oxygen content of the fresh air entering the cylinder (reactive part of the charge, direct consequence of the boost pressure), M_{H_2O} is the amount of water vapor of the fresh air (ϕ), M_{RG} represents the mass of residual gases and M_{EGR} the amount of external EGR. The model parameters k_{iRG} and k_{ERG}, which will be discussed later, are used to consider the impacts of the residuals and EGR on the mixture chemistry trying to summarize the internal mixing phenomena which affect the ID.

$$M_{eq} = M_{O_2} - M_{H_2O} - k_{iRG}M_{RG} - k_{EGR}M_{EGR} \qquad (60)$$

As mentioned before, M_{RG} and M_{ERG} can be easily calculated through the in-cylinder filling model, as reported in Equation 30 and Equation 33 respectively. On the other hand, M_{O_2} and M_{H_2O} can be obtained by using simply physical considerations.

The air inside the test cell, and consequently the air entering the cylinder, is a binary mixture composed by dry air and water vapor; in its turn, dry air is mainly composed by N_2 (75.5 %) and O_2 (23.19 %) plus other gases whose mass fractions are negligible with respect to those of nitrogen and oxygen. Therefore, it is reasonable to assume that without EGR during the intake stroke, N_2, O_2 and water vapor enter inside the cylinder. The Dalton's law states that in a mixture of non-reacting gases, the total pressure is equal to the sum of the partial pressures of the individual gases.

This implies that, assuming air as composed by water vapor, nitrogen and oxygen, the ambient pressure measured inside the test cell (namely the total pressure) can be expressed through Equation 61.

$$p_{amb} = p_{dry\ air} + p_{water\ vapor} \cong p_{O_2} + p_{N_2} + p_{H_2O} \quad (61)$$

Accordingly, the mass of air entering the intake duct and consequently the cylinder (without EGR) is reported in Equation 62, in which the sum of $M_{O_2} + M_{N_2}$ represents the mass of dry air. Since the ratio between nitrogen and oxygen is almost constant, only the mass of oxygen will be considered as the reactive part of the mixture.

$$M_{air_{model}} = M_{dry\ air} + M_{H_2O} \cong M_{O_2} + M_{N_2} + M_{H_2O} \quad (62)$$

To evaluate the mass of oxygen and the mass of water vapor entering the cylinder, the pressure and temperature measurement inside the test cell as well as the relative humidity are exploited. The relative humidity (ϕ), expressed as a percentage, defines how much water vapor can the dry air contain at a given temperature and it is defined in Equation 63, in which $p_{water\ vapor}$ is the partial pressure of water vapor in the air-water mixture and p_{sat} (i.e., the saturation pressure) is the pressure exerted in a closed system at a given temperature when water vapor is in thermodynamic equilibrium with its condensed phase.

$$\phi = \frac{p_{water\ vapor}}{p_{sat}} * 100 \quad (63)$$

For this application, the p_{sat} is evaluated as a function of temperature as expressed in Equation 64, where T [°C] is the measured test cell temperature.

$$p_{sat} = 610.8\, exp\left(\frac{17.27 * T}{237.3 + T}\right)\ [Pa] \quad (64)$$

Once the relative humidity as well as the temperature inside the test cell are known, it is possible to calculate the partial pressure of water vapor as reported in Equation 65.

$$p_{water\ vapor} = \frac{\phi}{100} * p_{sat} \quad (65)$$

Now that the partial pressure of water vapor is known, it is possible to calculate the mass fraction of water vapor (i.e., $x_{mixture}$) as follow, Equation 66:

$$x_{mixture} = \frac{M_{H_2O}}{M_{air_{model}}} = 0.622 * \frac{p_{water\ vapor}}{p_{amb} - p_{water\ vapor}} \quad (66)$$

Once $x_{mixture}$ and the mass of air entering the cylinder are calculated, the mass of dry air and the mass of water vapor entering the cylinder are evaluated as reported in Equation 67 and Equation 68 respectively.

$$M_{dry\ air} = \frac{M_{air_{model}}}{1 + x_{mixture}} \quad (67)$$

$$M_{H_2O} = M_{air_{model}} - M_{dry\ air} \quad (68)$$

Finally, being the mass fraction of oxygen contained inside dry air equal to 23.19 %, the mass of oxygen entering the cylinder can be evaluated through Equation 69.

$$M_{O_2} = 23.19\%\ M_{dry\ air} \quad (69)$$

Once defined the model parameters, the ID model was derived by the analysis of several engine operating conditions in term of ID. By using a 2nd order polynomial function, it was possible to obtain the link between the ID of the switched cycles (in that way only the first combustion stage is considered, excluding mutual influences between the two combustion stages, premixed and diffusive) and the developed thermodynamic and chemical-physical parameters ($T_{SOI_{PIL}}$ and M_{eq}). The analytical expression used to model the ignition delay of GCI combustions is reported in Equation 70, in which the values of the model constant are summarized in Table 20.

$$ID = a + b * T_{SOI_{PIL}} + c * M_{eq} + d * T^2_{SOI_{PIL}} + e * T_{SOI_{PIL}} * M_{eq} + f * M^2_{eq} \qquad (70)$$

Model Parameter	Calibrated Values
a	25.69
B	-0.1127
c	-0.01435
d	$1.405e^{-4}$
e	$-1.191e^{-5}$
f	$5.235e^{-5}$

Table 20. Constants of ID model

Table 21 reports the engine operating conditions used to calibrate the ID model performing the switching pattern testing methodology over a wide range of engine operating conditions. Since the effect of EGR on ID is almost linear, the ID model was calibrated without considering the EGR. To further increase the calibration points for ID model, additional operating conditions were added running the engine with complete injection pattern without EGR and retarded combustion (MFB50 equal to 14 deg aTDC). In such conditions, reported in Table 22 and called EGR sweep tests, the retarded main injection positioning (which generates retarded MFB50) allows to separate the combustion stages (premixed and diffusive) and, therefore, accurately identify the SOC.

Engine Speed [rpm]	IMEP [bar]	MFB50 [deg aTDC]	Boost Pressure [barA]	Intake Temperature [C]	Exhaust Pressure [mbarA]	SOI Pil [deg bTDC]	SOI Pre [deg bTDC]	Relative Humidity [%]
2000	8	9	1.8	75	3.1	34	20	46
2000	9	12	1.7-1.6	70	2.5	43	29	38
2000	9	12	[1.9:0.1:1.6]	70	2.7	43	29	38
2000	12	12	2.1	72	3	35	21	40
2000	12	12	2.1	72	2.8	35	21	38
2000	12	12	[2.2:0.1:1.8]	74	3	35	21	25
2000	9	12	[1.9:0.1:1.6]	60	2.7	43	29	35
2000	9	12	1.8-1.7	60	2.5	43	29	35
2000	12	12	2.1	50	3	35	21	37
2000	12	12	2.1	50	2.8	35	21	37
2000	12	12	[2.2:0.1:1.9]	50	3	35	21	21
2000	12	12	[2.1:0.1:1.7]	50	2.8	35	21	21
2000	14	12	[2.2:0.1:2]	52	3	35	21	20
2000	14	12	[2.1:0.1:1.8]	52	2.8	35	21	20

Table 21. Engine operating conditions for ID model calibration running switching pattern methodology

Engine Speed [rpm]	IMEP [bar]	MFB50 [deg aTDC]	Boost Pressure [barA]	Intake Temperature [C]	Exhaust Pressure [mbarA]	SOI Pil [deg bTDC]	SOI Pre [deg bTDC]	Relative Humidity [%]
2000	8	14	1.5	40	1.9	32	18	44
2000	8	14	1.6	40	2.2	32	18	45
2000	12	14	1.6	46	1.8	34	20	44
2000	12	14	1.7	46	2	34	20	49
2000	14	14	1.9	43	2.2	35	21	45
2000	14	14	2	49	2.4	35	21	40

Table 22. Engine operating conditions for ID model calibration running GCI mode with EGR rate equal to zero

It is important to mention that the all the considered engine conditions are characterized by same engine speed (2000 rpm) and injection pressure (500 bar). Since the aim of the presented model is to predict the ID of GCI combustion, the baseline calibration of the engine must generate stable and reliable dual stage combustion. As a result, even if engine speed and injection pressure strongly modify the ID of the pre injections, the baseline injection phasing calibration shall be able to produce a GCI dual stage combustion. Future steps of this activity will be aimed to verify the ID model changing rpm and injection pressure.

As shown by Equation 60, the ID of GCI combustion is strongly affected by physicals and chemicals effects of the residual gases and, therefore, the chemical-physical parameter M_{eq} consider such dependencies by using k_{iRG}. Since it was demonstrated during the ID sensitivity analysis, that both temperature and quantity of residuals modify the gasoline autoignition dynamics, k_{iRG} was evaluated with respect to the product between the cylinder pressure ratio ($\frac{p_{exhaust}}{p_{intake}}$, which defines the amount of residual gases) and the charge temperature when residuals met the fresh charge (T_{IVC}). By using the tests listed in Table 21 and Table 22, in which different amount and temperature of residuals were performed, it was possible to calibrate k_{iRG} , reported in Figure 125, without external EGR, minimizing the distance between measured and estimated SOC.

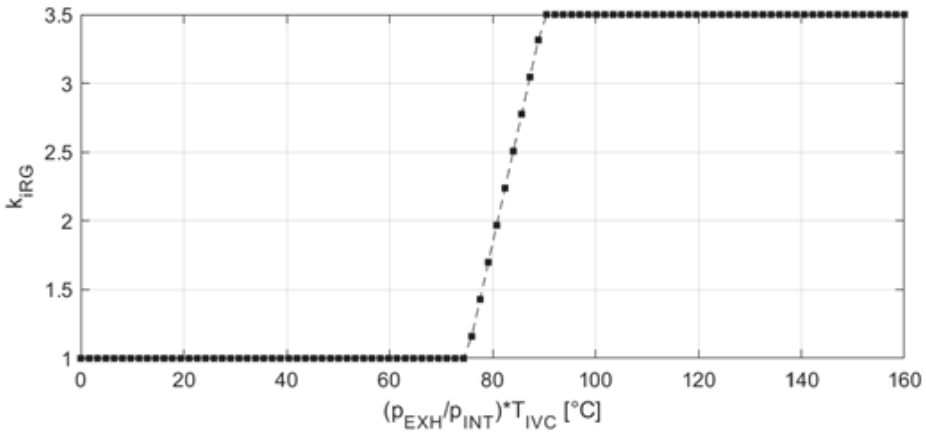

Figure 125. Calibration of k_{iRG} as function of the variable $\frac{p_{exhaust}}{p_{intake}} * T_{IVC}$

Figure 126 shows the ID model together with the calibration points coming from the before mentioned tests used to build it. Looking at both the x-z and y-z planes, it is clearly visible that for a given value of equivalent mass, the ignition delay increases if the temperature at the start of injection of the pilot injection reduces. Similarly, for a given $T_{SOI_{PIL}}$, the ignition delay increases if the equivalent mass (which basically represents the amount of oxygen entering the cylinder) reduces.

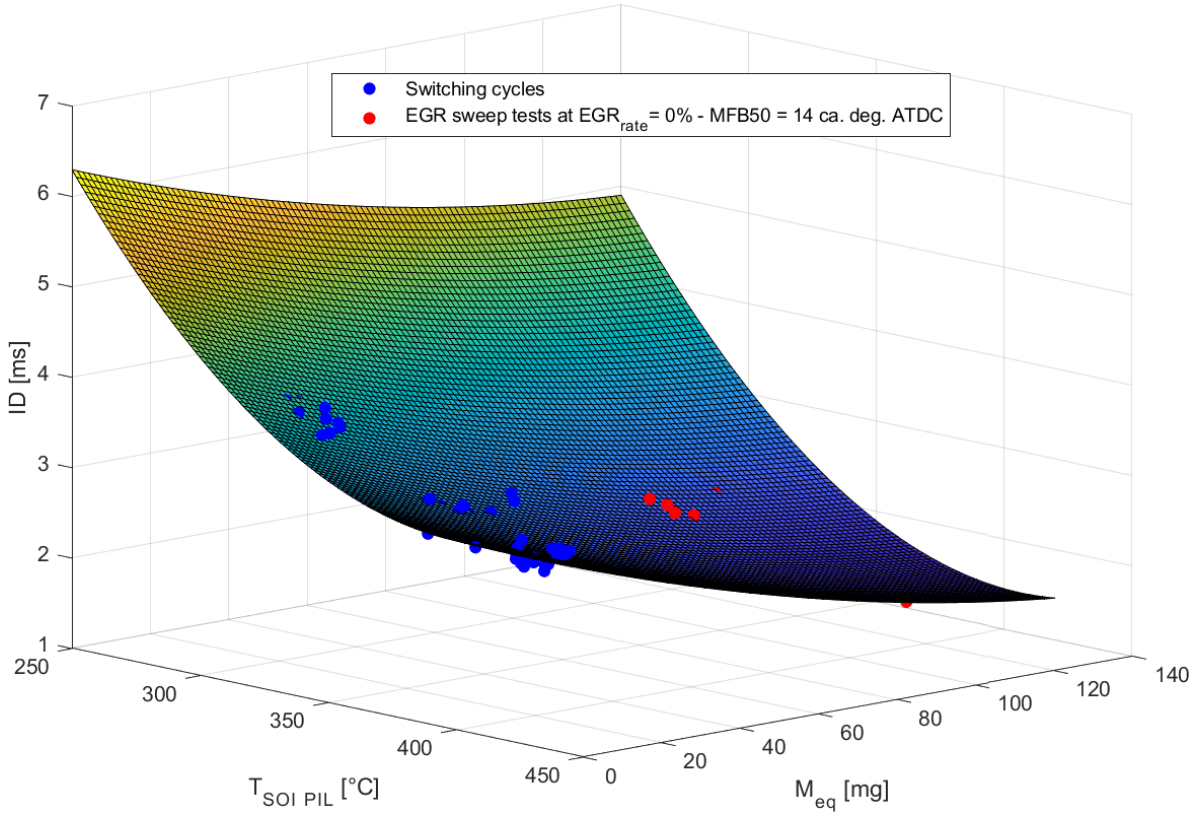

Figure 126. ID model

Since GCI mode needs big amount of external EGR to effectively reduce both pollutants and emissions, the ID model was used even with different EGR rates. As described during the ID sensitivity analysis, the external EGR obstacles the internal mixing process retarding the SOC positioning. Moreover, it was demonstrated that increasing the EGR rate, the SOC rises almost linearly. Therefore, k_{EGR} was calibrated as linear function of EGR rate to bring back SOC at the measured value without EGR. Figure 127 shows the calibration of k_{EGR} as a function of EGR rate running the GCI operating condition summarized in Table 22. It is important to notice that the impact of EGR can be neglected at EGR rates lower that 5%. As proved during the ID sensitivity analysis, the increment in charge temperature given by EGR compensates the chemical inertia of the recirculated exhaust gases.

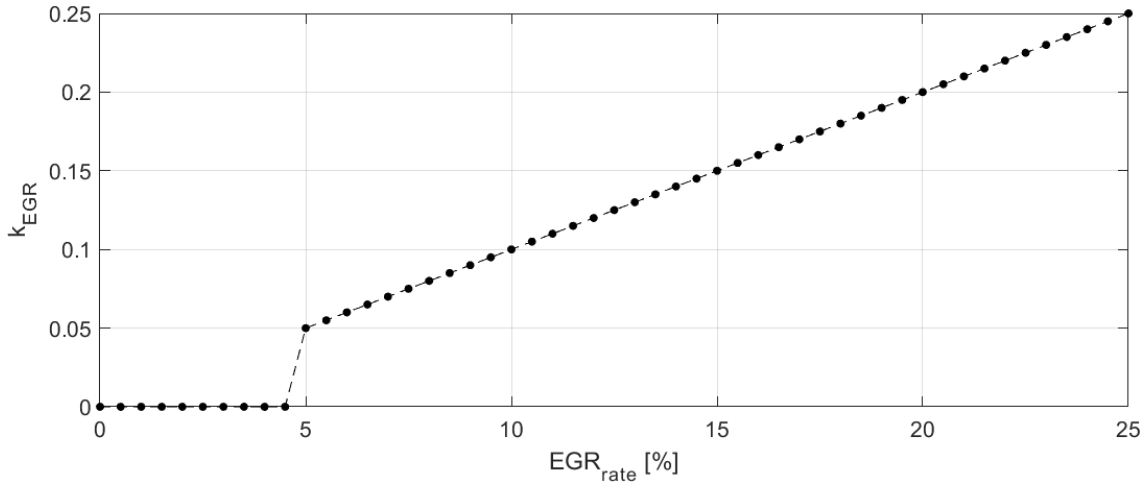

Figure 127. Calibration of k_{ERG} as function of the EGR rate

During the ID sensitivity analysis, it was demonstrated the mutual effects of residual gases and EGR on ID, especially at very low EGR rates. Mainly because of the amount of EGR (generally bigger than residuals) and its temperature (colder), the impact of residual gases on ID progressively decreases. By looking at Figure 128 which shows the ratio between residuals and external EGR, it clearly arises that the residuals rapidly decrease performing an EGR rate sweep following an exponential trend, i.e., $1/(p_{EXH}/p_{INT})\text{^}4$.

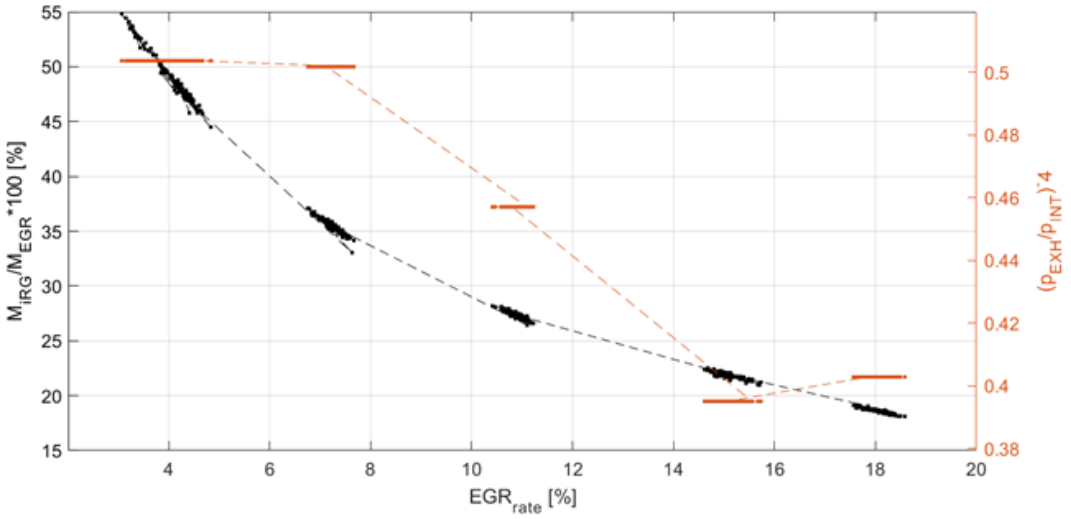

Figure 128. Percentage of residual gases with respect to mass of EGR and $1/(p_{EXH}/p_{INT})\text{^}4$ as a function of EGR rate

As a result, to decrease the impact of residuals on internal mixing and ID when external EGR was used, k_{iRG} was multiplied by the afore-mentioned residuals magnitude coefficient, defined by the relation: $1/(p_{EXH}/p_{INT})\text{^}4$. Figure 129 shows the calibration of k_{iRG}, i.e., the impact of residuals on ID, as a function of $\frac{p_{exhaust}}{p_{intake}} * T_{IVC}$ in two different cases: without EGR (k_{iRG}) and with EGR ($k_{iRG} * 1/(p_{EXH}/p_{INT})\text{^}4$). By observing at Figure 129 it clearly arises that the impact of residuals must be reduced because of differences on internal mixing, chemistry, and local temperature with EGR. Once defined and calibrated the model and its coefficients, the following section of the PhD dissertation describes the obtained results by applying the ID model on GCI mode.

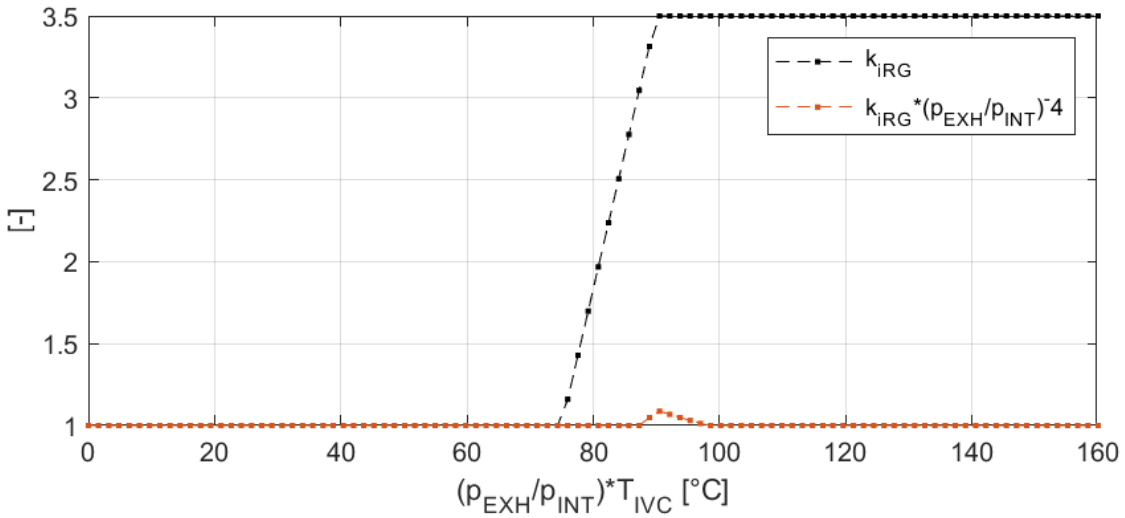

Figure 129. Comparison between the calibration of k_{iRG} in case of EGR (orange) and without EGR (black)

2.5.3 Ignition Delay Model: Results

After defining and calibrating the ignition delay model and their coefficients, to validate the presented approach the cycle-by-cycle ID estimation was performed for all the engine operating conditions reported in Table 21 and Table 22. Figure 130 shows a schematic of SOC modelling and summarizes the calculation of the two main parameters: T_{SOIPIL} and M_{eq}.

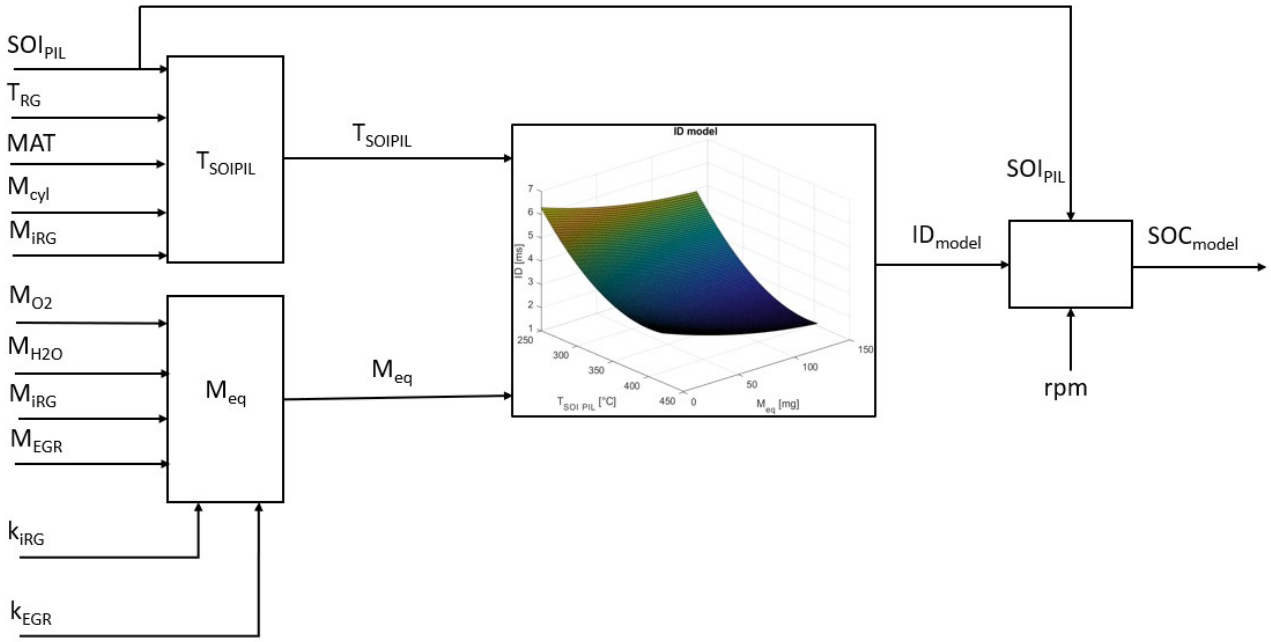

Figure 130. Schematic of SOC estimation based on ID model and T_{SOIPIL} and M_{eq} calculation

The model accuracy was evaluated as the difference between measured and estimated SOC defined by Equation 71. Since it was demonstrated that the SOC positioning for GCI mode is crucial to guarantee the whole combustion process stability, the maximum error was fixed at ±5°.

$$e_{model} = SOC_{exp} - SOC_{model} \qquad (71)$$

Figure 131 and Figure 132 show the accuracy of the cycle-by-cycle SOC estimation obtained applying the developed ID model performing MFB50 sweeps, from knocking to misfire limits, for each engine operating condition reported in Table 21 and Table 22. By looking at both Figures the model accurately predicts the ID of GCI combustion for very different engine conditions. It is important to point out that, considering the switching pattern tests (identified by blue dots), only few cycles (around cycle 5500) remarkable exceed the target error of ±5°. In such conditions, characterized by very low load for GCI combustion, extremely lean condition does not guarantee proper internal mixing and, therefore the cycle-by-cycle variability of the whole combustion will increase decreasing the combustion efficiency. As a result, poor combustion process will generate different residuals (temperature, chemical composition, and quantity) which modify T_{SOIPIL}, M_{eq} and the mixing dynamics considered through k_{iRG}, leading in a decrement of the accuracy of the ID estimation.

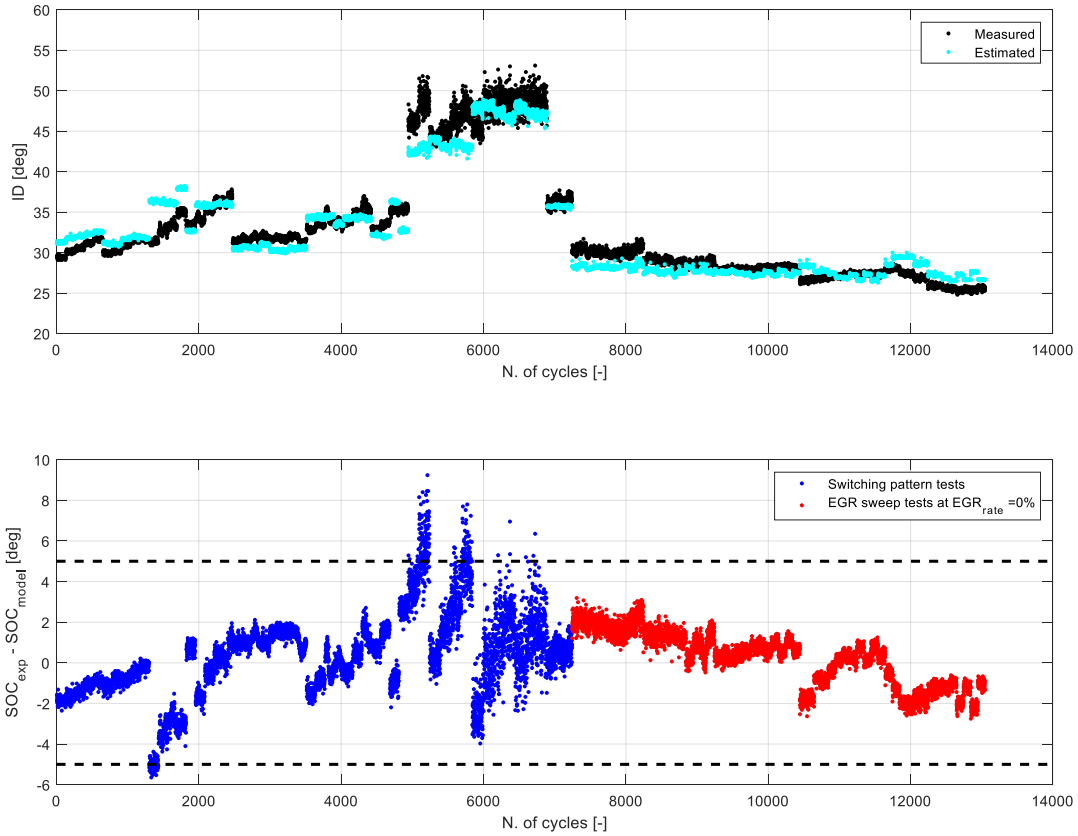

Figure 131. Accuracy on cycle-by-cycle SOC estimation for switching pattern tests: top subplot comparison between measured and estimated ID, bottom subplot error evaluation

It is important to notice that also the condition around cycle 1250 (CA50 sweeps at IMEP 14 bar), in which the relative humidity was very different (20%) compared to the all the analyzed conditions (approximately 40%), slightly exceeds the accuracy limit of -5°. Since the model was calibrated considering only one engine cycle for each condition showed in Table 21 and Table 22, the very low magnitude of such errors (very close to -5%) suggests that an improved ID model calibration (by averaging two or three switched cycles in similar conditions) might eliminate that inaccuracy. By observing Figure 132, it is possible to notice that even performing EGR sweeps (for each value of MFB50 tested during the sweeps) the model can accurately predict the ID in different engine operating conditions (shown in Table 22).

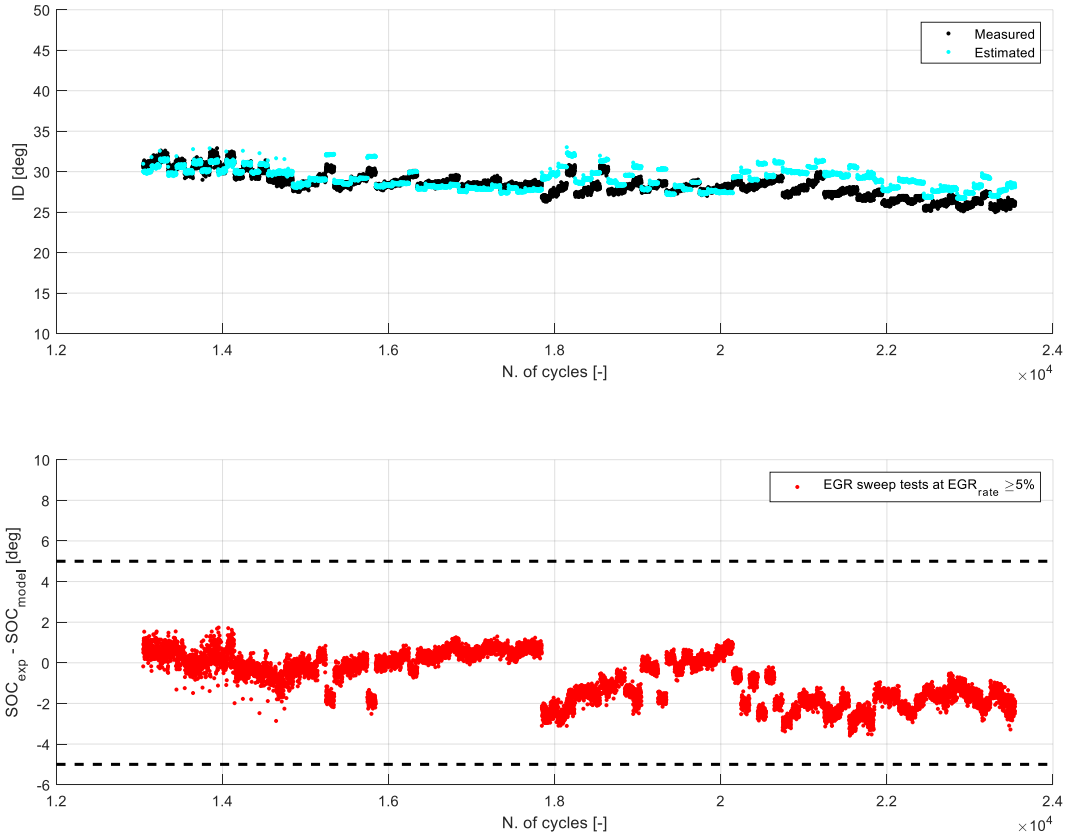

Figure 132. Accuracy on cycle-by-cycle SOC estimation for EGR sweep test: top subplot comparison between measured and estimated ID, bottom subplot error evaluation

Moreover, despite the schematic shown in Figure 130 was effective for control purpose (all the quantity are real-time available cycle-by-cycle), by the shape of GCI combustion (dual stage with premixed and diffusive stages), the evaluated SOC can be compared to another measured SOC coming from a non-intrusive sensor. As a result, thanks the knowledge of the real SOC the ID model can be re-centered with corrective factor through an adaptive strategy. The following section shows the experimental results about the SOC estimation based on accelerometer and the comparison with the calculation of the same index through the in-cylinder pressure sensor.

2.5.4 Accelerometer Based Start of Combustion detection for GCI combustion

As described in the previous section of this PhD dissertation, GCI combustion proved to be an effective way to increase the thermal efficiency and reduce pollutants of ICE. However, to make the GCI combustion stable and controllable assuring the before-mentioned benefits, very complex control strategies are needed. As a matter of fact, it was demonstrated that GCI controllability is achievable by using multiple injections pattern. The rise of temperature and pressure in the combustion chamber given by the combustion of small amount of fuel (pilot injections) early injected in the engine cycle, allows to significantly reduce the ignition delay of the following main fuel jet and, consequently, control the torque production and combustion phasing over its whole operating range. By the analysis of the GCI combustion, it was observed that by using multiple injections, the combustion shape is typically composed by two stages: premixed stage followed by a diffusive stage. The premixed stage, generated by the simultaneous energy release of the fuel injected through pilot injections, is the main responsible of the GCI controllability and therefore, its stability and efficiency must be guaranteed. Since the premixed stage is a chemically driven process, slight variations of the cylinder thermal conditions might compromise the combustion stability and, consequently, engine reliability. As a result, to further increase the stability of GCI combustion, complex control strategies were developed based on both feedforward and feedback contributions.

As an example of feedforward contribution for combustion control, an ignition delay estimation for the first combustion stage of GCI combustion was presented in the previous paragraph of this dissertation. By using this model-based information, the combustion controller will manage the injection phasing stabilizing the ignition process of GCI combustion when the engine run far from the calibration conditions. However, despite model-based contributions improve the effectiveness of the control strategy, they intrinsically contain uncertainties that might compromise the performance of the engine. As a result, to improve the robustness and reliability of these control strategies, combustion indexes of feedback were introduced.

For ICEs, the most common sensor which provides combustion feedback is the in-cylinder pressure sensor. However, pressure sensors on-board installation is still uncommon, mainly due to problems related to their reliability and cost. To overcome these problems, over the past years, several remote combustion sensing methodologies were developed to extract information about combustion process, such as SOC, MFB50, within the engine cycle through the real-time processing of signals coming from low-cost sensors (such as speed sensors or accelerometers) mounted on the engine [21]. Since it was demonstrated that the ignition process in GCI mode represent the key factor guaranteeing the stability of the whole combustion process, this section shows the results of the experimental activity aimed at verifying the SOC detection by using an accelerometer sensor mounted on the engine.

Figure 133. PCB Piezotronic 352C33 vibrational sensor

To measure engine block vibration, one high-accuracy accelerometer PCB Piezotronic 352C33, reported in Figure 133, was installed in the middle of the cylinder head between cylinder 2 and 3, as shown in Figure 134. To maximize the sensibility (i.e., magnitude of vibration and range of frequencies), the sensor was coupled through a mechanical thread.

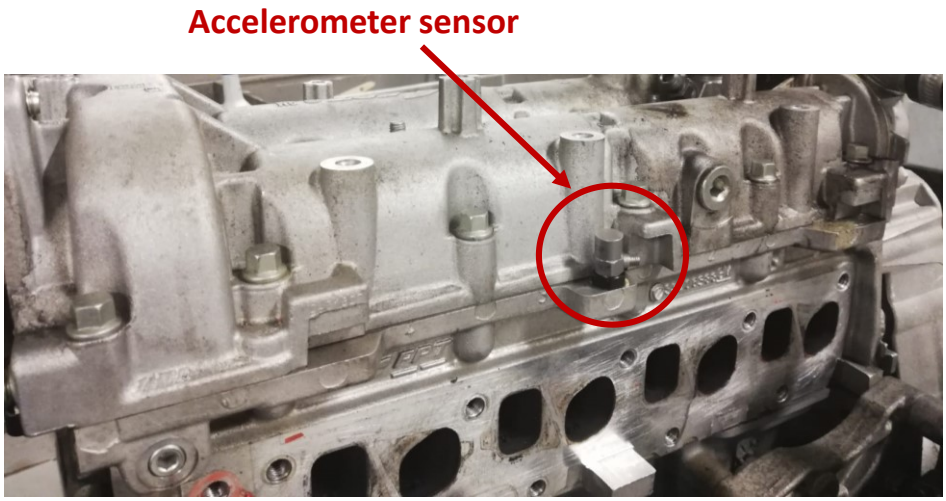

Figure 134. Accelerometer positioning on the engine: head placing

Many works on combustion indexes estimation using remote sensing demonstrate the correlation between engine block vibrations and the way combustion process takes place in the combustion chamber [21, 67, 68]. Cylinder pressure and accelerometer signal show high coherence in the frequency range usually associated to the combustion process, i.e., for frequencies lower than 4 kHz. The highest coherence values occur at the engine firing frequency and its multiples, indicating that the firing frequency and its harmonics dominate the response of the engine structure and the response captured by both cylinder pressure transducer and accelerometer.

Previous results reported in literature demonstrate that engine block acceleration is usually correlated with cylinder pressure first derivative, except for the delay between the signals, that corresponds to the time delay existing between the combustion event and the moment in which the effect is captured by the acceleration transducer. Considering conventional combustion processes, the highest accelerometer peak is usually correlated to the start of the combustion position, while the following zero-crossing provides information about the angular location of in-cylinder pressure peak. Despite GCI combustion is characterized by different combustion shape (with respect to CDC), Figure 135, which reports in-cylinder pressure derivative and engine block acceleration (all normalized with respect to their maximum values), confirms the existence of such correlation also in GCI operating mode.

Due to the typical shape of GCI combustion, only the premixed combustion stage generates a remarkable engine block vibration because it releases a big amount of energy in a short time. The following combustion stage, characterized by smoother heat release, generates very low vibration which could be confused with the mechanical vibration of the engine or, in the worst case, with the propagation tail of the oscillation generated by the previous combustion stage. As a result, for GCI combustion only the SOC detection of the first combustion stage can be considered effective and then, to make them more reliable, the developed methodology considers the RoHR derivative.

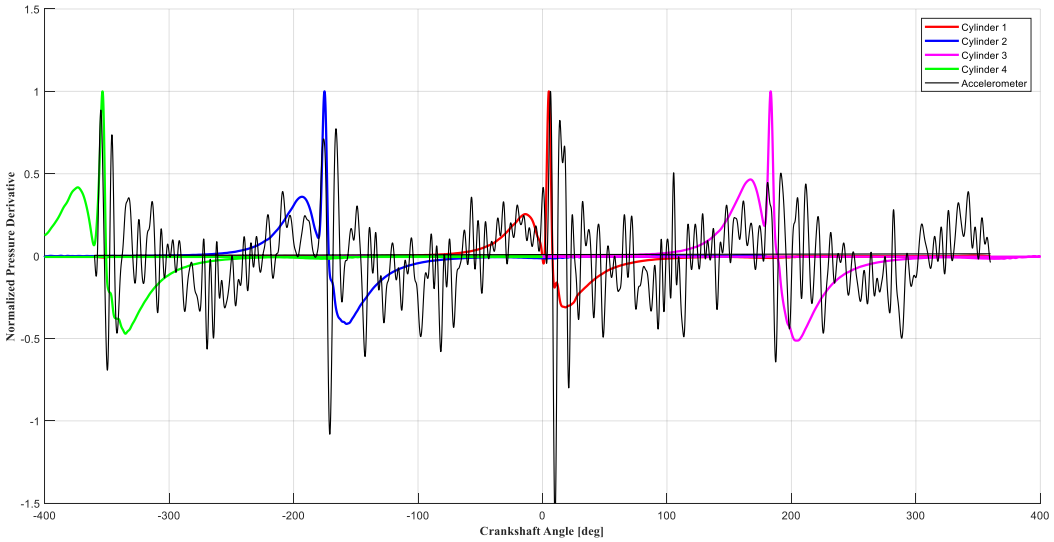

Figure 135. Comparison between (normalized) in-cylinder pressure derivative and accelerometer signals

The methodology, reported in this work, filters the acquired accelerometer signal using a bandpass filter with cutoff frequencies equal to 0.3 kHz and 2.5 kHz. Then, the filtered signal is resampled in the angular domain and properly windowed around the top dead center (TDC) of each cylinder. Finally, the algorithm automatically detects, for each cylinder, the major peak of the windowed signal that provides a reliable estimation of SOC position within the engine cycle. It is important to point out that due to the different vibration propagation on the engine block (which is typically function of the engine speed), the time delay of the accelerometer signal was characterized offline cylinder-by-cylinder. An example of signals processing (RoHR derivative and accelerometer signal respectively) for SOC detection is reported in Figure 136.

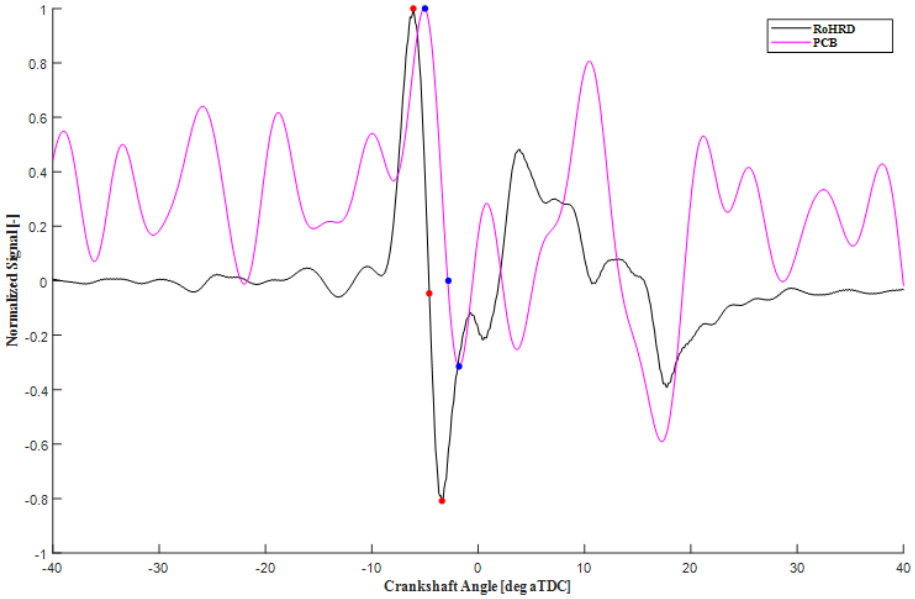

Figure 136. Signals processing of non-intrusive SOC detection

Once defined the accelerometer signal processing algorithm, the correlation between measured and estimated SOC was obtained running GCI engine at 2000 rpm changing the control parameters which typically affect the SOC positioning. Table 23 summarizes the operating conditions tested to calibrate the measured and estimated SOC correlation. By looking at Figure 137 it clearly arises the strong correlation between SOC position evaluated through in-cylinder pressure and accelerometer signals for the cylinder 3 (100 consecutive engine cycles was considered for each condition). It is important to point out that especially for engine conditions characterized by low temperature, which generates the decline of the ignition phase, the reliability of the SOC estimation decreases.

Engine Speed [rpm]	IMEP [bar]	MFB50 [deg aTDC]	Boost Pressure [barA]	Intake Temperature [C]	Exhaust Pressure [mbarA]	Gasoline Pressure [bar]	SOI Pil [deg bTDC]	SOI Pre [deg bTDC]	Relative Humidity [%]
2000	12	12	2	79	1.9	350:50:900	32	18	40
2000	12	12	2	54	2.2	350:50:900	32	18	45
2000	12	12	2.1-1.8	54	3.5-3.3	500	34	20	41
2000	12	12	2.1-1.8	79	3.5-3.3	500	34	20	43
2000	14	12	2.1-1.8	54	3.5-3.3	500	35	21	45
2000	14	12	2.1-1.8	79	3.5-3.3	500	35	21	39

Table 23. GCI operating conditions during the calibration of SOC estimation with accelerometer signal

As mentioned before, in GCI combustion, the SOC is mainly related to the premixed combustion stage efficiency. As a result, lowering the intake temperature, the ID of the pre injections (responsible of the first combustion stage) will increase modifying the whole RoHR shape. Figure 138 shows the RoHR of the engine running at the same engine condition (2000 rpm – 12 bar IMEP) but different intake temperatures. By looking at the RoHR, the remarkable differences on the first combustion stage explains the worsening on the SOC detection by the accelerometer: the high temperature condition (at left) shows two clearly-defined combustion stages with high energy released in the first part; on the contrary, decreasing the intake temperature (at right) the typical GCI dual stage combustion collapses in only one phenomenon. The lack of a well-defined premixed combustion is the cause of wrong SOC detections reported in Figure 137.

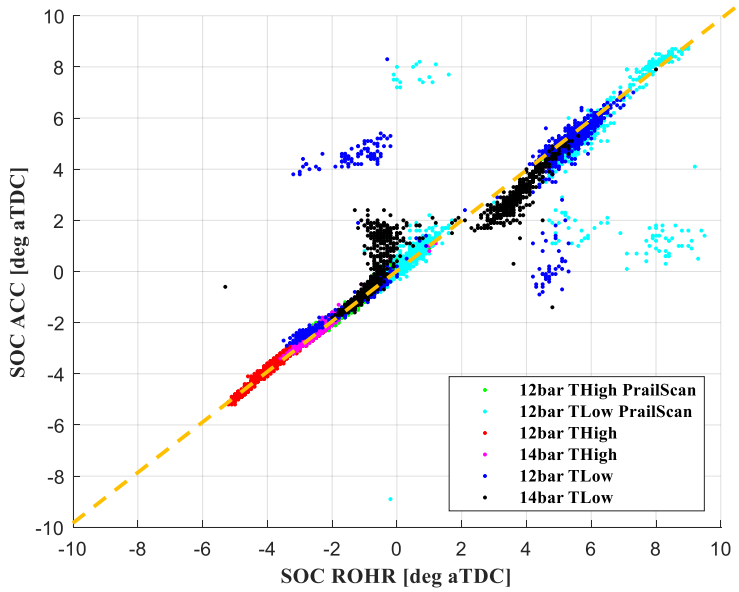

Figure 137. Comparison between SOC detections through cylinder pressure signal and accelerometer

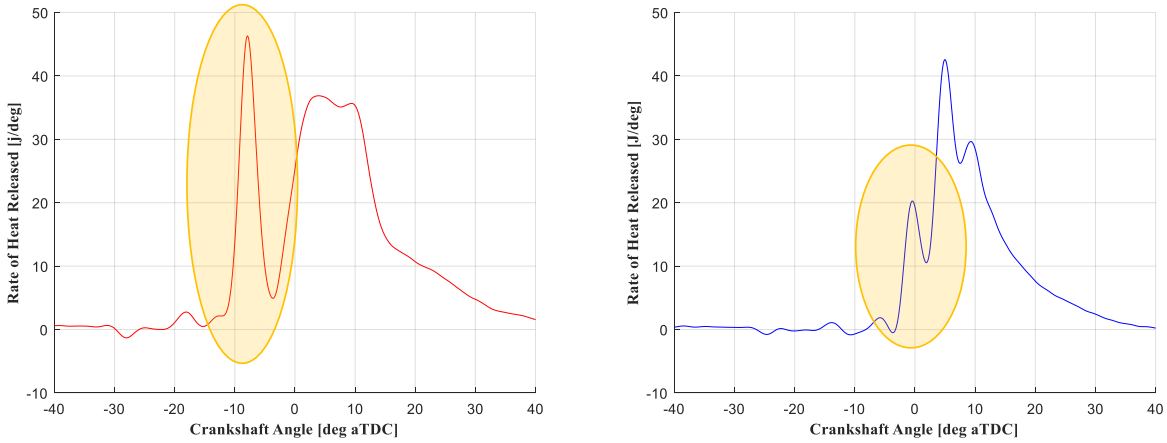

Figure 138. RoHR for different GCI operating conditions at 2000 rpm: high load (left) and low load (right)

Despite it was demonstrated that the SOC position can be effectively obtained by the analysis of the vibrational sensor, due to the different propagation of vibrations on the engine block, the accuracy of the presented estimation methodology is strongly affected by the sensor positioning. As a matter of fact, the sensitivity on vibrations changes from cylinder to cylinder manly because the distance between the sensor and the cylinders are different. To clarify that aspect, Figure 139 shows the SOC detection performed cylinder-by-cylinder running the GCI engine at 2000 rpm with IMEP 8 bar and performing MFB50 sweep from 8 to 14 deg aTDC (gasoline pressure was set equal to 500 bar). Despite the unfavorable conditions for GCI combustion (very low load), the accuracy of SOC estimation trough the accelerometer remains high for cylinders 2 and 3, while significantly decreases for cylinder 1 and 4. By the analysis of the reported results in Figure139, it clearly arises that to guarantee the SOC estimation reliability using the accelerometer, the sensor positioning plays a crucial role.

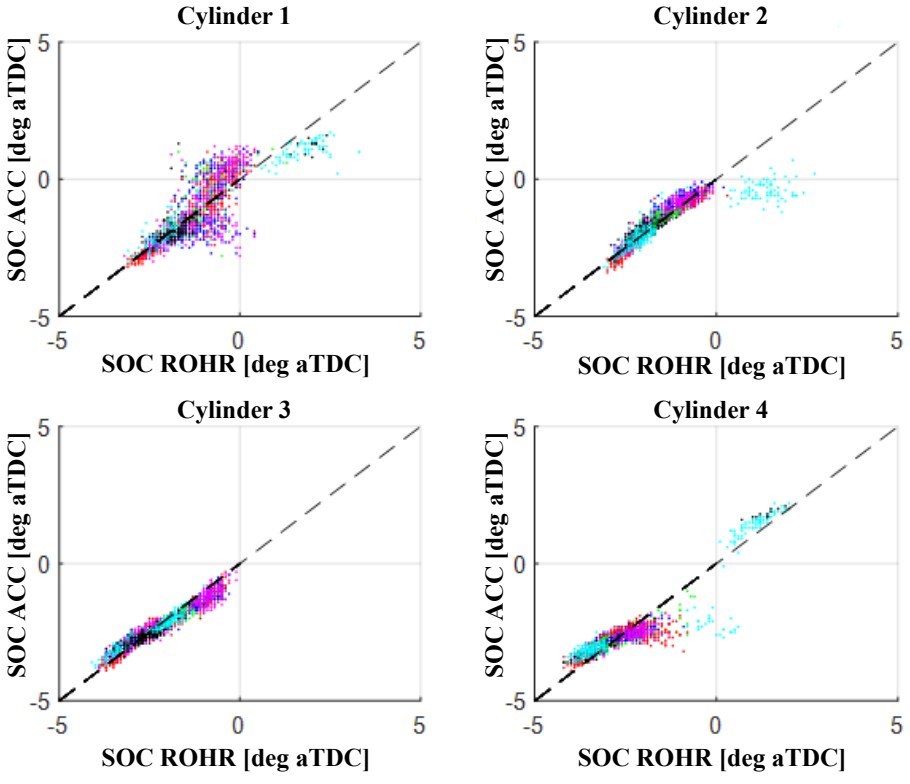

Figure 139. SOC detection with accelerometer: sensitivity on sensor positioning

With the aim of finding the sensor position on the engine block which guarantee good accuracy on SOC estimation for all cylinders, a wide experimental activity was carried out running the engine in the same conditions and changing the sensor position. Figure 140 shows the three different tested sensor positions (dummy sensors are shown): two on the exhaust side of the engine (at right) and only one on the intake side (at left). The whole experimental activity was conducted using the same vibrational sensor (PCB Piezotronic 352C33). Since the literature on remote sensing methodologies using accelerometer demonstrated that to maximize the sensitivity on vibration the sensor must be placed on the engine block (bottom part is preferred), the sensor positions highlighted by Figure 140 were chosen following this guideline.

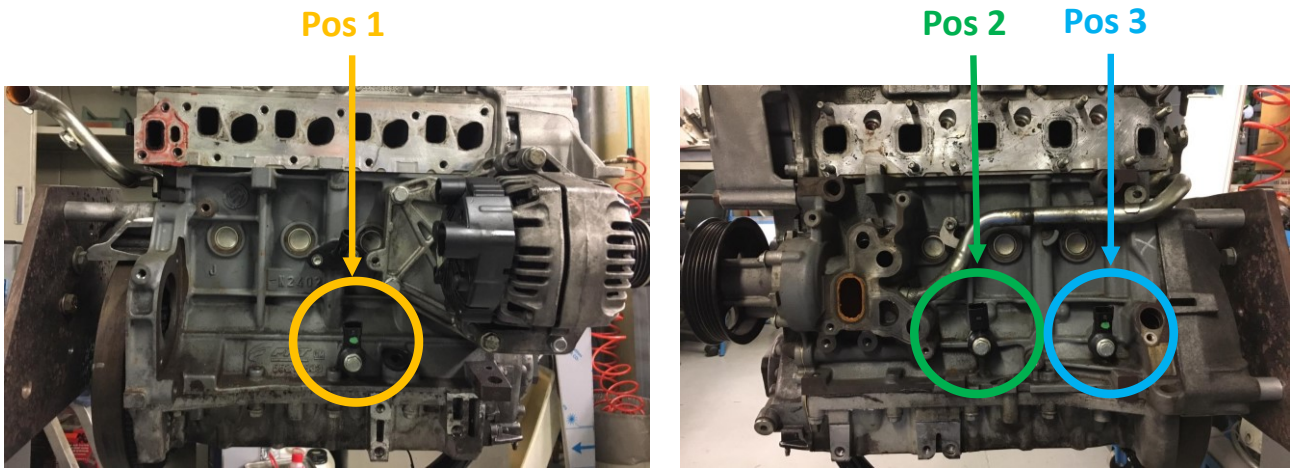

Figure 140. Different sensor (accelerometer) positioning on the engine block: at left the intake side, at right the exhaust side.

By using the engine calibration obtained through previous activities on GCI engine reported above, two different engine loads were tested: low load, with IMEP equal to 10 bar; high load, with IMEP equal to 14 bar. As widely explained before, rising the engine speed might compromise the SOC detection mainly because the worsening of the signal-to-noise ratio. As a result, to verify the accuracy of the presented non-intrusive SOC detection methodology, five different engine speed were tested: 2000, 2250, 2500, 2750, 3050 rpm. To quantify the performance of the presented SOC estimation methodology and determine the best sensor positioning, 150 consecutive engine cycles for each tested condition were considered and the error between measured SOC through in-cylinder pressure signal and accelerometer was calculated. All the engine cycles with SOC estimation error greater than +/- 3 degrees were considered unrecognized.

Figure 141 shows the results of the analysis on sensor positioning in different engine operating conditions. By the comparison of the reported results, it clearly arises that the position 2 can be considered the best sensor placement both in terms of accuracy and cylinder-by-cylinder variability. As a matter of fact, despite the performance of the algorithm decrease at low load (due to low signal to noise ratio generated by the low energy released in the first combustion stage and the high cycle-by-cycle variability), with the sensor in position 2 a consistent and accurate SOC estimation can be obtained for all the tested engine speed, meaning that the signal-to-noise ratio (in that position) does not strongly decreases. Furthermore, the SOC estimation by placing sensor in position 2 is almost constant (and quite accurate) for all the 4 cylinders. On the contrary, the results obtained with the sensor in position 1 and 3 are generally worse both in terms of accuracy with high variability changing the engine speed and cylinder-by-cylinder variability.

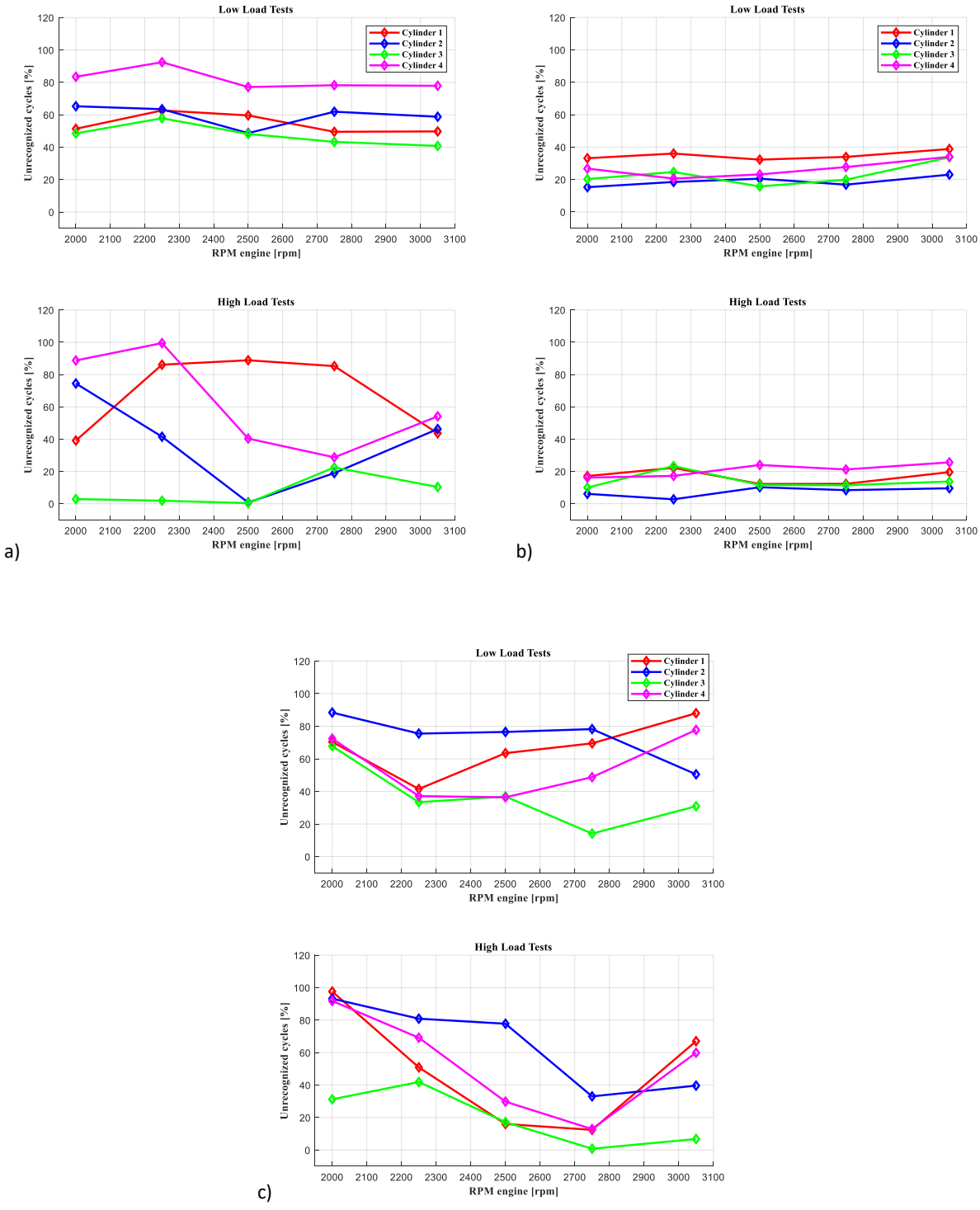

Figure 141. Accuracy of non-intrusive SOC detection methodology in different engine operating points and sensor positions: a) Position 1, b) Position 2 and c) Position 3on the engine crankcase

The presented results confirm the reliability of remote sensing methodologies even for GCI combustion. Due to its typical combustion shape, it was demonstrated that the start of combustion position for GCI combustion can be obtained by using an accelerometer sensor mounted on the engine block. Since the stability of the ignition phase (and consequently SOC position) plays a crucial role on the GCI combustion management, the SOC estimation through accelerometer, coupled with the previously-described ID model (feedforward contribution), could be effectively used as feedback improving the injection management strategy.

3. Conclusions

The presented thesis work is focused on the study of one of the most promising Low Temperature Combustion methodology, called gasoline Partially Premixed Combustion (GCI), which could be applied to reduce the impact of transports during the green transition on course. To do that, several experimental activities were conducted in a standard 1.3L compression ignited engine verifying the potential of the mentioned advanced combustion both in terms of engine-out emissions and thermal efficiency.

First, to verify the applicability of GCI combustion in the considered engine, a preliminary activity was conducted with the called "Cylinder Laboratory" mode, fueling only one cylinder with gasoline while the others 3 cylinders keep the engine in stable operating point. To do that, an additional injection system was added, and the test bench control systems was updated integrating the external hardware (Rapid Control Prototyping system) and respective control strategies for the gasoline cylinder management. By using the Cylinder Laboratory mode, the effects of the main control parameters, such as injection pattern management (number of injections, injections positioning), gasoline pressure, boost pressure, intake temperature, on GCI combustion stability and management were highlighted. The main outcome of the Cylinder Laboratory mode activity was to obtain a reference calibration which guarantee the stability of GCI combustion without compromise the engine reliability.

Then, once obtained a reliable set of control parameters able to perform GCI combustion, the activity was focused on updating test bench and engine layouts to run all the 4 cylinders of the engine in GCI mode. To do so, external supercharger and diathermic heater were added and integrated in the intake line of the engine. Moreover, to overcome the limitations of standard ECU when running the engine far from the manufacturer calibration conditions, the engine was controlled using the fully programmable SPARK ECU in which are developed and implemented all the control strategies needed to properly investigate GCI combustion in a fully converted engine. To verify the benefit of GCI combustion, engine-out emissions (NOx and FSN) and high accuracy fuel consumption measurement systems were added and integrated in the existing test bench layout. By using the updated experimental layout, GCI engine was tested over its whole engine operating range assuring high reliability and controllability. By using high EGR rates, the benefits of that combustion methodology both in terms of engine-out emissions and fuel consumption reductions were proved. By the comparison with the performance of the same engine run in CDC mode, GCI combustion demonstrated to be convenient (lower fuel consumption and pollutants) and therefore, a suitable solution developing cleaner transport.

Despite GCI combustion proved to be effective reducing pollutants and fuel consumption, the main limitations which hinders the diffusion in production applications is related to the control of the combustion process. As a matter of fact, since GCI combustion is characterized by the spontaneous ignition of a lean air and low reactivity fuel mixture, to guarantee an efficient combustion process a stable and reliable ignition stage is needed. Thus, it was demonstrated that it was possible to stabilize the GCI ignition process by using multiple injections of small amount of fuel early injected on the engine cycle. However, since this phenomenon is chemically driven, slight variation of cylinder thermal conditions or inaccuracy on the injected fuel with pre-injections might compromise the mixture ignitability and, therefore, the whole combustion stability producing misfire or knocking. For these reasons, to properly control the injected fuel with pre-injections, a wide experimental activity on studying the pressure waves propagation in the injection system of the engine was performed and a control-oriented model-based fuel quantity correction strategy was developed. Moreover, to reduce the impact of the cylinder thermal condition on combustion stability, a control-oriented physical based ignition delay model was developed. After developing the model parameters, T_{SOIPIL} and M_{eq}, the ID model was calibrated performing specific testing methodology called "Switching Pattern", which consist in a deactivation of the main injection after a certain number of cycles with complete injection pattern. By the

analysis of the switched cycle (engine cycle obtained actuating only the pre-injection), it was possible to study in deep the ID of the small amount of fuel injected without interaction of the main injection focusing the attention only on this stage of combustion. The results of this modeling highlighted a good accuracy on the ID estimation over the whole GCI operating range (different loads, intake, and exhaust conditions and EGR rates were tested) and therefore, the ID model could be considered as an effective feedforward contribution for the injection control strategy. Moreover, to further improve the robustness of GCI combustion control strategies, a remote sensing methodology for combustion indexes estimation based on vibrational sensor was developed. Since the typical GCI combustion shape shows a first stage with high energy released in a short time, it was demonstrated that SOC information can be easily obtained by using vibrational sensor. As a result, a specific experimental activity was carried out to verify the accuracy on SOC estimation running GCI combustion in different engine operation conditions and different sensor positions. The analysis of the obtained results confirmed that the developed algorithm for SOC estimation can be successfully applied even for the advanced combustion considered in this study. Furthermore, by the high accuracy and reliability of the SOC estimation through the accelerometer cycle-by-cycle, such information can be used as feedback improving the performance of the combustion control strategy, i.e., adjusting the ID model.

4. Acknowledgements

The authors gratefully acknowledge Marelli Holdings Co., Ltd. Powertrain division for the support during the whole experimental activity (engine).

University of Bologna (Forlì) and Alma Automotive s.r.l. are acknowledged respectively for the testing facilities and instrumentation.

5. Appendix 1: Sensors Characteristics

In-cylinder pressure: necessary to calculate all combustion indexes (IMEP, CA50, PPRR)

Sensor Name	AVL GH14P
Measuring range	0-250 bar
Overload	300 bar
Sensitivity	15 pC/bar
Linearity	≤ ± 0.3%
Calibrated ranges	0 ... 80 bar 0 ... 150 bar 0 ... 250 bar
Natural frequency	115 kHz

Fuel consumption: necessary to evaluate the total fuel injected mass for each condition and, therefore, to calculate combustion efficiency (ISFC)

Sensor Name	Flowsonic LF
Repeatability	+/- 0.15% of reading
Uncertainty	+/- 0.5% of reading
Measurement flow range	8-4000 ml/min
Measurement rate	2.2 kHz
Fluid temperature range	-20°C to +120°C
Ambient temperature range	-40°C to +120°C

NOx: necessary to evaluate the GCI combustion nitrogen oxides production

Sensor Name	Continental Uni-NOx SNS14
Measurement Principle	ZrO_2 based multilayer sensor with integrated heater and 3 oxygen pumps
Measured value output	NOx, linear λ and binary λ
Measurement Range	NOx: 0 – 1500 ppm Lin λ: 0.75 to 14 Bin λ: > 0.75V at λ=0.9; < 0.2V at λ=1.1
Time for readiness NOx	< 100 s
Operating gas temperature	100 - 800 °C

FSN: necessary to evaluate the GCI combustion particulate matter production

Sensor Name	AVL Smoke Meter 415s
Measurement Principle	Filter paper blackening
Measured value output	FSN (Filter Smoke Number), mg/m^3(soot concentration)
Measurement range	0 to 10 FSN
Detection limit	0.0002 FSN or 0.02 mg/m^3
Exhaust pressure ranges	0 to 3000 mbar (High Pressure Option)
Maximum exhaust temperature	800 °C (long probe configuration)
Repeatability	+/- (0.005 FSN + 3% @ 10 seconds intake time)

Piezoresistive pressure sensor: necessary to evaluate the pressure wave on the injection system feed duct

Sensor Name	Kistler 4067A
Measuring range	0-2000 bar
Overload	2500 bar
Sensitivity	5 (±0,5 % at 25 ºC)
Linearity	≤ ± 0.5%
Natural frequency	> 100 kHz

Accelerometer: necessary to evaluate the engine block vibration

Sensor Name	PCB Piezotronic 352C33
Measuring range	±490 m/s² pk
Sensitivity	10.2 mV/(m/s²)
Linearity	≤1 %
Natural frequency	≥50 kHz

6. References

1. https://world101.cfr.org/global-era-issues/climate-change/paris-agreement
2. https://ourworldindata.org/emissions-by-sector
3. Dhingra, Devakar & Chatterjee, Aniruddha & Jain, Samit. (2019). Episode III: Staying Cool inside the Building Using Phase Change Materials (PCM).
4. https://www.zmescience.com/ecology/almost-all-countries-are-failing-their-paris-agreement-contributions
5. https://www.evgo.com/ev-drivers/types-of-evs
6. https://thedriven.io/2018/08/28/what-is-a-fuel-cell-electric-vehicle
7. https://afdc.energy.gov/vehicles/how-do-gasoline-cars-work
8. https://nissan-global.com
9. https://www.greencarcongress.com/2021/07/20210721-icct.html
10. Dempsey, A. B., Curran, S. J., & Wagner, R. M. (2016). A perspective on the range of gasoline compression ignition combustion strategies for high engine efficiency and low NOx and soot emissions: Effects of in-cylinder fuel stratification. *International Journal of Engine Research*, 17(8), 897–917. https://doi.org/10.1177/1468087415621805.
11. Dempsey, AB, Curran, S, Wagner, R, Cannella, W, & Ickes, A. "Gasoline Compression Ignition (GCI) on a Light-Duty Multi-Cylinder Engine Using a Wide Range of Fuel Reactivities and Heavy Fuel Stratification." Proceedings of the ASME 2020 Internal Combustion Engine Division Fall Technical Conference. ASME 2020 Internal Combustion Engine Division Fall Technical Conference. Virtual, https://doi.org/10.1115/ICEF2020-2929
12. M.B. Luong, R. Sankaran, G.H. Yu, S.H. Chung, C.S. Yoo, "On the effect of injection timing on the ignition of lean PRF/air/EGR mixtures under direct dual fuel stratification conditions", Combustion and Flame 183 (2017), https://doi.org/10.1016/j.combustflame.2017.05.023
13. Bunce, M. and Blaxill, H., "Sub-200 g/kWh BSFC on a Light Duty Gasoline Engine," SAE Technical Paper 2016-01-0709, 2016, https://doi.org/10.4271/2016-01-0709.
14. Chiodi, M., Kaechele, A., Bargende, M., Wichelhaus, D. et al., "Development of an Innovative Combustion Process: Spark-Assisted Compression Ignition," SAE Int. J. Engines 10(5):2017, https://doi.org/10.4271/2017-24-0147.
15. Heywood J., Internal Combustion Engine Fundamentals, May 1st, 1988.
16. https://www.depusa.com/engine-development/
17. https://www.kistler.com
18. http://resources.edb.gov.hk/physics/articleIE/smartmaterials/SmartMaterials_e.htm
19. https://electronics.stackexchange.com/
20. https://biodieselmagazine.com
21. Ravaglioli, V., Carra, F., Moro, D., De Cesare, M. et al., "Remote Sensing Methodology for the Closed-Loop Control of RCCI Dual Fuel Combustion," SAE Technical Paper 2018-01-0253, 2018, https://doi.org/10.4271/2018-01-0253
22. Singh A. P., Agarwal A. K., "Low-Temperature Combustion: An Advanced Technology for Internal Combustion Engine", (2018), Springer Singapore
23. Maurya R. K., "Characteristics and Control of Low Temperature Combustion Engines", (2018), Springer International Publishing
24. Belgiorno, G., Dimitrakopoulos, N., Di Blasio, G., Beatrice, C., Tunestål, P., Tunér, M., "Effect of the engine calibration parameters on gasoline partially premixed combustion performance and emissions compared to conventional diesel combustion in a light-duty Euro 6 engine", *Applied Energy*, Volume 228, 2018, Pages 2221-2234, ISSN 0306-2619, https://doi.org/10.1016/j.apenergy.2018.07.098.
25. Belgiorno, G., Dimitrakopoulos, N., Di Blasio, G., Beatrice, C. et al., "Parametric Analysis of the Effect of Pilot Quantity, Combustion Phasing and EGR on Efficiencies of a Gasoline PPC Light-Duty Engine," SAE Technical Paper 2017-24-0084, 2017, https://doi.org/10.4271/2017-24-0084.
26. Sellnau, M., Foster, M., Moore, W., Sinnamon, J. et al., "Pathway to 50% Brake Thermal Efficiency Using Gasoline Direct Injection Compression Ignition," SAE Technical Paper 2019-01-1154, 2019, https://doi.org/10.4271/2019-01-1154..
27. Ravaglioli, V., Ponti, F., and De Cesare, M. (August 24, 2020). "Investigation of Gasoline Compression Ignition for Combustion Control." ASME. *J. Eng. Gas Turbines Power*. September 2020; 142(9): 091003. https://doi.org/10.1115/1.4048055
28. Stola, F., Ravaglioli, V., Silvagni, G., Ponti, F. et al., "Analysis of the Effects of Injection Pressure Variation in Gasoline Partially Premixed Combustion," SAE Technical Paper 2021-01-0517, 2021, https://doi.org/10.4271/2021-01-0517.
29. Stola, F., Ravaglioli, V., Silvagni, G., Ponti, F. et al., "Injection Pattern Investigation for Gasoline Partially Premixed Combustion Analysis," SAE Technical Paper 2019-24-0112, 2019, https://doi.org/10.4271/2019-24-0112
30. Ravaglioli, V., Ponti, F., Silvagni, G., Moro, D. et al., "Investigation of Gasoline Partially Premixed Combustion with External Exhaust Gas Recirculation," SAE Int. J. Engines 15(5):2022, https://doi.org/10.4271/03-15-05-0033.

31. Yazdani, A., Naber, J., Shahbakhti, M., Dice, P. et al., "Air Charge and Residual Gas Fraction Estimation for a Spark-Ignition Engine Using In-Cylinder Pressure," SAE Technical Paper 2017-01-0527, 2017, https://doi.org/10.4271/2017-01-0527
32. Sinnamon, J.F. and Sellnau, M.C., "A New Technique for Residual Gas Estimation and Modelling in Engines," SAE Technical Paper 2008-01-0093, 2008, https://doi.org/10.4271/2008-01-0093.
33. Signorelli, G., Cavani, A., Petrone, M., Petrecchia, S. et al., "GDI Very High-Pressure Injector for High Compression Gasoline Engine," in 42nd International Vienna Motor Symposium, Vienna, Austria, 2021.
34. Shahlari, A., Hocking, C., Kurtz, E., and Ghandhi, J., "Comparison of Compression Ignition Engine Noise Metrics in Low-Temperature Combustion Regimes," *SAE Int. J. Engines* 6(1):541-552, 2013, https://doi.org/10.4271/2013-01-1659.
35. An, Y., Mubarak Ali, M.J., Vallinayagam, R., AlRamadan, A. et al., "Compression Ignition of Low Octane Gasoline under Partially Premixed Combustion Mode," SAE Technical Paper 2018-01-1797, 2018, https://doi.org/10.4271/2018-01-1797.
36. Matsuura, K. and Iida, N., "Effect of Temperature-Pressure Time History on Auto-Ignition Delay of Air-Fuel Mixture," SAE Technical Paper 2018-01-1799, 2018, https://doi.org/10.4271/2018-01-1799.
37. Coppo, M., Dongiovanni, C., Negri, C., (2002), "Numerical analysis and experimental investigation of a common rail type diesel injector", *ASME ICEF* 2002, p.271-80, https://doi.org/10.1115/ICEF2002-507.
38. Boundy, F., Seers, P., (2009) "Impact of physical properties of bio-diesel on the injection process in a common-rail direct injection system", *Energy Conversion Management*, 2009, 50:2905-29102, https://doi.org/10.1016/j.enconman.2009.07.005
39. Su, H. F., Zhang, Y., T., Luo, X. And Liang J., W., "Dampling the Water Hammer Pressure Wave in the High Pressure Common Rail System", *Transaction of CSICE*, 04:379-383, 2013
40. Gupta, V. K., Zhang, Z., and Sun, Z., "Modeling and control of novel pressure regulation mechanism for common rail fuel injection system", *Applied Mathematical Modelling*, https://doi.org/10.1016/j.apm.2011.01.008.
41. Bianchi, G. M., Falfari, S., Brusiani, 2005, "High-Pressure Wave Propagation Induced by Multiple-Injection Strategy operated in a Common Rail Injection System Equipped by a Fast-Actuation Solenoid Injector", 2005, 60th *Congresso Nazionale ATI*, Roma 13-15 settembre 2005, Contributo in Atti di Convegno ART. 07/08.
42. Bianchi, G. M., Falfari, S., Brusiani, F., Osbat, G., Parotto, M., Pelloni, P., 2005, "Numerical Investigation of Critical Issues in Multiple-Injection Strategy Operated by New C.R. Fast-Actuation Solenoid Injector", *SAE Technical Paper* 2005-01-1236, 2018, https://doi.org/10.4271/2005-01-1236.
43. Ferrari, A., Paolicelli, F., "Modal Analysis of Fuel Injection System and Determination of a Transfer Function Between Rail Pressure and Injection Phase" ASME. *J. Eng. Gas Turbines Power*, https://doi.org/10.1115/1.403948
44. Ferrari, A., Paolicelli, F., "Modal Analysis as a Design Tool for Dynamical Optimization of a Common Rail Fuel Injection System", *SAE Technical Paper* 2015-24-2467, https://doi.org/10.4271/2015-24-2467.
45. Catania, A., Ferrari, A., Manno, M., Spessa, E., "Experimental Analysis of Transient Flow Phenomena in Multi-Jet Common Rail System", *SAE Technical Paper* 2005-24-048, https://doi.org/10.4271/2005-24-048.
46. Bai, Y., Gu, Y., Lan, Q., Fan, Y., MA, X., "Correction Strategy of Fuel Injection Quantity During Pilot-Main Injection of Common Rail System", *Journal of Mechanical Science and Technology* 34(6)2020, https://doi.org/10.1007/s12206-020-0538-0.
47. Silvagni, G., Ravaglioli, V., Ponti, F., Corti, E. et al., "Development of a Predictive Pressure Waves Model for High-Pressure Common Rail Injection Systems," SAE Int. J. Engines 15(5):2022, https://doi.org/10.4271/03-15-05-0039.
48. Lee, J., Lee, C.H., "An Uncertainty analysis of the time-resolved fuel injection pressure wave based on BOSCH method for a common rail diesel injector with varying current wave pattern", *Journal of Mechanical Science and Technology* 32(12)2018, https://doi.org/10.1007/s12206-018-1145-1.
49. Belgiorno, G., Dimitrakopoulos, N., Di Blasio, G., Beatrice, C. et al., "Parametric Analysis of the Effect of Pilot Quantity, Combustion Phasing and EGR on Efficiencies of a Gasoline PPC Light-Duty Engine", *SAE Technical Paper* 2017-24-0084, 2017, https://doi.org/10.4271/2017-24-0084.
50. Ubertini, S., (2006), "Injection pressure fluctuations model applied to a multidimensional code for diesel engines simulation", *J. Eng. Gas Turbines Power*, 2002, 128:694-701, https://doi.org/10.1115/1.2135813.
51. Mohebbi M., Azhar A. A., Hamidi A., Hajialimohammadi A., Hosseini V., "Modeling of pressure line behavior of common rail diesel engine due to injection and fuel variation", *J. Braz. Soc. Mech. Sci. Eng.*, 2016, https://doi.org/10.1007/s40430-016-0573-z.
52. Li, P., Zhang, Y., Li, T., Xie, L., "Elimination of Fuel Pressure Fluctuation and Multi-Injection Fuel Mass Deviation of High Pressure Common Rail fuel Injection System", *Chinese Journal of Mechanical Engineering*, https://doi.org/10.3901/CJME.2014.1216.180.
53. Peng, J., Ma, M., Weizhi, W., Bai, F., Du, Q., "Characterization of Rail Pressure Fluctuation under Two Injection Condition and the Control Strategy Based on ANN", *SAE Technical Paper* 2017-01-1242, https://doi.org/10.4271/2017-01-1242.
54. Kelly, S.G., Mechanical Vibration Theory and Applications, SI (Global Engineering, USA, 2012)

55. Baratta, M., Catania, A. E., Ferrari, A., “Hydraulic Circuit Design Rules to Remove the Dependence of the Injected Fuel Amount on Dwell Time in Multijet CR Systems”, *Journal of Fluid Engineering*, https://doi.org/10.1115/1.2969443.
56. Wu, D., Sun, B., Xu, A., An, X., Ge, Y., “Study on Pressure Fluctuation of a Constant Pressure Fuel System”, *SAE Technical Paper* 2012-01-0828, https://doi.org/10.4271/2017-01-0828.
57. Zhang, M., Xu, L., Derafshzan, S., Bai, X., Richter, M., Lundgren, M., “Impact of Multiple Injection Strategies on Efficiency and Combustion Characteristics in an Optical PPC Engine”, 2020, *SAE Int. J. Engines*, https://doi.org/10.4271/2020-01-1131.
58. Yin, L., Ingesson, G., Shamun, S., Tunestal, P. et al., "Sensitivity Analysis of Partially Premixed Combustion (PPC) for Control Purposes," *SAE Technical Paper* 2015-01-0884, 2015, https://doi.org/10.4271/2015-01-0884.
59. Dec, J., Dernotte, J., and Ji, C., "Increasing the Load Range, Load-to-Boost Ratio, and Efficiency of Low-Temperature Gasoline Combustion (LTGC) Engines," 2020, *SAE Int. J. Engines,* https://doi.org/10.4271/2017-01-0731.
60. Cho, K., Latimer, E., Lorey, M., Cleary, D. et al., "Gasoline Fuels Assessment for Delphi’s Second-Generation Gasoline Direct-Injection Compression Ignition (GDCI) Multi-Cylinder Engine" 2017, *SAE Int. J. Engines*, https://doi.org/10.4271/2017-01-0743.
61. Catania, A. E., Ferrari, A., and Manno, M., 2005, “Development and Application of Complete Common Rail Injection System Mathematical Model for Layout Hydro-Dynamic Analysis”, ASME ICED Spring Conference and ASME *J. Eng. Gas Turbines Power*, https://doi.org/10.1115/ICES2005-1018.
62. Bing-Qi, J., Li-Yun, F., Xiu-Zheng, M., Hayot, Q., Yang, L., Hao, W., “Investigation of Main Injection Quantity Fluctuation due to Pilot Injection in a High Pressure Common Rail Fuel Injection System”, *International Journal on Smart Sensing and Intelligent Systems*, https://doi.org/10.21307/ijssis-2017-683
63. Matsuura, K. and Iida, N., “Effect of Temperature-Pressure Time History on Auto-Ignition Delay of Air-Fuel Mixture”, *SAE Technical Paper* 2018-01-1799, 2018, https://doi.org/10.4271/2018-01-1799.
64. Ravaglioli, V, Ponti, F, Silvagni, G, & De Cesare, M. "Development of a Methodology for the Investigation of Residual Gases Effects on Gasoline Compression Ignition." Proceedings of the ASME 2020 Internal Combustion Engine Division Fall Technical Conference. ASME 2020 Internal Combustion Engine Division Fall Technical Conference. Virtual, Online. November 4–6, 2020. V001T04A006. ASME. https://doi.org/10.1115/ICEF2020-2996
65. Lee, Y., Lee, S., and Min, K., “Ignition Delay Model of Multiple Injections in CI Engines,” SAE Technical Paper 2019-24-0071, 2019, https://doi.org/10.4271/2019-24-0071.
66. Cavina, N., Rojo, N., Businaro, A., Brusa, A. et al., "Investigation of Water Injection Effects on Combustion Characteristics of a GDI TC Engine," SAE Int. J. Engines 10(4):2209-2218, 2017, https://doi.org/10.4271/2017-24-0052.
67. Arnone, L., Boni, M., Manelli, S., Chiavola, O. et al., "Block Vibration Measurements for Combustion Diagnosis in Multi-Cylinder Common Rail Diesel Engine," SAE Technical Paper 2009-01-0646, 2009, https://doi.org/10.4271/2009-01-0646.
68. Ponti, F., Ravaglioli, V., Cavina, N. and De Cesare M., "Diesel Engine Combustion Sensing Methodology Based on Vibration Analysis." ASME. J. Eng. Gas Turbines Power. November 2014; 136(11): 111503. https://doi.org/10.1115/1.4027363.

7. Symbols/Acronyms Index

A_p	Piston Bore
BEVs	Battery Electric Vehicles
BSFC	Brake Specific Fuel Consumption
CAN	Controller Area Network
CA50, MFB50	Center of combustion
CA90	End of Combustion
CDC	Conventional Diesel Combustion
CHR	Cumulative Heat Release
CI	Compression Ignition

CO	Carbone oxide
CO2	Carbone dioxide
CR	Common Rail
DI	Direct Injection
DI-PWR	Double Injection Pressure Wave Reconstruction
DT	Dwell Time
E_a	Mixture Activation Energy
ECU	Electronic Control Unit
EGR	Exhaust Gas Recirculated
EGRrate	Mixture dilution Factor
EOI	End of Injection
ET	Energizing Time
ET1	First Injection Energizing Time
ET2	Second Injection Energizing Time
FCEVs	Fuel Cell Electric Vehicles
FQC	Fuel Quantity Fluctuation Correction
GHG	Green House Gases
GCI	Gasoline partially premixed Compression Ignition combustion
HC	Unburned Hydrocarbon
HCCI	Homogeneous Charge Compression Ignition
HEVs	Hybrid Electric Vehicles
HSF	Heavy Fuel Stratification
Hy-ICE	Hydrogen Internal Combustion Engines
ICE	Internal Combustion Engine
ID	Ignition Delay
IMEP	Indicated Mean Effective Pressure
ISFC	Indicated Specific Fuel Consumption
K	Bulk Modulus

L_i	Indicated Work
LTC	Low Temperature Combustions
$M_{CYL_{intake}}$	Amount of fresh Charge
M_{EGR}	Exhaust Gases Mass
M_{eq}	Equivalent Mass (Chemical-Physical Index)
M_{H_2O}	Water Vapor Mass
M_{O_2}	Oxygen mass
M_{RG}	Residual gases Mass
$M_{air_{model}}$	Amount of Fresh Air, output of the cylinder filling model
$M_{dry\ air}$	Dry Air Mass
MSD	Mass-Spring-Damper
MSF	Moderate Fuel Stratification
N_2	Molecular Nitrogen
NOx	Nitrogen Oxides
O_2	Molecular Oxygen
P_i	Indicated Power
PFI	Port Fuel Injection
PFS	Partial Fuel Stratification
PHEVs	Plug-in Hybrid Electric Vehicles
PPCI	Partially Premixed Compression Ignition combustion
Pkist Inj Side	Piezoresistive fuel pressure sensor Injector Side
Pkist Rail Side	Piezoresistive fuel pressure sensor Rail Side
PM	Particulate Matter
P_{exh}, $p_{exhaust}$, p_{EXH}	In-cylinder pressure averaged during exhaust stroke
P_{Int}, p_{intake}, p_{INT}	In-cylinder pressure averaged during intake stroke
P_{r_x}	Relative Power Ratio

$\mathbf{P_x}$	Amplitude of x-carrier
PPRR, $\boldsymbol{R_{max}}$	Peak Pressure Rise Rate
PRail	Rail Pressure
PWM	Pulse Width Modulation
R	Specific Gas Constant
$\boldsymbol{R_{air}}$	Air Specific Gas Constant
$\boldsymbol{R_u}$	Universal Gas Constant
RCCI	Reactivity Controlled Compression Ignition combustion
RCI	Relevance Carrier Index
RCP	Rapid Control Prototyping
RMSE	Root Mean Square Error
RoHR	Rate of Heat Release
RON	Research Octane Number
RPM	Revolutions per Minute
SACI	Spark Assisted Compression Ignition combustion
SCCI	Stratified Controlled Compression Ignition combustion
SOC	Start of Combustion
SOI	Start of Injection
SI	Spark Ignited
SI-PWR	Single Injection Pressure Wave Reconstruction
$\boldsymbol{T}$	Temperature
$\boldsymbol{T_{cyl}}$	Gas Temperature during combustion process (from cylinder pressure signal)
$\boldsymbol{T_{Exh}}$	Exhaust gas Temperature (from the cylinder pressure signal)
$\boldsymbol{T_{IVC}}$	Mixture Temperature at Intake Valve Closing timing
$\boldsymbol{T_{man}}$	Manifold Air Temperature
$\boldsymbol{T_{RG}}$	Residual Gases Temperature
$\boldsymbol{T_{SOI_{PIL}}}$	Mixture Temperature at SOI Pil

T_i	Indicated Torque
TDC	Top Dead Center
TI	Torch Ignition
TJI	Turbulent Jet Ignition
V_{BDC}	Volume at Bottom Dead Center angle
Vcc	Combustion chamber volume
Vcyl	Maximum geometrical volume of the cylinder
V_{IVC}	Volume at Intake Valve Closing angle
$V_{SOI_{PIL}}$	Volume at SOI Pil
VGT	Variable Geometry Turbine
aTDC	After Top Dead Center
bTDC	Before Top Dead Center
dL	Work done by gases on piston
dP	Derivative pressure
dQ_n	Infinitesimal Net Energy released during combustion
dU_s	Internal energy variation of open system considered
dV	Derivative volume
$d\theta$	Derivative angle
c	Fuel damping
cp	Heat capacity at constant pressure
cv	Heat capacity at constant volume
dp	Pressure derivative
$d\rho$	Density derivative
k	Fuel stiffness of the feed duct and injector
k_{EGR}	ID model coefficient for External EGR
k_{iRG}	ID model coefficient for Residuals

$\boldsymbol{hdm}$	Enthalpy lost due to gas leak through elastic tights
$\boldsymbol{m}$	Fuel inertia
$\boldsymbol{m_{Air}}$	Fresh Air mass
$\boldsymbol{m_{Air_{Flow\,rate}}}$	Air Flow Rate measurement
$\boldsymbol{m_{EGR}}$	Exhaust gas recirculated mass
$\boldsymbol{m_f}$	Fuel mass flow rate
$\boldsymbol{m_{RG}}$	Residual Gases mass
$\boldsymbol{l_{rod}}$	Conrod Length
$\boldsymbol{m_{inj}}$	Injected mass
$\boldsymbol{m_{inj\,1}}$	First pulse injected mass
$\boldsymbol{m_{inj\,2}}$	Second pulse injected mass
$\boldsymbol{p_{H_2O}}$, $\boldsymbol{p_{water\,vapor}}$	Partial pressure of water vapor in the air-water mixture
$\boldsymbol{p_{N_2}}$	Partial pressure of nitrogen in the air-water mixture
$\boldsymbol{p_{O_2}}$	Partial pressure of oxygen in the air-water mixture
$\boldsymbol{p_{cyl}}$	In-cylinder pressure
$\boldsymbol{p_{amb}}$	Ambient pressure of the test cell
$\boldsymbol{p_{dry\,air}}$	Partial pressure of air in the air-water mixture
$\boldsymbol{p_{sat}}$	Air saturation pressure
$\boldsymbol{r}$	Radius of crank
$\boldsymbol{s}$	Piston Stroke
$\mathbf{t}$	Time
$\boldsymbol{x_{mixture}}$	Mass fraction of water vapor
$\boldsymbol{x_0}, \boldsymbol{v_0}$	Initial Conditions
$\boldsymbol{x_{01}}, \boldsymbol{v_{01}}$	First main carrier estimated initial conditions
$\boldsymbol{x_{02}}, \boldsymbol{v_{02}}$	Second main carrier estimated initial conditions
$\boldsymbol{\delta Q_{ch}}$	Heat released during combustion
$\boldsymbol{\delta Q_{ht}}$	Heat exchanged through walls

ΔV_1	Re-expansion reduction volume contribution
ΔV_2	Late intake valve reduction volume contribution
Δ_ω	Natural frequency difference by different fuel type
γ	Adiabatic index
γ_{comp}	Adiabatic index of mixture during compression stroke
γ_{Exh}	Adiabatic index of mixture during expansion stroke
γ_θ	Adiabatic index function
λ	Air-fuel Ratio
ξ_1	First main carrier estimated damping ratio
ξ_2	Second main carrier estimated damping ratio
ϑ	Crankshaft Angle
$\theta_{RoRH\_0.15}$	Angular position at which RoHR reaches 0.15 J/deg
θ_{RoRH_5}	Angular position at which RoHR reaches 5 J/deg
ϕ	Relative humidity
φ	Local Air-fuel Ratio
ρ_g	Gasoline density
ρ_d	Diesel density
ω_d	Damped frequency
ω_{n1}	First main carrier estimated natural frequency
ω_{n2}	Second main carrier estimated natural frequency

8. Figures Index

9. Equations Index

10. Table Index